Evaluation of the Properties of Pyrolytic Char Modified Asphalt Binders and Mixtures

A thesis submitted in partial fulfilment of the

requirements for the award of the degree of

DOCTOR OF PHILOSOPHY

in

CIVIL ENGINEERING

by

Abhinay Kumar

Under the supervision of

Prof. Rajan Choudhary

Department of Civil Engineering
Indian Institute of Technology Guwahati
Guwahati – 781039, India

March, 2022

Department of Civil Engineering
Indian Institute of Technology Guwahati
Guwahati – 781039, Assam, India

CERTIFICATE

This is to certify that this thesis titled "**Evaluation of the Properties of Pyrolytic Char Modified Asphalt Binders and Mixtures**", submitted by **Mr. Abhinay Kumar** bearing registration number 156104009 in partial fulfilment of the requirement for the award of the degree of Doctor of Philosophy (Ph.D.) in Civil Engineering to Indian Institute of Technology Guwahati is a record of candidate's own work carried out under my supervision in the Department of Civil Engineering, Indian Institute of Technology Guwahati. This thesis, in my opinion, has reached the requisite standard fulfilling the requirement for the degree of Doctor of Philosophy.

Date: 23-03-2022

Place: Guwahati

(Dr. Rajan Choudhary)
Thesis Supervisor
Professor
Department of Civil Engineering
Indian Institute of Technology Guwahati
Guwahati, Assam – 781039, India

DECLARATION

I hereby declare that this written submission represents ideas in my own words and where other ideas and words/illustrations have been included, I have adequately cited and referenced the original sources. The work reported herein has not been submitted to any other institute for any degree or diploma. I also declare that I have adhered to all principles of academic honesty and integrity and have not misinterpreted or fabricated or falsified any idea/ data/ fact/ source in my submission. This thesis, in any way, does not purport to endorse any proprietary products or technologies.

Date: 23-03-2022

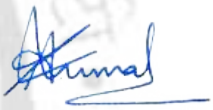

(Abhinay Kumar)
Registration No. 156104009
Department of Civil Engineering
Indian Institute of Technology Guwahati
Guwahati, Assam – 781039, India

Dedicated to:

My parents (Sunil Kumar and Nitu Karn), my brother (Abhishek), my sister (Rama), and Shivani: your unwavering love, patience, faith, and encouragement have enriched my soul and inspired me to complete this research.

ABSTRACT

The road transportation sector accounts for 4-5 percent of India's gross domestic product (GDP). The total road network length of 6.2 million kilometres in India is the second largest in the world. The major share of roads in India is built as flexible pavements. Flexible pavement structure usually consists of bituminous wearing and binder courses built over a granular base and sub-base course, and these courses lie on a compacted soil subgrade. The most common types of distresses in flexible pavements have been recognised as rutting, moisture damage, and fatigue. To alleviate pavement distresses and address the higher temperatures, tyre pressures, and axle load levels experienced by pavements, asphalt binder is typically modified for better performance under diverse loading and climatic circumstances, with the goal of extending the pavement service life. Some of the commonly used asphalt modifiers include styrene-butadiene-styrene (SBS), crumb rubber, ethylene-vinyl acetate (EVA), and styrene-butadiene rubber (SBR).

In recent years, there has been a strong push toward developing sustainable solutions for managing post-consumer tyre and plastic waste streams. In this regard, pyrolysis technology has garnered scientific attention for its ability to minimise waste volume while also allowing for energy valorisation and overcoming the challenges/concerns related to waste tyres and plastic disposal. The two primary pyrolysis products are liquid oils and gases, which have high potential as fuels, monomers, and precursors to important petrochemicals. The third product, solid carbonaceous pyrolytic char, is considered a by-product with relatively few applications/uses.

Carbon black, toner ink, and coke dust are examples of carbon-based materials/carbonaceous substances that have been used as asphalt additives/modifiers for asphalt pavements. The use of pyrolytic chars in the modification of asphalt binder is a relatively new research area. The current investigation on tyre pyrolytic char (TPC) and plastic pyrolytic char (PPC) modified asphalt binders and mixtures was inspired by previous findings with other carbon-based asphalt modifiers, as well as the possibility of incorporating a carbonaceous by-product of the pyrolysis process for asphalt modification.

This study evaluated the effect of TPC and PPC on the properties of asphalt binders as well as on the design and performance attributes of bituminous concrete mixes containing TPC and PPC modified asphalt binders. The study focused on a multi-faceted investigation that included: (a) characterisation of the two pyrolytic chars (TPC and PPC), (2) characterisation of the TPC and PPC modified asphalt binders focusing on conventional, storage stability, rheological, ageing, microscopic, and thermo-chemical evaluations, and (3) characterisation of asphalt mixtures fabricated with TPC and PPC modified asphalt binders focusing on their design, and performance against rutting, moisture damage,

cracking, and fatigue. Leachate toxicity tests were also conducted on asphalt mixtures fabricated with char modified binders to ensure that their use is safe for the environment. Pavement structural analysis was then carried out using IITPAVE software as per the Indian specification for flexible pavement design based on the resilient modulus of the mixes. A total of nine modified binders/mixtures were studied with a control binder and four binders, each with TPC and PPC modification levels of 5, 10, 15, and 20% by weight of binder.

The objectives of this study were grouped into six independent tasks. Task 1 of the study involved the physical and chemical characterisation of TPC and PPC and the microstructural and thermo-chemical characterisation of char-modified asphalt binders. Task 2 of the study involved evaluating the storage stability of the TPC and PPC modified binders. The thermal storage stability was evaluated at multiple dosages of two cross-linking agents: polyphosphoric acid (PPA) and sulfur. Task 3 of this study covered the rheological characterisation of TPC and PPC modified binders through frequency sweep, high-performance grade (PG) measurement, multiple stress creep and recovery (MSCR) evaluation, G* and δ master curves, G*sin δ evaluation, linear amplitude sweep (LAS) tests, and an additional high temperature/rutting evaluation. Task 4 of this research study aimed to evaluate the ageing resistance/characteristics of TPC and PPC modified binders using rheology-based and Fourier transform infrared (FTIR) spectroscopy-based ageing indices. Under Task 5, the production temperatures (mixing and compaction temperatures) were determined for the control, and TPC and PPC modified binders using four approaches: equiviscous method, high shear viscosity method, steady shear flow method, and phase angle method. Task 6 of the study included mix design and evaluation of toxicity potential and performance of asphalt (bituminous concrete) mixtures fabricated with control and TPC/PPC modified binders. For performance evaluation, asphalt mixtures were evaluated for resistance against rutting (through static creep, dynamic creep, and Hamburg wheel tracking device (HWTD) tests), moisture damage (through tensile strength ratio (TSR) and retained Marshall stability (RMS) tests), cracking (through semi-circular bend (SCB) test), and fatigue (through indirect tensile fatigue test (ITFT)).

Characterisation of the two pyrolytic chars showed that TPC had a finer particle size distribution with a lower volatile matter content and more stable thermal characteristics than PPC. PPA content of 1.0% and sulfur content of 0.3% produced the lowest storage separation for TPC modified binders. Storage stability analysis of PPC modified binders also showed that the 0.3% sulfur dosage resulted in the best performance. Asphalt binder modification with TPC and PPC improved the rheological performance of binders at multiple test temperatures based on multiple rutting parameters. The rutting performance improved with the increase in char dosages up to 20%. Based on the LAS fatigue test on binders, it was found that the optimum performance was achieved at a 10% dosage of both TPC and PPC. Rheological as well as FTIR based ageing indices showed that TPC modified asphalt binder suffered lower ageing compared to the control and PPC modified binder.

An increase in the production temperatures was observed with an increase in pyrolytic char content across all methods used. Leaching tests showed that TPC and PPC could be safely used in asphalt mixtures for pavement construction. Stiffness and rutting performance of the mixtures showed a consistent increase with an increase in TPC and PPC dosage up to 20%, as also observed in binder testing. Comparing the fatigue, cracking, and moisture damage results, it was found that the optimum performance was achieved at 10% dosage of both TPC and PPC. Pavement structural analysis conducted with IITPAVE software showed that the use of TPC and PPC in the top wearing course layer contributed to an increased traffic carrying capacity of the pavement, owing to the higher resilient moduli. The overall findings of this study show that 10% dosage of these chars is the most favourable dosage considering rheological characteristics and the improvements in rutting, moisture damage, cracking, and fatigue performance of asphalt mixtures.

Keywords: asphalt binder modification; pyrolysis; tyre pyrolytic char; plastic pyrolytic char; asphalt rheology; asphalt mixture; waste utilisation

ACKNOWLEDGEMENTS

I would like to express my sincere gratitude and thanks to my supervisor Prof. Rajan Choudhary for his excellent technical guidance. I am always indebted to him for the timely advice, meticulous scrutiny, scholarly advice and scientific approach. He was engrossed in the research project from its inception to its conclusion. I am grateful for his generous personality and all of the valuable time he spent with me throughout the course of my studies. I am highly thankful to him for the invaluable assistance and suggestions that will help shape my career.

I wish to express my deep sense of gratitude to the doctoral committee members Prof. Akhilesh Kumar Maurya, Prof. Bimlesh Kumar, and Dr. Dilwar Hussain for the insightful discussion, for offering brilliant advice, and for their encouragement during the whole duration of the research. The thesis's final form would not have been conceivable without their invaluable suggestions.

I am thankful to the Ministry of Education (Govt. of India) for providing the research fellowship. I also express my gratitude to the Director of the Institute, Head of the Civil Engineering Department, Dean (Academics), and Dean (Research & Development) of IIT Guwahati for strengthening the research environment and providing the requisite support to conduct my research.

I also thank Prof. Rupam Kataki (Tezpur University), who graciously spent his precious time during the early stages of my PhD, providing assistance and comments that helped shape the course of the research. I thank all the editors and anonymous reviewers for their constructive feedback during the review process of my journal and conference publications. I thank the Central Instruments Facility, IIT Guwahati, for support in analysing asphalt binder and char samples. I also sincerely appreciate the support and contribution of Mr. Manojj Natarrajan (Innova Engineering & Fabrication, Mumbai) for providing pyrolytic products and related technical assistance during my PhD research.

My journey as a researcher began as a summer intern after the second year of my undergraduate degree, as I got the opportunity to work with Prof. GL Sivakumar Babu (IISc Bangalore). No words of thanks can sum up the gratitude that I owe to him for inculcating in me the learning attitude towards research. I owe a deep sense of gratitude to my teachers at NERIST (Itanagar), particularly Prof. Sukumar Baishya, Dr. Dipika Devi, and Dr. Archana Kumari; it was because of their enthusiasm, counsel, and trust in me that I chose to enrol in the PhD programme.

I extend thanks to the staff at Transportation Engineering Lab: Mr. Kuldeep Kalita, Mr. Mrinal Sarmah, and Mr. Balen Kalita, for their constant help and administrative assistance

during the experimental phase of the work. I would like to reserve a memory lane for (Late) Shri Sanatan Patoway, lab attendant, who helped me during material collection and initial experimentation works. I pray for eternal peace to the departed soul. I would like to express my heartfelt gratitude to lab attendants Shri KC Bhuyan, Shri Prasanna Baishya, and Shri Habijur Rahman for their continuous help during the experimentation.

My special thanks go to Dr. Ashok Julaganti, who has been my mentor since my summer internship after the third year of undergraduate studies to this day. I thank you for introducing me to the field of asphalt technology, for nurturing me, for providing valuable insights and suggestions, and for always helping me solve problems during the research. I wish to express my special thanks to Dr. Sanjay Deori (NEIST, Jorhat) for the assistance and encouragement provided during the course of my PhD. Thanks to Mr. Ankush Kumar, with whom I share the bond of a brother rather than a PhD colleague. Thank you for the several long and engaging research discussions over the infinite cups of tea that helped me in this PhD journey. I wish you nothing but the best in your career and life!

I would like to express my gratitude to my supervisor's family for ensuring that I didn't miss home during my time at IIT Guwahati. My acknowledgements are devoted to the excellent group of seniors and friends I met at IIT Guwahati: Dr. Madhu Lisha Pattanaik, Santanu Pathak, Pubali Nazir, Dr. Bhaskar Pratim Das, Suresh Nama, Chandrabhanu Gupt, Dr. Sudheer Kumar Yamsani, Dr. V. Srikanth, Rajnish Kumar, Deepa Sachan, Dr. Surjith Ramasamy, Dr. Santanu Ghosh, Dr. Anisha Purkait, and Ashish Sharma. You all helped me in various phases of my work and made my doctoral experience one I will never forget, and I look forward to continuing to enjoy your friendships now and in the future.

I received incredible support from my father (Mr. Sunil Kumar), my mother (Mrs. Nitu Karn), my siblings (Abhishek and Rama), and Shivani: without your unflinching love, patience, and encouragement, none of this would indeed be possible. They kept me motivated and gave me a free hand without letting me know the difficulties they were facing. This thesis would not have been possible without their unwavering support and boundless affection. I thank them all from the bottom of my heart. I also thank and acknowledge my late grandparents, who have showered their blessing upon me through every step of this incredible journey.

Last but not least, I bow down to SitaRamji, Hanumanji and Maharajji, who granted countless blessings and endless grace, and opened before me unexpected avenues and enlightened my thoughts. Charan sparsh.

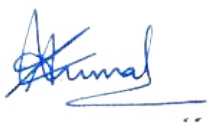

Abhinay Kumar

TABLE OF CONTENTS

LIST OF FIGURES

LIST OF TABLES

SYMBOLS AND ABBREVIATIONS

Symbols

A	Absorbance [arbitrary units]
a	notch depth [m]
a_T	shift factor at temperature T [unitless]
α	difference between values of upper and lower asymptotes in Sigmoidal model [unitless]
β	parameter defining shape between asymptotes and inflection point [unitless]
c	velocity of light [m/s]
C	factor for volumetrics of binder course layer [unitless]
D	specimen diameter [m]
D_{30}	particle size at 30% passing [m]
D_{50}	particle size at 50% passing [m]
D_{60}	particle size at 60% passing [m]
D_{90}	particle size at 90% passing [m]
δ	phase angle [°]
$\Delta\varepsilon_{nr}$	non-recoverable strain rate in MSCR test [%/cycle]
Δh	axial deformation [m]
ΔH_r	recovered horizontal deformation [m]
δ_L	rise (or fall) on left side of plateau [°]
δ_P	plateau phase angle [°]
E	light energy; elastic modulus [Pa]
ε	shear strain [unitless]
ε_0	strain applied during load cycle [unitless]
ε_c	creep strain in an MSCR cycle; vertical compressive strain [unitless]
ε_{nr}	non-recovered strain in an MSCR cycle [unitless]
ε_r	recovered strain in an MSCR cycle [unitless]

ε_t	horizontal tensile strain [unitless]
η	dynamic viscosity [Pa.s]
η_0	zero shear viscosity in Cross model [Pa.s]
η_∞	infinite shear viscosity in Cross model [Pa.s]
η'	storage viscosity [Pa.s]
η^*	complex viscosity [Pa.s]
f	frequency [Hz or rad/s]
f_P	plateau frequency [Hz]
f_r	reduced frequency [Hz]
G''	loss modulus [Pa]
G'	storage modulus [Pa]
G^*	complex shear modulus [Pa]
γ	shear rate [s^{-1}]
G_{mb}	bulk specific gravity of compacted mix [unitless]
G_{mm}	maximum specific gravity of loose mix [unitless]
G_{sb}	bulk specific gravity of the aggregates [unitless]
G_{se}	effective specific gravity of the aggregates [unitless]
h	thickness (height) of specimen [m]
h_P	Planck's constant [m^2 kg / s]
I	intensity in sample spectrum [W]
I_0	intensity in incident spectrum [W]
J_{nr}	MSCR non-recoverable compliance [Pa^{-1}]
J_c	critical strain energy release rate (J-integral) [J/m^2]
K,m	Cross model parameters [unitless]
k,n	Cross-Williams model parameters [unitless]
L	effective spindle length [m]
M_R	resilient modulus [Pa]
$M_{R,b}$	resilient modulus of bituminous mix used in binder course [Pa]
m-value	slope of stiffness versus time curve in BBR test [unitless]
μ	Poisson's ratio [unitless]

N_f	number of cycles to failure in LAS test [unitless]
v	lower asymptote [unitless]
ω	rotational speed [rad/s]
ω_{86}	frequency corresponding to phase angle of 86° [Hz]
P	peak load [N]
P_i	applied load at i^{th} load step [N]
P_s	percent aggregate [%]
ψ	parameter defining shape between asymptotes and inflection point [unitless]
r	radius of specimen [m]
R_c	container radius [m]
R_s	spindle radius [m]
S_L	slope of the master curve to the left side of plateau [unitless]
S_R	slope of the master curve to the right of plateau [unitless]
S-value	flexural creep stiffness in BBR test [Pa]
σ, σ_0	stress level [Pa]
SMC	spindle multiplier constant [unitless]
SP	softening point [°C]
t	Thickness [m], time [s]
T_F	fatigue life of bituminous layer [msa]
T_i	initial decomposition temperature [°C]
T_{max}	maximum decomposition temperature [°C]
T_R	subgrade rutting life [msa]
τ	torque applied [N.m]
θ	angular rotation [radian]
TK	torque constant [unitless]
U	strain energy to failure [Joule]
u	cross-head displacement [m]
W	Wavenumber [m^{-1}] ; weight [g]
W_c	dissipated energy per load cycle [Joule]
x	radial location to calculate shear rate [m]

Abbreviations

AAS	atomic absorption spectroscopy
AASHTO	American Association of State Highway and Transportation Officials
AC	asphalt cement
AFM	atomic force microscopy
AHO	aromatic hydrocarbon oil
AI	ageing index
ANOVA	analysis of variance
APA	Asphalt pavement analyzer
ASTM	American Society for Testing and Materials
ATR	attenuated total reflection
BBR	bending beam rheometer
BC	bituminous concrete
BET	Brunauer-Emmett-Teller
BIS	Bureau of Indian Standards
BS	British standard
CB	carbon black
CC	commercial charcoal
CI	carbonyl index
CMB	pyrolytic char modified binder
COC	Cleveland open cup
CTE	coefficient of thermal expansion
DSR	dynamic shear rheometer
EDX	energy dispersive X-ray
ESCA	electron spectroscopy for chemical analysis
EV	equiviscous
EVA	ethylene-vinyl acetate
FESEM	field emission scanning electron microscopy
FHWA	Federal Highway Administration

FTIR	Fourier transform infrared
GDP	gross domestic product
GPC	gel-permeation chromatography
HMA	hot mix asphalt
HSM	high shear mixer
HSV	high shear viscosity
HWTD	Hamburg wheel tracking device
INR	Indian Rupee
IR	infrared
IRC	Indian Roads Congress
IS	Indian Standard
ITFT	indirect tensile fatigue test
ITS	indirect tensile strength
ITSM	indirect tensile stiffness modulus
LAS	linear amplitude sweep
LVDT	linear variable displacement transducer
LVE	linear viscoelastic
MCR	Modular Compact Rheometer
MoRTH	Ministry of Road Transport and Highways
MSCR	multiple stress creep and recovery
NA	natural ageing
NCHRP	National Cooperative Highway Research Program
NHDP	National Highways Development Programme
NMAS	nominal maximum aggregate size
NMR	nuclear magnetic resonance
OBC	optimum binder content
PA	phase angle
PAV	pressure ageing vessel
PCB or CB_p	pyrolytic carbon black
PG	performance grade

PMB	polymer-modified bitumen
PMGSY	Pradhan Mantri Gram Sadak Yojana
PPA	polyphosphoric acid
PPC	plastic pyrolytic char
PPCMA	PPC modified asphalt
R&B	Ring and ball
RMB	rubber-modified bitumen
RMS	retained Marshall stability
rpm	revolutions per minute
RTFO	rolling thin film oven
SB	styrene-butadiene
SBR	styrene-butadiene rubber
SBS	styrene-butadiene-styrene
SCB	semi-circular bend
SEM	scanning electron microscopy
SHIP	State Highways Improvement Programme
SHRP	Strategic Highway Research Program
SI	separation index; stability index; sulfoxide index
SIMS	secondary ion mass spectrometry
SPD	softening point difference
SRP	Shenoy rutting parameter
SSD	saturated surface dry
SSF	steady shear flow
TCLP	toxicity characteristics leaching procedure
TFO	thin film oven
TGA	thermogravimetric analysis
TLC	thin-layer chromatography
TPC	tyre pyrolytic char
TPCB	tyre pyrolytic carbon black
TPCMA	TPC modified asphalt

TSR	tensile strength ratio
TTSP	time-temperature superposition principle
USD	United States dollar
USEPA	United States Environmental Protection Agency
UTM	universal testing machine
UV	ultraviolet
VFB	voids filled with bitumen
VG	viscosity grade
VMA	voids in mineral aggregates
ZSV	zero shear viscosity

Chapter 1

INTRODUCTION

1.1 Background

In India, the construction sector encompasses the second-largest economic activity after agriculture. It includes roads, railways, water supply, ports, urban infrastructure, *etc*. Out of these, road construction is a predominant segment that plays a vital role in the country's economy. Globally, India's road network is the second largest with a total length of 6.2 million km (MoRTH, 2021). The road transportation sector has a significant share of about 4-5% in the India's gross domestic product (GDP). The main high speed corridors comprising of national highways and expressways, which form only a 2% share of the total road network, cater to about 87% of passenger traffic and 60% of freight traffic movement in the country. The road infrastructure is therefore continuously undergoing rapid expansion under various ambitious programs/schemes, including National Highways Development Programme (NHDP), State Highways Improvement Programmes (SHIPs), Bharat Nirman, Bharatmala, Pradhan Mantri Gram Sadak Yojana (PMGSY), *etc*. With more highway development projects in the pipeline, the requirements of adequate quality construction materials especially aggregates and bituminous/asphalt binder[1] are expected to increase manifolds.

In India, the majority of roads are constructed as flexible pavements. A flexible pavement primarily consists of bituminous wearing and binder courses built over a granular

[1] Note on terminology: The terms 'bitumen', 'asphalt binder', and 'bituminous binder' are synonyms and have been used interchangeably in this thesis. Similarly, the terms 'asphalt mix', 'asphalt mixture', and 'bituminous mix' are also used interchangeably.

base course and sub-base course, and all these courses finally rest upon the compacted soil subgrade. Conventional bituminous mixes used in wearing and binder/base courses are prepared and constructed at relatively high temperatures (125-175 °C) and are also called as hot mix asphalt (HMA). HMA has continuously evolved over the last 130 years, and is the most preferred paving material globally. Dense-graded HMA comprises about 93-95% by weight of aggregates (consisting of stone, gravel, and sand) bound together by asphalt binder/bitumen. Although bitumen occupies a small proportion (5-7%) of HMA by weight, it is the costliest component (40-50% of the total mix cost) and plays a vital role in the HMA performance.

In general, an asphalt binder must remain flexible enough during the construction and the service life of the pavement to avoid cracking at ambient and low temperatures, but at the same time, it must also be stiff to resist the permanent deformation at high in-service temperatures during summer. Rutting, moisture damage, and fatigue have been identified as the most prominent distress types in flexible pavements. To alleviate such distresses and tackle the increased temperatures, tyre pressures, and axle load levels experienced by the pavements, asphalt binder is frequently modified for enhanced performance under different loading and climatic conditions striving to lengthen the service life of pavements.

Recently, there has been growing interest in using recycled or scrap materials as potential candidates for bitumen modification. This interest primarily originated due to increased costs involved with the use of virgin polymers (Kalantar et al., 2012) and to explore channels for sustainable reutilisation of materials, which otherwise would likely land up in landfills. Examples of some waste materials investigated for use in asphalt modification are crumb rubber from scrap tyres, different types of waste plastics, waste glass, waste cooking oil, waste engine oil, palm oil fuel ash, and others (Rahman et al.,

2020). Thus, from an environmental and economic point of view, the use of waste materials in the production of modified bitumen is an interesting alternative.

Population growth, coupled with urbanisation and a rise in the standard of living, has led to an explosion in the quantity of solid wastes generated globally. Two such highly visible polymeric solid wastes are waste tyres and plastics. There is a continuous increase in quantities of these wastes, creating an ever-growing and pervasive environmental problem. Sustainable and responsible management of waste tyres and plastics has been a growing issue plaguing many countries, including India. Cumulatively, since the 1950s till 2015, an estimated 8.3 billion metric tons of plastic waste was generated globally, of which 9% was recycled, 12% was incinerated, and 79% found its way to the landfills or was left unattended (University of Georgia, 2017). Waste/end-of-life tyres have also become a significant component of the waste stream, with global quantities estimated at 4 billion tons (Sathiskumar and Karthikeyan, 2019). Waste tyre disposal is a difficult task since landfill disposal has been banned in several countries (Martínez et al., 2013), and incineration leads to harmful emissions (dioxins, particulate matter, volatile organic compounds, polycyclic aromatic hydrocarbons) (Levendis et al., 1996; Mastral et al., 1999). Both plastics and tyres take innumerable years to degrade in landfills and thus create severe challenges regarding their management.

With recent research and developments in waste management technologies, various methods are being tried and explored to manage these wastes in an environmentally friendly and clean manner. Pyrolysis is one method that has gained significant interest as a sustainable and reliable technique for managing and energy valorisation of waste plastics and tyres. Pyrolysis essentially involves the thermo-chemical decomposition of polymer (tyre or plastic) materials in a low or nil oxygen environment at low (<400 °C), medium (400-600 °C), or high temperatures (>600 °C) (Scheirs and Kaminsky, 2006), causing

irreversible changes in the chemical composition. Pyrolysis of wastes generates liquid, solid, and gaseous products. The liquid product, also called pyrolytic oil (the vapour released in the process is condensed to obtain the pyrolytic oil), can be suitably refined and fractionated to have properties similar to fuel oil/gasoline. Such a fractionation makes these oils profitable in the market. The gases produced are combustible and thus mainly used to power the pyrolysis reactor, making its operation self-sufficient/economical.

The solid char is generated as a by-product in the plastic and tyre waste pyrolysis. Char is a carbonaceous, fine powdery material and has yet to find a continuous/appreciable level of application routes (Miandad et al., 2016; Sharuddin et al., 2016; Xu et al., 2020a). The importance of broadening the range of applications for pyrolytic char has been emphasised as critical to the commercial success of the pyrolysis process. The use of pyrolytic chars in asphalt binder modification is an emerging area of research. Positive results reported with other carbon-based asphalt additives (such as carbon black, carbon nanotubes), together with the possibility of using a carbonaceous by-product of the waste pyrolysis processes, motivated the present study on tyre pyrolytic char (TPC) and plastic pyrolytic char (PPC) modified asphalt binders and mixtures.

1.2 Problem Statement

Most of the previous research studies on asphalt modification by TPC pertained to evaluating the properties of modified binders only (Chaala et al., 1996; Chebil et al., 1996; Feng et al., 2016, 2021; Wang et al., 2019). The application of PPC in asphalt modification is quite new and the present study, to the best of author's knowledge, is the first one to explore its use in asphalt binder and mixtures. It is thus quite important to evaluate and compare the performance of asphalt binders and mixtures containing TPC and PPC at various dosages in asphalt binder modification. Understanding the changes in the performance of modified binders and mixtures with pyrolytic chars can be aided through

their physicochemical characterisation. From a chemical perspective, the existing literature is quite limited especially in terms of the nature of interactions between asphalt binders and pyrolytic chars. It therefore raises the need of a study involving assessment of the char properties, chemical and rheological properties of TPC and PPC-modified asphalts and their impact on the performance characteristics of the resulting asphalt mixtures. TPC and PPC originating from two different waste raw materials are expected to have variable effects on the physico-chemical and ageing properties of the resulting modified binders. A comparative evaluation is also required in terms of the ageing behaviour for asphalt binders modified with the two chars, which plays a vital role in the long-term performance. These gaps in the existing literature/knowledge create the need for an evaluation concerning the characterisation of the chars; chemical, ageing, and rheological properties of TPC and PPC-modified asphalts, and the effect on the performance characteristics of the resulting asphalt mixtures.

Under this perspective, this study evaluates the effect of TPC and PPC (by-products from waste tyre and plastic pyrolysis industries) on the rheological properties of asphalt binders, and the performance of bituminous concrete mixtures containing TPC and PPC modified asphalt binders. To fulfil the identified research gaps, the present study focused on a multi-faceted investigation considering: (a) characterisation of the two pyrolytic chars (TPC and PPC), (2) characterisation of the TPC and PPC-modified asphalt binders focusing on conventional, rheological, ageing, microscopic, and thermo-chemical tests, and (3) characterisation of asphalt mixtures fabricated with TPC and PPC-modified asphalt binders focusing on their design properties, and rutting, moisture damage, cracking, and fatigue performance. A total of nine modified binders and mixtures were studied with a control binder and four binders, each with TPC and PPC-modification levels of 5%, 10%, 15%, and 20%.

1.3 Research Objectives

The main aim of this study is to evaluate the characteristics of the tyre and plastic pyrolytic char (TPC and PPC) modified asphalt binders and asphalt mixtures. The specific objectives formulated for the study are:

1. Characterisation of materials used in the study (aggregates, asphalt binders, TPC, and PPC).
2. Evaluation of thermal storage stability of asphalt binders modified with TPC and PPC.
3. Physical and rheological characterisation of modified asphalt binder blends with different contents of TPC and PPC (0% (control), 5%, 10%, 15%, and 20% by weight of binder).
4. Evaluation of ageing characteristics of control and asphalt binders modified with TPC and PPC.
5. Determination of mixing and compaction temperatures (production temperatures) for control and asphalt binders modified with TPC and PPC.
6. Design and evaluation of bituminous concrete mixes with control and TPC and PPC modified asphalt binders.
7. Evaluation and comparison of the performance of asphalt mixes fabricated with control and TPC and PPC modified binders in terms of resistance against permanent deformation, moisture damage resistance, cracking resistance, and fatigue damage.

1.4 Organisation of the Thesis

The contents of the thesis are organised into nine chapters. **Chapter 1** provides a background to the research area, highlights the research problem and the motivation of

study, and lists the formulated objectives of the research work. **Chapter 2** discusses the review of literature on pyrolysis technology and the pyrolytic products, the use of pyrolytic chars in asphalt materials, and their effects on binder and mixture properties. The chapter ends with identifying research gaps that helped to formulate the aim and objectives for the present study. **Chapter 3** presents the selection of materials, their characterisation approaches, details of the preparation of modified binders and mixtures, experimental programme, and test procedures used to achieve the framed objectives of this study. **Chapter 4** is devoted to present the characterisation of materials used in this research. It also presents the physical and chemical characterisation results of the pyrolytic chars and asphalt binders used in the study. **Chapter 5** provides the results and discussion on thermal storage stability evaluation of TPC and PPC modified binders. **Chapter 6** reports the results and discussion on rheological characterisation of TPC and PPC modified binders, the results of ageing performance evaluation, and advanced rutting characterisation. The results of the determination of production temperatures for the control and modified binders are presented in **Chapter 7**. **Chapter 8** explains the mixture designs, followed by the presentation of results on the evaluation of performance characteristics of various asphalt mixtures in terms of rutting, moisture damage, cracking, and fatigue, and pavement structural analysis. Finally, **Chapter 9** summarises the study, presents the key findings and conclusions drawn from this research, and provides suggestions for future research.

Chapter 2

LITERATURE REVIEW

2.1 Introduction

This chapter presents a comprehensive review of literature on pyrolytic chars from different sources and their use for asphalt binder modification. The chapter begins with a condensed account of research works performed on carbonaceous materials in asphalt binder modification. The emergence of pyrolytic chars is then discussed. A brief background on pyrolysis technology and the pyrolysis products is also provided. The chapter then provides a state-of-the-art review in the field of pyrolytic char modified asphalt binders and identifies the path to the contribution of this study. The performance of pyrolytic char modified binders, ageing and chemical characterisation of the char-modified binders, and the effect of pyrolytic chars on the asphalt mixture properties are also reviewed. The chapter concludes with a presentation of the critical appraisal of the literature review identifying key research gaps that contributed to the formulation of objectives for this study.

2.2 Application of Carbonaceous Additives in Asphalt Binder Modification

Carbonaceous materials have long been used as asphalt additives because they are made of carbon and are considered inherently compatible with asphalt binder that is also a hydrocarbon (Abtahi et al., 2010; Zhao et al., 2014b). This expectation has motivated numerous studies since the 1960s to modify asphalt binders with carbon-based materials for improved performance. Carbon black (Alliotti, 1962; Rostler et al., 1977; Sasaki et al., 2003; Yamaguchi et al., 2005; Ahmedzade and Geckil, 2007; Apeagyei, 2011; Cong et al.,

2014), toner ink (Solaimanian et al., 1998), and coke dust (Taha et al., 1998) are some main carbon-based materials that have been used as asphalt additives/modifiers.

Carbon black is an industrial product used chiefly as a reinforcing agent in rubber tyres and colouring pigment for ink and paints. Chemically, it is nearly pure elementary carbon with minor amounts of hydrogen and oxygen and ash contents less than 1 percent. The particle size ranges from 0.005 to 0.5 μm. Carbon black is well known for improving natural and unsaturated synthetic rubbers; for example, it increases the performance life of tyres by a factor of up to 40. The carbon blacks form chemical bonds with the rubbers at active sites, which are produced by the formation of free radicals when the rubber is ruptured during mastication. The resulting network of rubber and carbon improves properties such as modulus, hardness, and resilience. Due to these properties, its use has also been attempted as an asphalt additive.

Alliotti (1962) discussed the rationale behind the use of carbon black and proposed that because of its predominant use as a reinforcing agent in rubber polymers, it might also show a beneficial influence as an additive to asphalt binders. One of the earliest studies on carbon black as an additive to bituminous binders was performed by Martin (1962) with pelletised rubber grade carbon blacks. It was reported that distributing 3% carbon black (by weight) had no discernible influence on the temperature susceptibility of the bituminous binder. It was challenging to use carbon black in asphalt reinforcement because a dispersion could not be achieved through conventional mixing protocols.

Rostler et al. (1977) is one of the important later works on carbon black reinforcement in asphalt. It was suggested that the discouraging results noted in Martin's work were due to poor dispersion, low contents of carbon black, and the addition of fluxing oil. The authors developed carbon black pellets consisting of high structure carbon black combined with a fluxing oil (similar to maltene fraction of asphalt binders). Maximum asphalt reinforcement

was obtained at 11-15% carbon black content by the combined weight of asphalt binder, carbon black, and oil. The 75:25 ratio of carbon black to oil was identified as suitable for practical applications. Pellet abrasion tests were performed on asphalt binder-carbon black-Ottawa sand mixtures to evaluate the impact resistance of the specimens. The results showed that carbon black functioned as an effective reinforcing agent for asphalt when adequately dispersed. The authors also reported seven field trials with the carbon black used as a micro-filler in asphalt mixtures. Observations during the trial operations indicated well dispersion of the carbon black, absence of undispersed pellet fragments, and no dust problem during the production of mixtures. Following this study, the pelletised form of carbon black was allotted the tradename 'Microfil', which was used in many of the later studies (Vallerga and Gridley, 1980; Yao and Monismith, 1986; Khosla, 1991). In general, the use of carbon black improved the high-temperature stiffness and resistance to permanent deformation of binders and mixtures (Vallerga and Gridley, 1980; Yao and Monismith, 1986; Button et al., 1987; Khosla, 1991), while it did not have much effect on fatigue and tensile properties of the mixtures (Yao and Monismith, 1986).

Sasaki et al. (2003) used 10% carbon black (CB) modified asphalt and compared the performance of the modified binder with the unmodified one. The base binder was an 80/100 pen grade (‘pen’ stands for penetration). The findings revealed that CB minimised rutting in hot conditions while also reducing cracking in cold environments. The properties of CB modified binder were found superior to the base binder under different ageing conditions (original (unaged), TFO-aged, PAV-aged, and UV-aged) [TFO: thin film oven; PAV: pressure ageing vessel; UV: ultraviolet ageing]. The efficiency of CB as an anti-weathering agent was noticed for asphalt materials due to its UV shielding (absorbent) effects, which is also widely recognised in the polymeric industry.

Yamaguchi et al. (2005) investigated the high and low temperature properties of asphalt binder modified with 10 and 20% CB. CB enhanced the elastic modulus, lowered the viscosity, and raised the binder high PG grade at high test temperatures. The addition of CB increased the modified asphalt's failure strain at low test temperatures. The researchers attributed the improved findings at low temperatures to the modified asphalt's lower coefficient of thermal expansion (CTE) than the original asphalt. The addition of 10% and 20% CB reduced the CTE values by 8% and 13%, respectively. CB was considered to be an excellent filler for improving asphalt characteristics at both high and low temperatures.

Ahmedzade and Geckil (2007) investigated the use of CB as a filler in asphalt mixtures and determined the mechanical characteristics of the mixtures by Marshall stability, indirect tensile stiffness modulus (ITSM), creep stiffness, and indirect tensile strength (ITS) tests. The control mixture was made with limestone aggregates as coarse and fine aggregates and a filler. In the second mixture type, limestone aggregates were coarse and fine but CB replaced the limestone filler by volume. Two asphalt binders (AC-5 and AC-10) were used in the study. Results showed that the mixtures with CB as filler showed higher stability, lower flow, higher ITSM (at 40 °C), higher creep stiffness, and higher ITS values than the control mixture. It was concluded that CB improved all mechanical properties of the asphalt mixtures resulting in improved performance.

Apeagyei (2011) evaluated the effects of carbon black as a potential anti-oxidant on the age-hardening of asphalt binders. The base binder was a PG 64-22. It was reported that carbon black could act as a primary anti-oxidant and a hydroperoxide decomposer. Compared to the control binder, the addition of carbon black to the asphalt reduced age-hardening by 24%. Carbon black's efficiency was ascribed to the presence of chemical groups such as phenols, carboxyphenols, lactones, and quinones on its structure. Improved resistance to ageing was also reported by Cong et al. (2014) with three grades of carbon

black used with a styrene-butadiene-styrene (SBS) triblock copolymer modified binder based on the findings of Fourier transform infrared (FTIR) spectroscopy.

Geckil et al. (2018) evaluated the CB modified binders prepared at multiple CB contents (5, 10, 15% by weight of binder) added to a PG 58-28 base binder. The temperature susceptibility of bitumen decreased, and the elastic characteristics increased with the addition of CB. The Superpave PG grades of control and CB modified binders at 5, 10, and 15% dosages were respectively determined as PG 58-28, PG 58-28, PG 64-28, and PG 70-22. Based on the low and high temperature results, 10% CB content was determined as the most suitable.

Toner manufacturers generate a massive amount of waste toner from printers and copiers. Some of the toner is also discarded as waste as it does not meet the quality requirements during manufacturing, while another significant quantity of spent and used toner is dumped in landfills for lack of a better utilisation approach (Solaimanian et al., 1998). Earlier, only carbon powder was used to produce toner. Nowadays, different polymers such as styrene acrylate copolymer and styrene-butadiene copolymer are also added with carbon powder to improve printing quality. Several studies have attempted to utilise this waste material as an asphalt modifier.

Khedaywi (2014) attempted to explore waste toner from copier machines and laser printers as a potential asphalt modifier. The waste toner refers to dry ink used in copiers of black colour and with a slight plastic odour. The waste toner was added to a neat 60/70 pen grade asphalt binder at five contents (0, 5, 10, 15, and 20% by volume of the asphalt cement). The basic properties of binder-toner blends were evaluated. Results showed that penetration and ductility decreased as the percentage of waste toner in the binder increased. Specific gravity, softening point, flash point, fire point, and viscosity increased with the waste toner content.

Yildirim et al. (2004) described the results of three demonstration projects in Texas where waste toner was used as an asphalt binder modifier. Non-magnetic toners were used at two locations, while a magnetic toner was used at the other. Different parameters were observed for each of these projects, including blending time, performance grading, storage stability, and mixing and compaction temperatures. Blending times were similar for the three projects, taking 60 to 90 min to get a homogeneous blend in all cases. Further, magnetic toners presented a better response at low temperatures in the neighbourhood of and below 10% toner levels. Brittleness of the binder, as defined by the m-value (from bending beam rheometer (BBR) tests), increased at low temperatures as the toner level increased. This indicated a low capacity of the binder to release the carried load, stepping up the low temperature cracking potential of the pavement. It was noted that toner-modified asphalt binder needs to be agitated before mixing with aggregates for adequate storage stability.

Solaimanian et al. (1998) investigated waste toners from different sources by blending them with asphalt cement at different ratios (0, 5, and 16%) and evaluated binder and mixture properties. It was shown that at least 2 h of stirring of the waste toner in asphalt at temperatures above the melting point of the waste toner is required to obtain a homogeneous blend. The results indicated that as the amount of waste toner in the blend increased, the stiffness and viscosity of the modified binder increased. The mixture analysis also indicated higher strength and stability for toner-modified asphalt concrete compared with unmodified mixtures. The toner-modified binder performed satisfactorily in areas where permanent deformation was of great concern. It was also reported that a PG 64-28 asphalt would grade as a PG 70-22 with 10% waste toner.

Taha et al. (1998) considered coke dust produced during calcination of hearth as an additive to asphalt binders. Physically, coke dust particles were black in appearance, of

very small size (much finer than 0.074 mm), and had a carbon content of over 90%. Concentrations used were 3, 5, 7, 12, and 18% by binder weight. Penetration values were reduced with increased coke dust percentage, and the effect was more pronounced for the softer base binder (AC-5). Considering the requirements of higher stiffness at high service temperatures and lower stiffness and low service temperatures, the best performance was obtained using 18% coke dust followed by 12% coke dust.

2.2.1 The emergence of pyrolytic chars for asphalt modification

The direction of research on carbonaceous additives diverged in the mid-1990s, and the first research studies on pyrolytic chars appeared (Lesueur et al., 1995; Chaala et al., 1996; Chebil et al., 1996; Park et al., 1997). The early studies utilised pyrolytic char from scrap tyre pyrolysis (also referred to as 'pyrolytic carbon black (CB_p)') as an economical substitute to commercial carbon black. Park et al. (1997) reported the cost of commercial carbon black as USD 1.6/kg compared to USD 0.4/kg for the pyrolytic carbon black. The use of biochar for asphalt modification was first reported by Chebil et al. (2000), where biochar was derived from the pyrolysis of softwood bark residue. However, the extensive interest in other modifiers such as recycled tyre rubber and various polymeric modifiers constrained further advancements on the use of pyrolytic chars as asphalt modifiers (Zhao et al., 2014b).

In recent years, there has been a renewed interest in pyrolytic char usage in asphalt (Zhao et al., 2014a, b; Feng et al., 2016, 2021; Kumar et al., 2018; Li et al., 2018; Wang et al., 2019; Dong et al., 2020). The recently regained interest in the use of pyrolytic chars is likely due to developments in industrial-scale pyrolysis technology, currently being widely used for the treatment and management of vast volumes of waste materials (such as scrap tyres and plastics) produced globally. Over the past two to three decades, numerous industrial/commercial scale pyrolysis plants for end-of-life tyres and plastic wastes have

been installed worldwide and in India. Recent studies have highlighted the necessity to expand the application avenues of pyrolytic char in order to make the pyrolysis process commercially successful, and their use in asphalt modification offers the potential for their bulk and promising utilisation.

The following section introduces pyrolysis technology and further discusses the motivation to use waste tyre and waste plastic pyrolytic chars for asphalt modification.

2.3 Pyrolysis Technology

2.3.1 Overview of pyrolysis process and products

Etymologically, the word 'pyrolysis' originates from two Greek words: '*pýr*' (meaning 'fire') and '*lýsis*' (meaning 'splitting' or 'cracking') (Dahiya, 2014). Pyrolysis refers to thermochemical cracking (or decomposition) of a feedstock at high temperatures under a low oxygen environment. With recent technological advancements in pyrolysis techniques, it is widely used to convert solid materials (such as biomass, waste tyres, waste plastics, or their combinations, *etc*.) into solid carbonaceous char and fuel (in terms of condensable liquid oil and gases). Nowadays, pyrolysis is receiving widespread consideration for its flexibility in producing these three components (solid char, liquid oil, and gases) in different desired proportions by varying the reaction variables such as treatment temperature, residence time, and heating rate (Czajczyńska et al., 2017). Consequently, pyrolysis processes can be categorised as slow, fast, catalytic fast, intermediate, or vacuum type (Czajczyńska et al., 2017). Pyrolysis is quite popular in the management of different types of domestic and industrial wastes such as wood waste, agricultural residues, forestry residues, paper waste, scrap tyres, waste plastics, yard waste, food waste, textile waste (Moraes et al., 2012; Chen et al., 2014; Czajczyńska et al., 2017). Pyrolysis plants can be developed at more flexible scales than incineration plants, and pyrolysis also has low

emission of air pollutants (*e.g.* polybrominated diphenyl ethers) compared to combustion (Wyrzykowska-Ceradini et al., 2011; Chen et al., 2014).

Each year, the world generates about 1.4 billion scrap (or end-of-life) tyres, with an estimated 4 billion currently lying in landfills and stockpiles (Martínez et al., 2013). As of 2015, about 6.3 billion tonnes of plastic waste have accumulated globally, 79% of which lies dumped in the open or in landfills (Geyer et al., 2017). Both wastes have long-lasting environmental concerns and take several decades for complete degradation. Consequently, there has been a significant drive toward establishing sustainable solutions for managing post-consumer tyre and plastic waste streams. In this direction, pyrolysis technology has garnered broad scientific interest to reduce waste volume while allowing for energy valorisation and overcoming the challenges/concerns associated with the disposal of waste tyres and plastics (Martínez et al., 2013; Wijesekara et al., 2021). Although pyrolysis is an ancient method that has been used to make vegetable charcoal since the Bronze Age, the first advancements for waste tyre pyrolysis began in the 1970s with the first oil crisis (Martínez, 2021). The main advantage of pyrolysis is its capacity to deal with wastes that are difficult to recycle, as the waste feedstocks can be turned into value-added fuels, chemicals, and monomers (Martínez et al., 2013; Hu et al., 2021). Recovering valuable hydrocarbons from discarded tyres for energy and chemical feedstocks would reduce reliance on fossil fuels, hence reducing the risks of diminishing fossil fuel reserves and climate change (Quek and Balasubramanian, 2013).

Figure 2.1 shows a typical industrial scale tyre pyrolysis setup. A typical tyre pyrolysis system consists of a grinder, dryer, heating source, reactor, cyclone, and condenser. Before being discharged into the pyrolysis reactor, the waste tyre goes through a series of pre-treatments, including drying and grinding. N_2 gas is purged into the reactor to remove O_2 and maintain oxygen-free conditions for the pyrolysis reactions. The reaction mixture is

passed through a cyclone at the end of the reaction to collect the char, and the remaining reaction mixture is condensed to separate condensates from non-condensable gases. After that, the condensates are collected and turned into tyre pyrolytic oil. The gases can be collected or recycled to generate heat for the pyrolysis process (Hu et al., 2021).

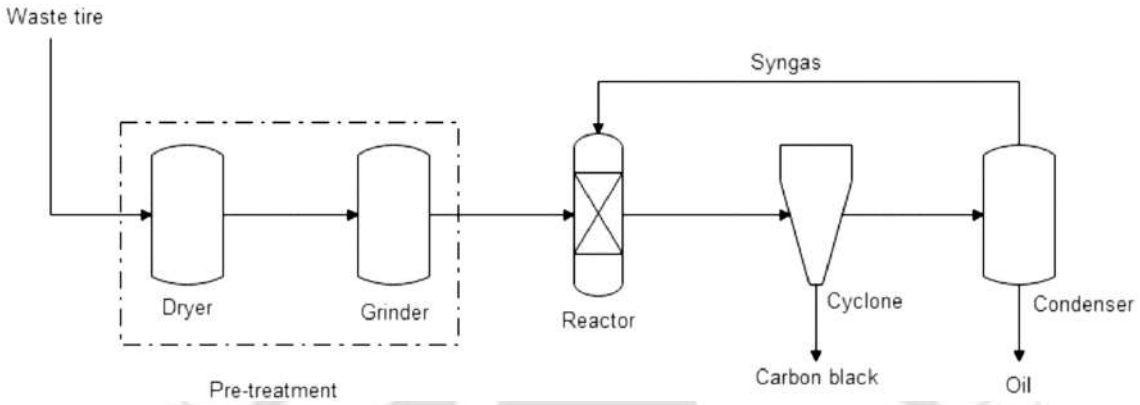

Figure 2.1 Schematic diagram of tyre pyrolysis setup (Hu et al., 2021)

[Reprinted by permission from Springer Nature Customer Service Centre GmbH: Springer Nature, Journal of Material Cycles and Waste Management, Valorization of waste tire by pyrolysis and hydrothermal liquefaction: a mini-review, Hu, Y., Attia, M., Tsabet, E., Mohaddespour, A., Munir, M. T., & Farag, S. Copyright (2021).]

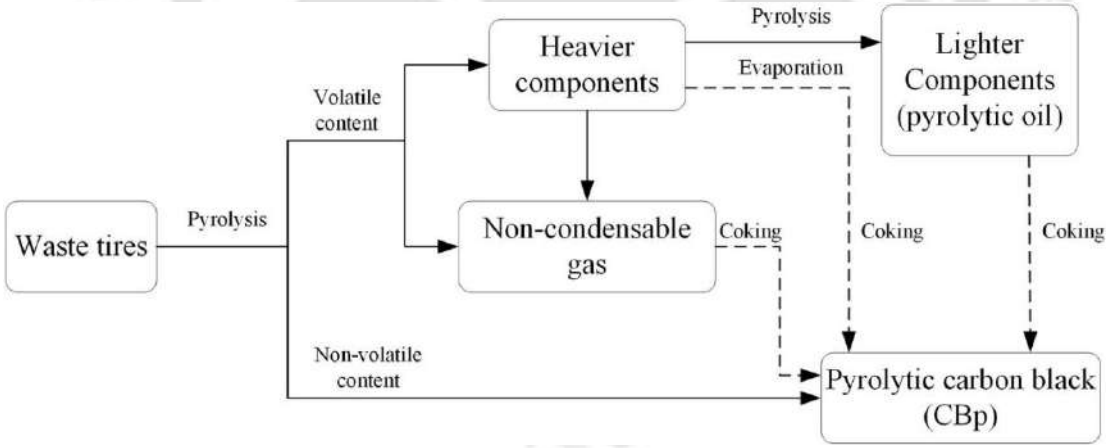

Figure 2.2 Schematic diagram of tyre pyrolysis showing char formation processes (Xu et al., 2020a)

[Reprinted from Science of the Total Environment, Vol. 742, Xu, J., Yu, J., Xu, J., Sun, C., He, W., Huang, J., & Li, G., High-value utilization of waste tires: A review with focus on modified carbon black from pyrolysis, Page 9, Copyright (2020), with permission from Elsevier.]

The main tyre pyrolysis products are (by weight) 40-60% liquid pyrolytic oil, 30-40% solid char, and 5-20% gases (Karthikeyan et al., 2012). Factors affecting product

distribution and properties are the type of the reactor, pyrolysis method, temperature, pyrolysis time, tyre particle size, heating rate, and pressure (Xu et al., 2020a). Tyre pyrolytic char (shown as pyrolytic carbon black in Figure 2.2) is made up of carbon black and inorganic fillers used in tyre production and coke material created during the pyrolysis process (Xu et al., 2020a). Figure 2.2 shows the processes leading to char formation due to non-volatile content and the coking of volatile content produced during the tyre pyrolysis.

The typical process for plastic waste pyrolysis is shown in Figure 2.3, which is quite similar to that for waste tyre pyrolysis. The dried and ground plastic waste is fed into the reactor operating at a heating rate of about 0.1–1 °C/s. The liquid pyrolytic oil is obtained after condensation of the pyrolysis yield. In some cases, the char is also reused as a heat insulator to reduce heat transfer to the plastic (Maqsood et al., 2021), as indicated in Figure 2.3. After undergoing up-gradation and fractionation procedures, the liquid oil can be used in multiple applications such as boilers, furnaces, and turbines (Sharuddin et al., 2016). Gases produced are usually consumed to fulfil the energy needs of the pyrolysis reactor. In plastic waste pyrolysis, char formation is attributed to non-volatilisation of the plastic and re-condensation/recombination of pyrolytic cracking products (Bernardo et al., 2012). This char is primarily made up of a carbon-rich matrix containing inorganic compounds found in raw plastic trash as well as condensed by-products created during pyrolysis that are distributed throughout the solid porous structure (Bernardo et al., 2012). Char formation also involves side-chain reactions that maintain C-C bonds, remove small molecules such as H_2O, CO_2, or hydrogen, and contain residual groups from the original polymer (Moldoveanu, 2005). Char formation is also attributed to secondary repolymerisation reactions among the polymer-derived products (Gao, 2010; Lopez et al., 2011) and may include coke and undegraded polymer (Buekens and Huang, 1998).

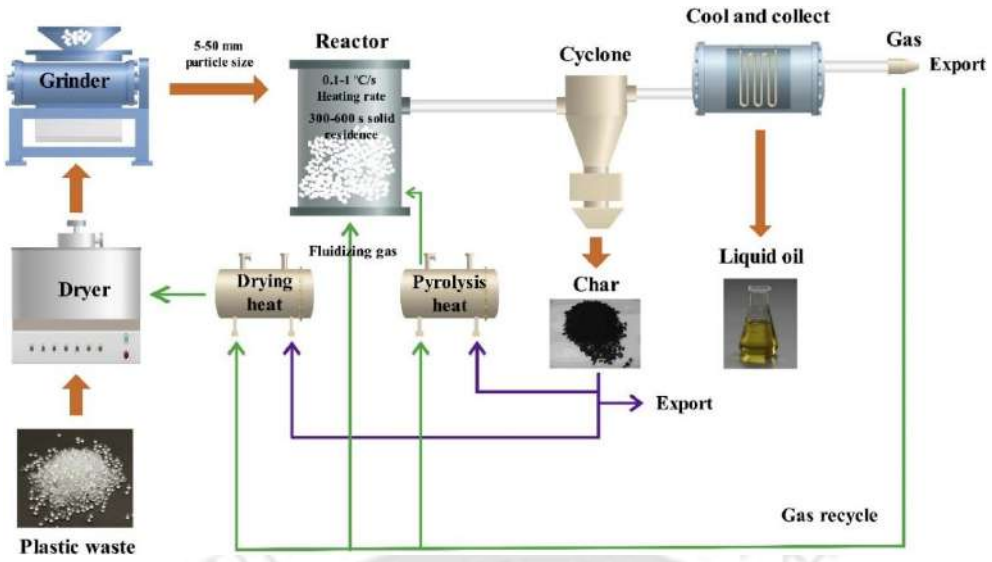

Figure 2.3 Schematic diagram of waste plastic pyrolysis process (Maqsood et al., 2021) [Reprinted from Journal of Analytical and Applied Pyrolysis, Vol. 159, Maqsood, T., Dai, J., Zhang, Y., Guang, M., & Li, B., Pyrolysis of plastic species: a review of resources and products, Page 4, Copyright (2021), with permission from Elsevier.]

Pyrolysis has several advantages over other traditional waste plastic handling methods. Most waste plastics are downcycled during recycling, and recycled plastics are utilised to make lower-quality and application-specific items. This is due to the fact that as plastic is recycled, it loses qualities such as clarity, strength, and flexibility. On the other hand, pyrolysis transforms trashed plastics into valuable resources, including monomers, fuel, and other materials. Second, the cost of sorting, washing, and blending waste plastics before they are mechanically recycled is completely eliminated in the pyrolysis approach. Mechanical recycling also entails melting and remoulding waste polymers into new products. This means that only wastes made of thermoplastic materials are acceptable for this process; therefore, thermoset polymers will persist in landfills and dumpsites due to their inability to be remoulded. Both thermoset and thermoplastic wastes, on the other hand, can be employed as feedstocks in pyrolysis processes. Finally, depending on the feedstock composition, process environment (temperature, heating rate, reaction gas), and presence of a catalyst (catalytic pyrolysis) or lack of catalyst, pyrolysis allows for a wide range of product yield distributions (Eze et al., 2021). The work of researchers (Martínez et al.,

2013; Sharuddin et al., 2016; Eze et al., 2021; Hu et al., 2021) could be referred for further details on pyrolysis technologies, process variables, and chemical engineering aspects of tyre and plastic waste pyrolysis.

As the pyrolytic oil is of a higher commercial value in tyre and plastic pyrolysis, the reaction parameters are mainly aimed at maximising oil production. The chars generated during pyrolysis are considered a by-product. Currently, there is a lack of feasible and efficient valorisation applications for the chars. Tyres are made of 60-65 wt% rubber (both natural and synthetic rubbers are used), 25-35 wt% carbon black, and small amounts of fillers and accelerators (Martínez et al., 2013). Carbon black is added to provide resistance against abrasion and to strengthen the tyre rubber. Efforts have been made to recover the carbon black initially used in the tyre manufacturing from the tyre pyrolysis char but posed several challenges. The highest grades of carbon black used in tyre tread mostly get lost with time due to wearing and abrasion of the tyre. The carbon black present in the char has a lower reinforcing value compared to the high-grade virgin carbon black. Further, the extraction of carbon black from the char is also difficult and uneconomical. Therefore, it has been challenging to scale up the laboratory studies on char utilisation into a commercial manufacturing process (Fader et al., 1997). The plastic pyrolysis char has limited high-value application opportunities (Miandad et al., 2016; Sharuddin et al., 2016). To maximise the circularity of pyrolysis technology as a sustainable waste treatment method, it is necessary to find large-scale application routes for pyrolytic chars. The importance of broadening the range of applications for pyrolytic char has been emphasised as critical to the commercial success of the pyrolysis process (Xu et al., 2020a).

2.3.2 Use of pyrolysis products in asphalt binders

Table 2.1 presents the summary of pyrolysis product, pyrolyzed material, pyrolysis type and pyrolysis conditions reported by the researchers. Only those studies are reviewed

wherein the pyrolysis product was used in asphalt binder. The most commonly used pyrolysis temperatures are 450-500 °C, and the most commonly used pyrolysis types are fast and vacuum pyrolysis.

Table 2.1 Summary of pyrolyzed materials, products, pyrolysis type and conditions

Reference	Pyrolyzed material	Pyrolytic product used	Pyrolysis type	Pyrolysis conditions
Chebil et al. (2000)	Softwood bark residue	Char	Vacuum	Temperature = 500 °C Pressure = 5 kPa Biomass quantity in one batch = 1.4 kg Pyrolysis yield = 23 wt% char, 34 wt% oil, 34 wt% aqueous phase, 9 wt% gases.
Wang et al. (2019)	Scrap tyres	Char	Vacuum	Temperature = 480-520 °C Pressure = 20 kPa
Zhang et al. (2018a)	Waste wood	Char	Fast	Temperature = 500-650 °C Heating rate = 104-105 °C/s
Kumar et al. (2018)	*Mesua ferrea* seed cover waste	Char	Slow	Temperature = 450 °C Heating rate = 40 °C/min
Zhang et al. (2018a)	Waste wood	Oil	Fast	Heating temperature: 500-650 °C Heating rate: 104-105 °C/s Residence time: 2 s
Yousefi et al. (2000)	Waste tyre	Oil	Vacuum	Heating temperature: 550 °C Pressure: 10 kPa (vacuum pyrolysis)
Yang et al. (2013)	Waste wood		Fast	Heating temperature: 500 °C
Girimath and Singh (2019)	Waste wood	Oil	Fast	Not reported
Zhang et al. (2019)	Sawdust	Oil	Fast	Not reported
Bao et al. (2020)	Waste wood	Oil	Not reported	Not reported
Lei et al. (2018)	Waste corn stover	Oil	Fast	Not reported
Yang and You (2015)	Waste wood	Oil	Fast	Not reported
Yang et al. (2014)	Waste wood	Oil	Fast	Not reported

Many studies have not reported the details on pyrolysis conditions, likely due to the details being proprietary. Pyrolytic oil and char are the main products that have been attempted for use in asphalt binders. Further, the most commonly used waste biomass materials whose pyrolytic products have been used in asphalt binders are waste wood, seed shell/cover, and sawdust, while scrap tyre is the commonly used industrial waste.

2.3.3 Motivation to use pyrolytic chars in asphalt binders

Asphalt binder (or bitumen) is amongst the earliest known construction materials known to the mankind (Krishnan and Rajagopal, 2003). It is the material of choice for the construction of highways, airfield runways, driveways that serve as the lifeblood of modern society for transportation of both passengers and goods. Out of the total paved roads, asphalt pavements (or flexible pavements) have a share of about 98 percent in India (Kumar and Gupta, 2010). In recent times, there has been a continuous rise in traffic volume (especially heavy trucks), axle loads, tyre pressures, and extreme fluctuations in pavement temperatures (Gogoi et al., 2016; Julaganti et al., 2019). These factors have led to the premature onset of pavement distresses in many projects. To mitigate the impact of these factors, asphalt binders are typically modified to enhance the asphalt pavement resistance against major distresses (rutting, fatigue, thermal cracking, and ageing) and improve the engineering performance of the resulting asphalt mixtures. Some of the commonly used asphalt modifiers include crumb rubber, styrene-butadiene-styrene (SBS), ethylene-vinyl acetate (EVA), and styrene-butadiene rubber (SBR) (Yildirim, 2007).

As discussed earlier, pyrolysis produces solid char, liquid oil, and gases. Several factors motivate the use of pyrolytic char as a modifier in asphalt binders. Carbonaceous additives have long been used as modifiers in asphalt binders with encouraging results (Alliotti, 1962; Zhao et al., 2014b). Some examples of carbonaceous asphalt modifiers include commercial carbon black, waste toner ink, activated carbon, and coke dust. Further, biomass pyrolysis is primarily aimed at generating fuels through post-processing and up-gradation of oil, and the char produced is generally considered a by-product of the process (Zhao et al., 2014b; Kumar et al., 2018; Zhang et al., 2018a).

As noted earlier, the desire for the asphalt pavements to possess improved resistance against principal distresses (rutting, fatigue, thermal cracking) and higher durability have

actively motivated the modification of asphalt binders. During the years 1995-1997, the early research studies on the use of tyre char as an asphalt modifier were published (Lesueur et al., 1995; Darmstadt et al., 1996; Chaala et al., 1996; Park et al., 1997). In recent years, there has been increasing interest in using pyrolytic chars (Feng et al., 2016; Zhang et al., 2018a; Wang et al., 2019; Jerin et al., 2020). Therefore, the use of pyrolytic chars in asphalt binder modification is an emerging area of research and requires in-depth studies to assess the performance of char modified asphalt binders and mixtures.

2.4 Application of Pyrolytic Chars in Asphalt Binder Modification

Table 2.2 summarises the studies by various researchers on the effect of pyrolytic chars on binder properties and also shows the critical findings of each study. Table 2.3 summarises the literature on the effect of pyrolytic chars on binder chemical properties. Table 2.4 shows the findings on the effect of pyrolytic char on the properties of asphalt mixtures. The literature review shows that two categories of pyrolytic chars have been utilised for asphalt binder modification: (1) biochars from the pyrolysis of various biomasses, and (2) char from the pyrolysis of scrap tyres (also referred to as 'pyrolytic carbon black (CB_p)' in several studies).

Table 2.2 Summarised review of studies on use of pyrolytic chars in asphalt binder modification: binder characterisation

Reference	Pyrolytic char type	Experimental variables	Summary of findings
Chebil et al. (2000)	Charcoal (biochar) from vacuum pyrolysis of softwood bark residue	Two base binder sources (80/100 pen and 150/200 pen); Char size: passing 45 µm; Char contents: 5-25%	- Biochar reduced penetration, increased softening point values up to 25% char content. - Considering Fraass breaking point, the optimum content was 5-10%. - Master curves indicated higher G′ and G″ for modified binders at low frequency regions while having a small effect at high frequency regions. - G*/sin δ increased with an increase in biochar content. - Thermal susceptibility of the modified binders reduced compared to the unmodified binder.
Zhao et al. (2014a)	Biochar from slow pyrolysis of switchgrass	Base binder: PG 64-22; Char size: passing 75 µm; Char contents: 5 & 10%; Other additives: carbon black & carbon fibre	- Addition of biochar caused increase in G* at 64 °C while it had very little effect on G* measured at –10 °C, compared to the base binder. - Biochar showed the highest stiffening effect at 64 °C among other modifiers. - Biochar modified binder had reduced temperature susceptibility.
Zhao et al. (2014b)	Biochar from pyrolysis of switchgrass	Base binder: PG 64-22; Pyrolysis type: slow & fast; Pyrolysis temperature: 400 and 500 °C; Char contents: 5-20%; Char sizes: 75-150 µm and <75 µm	- Biochar modified binder had reduced temperature susceptibility. - Significant improvements observed in rutting parameter (G*/sin δ). - Up to 10% dosage, improvement in ageing resistance was also noted. - Fatigue properties (G*sin δ and G′/(η′/G′)) remained unchanged up to 10% dosage and deteriorated at higher dosages. - Slow pyrolysis, lower pyrolysis temperature, and finer particle size produced more effective modification.
Celoglu et al. (2016)	Biochar from pyrolysis of walnut crust and apricot seed shells	Base binder: 160/220 pen Char contents: 5, 10, 15%	- Addition of biochars increased the binder stiffness from reduced penetration, increased viscosity, softening point, G*/sin δ, and G* master curves. - Effect of biochars on binder phase angle (δ) was negligible. - Biochar from walnut had a higher effect on binder stiffness.
Zhang et al. (2018a)	Biochar from pyrolysis of waste wood resources	Base binder: PG 58-28; Char contents: 2, 4, 8%; Char sizes: 75-150 µm & <75 µm; Other additive: graphite (<75 µm size and 4% dosage)	- Biochar modified binders with smaller particles had higher viscosity, rutting resistance (G*/sin δ), ageing resistance, and low-temperature cracking resistance than those with larger particles. - All modified binders had BBR stiffness < 300 MPa at –18 °C. The BBR m-values decreased at higher biochar contents (4% and 8%).

Table 2.2 (continued)			
Kumar et al. (2018)	Biochar from pyrolysis of *Mesua ferrea* seed cover waste	Base binders: VG 30 (two sources); Char contents: 5-20%; Char size: <150 µm	- Increase in biochar dosage reduced binder viscosity, improved rutting resistance measured through G*/sin δ and MSCR J_{nr}, and improved binder ageing resistance. - Stress sensitivity of binders reduced with an increase in biochar content, as measured by J_{nr} difference parameter at 0.1 and 3.2 kPa stress levels.
Dong et al. (2020)	Biochar (source not reported)	Base binder: Pen 70; Char contents: 5-15%; Char size: <150 µm	- Anti-ageing performance of biochar modified asphalt binder was superior than that of base asphalt binder, according to ageing index and viscosity ratio analysis. - Because of its porous structure, biochar adsorbs asphalt binder components, and alleviates oxidative ageing of asphalt binder. - Biochar modified binder's low temperature performance based on BBR decreased but the reduction was not significant.
Gan and Zhang (2021)	Biochar from pyrolysis of crop straw	Base binder: Pen 70; Char contents: 2-12%; Char size: <75 µm; Other additive: commercial charcoal (CC) (<75 µm size)	- With increase in biochar or CC content, penetration and ductility decreased, and softening point increased. - The mixing and compaction temperatures of biochar modified asphalt (6% biochar content) were slightly higher than those for base asphalt.
Ma et al. (2022)	Biochar from pyrolysis of straw stalk	Base binder: Pen 70; Char contents: 5-15%; Char size: <150 µm	- High-temperature properties of the binders improved with the incorporation of biochar (increase in G* and G*/sin δ and decrease in δ). - Fibrous and porous structure of biochar caused an improved interaction between binder & biochar leading to improved binder properties. - Biochar reduced the low-temperature cracking performance of the binder.
Lesueur et al. (1995)	Char from pyrolysis of scrap tyres	Base binder: AC-10; Styrelf MAC-10 (SB copolymer modified); Char contents: 20 and 30%; Char size: <75 µm; Other additives: Mineral fillers	- The increase caused by 20% char in the base AC-10 was comparable to increases caused by 30% mineral fillers and polymer modification. - G* sin δ increased with an increase in char dosage. - BBR stiffness increased and m-value decreased with an increase in char dosage. The stiffening effect of the char was compensated by polymer modification.
Chaala et al. (1996)	Char from vacuum pyrolysis of scrap tyres	Base binder: 150/200 pen; Char contents: 5-30%; Char size: <150 µm	- Addition of char led to reduced penetration, and increased softening point, viscosity, G′ and G″, and ZSV.

Table 2.2 (continued)			
Chebil et al. (1996)	Char from vacuum pyrolysis of scrap tyres	Base binders: 80/100 and 150/200 pen; Char contents: 5-30%; Char size: <45 µm; Other additive: commercial carbon black	- Both modifiers reduced penetration, increased softening point, G′ and G″, G*/sin δ, and complex viscosity. -Differences in G′ and G″ master curves were less noticeable at high frequencies. - Lowest Fraass point was observed at 10% dosage. - Overall, 5-15% dosages were recommended.
Feng et al. (2016)	Char from vacuum pyrolysis of scrap tyres	Base binders: SK 70# and SK 90#; Char contents: 5, 10, 15%; Char sizes: 25 µm for PCB-1, 150 µm for PCB-2; Other additive: commercial carbon black	- Both PCB improved thermal and photo-oxidative ageing performance of binders. - Storage stability criterion was met up to 10% dosage and not at the higher dosage. - High-temperature properties (G* and G*/sin δ) enhanced by both chars with more positive role by PCB-2.
Li et al. (2018)	Char from pyrolysis of scrap tyres	Base binders: GF-70; Char content: 15%; Char size: 50-5000 nm	- Char modified asphalt showed a higher G* over the temperature range of –10 to 85 °C than the base asphalt. - Char modification showed poor performance in terms of BBR stiffness and m-value, which was improved by the addition of an aromatic hydrocarbon oil (AHO) at dosages of 0.3, 0.6, 0.9, and 1.2%.
Wang et al. (2019)	Char from vacuum pyrolysis of scrap tyres	Base binders: SH-70; Char content: 3-18%	- Addition of char led to an increase in the softening point and viscosity and a decrease in the penetration and ductility. - Char modified binders had poor storage stability. - Modified binders had higher G* and decreased δ. - MSCR tests showed a lower non-recoverable compliance (J_{nr}) and limited improvements in recovery, indicating better rutting performance with char. - Based on a rheological index (ratio of J_{nr}), ageing resistance of char modified binders enhanced with an increase in char dosage.
Feng et al. (2021)	Char from vacuum pyrolysis of scrap tyres	Base binders: SK 70#; Char contents: 5, 10, 15%; Char types: normal and pelletised	- Pelletised char particles had higher size and smoother surface than normal char particles. - Both char types improved the high temperature binder properties but worsened the low-temperature BBR properties. - Binders with pelletised char performed better in high temperature tests.

Table 2.3 Summarised review of studies on use of pyrolytic chars in asphalt binder modification: chemical characterisation of binders

Reference	Pyrolytic char type	Experimental variables	Summary of findings
Chebil et al. (2000)	Charcoal (biochar) from vacuum pyrolysis of softwood bark residue	Char size: passing 45 µm; Char contents: 5-25%	- ESCA spectroscopy showed that biochar particles were covered with asphaltenes from the bitumen during the blending.
Dong et al. (2020)	Biochar (source not reported)	Base binder: Pen 70; Char contents: 5-15%; Char size: <150 µm	- Main components of biochar were aromatic rings, alkanes and hydroxyl groups. - FTIR spectrum of biochar modified binder was similar to that of base binder. - The conclusion made was that biochar in modified asphalt binder was mainly blended physically with the asphalt binder.
Ma et al. (2022)	Biochar from pyrolysis of straw stalk	Base binder: Pen 70; Char contents: 5-15%; Char size: <150 µm	- Biochar modified asphalts showed a similar position of FTIR characteristic peaks as observed for base binder, indicating similar molecular structure of the two binder types. - SEM images showed micro-network structure of biochar in the modified binder.
Darmstadt et al. (1995)	Char from pyrolysis of scrap tyres	Base binder: 150/200 pen; Char content: 30%	- ESCA spectroscopy showed that char particles strongly adsorbed fraction of bitumen compounds. The char particles were covered with a 2 nm layer of asphaltenes. - Such strong adsorption was believed to have influence on the rheological properties of char modified bitumen.
Chaala et al. (1996)	Char from vacuum pyrolysis of scrap tyres	Base binder: 150/200 pen; Char contents: 5-30%; Char size: <150 µm	- ESCA and UV spectroscopy showed that the effect of char on asphalt was different from an inactive filler, and char had both physical and chemical interactions with asphalt.

Table 2.4 Summarised review of studies on use of pyrolytic chars in asphalt binder modification: mixture characterisation

Reference	Pyrolytic char type	Experimental variables	Summary of findings
Chebil et al. (2000)	Charcoal (biochar) from vacuum pyrolysis of softwood bark residue	Char size: passing 45 µm; Char content: 5% by wt. of binder	- Biochar modification resulted in an improvement in the mix rutting resistance, improved moisture-damage resistance, and better cohesive properties. - Low temperature mix performance was not sensitive to the biochar content.
Zhao et al. (2014a)	Biochar from slow pyrolysis of switchgrass	Char size: passing 75 µm; Char contents: 5 & 10%; Other additives: carbon black & carbon fibre; 9.5 mm NMAS aggregate gradation	- Biochar dosage increased the resilient modulus of the mixture up to 10% and also reduced the rut depth, indicating superior rutting resistance. - Biochar mixtures had the highest TSR, showing higher potential of improving moisture resistance than carbon black and carbon fibres. - Biochar increased the SCB J-integral value, improving cracking resistance of the mixture.
Sanchez et al. (2020)	Biochar from microwave pyrolysis of spruce sawdust	Base binder: PG 58-28; Char contents: 4, 8, 12%; Char size: <75 µm; 12.5 mm NMAS gradation with limestone aggregates	- Heated biochar was directly added to heated aggregates, then the binder was introduced to fabricate the asphalt mix specimens. - TSR increased with the addition of the biochar content, but it showed peak at 8% biochar content. - 12% biochar mixtures showed mix properties similar to the control mix.
Park et al. (1997)	Char from pyrolysis of scrap tyres	Base binder: AC-10 and AC-20; Char contents: 5-20%; Char size: <75 µm; 12.5 mm NMAS gradation with limestone and slag aggregates	- An increase in char content led to a higher Marshall stability, high shear resistance (from gyratory compaction), higher resilient modulus, higher stripping inflection point, and higher tensile strength (at 5 °C) than mixtures with commercial carbon black. - The 10% char content was the best considering mixture properties for both aggregate types and base asphalt binders.
Li et al. (2018)	Char from pyrolysis of scrap tyres	Base binders: GF-70; Binder: Composite with 15% char and 1.2% AHO; Char size: 50-5000 nm; 13 and 20 mm NMAS mixtures	- The rutting and low-temperature performance of mixtures were improved with the composite binder with aromatic hydrocarbon oil (AHO). - Decrease in retained Marshall stability (RMS) and TSR of the modified mixture was noted after freeze-thaw conditioning. - RMS and TSR of the modified mixture were higher than the standard requirements of 80% and 75%, respectively.
Jerin et al. (2020)	Char from pyrolysis of scrap tyres	Base binders: 60/70 pen grade; Char size: <75 µm; Char contents: 5, 10, 15%	- Highest Marshall stability found at 5% char dosage, thereafter the stability decreased at 10% and 15% dosages. - Flow values also peaked at 5% char dosage.

The detailed state-of-the-art review on pyrolytic char modified asphalt binders is presented in the subsections that follow. This literature review-based discussion is organised into five themes, each of which focuses on a specific aspect of pyrolytic char modification.

2.4.1 Theme-1: Pyrolytic char size and blending parameters

Pyrolytic char particles smaller than 150 µm and 75 µm have been commonly used for asphalt modification. In some cases, grinding and sieving of the chars was found necessary to bring them to the desired size prior to blending with the asphalt binder (Chaala et al., 1996; Chebil et al., 2000; Zhao et al., 2014b; Gan and Zhang, 2021). A smaller size facilitates homogeneous and uniform blending of the char particles in the base asphalt binder. Particle size also plays an essential role in an accurate/true rheological characterisation of the modified binder through a dynamic shear rheometer (DSR). ASTM D7175 (2015) states that the thickness of particulate material in the modified binder should be smaller than one-fourth of the thickness of the test specimen. Hence, for a gap of 1000 µm (1 mm) between the bottom and top plates of the DSR, particles with dimensions less than 250 µm are to be used.

Uniform dispersion of pyrolytic char during asphalt binder modification is one key factor in achieving the desired performance. Table 2.5 summarises the blending parameters (temperature, rpm, time) and dosages and mixing equipment used by researchers to prepare pyrolytic char modified asphalt binders. The most commonly used approach utilises high shear mixing. A high shear mixer mainly consists of a rotor and stator assembly that allows uniform dispersion of a modifier through high centrifugal forces that force the binder to exit from the space between rotor and stator. The rotational speed (rpm) has been reported in the range of 1000-4000 rpm, whereas blending time varied from 13 to 60 min. It is also recommended in the studies to dry the char at about 110-120 °C to ensure there is no

moisture prior to blending (Chebil et al., 2000). The maximum dosage of char is generally limited to about 20-30% from the considerations of mix workability, viscosity, and stability.

Table 2.5 Summary of dosages and blending parameters

Reference	Pyrolytic product used	Size (µm)	Dosages (% by wt of binder)	Blending equipment	Blending temperature (°C)	Blending shear rate (rpm)	Blending time (min)
Chebil et al. (2000)	Biochar	<45	5-30	NR	90-100	NR	13
Celoglu et al. (2016)	Biochar	<75	5, 10, 15	Four blade paddle mixer	180	1000	60
Zhang et al. (2018a)	Biochar	75-150; <75	2, 4, 8	HSM	120	NR	60
Dong et al. (2020)	Biochar	<150 mesh (89 µm)	5-15%	HSM	145	NR	45
Gan and Zhang (2021)	Biochar	<75	2-12%	HSM	150-160	NR	30
Ma et al. (2022)	Biochar	<150 mesh (89 µm)	5-15	HSM	150-160	5000	60
Wang et al. (2019)	Tyre char	<45	3-18	HSM	150	2000	60
Feng et al. (2016)	Tyre char	PCB-1: 25 µm; PCB-2: 150 µm	5-15	HSM	150	2500	60
Li et al. (2018)	Tyre char	50-5000 nm	15	HSM	155	4000	40
Feng et al. (2019)	Tyre char	NR	5-15	HSM	130	4000	60

Abbreviations:
HSM: High shear mixing
NR: Not reported

2.4.2 Theme-2: Conventional and rheological binder properties

Most existing studies/literature on the use of pyrolytic chars in asphalt modification have focused and mainly reported the results of conventional and rheological properties of the modified binders. The following paragraphs provide the common characteristics of the findings from the studies.

The conventional properties of asphalt binders include penetration, softening point, viscosity, and ductility. The penetration, softening point, and viscosity tests evaluate the asphalt binder consistency. Ductility indicates the flexibility and the ability of the asphalt binder to undergo tensile deformation. With the addition of pyrolytic chars, the penetration value and ductility decreased, while the softening point and viscosity increased (Chaala et al., 1996; Chebil et al., 1996, 2000; Celoglu et al., 2016; Feng et al., 2016, 2021; Li et al., 2018; Zhang et al., 2018a; Wang et al., 2019; Dong et al., 2020; Jerin et al., 2020; Gan and Zhang, 2021; Ma et al., 2022).

Based on viscosity determined at two or more elevated temperatures (temperatures greater than 100 °C), some studies reported the mixing and compaction temperatures (collectively also called production temperatures) of the pyrolytic char modified binders. The production temperatures were determined based on the equiviscous method (Asphalt Institute, 1997), wherein the mixing and compaction temperatures respectively correspond to the temperatures at viscosity values of 0.17±0.02 Pa.s and 0.28±0.3 Pa.s. The main finding was that the addition of pyrolytic chars increased the production temperatures, and higher temperatures were obtained for binders fabricated with a higher char dosage (Celoglu et al., 2016; Wang et al., 2019; Gan and Zhang, 2021). In the study by Celoglu et al. (2016), the addition of 15% walnut seed shell biochar increased the mixing temperature by 27.8 °C from 150.1 °C for the control (unmodified) binder to 177.9 °C for the 15% biochar modified binder.

The DSR prominently determines the rheological characteristics of asphalt binders. The main rheological tests reported on pyrolytic char modified binders include measurement/assessment through temperature sweep, frequency sweep, complex viscosity (η^*), complex modulus (G^*), phase angle (δ), Superpave rutting parameter ($G^*/\sin\delta$), Superpave fatigue parameter ($G^*\sin\delta$), and multiple stress creep and recovery (MSCR).

The Superpave rutting and fatigue parameters are commonly used to evaluate rutting and fatigue performances of the modified binders, respectively. Several studies have concluded that pyrolytic chars improved high-temperature rutting properties in terms of higher G*, η*, and G*/sin δ (Chaala et al., 1996; Chebil et al., 1996, 2000; Zhao et al., 2014a,b; Celoglu et al., 2016; Feng et al., 2016, 2021; Kumar et al., 2018; Li et al., 2018; Zhang et al., 2018a; Wang et al., 2019; Dong et al., 2020; Ma et al., 2022). Figure 2.4 shows the significant improvements in G*/sin δ values observed at increasing biochar contents from the study by Ma et al. (2022). Pyrolytic char from biomasses is rich in carbon and shows irregular, fibrous, porous and rough surface morphology (Zhao et al., 2014b; Kumar et al., 2018; Zhang et al., 2018a). Figure 2.5 shows the morphological images of biochar reported by Zhang et al. (2018a). Such a morphology allows char to have high specific surface area leading to better interaction with asphalt binders and a better high-temperature rheological performance (Zhao et al., 2014b; Zhang et al., 2018a). In terms of binder fatigue resistance, the addition of pyrolytic chars increased the G*sin δ parameter due to the stiffer nature of the modified binder (Lesueur et al., 1995; Zhao et al., 2014b; Kumar et al., 2018; Li et al., 2018).

Due to the limitations in the Superpave rutting and fatigue parameters, new test procedures for evaluating the binder's contribution to rutting and fatigue performance have been recommended and used. The MSCR test is the most recent method for determining asphalt binders' rutting resistance. The linear amplitude sweep (LAS) test is a recently developed test, which is utilised to evaluate the fatigue damage tolerance of asphalt binders in a short period of time. The use of the MSCR test for pyrolytic char modified binders has only been documented in a few publications (Kumar et al., 2018; Wang et al., 2019), while no publication was found on the use of the LAS test.

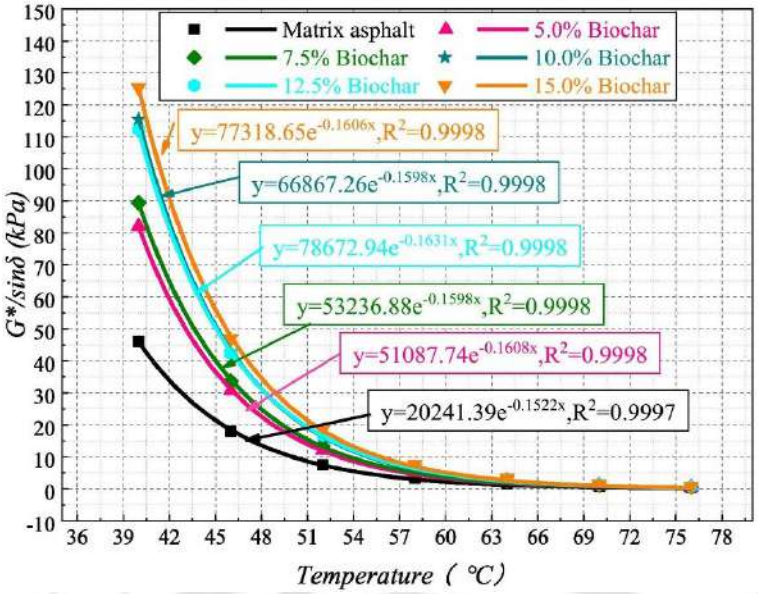

Figure 2.4 Variation of G*/sin δ at different biochar contents (Ma et al., 2022)
[Reprinted from Science of the Total Environment, Vol. 804, Ma, F., Dai, J., Fu, Z., Li, C., Wen, Y., Jia, M., Wang, Y. and Shi, K., Biochar for asphalt modification: A case of high-temperature properties improvement, Page 8, Copyright (2021), with permission from Elsevier.]

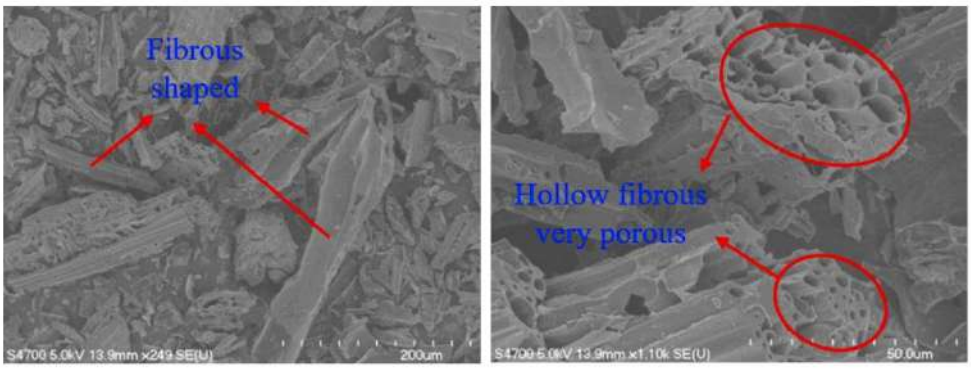

Figure 2.5 Scanning electron microscopy (SEM) images of biochar (Zhang et al., 2018a)
[Reprinted under the terms of the Creative Commons Attribution License.]

The low-temperature binder rheological performance was evaluated through the bending beam rheometer (BBR) tests, which provide a measure of stiffness (S-value) and relaxation properties (m-value) of asphalt binders at low temperatures. In general, the effect of pyrolytic chars was to increase the S-value and decrease the m-value, which indicate a lower performance against thermal stresses (Lesueur et al., 1995; Li et al., 2018; Zhang et al., 2018a; Dong et al., 2020; Feng et al., 2021; Ma et al., 2022). The stiffening effect of the pyrolytic chars could be compensated with the addition of another modifier, such as a

polymer (Lesueur et al., 1995) or a softening agent like aromatic hydrocarbon oil (Li et al., 2018). In some studies, the Fraass breaking point test was also used for low-temperature characterisation. Chebil et al. (1996, 2000) observed that the Fraass breaking point temperature reduced up to biochar and CB_p dosages of 5-10% and increased at higher dosages.

2.4.3 Theme-3: Storage stability properties of char-modified binders

A modified asphalt binder must have adequate storage stability to confirm that the binder maintains/retains its integrity and homogeneity during storage, handling, and transportation in the field. Typically, the separation tube test (also called the cigar tube test) is used to determine storage stability. The test comprises storing a modified binder sample in a narrow aluminium tube at 163 °C for 48 hours. After that, the tube is placed in a freezer, and then sawed into three equal segments. The binders from the top and bottom segments are removed and their properties are compared to assess the storage stability.

In the study by Chebil et al. (2000), the biochar concentrations in the top, middle, and bottom segments of the storage stability tube were determined for a 10% biochar modified binder. The concentrations in the top, middle and bottom segments were determined as 14%, 22%, and 64% by weight, respectively. Optical micrographs also revealed that the size of the biochar particles increased from the top to the bottom of the storage tube. The results indicated settlement of biochar particles towards the bottom of the tube during the hot storage at 163 °C. The authors suggested that the presence of biochar particles in the top segment was due to chemical interactions between the biochar and bitumen compounds.

Some past studies have reported inadequate storage stability with tyre pyrolytic char modification of asphalt binders. Feng et al. (2016) used softening point difference (SPD) to measure the storage stability of tyre pyrolytic char modified binders in three contents: 5, 10, and 15% by weight of the binder. Their results showed an increase in SPD with an

increase in char dosage. The SPD for the base binder was 0.3 °C, which increased to 3.2 °C and 4.4 °C at 15% dosages of two types of tyre pyrolysis chars. The poor storage stability was explained by the difference in densities of char and the binder, causing the char particles to settle at the bottom of the tube. It was also indicated that a larger TPC particle size would lead to a higher separation.

Wang et al. (2019) also used tyre pyrolysis char in three dosages: 6, 12, and 18% by weight of bitumen. A stability index based on non-recoverable creep compliance (J_{nr}) value was formulated to quantify the separation tendency of the modified binders (Equation 2.1):

$$SI = \frac{\left| J_{nr,top} - J_{nr,bottom} \right|}{J_{nr,average}} \quad (2.1)$$

where, SI is the stability index; $J_{nr,top}$ and $J_{nr,bottom}$ are the MSCR non-recoverable compliances of the sample from the top and bottom segments, respectively. $J_{nr,average}$ is the averaged J_{nr} among the samples from the top, middle, and bottom parts. A smaller SI value indicates better storage stability performance. Results (Figure 2.6) showed that the stability index increased with an increase in TPC percentages indicating lower storage stability. The authors used Stoke's law to explain the reason for separation and reported that a difference in densities (density of char: 1.871 g/cm^3; density of bitumen: 1.032 g/cm^3) attributed to the settling of the char particles under gravitational forces in the storage tube.

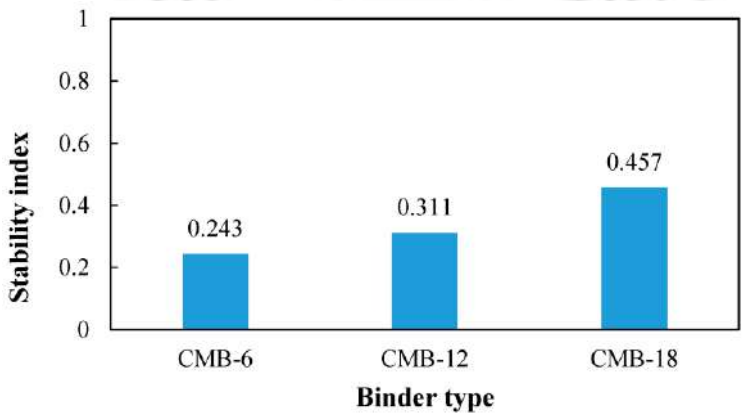

Figure 2.6 Storage stability index of pyrolysis char modified binders (CMB) (Wang et al., 2019) [Reprinted under the terms of the Creative Commons Attribution License.]

2.4.4 Theme-4: Ageing resistance and chemical properties of char-modified binders

Asphalt binder ages in two phases: (1) short-term ageing (during production, placement, and compaction of the asphalt mixture), and (2) long-term ageing (during the service life of the asphalt pavement when exposed to the environment). The effects of ageing have been generally characterised using ageing indices/ratios formulated based on a binder property in an unaged state to that in the aged state. The commonly used binder ageing procedures are thin film oven (TFO) and rolling thin film oven (RTFO) for short-term ageing, and pressure ageing vessel (PAV) for long-term ageing.

In the study by Zhao et al. (2014b), complex viscosity (η*) was measured after RTFO and PAV ageing to determine the effect of biochar on the ageing resistance of the binder. Results showed that the inclusion of biochar offset the effect of ageing, with the possible explanation that interaction of biochar with binder hindered the low weight molecule components from oxidation. Finer biochar size was more effective in reducing oxidation due to the high surface area. To compare the ageing properties of the binders, Zhang et al. (2018a) used an ageing index based on the ratio of viscosity (at 135 °C) of RTFO-aged binder to that of unaged binder. A lower value of the index indicated better performance against ageing. As shown in Figure 2.7, the anti-ageing characteristics of biochar modified asphalts enhanced as the biochar content increased. This was explained by the stiffening effect of the high biochar concentration, which reduced the effects of ageing. The anti-ageing characteristics of biochar modified asphalts with smaller particles were better than those with bigger particles. Moreover, 2% BS, 4% BS, and 8% BS modified binders (BS: biochar with small size) had better ageing resistance than the control binder. The authors explained that biochar's unique fibrous and porous structure probably resulted in a better adhesion interaction between the biochar and the base binder molecules, thereby reducing oxidation.

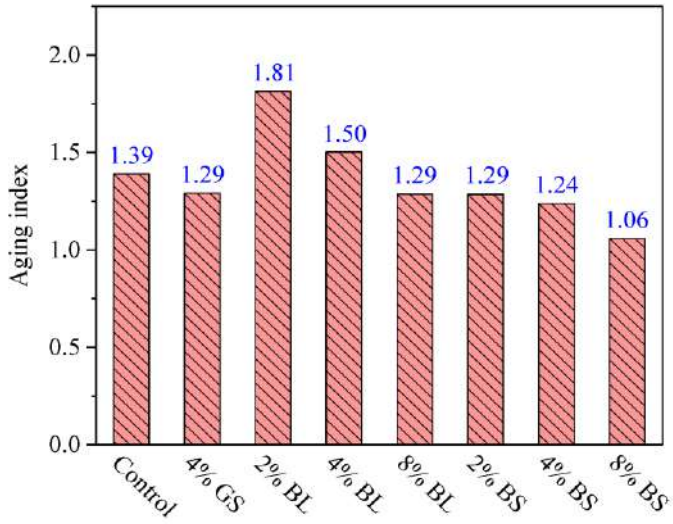

Figure 2.7 Ageing index of binders (Zhang et al., 2018a) (GS: graphite; BL and BS: biochar of large and small size)

[Reprinted under the terms of the Creative Commons Attribution License.]

Dong et al. (2020) evaluated the ageing properties of biochar modified binders using TFO and PAV procedures to simulate short-term and long-term ageing, respectively. The penetration ratio (penetration of short-term aged to unaged binder) was greater for biochar modified binders than that of the base (unmodified) binder. This indicated that the biochar could reduce the ageing sensitivity of the binder and thus improve ageing resistance. The observation was explained by ionic adsorption characteristics and porous morphology of biochar particles, due to which biochar could adsorb asphalt components and interact with the binder. A similar improvement in the ageing performance was also observed on comparing the binder viscosity. FTIR spectroscopic analysis indicated that the interaction of biochar with asphalt binder was a physical phenomenon. However, FTIR-based ageing indices (such as carbonyl and sulfoxide indices) were not determined.

Feng et al. (2016) used two types of tyre pyrolytic carbon blacks (PCB-1 and PCB-2) with particle sizes of 25 µm for PCB-1 and 150 µm for PCB-2. The base binder was designated as SK70# and was modified with three PCB dosages: 5, 10, and 15%. The ageing procedures used were TFO, PAV and a 'natural ageing' (NA). In the NA procedure,

a binder sample was aged by subjecting it to the exposure of sunlight followed by water scouring. The ageing indices used in this study were formulated based on ratios/differences of conventional properties (penetration, softening point, ductility) and viscosity (60 °C) before and after ageing. The results showed that the addition of both pyrolytic carbon blacks improved the ageing performance of the binders considering both thermo-oxidative (simulated by TFO and PAV) and photo-oxidative (simulated by NA procedure) ageing states.

Wang et al. (2019) evaluated the ageing properties of tyre pyrolytic carbon black (CB_p) modified binders at three CB_p dosages (6, 12, 18%). An ageing index (*AI*) derived as the ratio of MSCR J_{nr} of aged binder to unaged binder (Equation 2.2) was used to quantify ageing resistance.

$$AI = \frac{J_{nr,aged}}{J_{nr,unaged}} \tag{2.2}$$

A binder with *AI* value near unity is considered to be more ageing resistant. Results (Figure 2.8) showed that the increase in CB_p content significantly improved the ageing resistance under both RTFO and PAV states. The possible mechanism for better ageing resistance for CB_p modified binder was explained based on the results of electron spectroscopy for chemical analysis (ESCA), infrared, and ultraviolet spectroscopic studies on CB_p modified bitumen by Chaala et al. (1996). When char particles are added to bitumen, the CB_p particles absorb the maltenes, and a thin border layer of asphaltenes forms on the CB_p surface. The depletion of maltenes and the production of additional asphaltene-like compounds are also the main causes of bitumen ageing. When the binder is aged, a system like this (CB_p particle surrounded by asphaltenes) helps prevent maltene depletion and improves the binder's ageing resistance. Another reason for the improved ageing

resistance was the presence of active functional groups on the CB_p surface that are more prone to reacting with oxygen than bitumen during ageing processes.

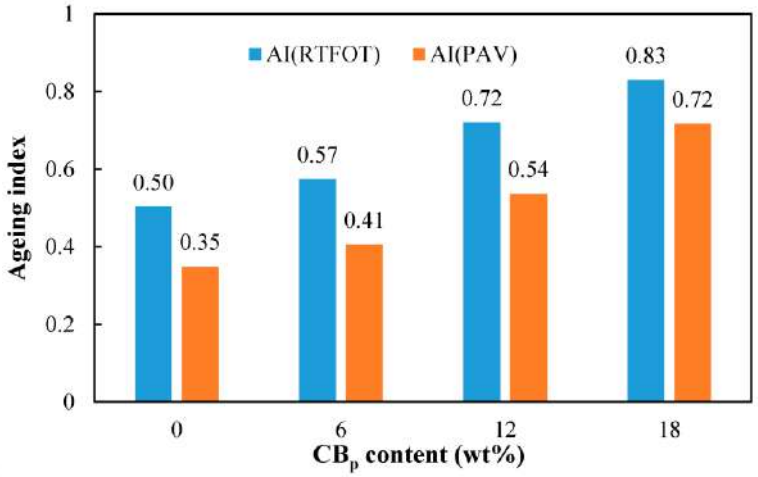

Figure 2.8 Ageing index of binders (Wang et al., 2019)
[Reprinted under the terms of the Creative Commons Attribution License.]

Darmstadt et al. (1995) investigated the interaction between tyre pyrolytic carbon black (CB_p) and bitumen using electron spectroscopy for chemical analysis (ESCA), secondary ion mass spectrometry (SIMS), and the infrared spectroscopy. CB_p was extracted from CB_p modified bitumen and it was observed that the extracted CB_p was covered with a layer of about 2 nm thickness composed of asphaltenes. Another study expounding on the chemical behaviour of CB_p-modified asphalt was conducted by Chaala et al. (1996). Based on ESCA and ultraviolet (UV) spectroscopy, CB_p had both physical and chemical interactions with asphalt. CBp has been proven to 'trap' some asphaltenes in the maltenes, lowering their concentration. A border layer (film) of roughly 2 nm thickness encircled the CB_p particles, primarily made up of asphaltenes. It was concluded that the effect of CB_p on asphalt binder was different from an inactive filler. Chebil et al. (2000) utilised the same analytical technique (ESCA) on a 10% biochar modified asphalt binder and found that the extracted biochar particles had a surface area of 15 m^2/g compared to 150 m^2/g for the raw biochar particles. It was concluded that the biochar particles had a high adsorption capacity and

were covered with asphaltenes from the binder during the modified binder blend preparation process.

2.4.5 Theme-5: Properties of asphalt mixtures

As seen from Table 2.4, a limited number of studies have been conducted on pyrolytic char modified asphalt mixtures. Park et al. (1997) evaluated the performance properties of asphalt mixtures with pyrolytic carbon black, CB_p, with two binders (AC-10 and AC-20) and two aggregate types (limestone and slag). Higher dosages of the char led to higher stability, attributed to the higher viscosity of the char modified binder. At the same compactive effort, there was an increase in mix air voids with an increase in CB_p content. The resilient modulus also increased with the CB_p dosage, but the maximum moduli values were observed at 15% dosage. The low-temperature ITS (measured at 5 °C) increased with an increase in CB_p dosage, indicating that the cracking potential of the mixtures was reduced with the addition of CB_p. The inclusion of CB_p also increased the stripping inflection point in the Hamburg wheel tracking test; however, the trends were influenced by the base binder and the aggregate type. The best performances were noted at 10% CB_p content for mixtures prepared with AC-10 and AC-20 binders.

Zhao et al. (2014a) studied the laboratory performance of asphalt mixtures modified with biochar obtained from slow pyrolysis of switchgrass. Commercially available carbon fibres and carbon black were used as reference additives in the study. All three additives were used at 5% and 10% by weight of the base binder (PG 64-22). A gravel aggregate was used with a 9.5 mm nominal maximum aggregate size (NMAS) gradation. A constant binder content of 5.7% by weight of mix was used to fabricate all mixture specimens. The 5.7% binder content was determined as the optimum for the mixture with the control binder (PG 64-22). Figure 2.9a shows the results of resilient moduli of the different mixtures at 25

°C. It was found that the 10% biochar-modified mixture had the highest modulus indicating that biochar had a better interaction with the binder during mixing.

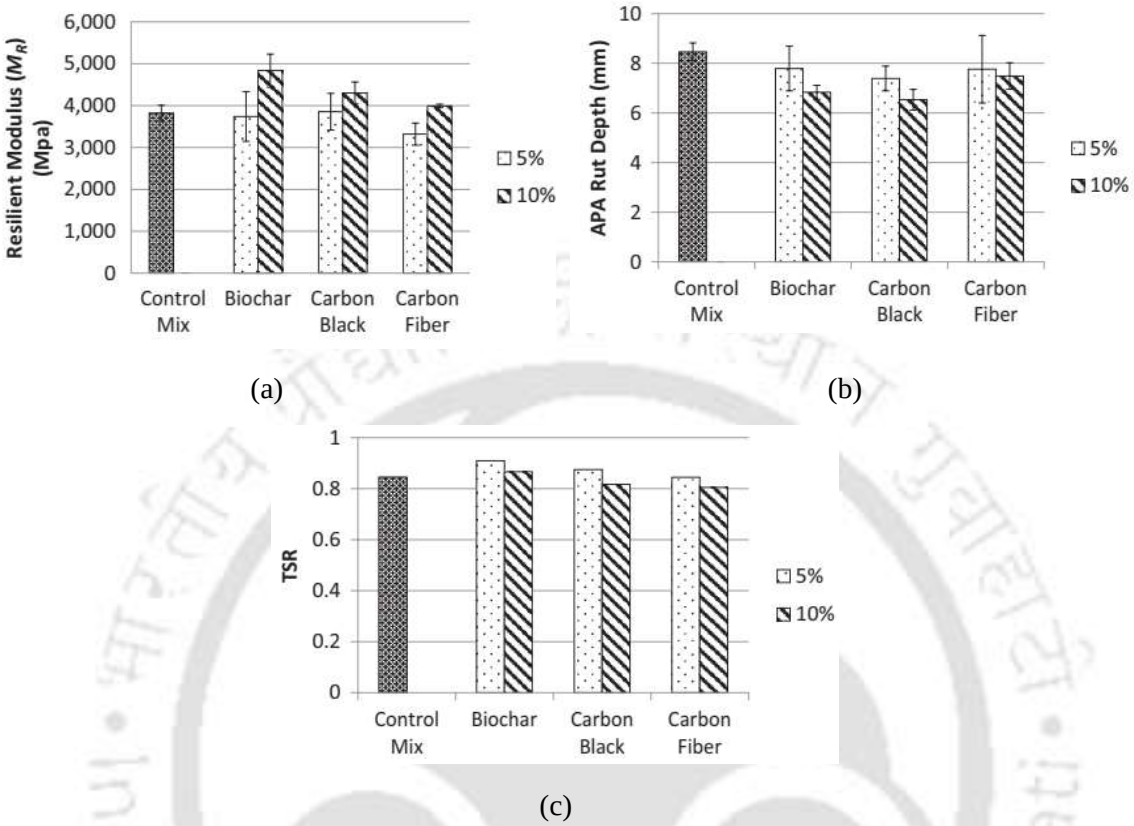

Figure 2.9 (a) Resilient modulus, (b) rut depth, and (c) TSR results for asphalt mixtures (Zhao et al., 2014a)

[Reprinted from Transportation Research Record, Vol. 2445 (Issue 1), Zhao, S., Huang, B., Shu, X., & Ye, P., Laboratory investigation of biochar-modified asphalt mixture, Pages 60-61, Copyright (2014), with permission from SAGE Publishing.]

The results of Asphalt Pavement Analyzer (APA) rut depth tests conducted at 64 °C (Figure 2.9b) also showed that the additives improved the rutting performance, especially biochar and carbon black at higher contents. However, an increase in additive dosages from 5% to 10% reduced the resistance against moisture-induced damage, as seen from Figure 2.9c. Biochar-modified mixtures met the minimum 80% TSR requirement showing that biochar had a more significant effect on moisture resistance than other additives. Considering the cracking performance, the biochar increased the J-integral value in the semicircular bend (SCB) tests performed at 25 °C, indicating an improved cracking resistance.

Li et al. (2018) used two mixture types (AC-13 and AC-20 of 13 mm and 20 mm NMAS, respectively) to investigate the influence of tyre pyrolytic carbon black (TPCB) on the performance of asphalt mixtures. Crushed basalt aggregates were used as coarse and fine aggregates with limestone as the filler. Two binders were used: (1) control (unmodified) binder (designated as GF70), (2) binder modified with 15% TPCB and 1.2% aromatic hydrocarbon oil (AHO). The binder contents were approximately the same for a particular mix type (about 4.5% for AC-13 and 5.1% for AC-20). The use of the modified binder reduced the rut depth in the wheel tracking test by 29.8% and 14.8%, respectively, for AC-13 and AC-20 mixtures. Improved rutting performance was also observed from the increase in dynamic stability parameter (Figure 2.10). The dynamic stability indicates the number of wheel passes required for a unit rut depth on the specimen, and higher values are desirable. The authors attributed the better rutting performance to the large specific surface area of TPCB. In low-temperature mix characterisation, the modified binder improved performance with a lower flexural modulus and a higher flexural strain at –10 °C compared to the mix with the control binder. The moisture damage resistance, measured using retained Marshall stability and TSR tests, showed a decrease when the modified binder was used for both mix types. For example, the TSR of the AC-13 mix type decreased from 89.3% to 81.7% when the modified binder was used compared to the control binder.

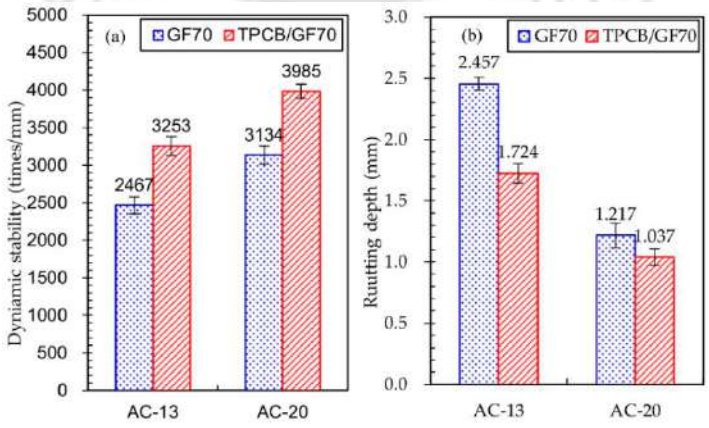

Figure 2.10 Rutting performance of mixtures (a) dynamic stability, (b) rut depth (Li et al., 2018) [Reprinted under the terms of the Creative Commons Attribution License.]

Gao et al. (2019) used 5% and 10% dosages of char derived from tyre pyrolysis and evaluated the results of TSR and wheel tracking tests. The base binder was a PG 58-28, and a 12.5 mm NMAS aggregate gradation was used for mix preparation with 6.1% and 6.7% binder contents for the control and the modified mixtures, respectively. All mixtures satisfied the minimum TSR criterion of 80% in the TSR tests, while the mix with 10% char showed the highest TSR of 92.7% compared to 86.6% for the control mix. In the wheel tracking tests, the control mix reached the failure rut depth (20 mm) at 9,849 passes, while the mixes with 5% and 10% char failed at 6,717 and 6,979 passes, respectively. It was concluded that the modified mixtures had reduced rutting resistance. Jerin et al. (2020) used 5, 10, and 15% dosages of tyre pyrolysis char and evaluated the Marshall stability and flow of the modified mixtures. The highest stability and flow values were obtained at 5% char content. For 10% and 15% char dosages, the stability and flow decreased. The studies by Gao et al. (2019) and Jerin et al. (2020) show that the results with pyrolytic chars may not follow strictly increasing or decreasing trends with the char dosage/content.

Sanchez et al. (2020) used biochar (derived from microwave pyrolysis of wood pellets made from spruce sawdust) as a direct additive when preparing asphalt mixtures in the dosages of 4, 8, and 12% by weight of the binder. The base binder was a PG 58-28, and a 12.5 mm NMAS aggregate gradation was used for mix preparation. A binder content of 6.1% was used during the fabrication of all mixtures. Contrary to earlier studies, biochar served as a compaction aid in this study since less compaction effort was required to achieve the same air void content as for the control mixture. The addition of biochar also reduced the bulk specific gravity of the compacted mixtures, which was attributed to lightweight biochar particles with less density. The TSR values of the control, 4, 8, and 12% biochar-modified mixtures were determined as 67.3, 70.7, 72.1, and 66.8%,

respectively. The TSR increased with the addition of biochar and peaked at 8% biochar content.

2.5 Selection of Pyrolytic Chars for this Study

A survey of pyrolysis enterprises in India was done to select the pyrolytic chars for this study for asphalt modification. Visits to nearby pyrolysis plants and telephonic discussions with other enterprise owners were part of the survey. According to the survey's findings, tyre and plastic wastes are currently the most commonly pyrolyzed materials in India. The majority of pyrolysis companies pyrolyze tyres, plastics, or both. The approach generates a significant quantity of pyrolytic chars as a by-product, which can be available in adequate amounts if they are found feasible for use in pavement construction projects. On the other hand, biomass pyrolysis has not achieved the same traction as tyre/plastic pyrolysis since the quality of biooil is inferior to tyre/plastic pyrolysis oil (lower calorific value, high oxygen content). Oils extracted from the tyre/plastic pyrolysis are found to be more profitable. Furthermore, biomass wastes are easily compostable; thus, pyrolysis is not the most attractive alternative. Tyre and plastic wastes, on the other hand, cannot be composted because they are non-biodegradable. As a result, their pyrolysis is technically more attractive and commercially viable. For these reasons, tyre and plastic pyrolytic chars were considered as the two pyrolytic chars in this research, produced from the pyrolysis of waste tyres and plastics, respectively.

Figure 2.11 shows photographs of stockpiles of the tyre and plastic pyrolytic chars stored in sacks near pyrolysis plants. Information provided by plant owners revealed that the chars are presently sold as low-grade fuel in brick kilns at meagre prices (INR 4 per kg ~ USD 0.05 per kg), else discarded in nearby landfills/open areas. Expanding the application avenues of pyrolytic char is necessary for the commercial success of the

pyrolysis process. The use of the tyre and plastic pyrolytic chars in asphalt binder modification can help enhance the performance of asphalt binders and asphalt mixtures. The use of chars in asphalt materials will also support the sustainable management of plastic and tyre wastes through pyrolysis technology by providing a channel for bulk utilisation of these by-product materials.

(a)

(b)

Figure 2.11 Photographs of stockpiled pyrolytic chars (a) tyre char and (b) plastic char
[Figure 2.11a – Photograph taken by Derick Norman, reused with permission;
Figure 2.11b – Photograph taken by Mayur Bhole, reused with permission.]

2.6 Critical Appraisal of Literature and Identification of Gap Areas

According to the literature review, biochar and tyre pyrolytic char have been researched for asphalt binder modification. However, no research on plastic pyrolytic char could be found.

As discussed in the previous section, waste tyres and plastics are the two most pyrolyzed waste materials in India. Pyrolysis of plastic waste has also gained popularity in India and several other countries to extract valuable compounds from plastic wastes. To the best of the author's knowledge, this study was the first to use plastic pyrolytic char for asphalt binder modification. The tyre pyrolytic char was the second pyrolytic char used in the investigation.

The majority of previous studies used a single char type, or if other modifiers were included, they were generally carbonaceous modifiers like carbon black. A comparison study is needed to determine the variations in modified binder and mixture characteristics when different char types are considered for binder modification. A comparison of char types will aid in understanding the impact of char type on a variety of asphalt binder and mixture performance attributes. An assessment with tyre and plastic pyrolytic chars, in particular, will be helpful in identifying high-value application pathways for these pyrolysis by-products as asphalt binder modifiers.

Understanding the differences in the performance of pyrolytic char modified binders and mixes requires materials science-based understanding of pyrolytic chars. However, only a few studies have attempted to explain how the inherent material qualities of the chars affect the properties of the resulting modified binders and asphalt mixtures. As a result, the microstructural and thermo-chemical attributes of the chars were included in Objective 1 of the study (research objectives were presented in Section 1.3 of the thesis). These attributes included FTIR, proximate analysis, specific surface area, thermogravimetric analysis, chemical composition, and microscopy. The objective also included microstructural and thermo-chemical characterisation of the modified asphalt binders and their comparison with the control (unmodified) binder.

Past research studies have indicated that storage separation in tyre char modified binders is indeed a concern (Feng et al., 2016; Gao et al., 2019; Wang et al., 2019). The application of cross-linking agents (such as sulfur, polyphosphoric acid) is a widely followed approach to alleviate storage stability issues with modified asphalt binders. However, no systematic research on the characterisation and potential remediation of separation issues in pyrolytic char modified binders has been conducted. Objective 2 of the study was formulated to evaluate the thermal storage stability of asphalt binders modified with tyre and plastic pyrolytic chars using cross-linking agents.

The use of advanced rheological tests such as MSCR and LAS for pyrolytic char modified binders has been very limited. For binder rutting evaluation, the use of multiple rutting performance evaluation methods (such as Shenoy rutting parameter, zero shear viscosity, MSCR) at multiple temperatures has not yet been attempted. In this study, the storage stable binders were characterised through classical (conventional) tests followed by rheological tests at various temperatures, frequencies, strain and stress levels, and ageing states. All tests were performed at multiple dosages of the pyrolytic chars. Objective 3 of the study was to determine the conventional and rheological properties of modified binders with different contents of the tyre and plastic pyrolytic chars.

Considering the ageing characteristics, limited studies have evaluated the effect of pyrolytic chars on the ageing performance of modified asphalt binders (Feng et al., 2016; Wang et al., 2019; Dong et al., 2020). New techniques for studying changes in asphalt chemical composition due to ageing have been developed, with FTIR spectroscopy being one of the most extensively employed. Peaks corresponding to two oxygenated functions, namely carbonyl (C=O) and sulfoxide (S=O), are used to evaluate changes caused due to ageing in asphalt binders (Lamontagne et al., 2001; Lu and Isacsson, 2002). A detailed study utilising spectroscopic studies coupled with rheological ageing indices is needed for

pyrolytic char modified asphalt binders under different ageing conditions to improve the understanding of ageing performance. Objective 4 of the study included the evaluation of ageing characteristics of asphalt binders modified with tyre and plastic pyrolytic chars.

It is essential to determine the appropriate mixing and compaction temperatures for pyrolytic char modified binders. The previous studies have been limited on this aspect and have mostly reported the equiviscous temperatures (Celoglu et al., 2016; Wang et al., 2019; Gan and Zhang, 2021). While being routinely used for neat/unmodified binders, the equiviscous method often results in disproportionately high temperatures for modified binders, which may cause unwarranted ageing of the binder, damage to the binder and/or modifier, increased fumes and emissions during mix preparation and compaction (Yildirim et al., 2000; Azari et al., 2003; West et al., 2010). For modified binders, recent studies have proposed new methodologies such as high shear viscosity, steady shear flow, and phase angle methods; however, they have not been elucidated for pyrolytic char modified binders. Objective 5 of this study focused on determining mixing and compaction temperatures (production temperatures) for the control and tyre and plastic pyrolytic char modified binders using the conventional and new approaches.

The toxicity characteristics evaluation test is desirable when industrial wastes/by-products are used as pavement materials (Oluwasola et al., 2016). However, evaluation of the toxicity characteristics of asphalt mixtures containing pyrolytic chars is not yet been reported. Limited studies have reported the properties of asphalt mixtures fabricated with pyrolytic char modified binders. Further, the impact of pyrolytic chars on mix design and volumetrics, along with performance parameters such as rutting, fatigue cracking, and pavement structural analysis, are not described in detail. To investigate these research gaps, Objectives 6 and 7 of the present study were formulated to understand mix design properties and performance of asphalt mixtures fabricated with tyre and plastic pyrolytic

chars modified binders in terms of resistance against permanent deformation, moisture damage resistance, cracking resistance, and fatigue damage. Leachate toxicity tests were conducted on asphalt mixtures to ensure that their use is safe for the environment. Pavement structural analysis was then carried out based on the resilient modulus of the mixtures.

2.7 Summary

This chapter presented the review of the literature on the use of pyrolytic chars in asphalt binder modification, including the effect of the chars on the binder conventional and rheological properties, chemical characteristics of the binders, and the properties of asphalt mixtures fabricated with the char modified binders. The chapter also discussed carbonaceous additives for asphalt binder modification, pyrolysis technology, and the motivation to use pyrolytic chars. Arguments were provided for the selection of tyre and plastic pyrolytic chars for this study. The chapter concluded with a critical appraisal of the different studies that helped identify research gaps that guided the formulation of objectives for the study.

Chapter 3

MATERIALS AND EXPERIMENTAL PROGRAMME

3.1 Introduction

This chapter describes materials used in the study, including the base asphalt binder, mineral aggregates, and pyrolytic chars. This is followed by a discussion on the experimental programme used to accomplish the objectives formulated for the study. A detailed description is then provided for the six tasks formulated to achieve the objectives of the study. The chapter provides the details of experimental techniques and test methods adopted to investigate the different properties of the pyrolytic chars, modified binders, and asphalt mixes corresponding to each task formulated for the study.

3.2 Materials

3.2.1 Base asphalt binder

A viscosity grade-30 (VG 30) asphalt binder (shown in Figure 3.1) was used as the base and the control binder and was supplied by a commercial binder manufacturer TikiTar Industries (Vadodara, India). VG 30 binder is quite often used for paving in different regions of India in place of the old 60/70 penetration grade binder. The VG 30 binder is recommended for use by IRC 111 (2009) in regions/locations with the highest daily mean air temperature of more than 30 °C and lowest daily mean air temperature of above –10 °C. As per the information provided by the binder supplier, VG 30 grade bitumen is also preferred as a base binder for the production of modified bituminous binders. The physical properties of the base binder were evaluated as per the specifications of IS 73 (2013) and are reported in Table 3.1.

Figure 3.1 Base asphalt binder (VG 30)

Table 3.1 Properties of base asphalt binder (VG 30)

Property	***Requirement****	***Results***	***Standard***
Absolute viscosity at 60 °C, poise	2400–3600	3410	IS 1206 (P-II) (1978)
Kinematic viscosity at 135 °C, cSt	min 350	525	IS 1206 (P-III)(1978)
Penetration at 25 °C, 100 g, 5 s, 0.1 mm	min 45	51.6	IS 1203 (1978)
Softening point (R&B), °C	min 47	52.7	IS 1205 (1978)
Flash point (COC), °C	min 220	280	IS 1209 (1978)
Solubility in trichloroethylene, %	min 99	>99	IS 1216 (1978)
Properties tested on rolling thin film oven (RTFO) residue			
Viscosity ratio, 60 °C	max 4	1.15	IS 1206 (P-II) (1978)
Ductility, 25 °C, cm	min 40	>100	IS 1208 (1978)

* Requirements as per IS 73 (2013)

3.2.2 Aggregates and aggregate gradation

Aggregates used in the study were obtained from a nearby aggregate crusher plant in Shillong (India). Physical properties of aggregates were evaluated to ensure that the requirements laid by Ministry of Road Transport and Highways (MoRTH) (MoRTH, 2013) for use in bituminous concrete (BC) were met. BC is a dense-graded mix most commonly used as a wearing course for flexible pavements in India. Table 3.2 enlists the test results of the physical properties of the aggregates. The BC-2 gradation with a 13.2 mm nominal maximum aggregate size (NMAS) was selected to prepare BC mixes. Figure 3.2 shows the aggregate gradation along with the upper and lower limits for the BC-2 aggregate gradation specified by MoRTH (2013). The aggregates obtained from the crusher plant were cleaned,

dried, and sieved into the respective size fractions as required for the selected BC-2 gradation (Figure 3.3).

Table 3.2 Properties of aggregates

Property	***Requirement****	***Results***	***Standard***
Combined flakiness and elongation index	Max 35%	17.8%	IS 2386 (P-I) (1963)
Aggregate impact value	Max 24%	21.3%	IS 2386 (P-IV) (1963)
Aggregate abrasion value	Max. 30%	23.4%	IS 2386 (P-IV) (1963)
Water absorption	Max 2%	0.35%	IS 2386 (P-III) (1963)
Stripping	Min retained coating 95%	100%	IS 6241 (1971)
Specific gravity			
Coarse aggregate	—	2.600	IS 2386 (P-III) (1963)
Fine aggregate	—	2.594	IS 2386 (P-III) (1963)
Filler	—	2.596	IS 2720 (P-III) (1980)

*Requirements as per MoRTH (2013)

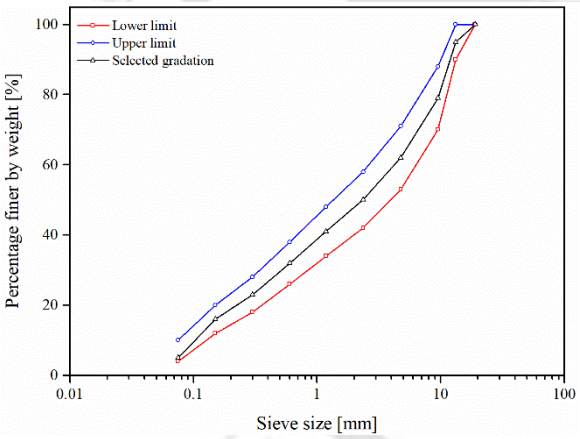

Figure 3.2 Selected BC-2 gradation along with upper and lower limits

Figure 3.3 Size fractions constituting the BC-2 gradation

3.2.3 Pyrolytic chars

The study used two pyrolytic chars: tyre pyrolytic char (TPC) and plastic pyrolytic char (PPC). Both TPC and PPC were provided by Innova Engineering & Fabrication (Mumbai, India). Figure 3.4 shows the physical appearance of the two chars. As per the information shared by the supplier, the tyre pyrolysis process broadly consisted of cleaning, debeading and shredding scrap tyres to about 1-inch (25 mm) size and then feeding them to the

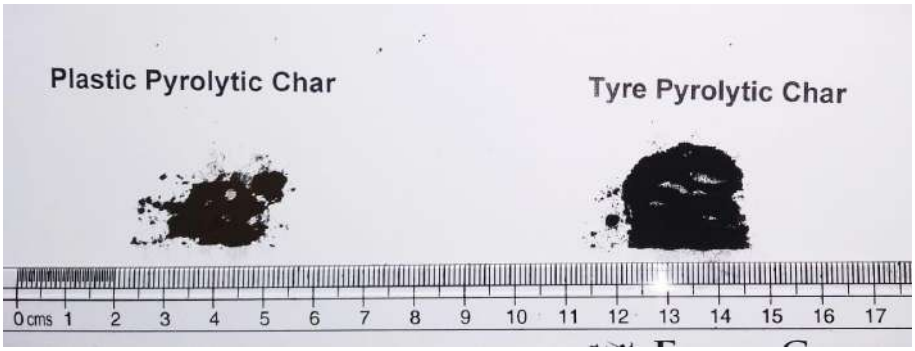

Figure 3.4 Physical appearance of the pyrolytic chars

pyrolysis reactor. At ~180 °C temperature, the tyre cracked and vapours released were condensed to pyrolysis oil and the uncondensed gases were taken to the reactor and used as fuel. The total process time was about 15 h for a 10 tonne batch. The pyrolysis yield was 35-40% liquid oil, 10-15% gases, and 35% pyrolytic char (the TPC). TPC consists of a mixture of carbon blacks originally added during tyre manufacturing, carbonaceous deposits, inorganic compounds (SiO_2, ZnO, K_2O, Fe_2O_3, *etc*.), and volatile matter (Cataldo, 2021). The inorganics originate from the tyre manufacturing process (Martínez et al., 2019; Urrego-Yepes et al., 2021).

In plastic pyrolysis process, the raw material, a mixture of municipal and industrial waste plastics (with polypropylene as the principal constituent), was first cleaned and shredded to a size of about 15-25 mm. At a temperature of ~250 °C, the plastic cracked and the vapours released were condensed to pyrolysis oil and the uncondensed gases were reverted to the reactor. The total process time was about 15 h for an 8 tonne batch. The pyrolysis yield was 70-80% liquid oil, 10-15% gases, and 15-25% pyrolytic char (the PPC). In plastic waste pyrolysis, char formation is attributed to non-volatilisation of the plastic and re-condensation/recombination of pyrolytic cracking products (Bernardo et al., 2012). PPC formation also involves side-chain reactions that maintain C–C bonds and remove small molecules such as H_2O, CO_2, or hydrogen, and thus may contain residual groups from the original polymer (Moldoveanu, 2005). PPC formation is also attributed to secondary

repolymerisation reactions among the polymer-derived products (Gao, 2010; Lopez et al., 2011) and may include coke and undegraded polymer (Buekens and Huang, 1998). Both TPC and PPC particles used in the study passed the 75 μm (No. 200) sieve.

3.3 Preparation of Pyrolytic Char Modified Binders

A high shear mixer device with a rotor-stator assembly was used to fabricate TPC and PPC-modified asphalt binders. The modification was performed at 5, 10, 15, and 20% char dosages (by weight of the neat binder). The chars were dried at 105 °C for 2 h, and the base binder was heated to 160 °C. The binder was then slowly charged with char particles with continued stirring of a glass rod. After the required quantity of char was introduced in the binder, the blend was subjected to high shear mixing for 30 min at 12000 rpm. Figure 3.5 shows the high shear mixer (Make and Model: IKA T25 Ultra-Turrax®) used. A 0.3% (by weight of the modified binder) dosage of elemental sulfur was added, and the mixing continued for 15 min. The sulfur was added to have the requisite thermal storage stability, and the selection of sulfur content was based on a detailed storage stability analysis with multiple sulfur contents (results of storage stability analysis are presented in Chapter 5).

The duration and speed selected in fabricating the modified binder blends were arrived from preliminary trials to ensure a good dispersion/mixing of the modifiers in the neat asphalt binder. During the operation of the high shear mixer, the rotor turns at the selected rotational speed within the stationary stator. The material is expelled radially outwards at a high velocity under intense hydraulic shear action. The mixing speed ensured an adequate degree of shearing action between the rotor and stator (shown in Figure 3.5), and thus helped to avoid the agglomeration of the modifiers. The nine binders used in the study are designated as follows: control, TPC-5, TPC-10, TPC-15, TPC-20, PPC-5, PPC-10, PPC-15, and PPC-20, where the number after ‘TPC’ or ‘PPC’ indicates the char dosage (by weight of neat binder) used.

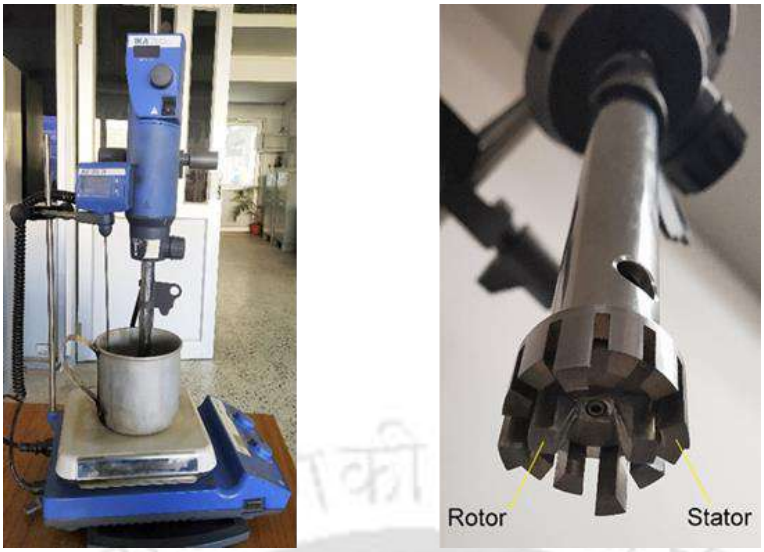

Figure 3.5 High shear mixer (left) and rotor-stator assembly of the high shear mixer (right)

3.4 Experimental Programme

The objectives of this study were arranged into six independent tasks. Table 3.3 shows the scope outlined for each of the six tasks. The following subsections describe the experimental design and test methods adopted for each task.

Table 3.3 Designation and scope of tasks of the study

Task	Scope
Task 1	Physico-chemical characterisation of materials
Task 2	Evaluation of storage stability of char modified binders
Task 3	Characterisation of char modified binders
Task 4	Ageing characterisation of char modified binders
Task 5	Determination of production temperatures
Task 6	Design and performance evaluation of asphalt mixes with char modified binders

3.4.1 Task 1: Physico-chemical characterisation of materials

To comprehend changes in the performance of TPC/PPC modified binders and mixtures, it is necessary to investigate the physico-chemical properties of the pyrolytic chars. Task 1 of the study involved physical and chemical characterisation of TPC and PPC and the

microstructural and thermo-chemical characterisation of asphalt binders. The analyses adopted to characterise chars included field emission scanning electron microscopy (FESEM), energy dispersive X-ray (EDX) spectroscopy, Brunauer-Emmett-Teller (BET) surface area analysis, particle size distribution analysis, proximate analysis, Fourier transform infrared (FTIR) spectroscopy, and thermogravimetric analysis (TGA). The binders were analysed through optical microscopy, TGA, and FTIR. Figure 3.6 presents the experimental plan for Task 1 of the study. The results of work performed under Task 1 are presented in Chapter 4. The following paragraphs provides a brief outline of each experimental technique used under Task 1.

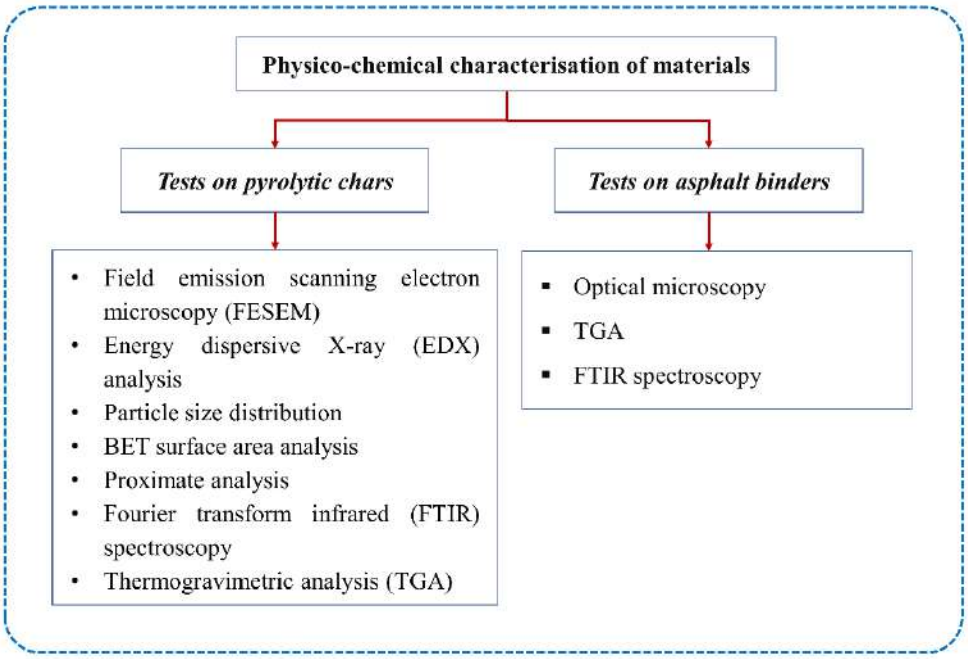

Figure 3.6 Experimental plan for Task 1

3.4.1.1 Experimental techniques and test procedures

***Field emission scanning electron microscopy (FESEM)*:** In FESEM microscopy, the surface of an object is scanned by electrons released by a field emission source. The electrons (primary electrons) are accelerated in a high electrical field gradient before being focused and deflected by electronic lenses to create a narrow scan beam that bombards the

object. Secondary electrons are thus emitted from each spot on the object as a result. The secondary electrons' angle and velocity are related to the object's topography. Secondary electrons are captured by a detector, which generates an electronic signal. This signal is amplified and transformed into a video scan image that can be viewed on a monitor or a digital image that can be saved and processed (Radboud University, 2021). Figure 3.7 shows the FESEM instrument used for the characterisation of the pyrolytic chars.

Figure 3.7 FESEM instrument

Energy dispersive X-ray (EDX) spectroscopy: EDX is used to determine a sample's elemental composition and the relative amounts of each element present in the sample. EDX is typically used in conjunction with FESEM. Atoms are made up of nuclei (protons and neutrons) with electrons orbiting around them at various energy levels. A high-energy electron beam strikes the sample during EDX operation. Some of these electrons collide with electrons at lower energy levels (present in the sample), leading to ejecting of electrons from the atoms of the sample's surface. As a result, an electron at a higher energy level jumps to a lower energy level. When an electron falls to a lower energy level, it emits energy in the form of X-rays to balance the energy difference between the two electrons' states. Since the electron transitions are characteristic of the element, the X-ray energy is also specific to the element, and thus EDX identifies the specific element(s) present in the

sample (University of Washington, 2020). Figure 3.8 shows the photograph of the EDX instrument used for the elemental characterisation of the pyrolytic chars.

Figure 3.8 EDX instrument

***Laser diffraction particle size analysis*:** Laser diffraction determines particle size distributions by recording the angular variation in the intensity of light scattered as a laser beam passes through a dispersed particulate sample. Small particles scatter light at small angles relative to the laser beam, whereas large particles scatter light at large angles. Using the Mie theory of light scattering, the angular scattering intensity data is then analysed to calculate the size of the particles that create the scattering pattern (Malvern Panalytical, 2021). Particle size distribution of TPC and PPC was performed using a Malvern Mastersizer 2000 laser diffraction analysis system shown in Figure 3.9.

Figure 3.9 Laser particle size analysis instrument

***BET surface area analysis*:** Stephen Brunauer, Paul Emmett, and Edward Teller developed the BET theory in 1938. This theory was named after the first letter of each researcher's surname. The BET theory is used to calculate the surface area of porous or solid materials under high-vacuum conditions. The volume of nitrogen (N_2) gas adsorbed on the sample surface is used to calculate the surface area of a material sample in a typical BET analysis. During the BET analysis, the sample temperature is kept constant (isothermal conditions) while the pressure of the adsorbing gas (N_2) is increased. With the increase in pressure, more gas molecules adsorb on the surface. By knowing the number of gas molecules (from the volume adsorbed), the surface area is calculated (Anton Paar, 2021; Raja and Barron, 2021).

***Proximate analysis*:** Proximate analysis determines a sample's moisture content, volatile matter, ash, and fixed carbon using a series of standard test methods. The proximate analysis procedure was designed to evaluate the products produced when a coal sample was heated under specific conditions (Speight, 2015). The results of proximate analysis of the two pyrolytic chars were provided by the supplier. The standard test methods used in proximate analysis were: ASTM D3172 (2013); ASTM D3173 (2017); ASTM D3174 (2012); ASTM D3175 (2020). The procedure for the determination of each of the quantities is briefly outlined below.

Moisture content: About 1 g of sample is weighed in a silica crucible and placed in a hot air oven maintained at 104-110 °C for 1 h. The crucible is then taken out, desiccated, and weighed for the loss in weight to give the moisture content.

Volatile matter: The components of a sample liberated at high temperatures in the absence of air are referred to as volatile matter. The volatile matter in coal is made up of paraffinic and aromatic hydrocarbons, as well as sulfur-containing compounds (Speight, 2015). This test method uses the sample obtained after the determination of moisture

content. About 1 g sample is placed in a platinum or nickel-chromium crucible with a closely fitting cover. The crucible is then placed in a muffle furnace maintained at 950±20 °C for 7 min. The crucible is then taken out, allowed to cool, desiccated, and the loss in weight determined to give the volatile matter content in the sample.

Ash content: Ash is the incombustible residue left after a sample is burned. This test method uses a dried sample obtained after the moisture content determination. About 1 g of sample is placed in a platinum crucible without cover. After being placed in a muffle furnace, the crucible is subjected to a two-stage ashing procedure: (1) heated at 500±10 °C for 1 h, followed by allowing the furnace chamber to heat to 750±15 °C for 2 h, and (2) heated at 750 °C for 2 h. The weight of the residue inside the crucible is taken after it is cooled and desiccated. Ash content is the weight of the residue remaining in the crucible expressed as percent of the original sample weight.

Fixed carbon: It is a calculated value obtained from the summation of moisture content, volatile matter content, and ash content subtracted from 100% (Equation 3.1).

$$\text{Fixed carbon} = 100 - (\text{moisture} + \text{ash} + \text{volatile matter}) \tag{3.1}$$

In Equation 3.1, all quantities are measured in percent.

Fourier transform infrared (FTIR) spectroscopy: FTIR is one of the most preferred infrared (IR) spectroscopy methods. Infrared spectroscopy involves passing IR radiation through a sample. Some of the infrared radiation is absorbed by the sample, while some is passed through (transmitted). The resulting spectrum represents molecular absorption and transmission, forming a molecular fingerprint of the sample. The absorption peaks correspond to the frequencies of vibrations between the bonds of the material's atoms (Thermo Nicolet, 2001). A typical FTIR spectrum consists of wavenumber on the *x*-axis and absorbance on the *y*-axis. The two terms are discussed as follows.

Wavenumber measures the number of cycles a light wave undergoes per unit length, measured in units of cycles per centimetre (cm^{-1}). For example, if a sample shows a peak in FTIR spectrum at 1000 cm^{-1} wavenumber, it means the sample absorbed infrared light that underwent 1000 cycles per cm (Smith, 2011). FTIR spectra are commonly plotted in the mid-infrared range (4000-400 cm^{-1}) or a subset of this range. The wavenumber is proportional to the energy of a light wave (photon) as follows:

$$E = h_P c W \tag{3.2}$$

where, E = light energy; h_P = Planck's constant; c = the velocity of light; W = wavenumber.

The frequency of a light wave is a measure of the number of cycles a wave undergoes per unit time, measured in cycles per second or Hertz (Hz). Wavenumber and frequency are related to each other by Equation 3.3:

$$c = \frac{f}{W} \tag{3.3}$$

where, c = the velocity of light; f = frequency; W = wavenumber. The absorbance spectrum of a sample is calculated from Equation 3.4:

$$A = \log\left(\frac{I_0}{I}\right) \tag{3.4}$$

where, A = absorbance; I_0 = intensity in the incident spectrum; I = intensity in the sample spectrum. Different types of molecular bonds in a material are distinguished by distinct vibration and rotation modes. Depending on the elements and the type of bond, molecular bonds in a material vibrate at different frequencies. The energy associated with these modes is quantified, and a higher level can be attained only if a quantity of energy exactly equal to the difference between two energy levels is transmitted to the molecule (Marsac et al., 2014). A specific type of bond can only achieve a higher activation level by absorbing a quantum that corresponds precisely to a specific infrared frequency. As a result,

characteristic bands in the absorption spectrum of IR radiation can be used to identify types of chemical bonds in a sample (Marsac et al., 2014; Hou et al., 2018). FTIR spectroscopy was performed on a PerkinElmer UATR Two spectrometer, working in attenuated total reflection (ATR) mode (Figure 3.10) with an accumulation of 32 scans in the range 400-4000 cm^{-1}. The analysis was performed on chars and control binder, TPC-10, and PPC-10 char modified binders. Binder samples were dissolved in tetrahydrofuran at a concentration of 10% w/v (weight per volume). A micropipette was used to drop 20 µl of the sample onto the sampling plate for acquiring the spectrum after allowing 5 min for solvent evaporation.

Figure 3.10 FTIR instrument

Thermogravimetric analysis (TGA): TGA is a technique that measures weight changes in a material as a function of temperature (or time) in a controlled environment under a controlled temperature program. During a TGA analysis, the temperature of a sample is gradually raised, and its weight is measured on a high-precision balance. To illustrate thermal transitions in the material, the weight of the sample is plotted against temperature. Such a plot is called the mass-loss curve. TGA is used to evaluate thermal stability and record thermal events in a material, such as loss of volatile components, decomposition temperatures, *etc*. In this study, TGA was performed to monitor the mass changes with temperature ramped from 20 to 1000 °C. A Netzsch STA 449F3 instrument (shown in Figure 3.11) was used with an alumina crucible and 10 °C/min heating rate. Argon gas was

used as purge gas at a 20 ml/min flow rate to prevent combustion throughout the range of temperatures studied. TGA was performed on TPC and PPC particles and the control, TPC-10, PPC-10, TPC-20, and PPC-20 binders.

Figure 3.11 TGA instrument

Optical microscopy: The control and char modified binders were evaluated through optical microscopy using a Leica DM 750 microscope shown in Figure 3.12. About 5 mg of well-stirred and heated binder sample was evenly spread on a glass slide. At a magnification of 40x, the images were acquired using a computer system connected to the microscope and viewed at room temperature (25 °C). The obtained photos were evaluated for a proper contrast between the binder and the chars using the open-source software 'ImageJ'. Original (unaged) binders were used for optical microscopy.

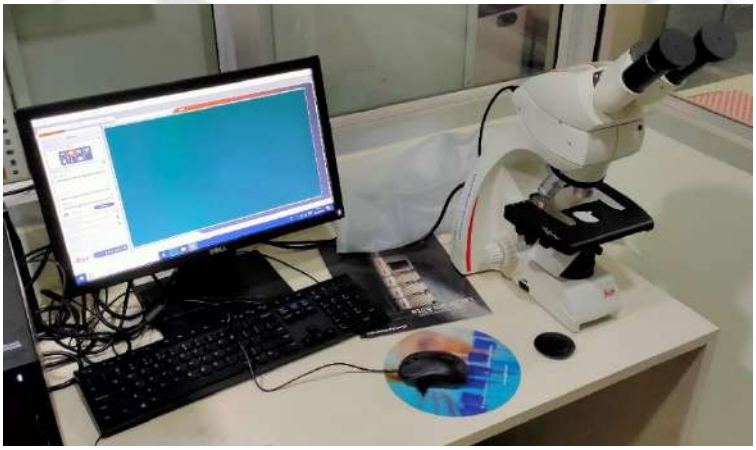

Figure 3.12 Optical microscope system

3.4.2 Task 2: Storage stability evaluation of char-modified binders

Adequate thermal storage stability is required for a modified asphalt binder to ensure the composite's integrity and homogeneity during storage, handling, transportation and construction in the field. A storage-stable formulation of TPC and PPC modified asphalt binders will help to realise the benefits of the modification and promote its use in pavement construction. Cross-linking agents are widely used in binder modification to have adequate storage stability and performance. Task 2 of the study involved evaluating the storage stability of the TPC and PPC modified binders and is further divided into two subtasks. The TPC modified binders were first evaluated under Subtask 2A, and based on the results, the work elements under Subtask 2B (on storage stability evaluation of PPC modified binders) were formalised. Chapter 5 of the thesis presents the results and discussion of works performed under Task 2. The two subtasks are discussed in the following subsections.

3.4.2.1 Subtask 2A: Storage stability evaluation of TPC modified binders

Two cross-linking agents, polyphosphoric acid (PPA) and sulfur, which are quite commonly used with modified binders, were tried at different dosages to ensure adequate storage stability of char modified binders. The thermal storage stability was evaluated for TPC modified binders at multiple dosages of the two cross-linking agents: PPA (0.5, 1.0, and 1.5% by weight of modified binder) and sulfur (0.15, 0.3, and 0.45% by weight of modified binder). Binder with the highest TPC dosage (20%) was used as the control binder in this case to check for storage stable formulation. Softening point difference (SPD) is the conventionally used parameter to quantify the storage stability of binders. In this phase of the study, eight rheology-based separation indices (SIs) derived from temperature sweep and multiple stress creep and recovery (MSCR) tests were also employed in addition to the SPD for storage stability testing. FTIR was also used to investigate storage stability through binder spectra, providing a chemical perspective on the binders' storage stability. Remixing

of the TPC modified binders was also performed to assess its benefits in the retrieval of homogeneity in a TPC modified binder. Figure 3.13 shows the experimental plan for the TPC storage stability evaluation component of Subtask 2A. The following paragraphs provide a brief outline of each experimental technique used along with the operating principles of the instruments.

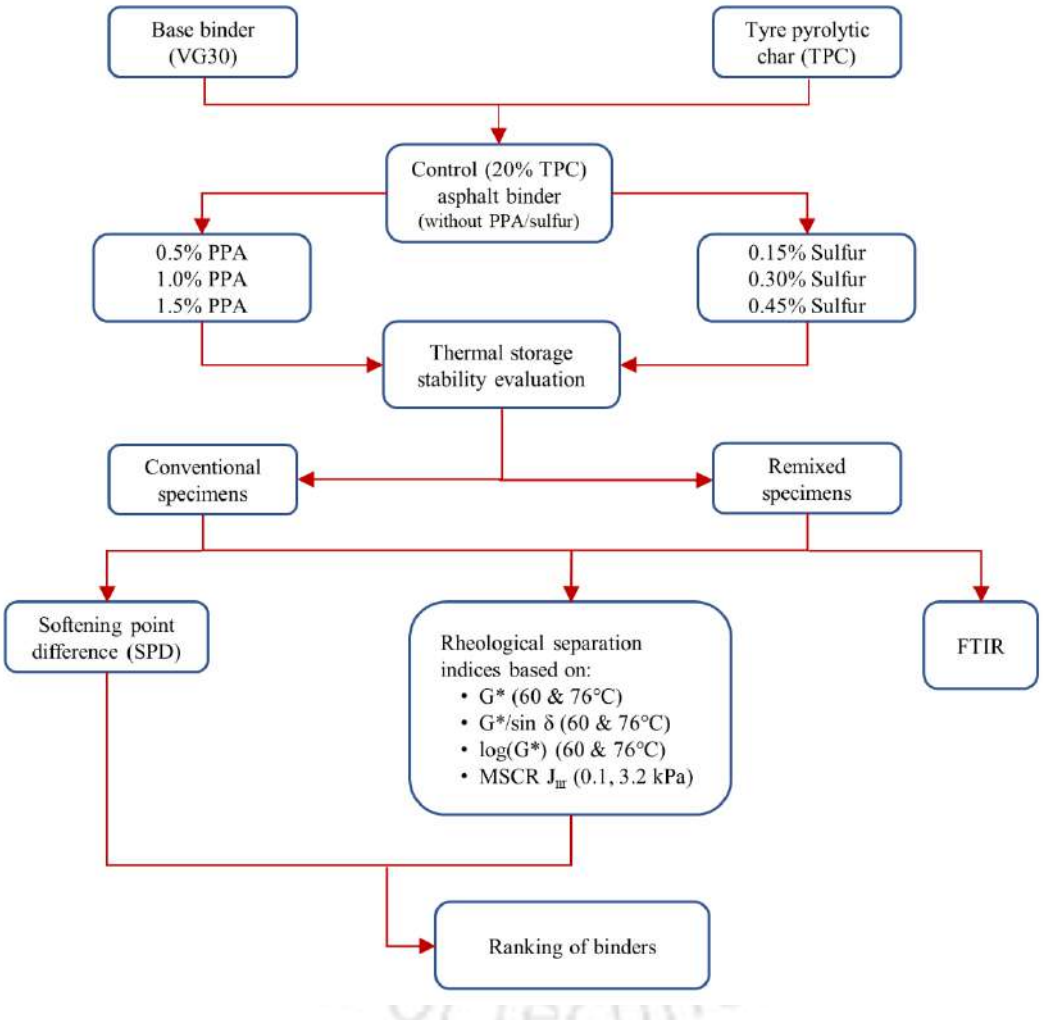

Figure 3.13 Experimental plan for Subtask 2A

Materials (cross-linking agents): The two candidate materials used as thermal stability improvers were PPA and sulfur. PPA is a liquid mineral polymer with a chemical composition of the form: $H_{n+2}P_nO_{3n+1}$, having a minimum of two phosphorous atoms. PPA containing more than 85 wt% phosphorous pentoxide (P_2O_5) was supplied by Zenith India Pvt. Ltd. (Guwahati, India). The elemental sulfur used in the study was supplied by TikiTar

Industries (Vadodara, India) and had a physical appearance of yellow powder with 99.9% purity. Figure 3.14 shows the physical appearance of the two cross-linking agents (PPA and sulfur).

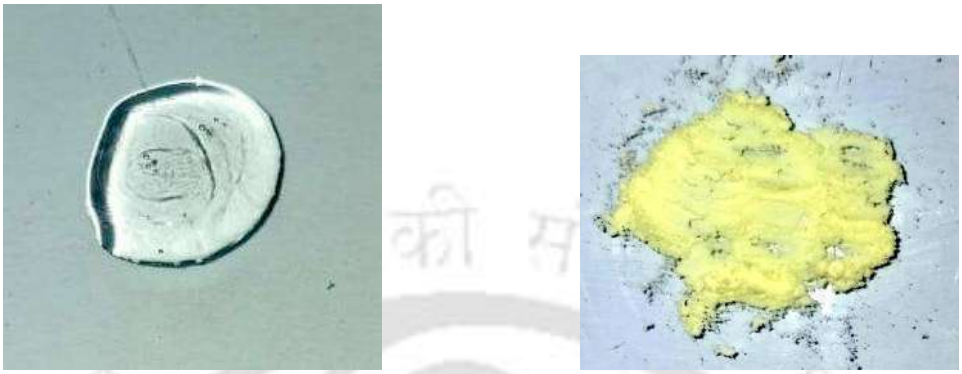

(a) (b)

Figure 3.14 Materials used for storage stability analysis: (a) PPA, (b) sulfur

***Conditioning for storage stability evaluation*:** The TPC modified binders with and without different dosages of sulfur and PPA were subjected to conditioning as per ASTM D7173 (2020). A 50 g properly stirred modified binder specimen was poured into an aluminium tube of 25 mm diameter and 140 mm height (Figure 3.15). The tube was sealed at the upper end using aluminium foil and was conditioned in an oven at 163 °C for 48 h. It was then immediately transferred to a freezer at –10 °C for 4 h. The tube was then sawed in three equal sections. It was ensured that the tube remained vertical throughout the duration of hot storage. Samples from the top and bottom sections were extracted for the evaluation of storage stability in terms of terms of softening point difference and separation indices.

***Softening point difference*:** The softening point of asphalt binders is determined using the ring and ball test. Asphalt's softening point is the temperature at which it softens to a specific degree. The test was carried out in accordance with IS 1205 (1978) specifications. The temperature at which a standard ball passes through a sample of bitumen placed in brass rings and falls through a height of 25 mm is defined as the softening point in the test.

The softening point apparatus used in the study is depicted in Figure 3.16. For quantifying the storage stability, the softening point difference (SPD) parameter for binder specimens extracted top and bottom section were used. The currently enforced Indian standards for polymer-modified bitumen (PMB) (IS 15462, 2019) and rubber-modified bitumen (RMB) (IS 17079, 2019) stipulate maximum SPD limits of 3 and 4 °C for PMB and RMB, respectively.

Figure 3.15 Aluminium tubes used in storage stability tests

Figure 3.16 Softening point apparatus

Separation indices: Table 3.4 presents the complete details of the SIs used in this subtask. Rheological separation indices (SIs) used to quantify storage separation are defined in two forms. In the first form, an SI is defined as the ratio of a rheological parameter measured for the top and the bottom sections. Examples include the ratio of G^*, δ or $G^*/\sin\delta$ measured at a specific temperature (generally a high-service or high-PG temperatures such as 60 °C or 76 °C) (Youtcheff et al., 2005; Al-Abdul Wahhab et al., 2017). It follows that a binder with zero separation would have SI = 1 (values near 1 are desirable). In the second form, SI is defined as the difference between the maximum and the average values of a rheological parameter belonging to either the top or bottom section, expressed as a ratio of the average value (*i.e.*, $(X_{max} - X_{avg})/X_{avg}$, where X is a rheological parameter).

Table 3.4 Details of separation indices for Subtask 2A

Expression for separation index (SI)	*Equation (#)*	*Description*	*Remarks*	*Interpretation*
$SI(G) = \frac{[G^*]_{top}}{[G^*]_{bottom}}$	(3.5)	Defined based on G* of top and bottom sections at 10 rad/s frequency from temperature sweep test	Test temperature: 60 °C for SI(G_60) and 76 °C for SI(G_76)	Values near 1 are desirable
$SI(GSD) = \frac{\left[G^*/\sin\delta\right]_{\max} - \left[G^*/\sin\delta\right]_{avg}}{\left[G^*/\sin\delta\right]_{avg}}$	(3.6)	Defined based on maximum and average G*/sin δ of top and bottom sections at 10 rad/s frequency from temperature sweep test	Test temperature: 60 °C for SI(GSD_60) and 76 °C for SI(GSD_76)	Values near 0 are desirable
$SI(\log G) = \log_{10}\left[\frac{[G^*]_{bottom}}{[G^*]_{top}}\right]$	(3.7)	Defined based on G* of top and bottom sections at 10 rad/s frequency from temperature sweep test	Test temperature: 60 °C for SI(logG_60) and 76 °C for SI(logG_76)	Values near 0 are desirable
$SI(Jnr) = \frac{[J_{nr}]_{\max} - [J_{nr}]_{avg}}{[J_{nr}]_{avg}}$	(3.8)	Defined based on maximum and average J_{nr} of top and bottom sections from MSCR test	Stress levels: 0.1 kPa for SI(Jnr_0.1); and 3.2 kPa for SI(Jnr_3.2) (test temperature: 60 °C)	Values near 0 are desirable
$SPD = SP_{bottom} - SP_{top}$	(3.9)	Defined based on softening point (SP) of top and bottom sections	—	Values near 0 are desirable

Examples of rheological parameters with SIs defined in this formulation include $G^*/\sin\delta$ (Xu et al., 2017; Goli et al., 2017) and J_{nr} (Xu et al., 2017; Wang et al., 2019). In this case, an ideal binder with zero separation would have the same value for the maximum and the average, implying SI = 0 (values near 0 are desirable). A slightly varied formulation is the logarithm (base 10) of the ratio of a rheological parameter for the top and bottom sections (Leng et al., 2019). It follows that lower values are desirable for such a formulation as a binder with zero separation would yield an SI = 0. In the present study, nine SIs (one SPD and eight rheology-based) were considered with the details of expressions presented in Table 3.4.

***Remixing procedure*:** The conventional cigar tube static separation test is not able to clearly capture the handling conditions of modified asphalt binder where they are typically subjected to agitation before being applied/used. In this study, a remixing procedure was also employed during the storage stability evaluation of TPC modified binders. This remixing is expected to provide a more realistic description of the binder separation performance. The purpose of evaluation of storage stability parameters after remixing was to ascertain the benefits of remixing to possibly reduce the degree of separation of a segregated TPC modified binder. Australian specifications have also standardised the remixing procedure (AG:PT/T108, 2006). For remixing, after being subjected to the 48 h static high-temperature storage at 163 °C, all binders were taken out of the oven, placed in a hot sand bath (163 °C), and gently stirred with a narrow glass rod (6 mm diameter) for 10 min (Figure 3.17). The sample tubes were then placed in a freezer at –10 °C for 4 h prior to sawing. Remixed binder samples corresponding to the top and bottom sections were extracted and subjected to the same testing regime as used for conventional (non-remixed) samples.

Figure 3.17 Remixing of storage stability specimens

Dynamic shear rheometer (DSR): As part of the Strategic Highway Research Program (SHRP) research, new methods and parameters were developed to measure more fundamental properties that can be easily related to pavement performance using sound engineering concepts (Bahia and Anderson, 1995a). Asphalt binders behave like a combination of viscous liquids and elastic solids at the temperatures where most pavements carry traffic. The mechanical response of an asphalt binder, a viscoelastic material, depends on temperature and loading frequency (or loading time). Within the linear domain, the behaviour of asphalt binder at any temperature and frequency is characterised by two properties: (1) complex shear modulus (G*)—a measure of the total resistance of the binder against deformation, and (2) phase angle (δ)—a measure of the relative distribution of the G* between elastic and viscous components. Both properties are essential to grading an asphalt binder through Performance Grade (PG) specifications (ASTM D6373, 2016).

DSR is used to determine the rheological viscoelastic properties of asphalt binders. The DSR principle is shown in Figure 3.18. An asphalt binder specimen is sandwiched in the gap between a fixed lower plate and oscillated by the top plate (spindle). To complete one

cycle, the top plate moves from point A to point B, then moves back to point C, and returns to point A. Such a geometry of fixed and oscillating plates is termed parallel-plate geometry. Two such geometries are frequently used with asphalt materials: (1) 25 mm diameter plate with 1 mm gap; and (2) 8 mm diameter plate with 2 mm gap. Frequency is the number of oscillation cycles performed by the DSR per unit time and is measured in rad/s or Hertz (Hz). The DSR oscillates with shear stress or shear strain so that the amplitude of stress or strain varies sinusoidally around zero. The G* is calculated as follows (ASTM D7175, 2015):

$$G^* = \frac{2h}{\pi r^4} \cdot \frac{\tau}{\theta} \tag{3.10}$$

where: τ = torque applied; θ = angular rotation, radians; h = thickness of specimen; r = radius of the specimen (or radius of plate). The phase angle (δ) is calculated by multiplying the time lag between applied stress and produced strain by the frequency. The values of δ for asphalt binders vary between 0° (characteristic of an elastic solid material) and 90° (characteristic of a viscous fluid material). The DSR software performs all measurements, and the final results are displayed to the user.

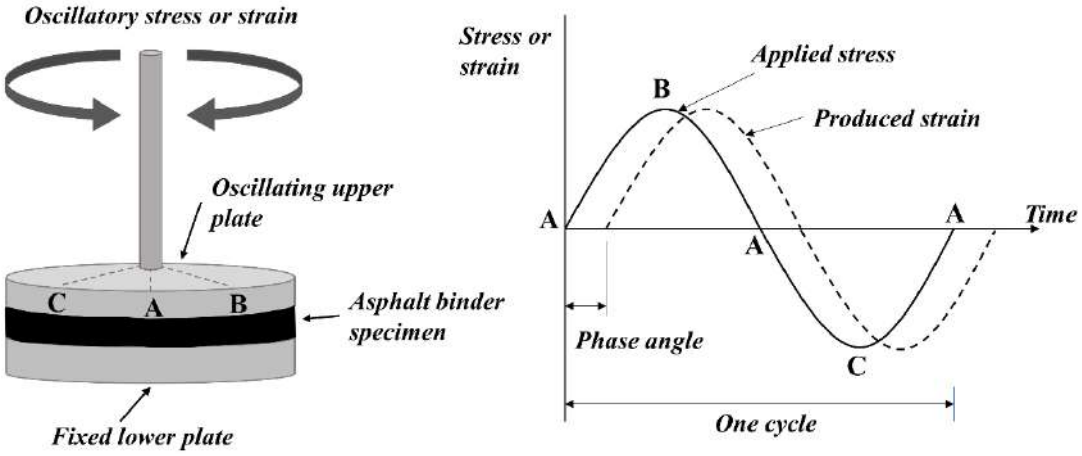

Figure 3.18 Operating principle of DSR oscillatory measurement

The DSR instrument used in this study is shown in Figure 3.19a, which is an Anton Paar Modular Compact Rheometer (MCR) (Model: MCR-102) device. The two test geometries described earlier are shown in Figure 3.19b. The temperature of the binder specimen in the DSR was controlled by solid-state Peltier elements surrounding the sample. The test specimens were prepared using silicone rubber moulds (Figure 3.19c). The asphalt binder was heated in an oven until it became sufficiently fluid to pour. The binder was stirred and then poured into the silicone rubber mould. The mould was allowed to cool to room temperature. The binder specimen was then loosened from the mould and placed on the lower plate. The upper plate (*i.e.*, the spindle) was moved down at pre-set gap (plus an additional gap to create specimen bulge). A trimming tool was used to trim the excess binder from the periphery to obtain a smooth surface and ensure the specimen diameter is the same as the diameter of the spindle and the base plate. The binder specimen was then allowed to reach thermal equilibrium at the desired test temperature for at least 10 min before beginning a test.

Temperature sweep test: Temperature sweep test measures the rheological changes that occur in an asphalt binder sample as it is subjected to a temperature ramp. The temperature sweep test was performed using the DSR with 25 mm parallel plate geometry and a 1 mm gap setting. The specimens tested were extracted from the top and bottom sections of the binder samples after being conditioned for storage stability without remixing protocol and binders extracted from the top and bottom sections of samples after being subjected to the remixing protocol. The temperature sweep test was employed to assess the binders' linear viscoelastic (LVE) properties over a wide temperature range. The tests were performed from 25 to 80 °C at 1.59 Hz (10 rad/s) frequency at low strain (0.1%) to ensure that the binders conformed to the LVE regime.

(a)

(b)

(c)

Figure 3.19 (a) DSR instrument used in the study; (b) DSR parallel-plate geometries: 25 mm (left) and 8 mm (right); (c) silicone rubber moulds: for 25 mm sample (left) and for 8 mm sample (right)

Multiple stress creep and recovery (MSCR): The MSCR test is a quite popular test for characterising rutting resistance of asphalt binders having good correlations with mix and field rutting (D'Angelo, 2009; Saboo and Kumar, 2016; Liu et al., 2021). The standard MSCR test involves ten creep and recovery cycles at two stress levels of 0.1 and 3.2 kPa (ASTM D7405, 2020). Figure 3.20 shows the stress and strain responses as a function of time in one MSCR creep-recovery cycle. The stress is applied for 1 s followed by recovery for 9 s. At the end of the recovery period, one can observe the non-recovered strain (ε_{nr}). From the MSCR test, non-recoverable compliance (J_{nr}) is calculated using Equation 3.11:

$$J_{nr} = \frac{\varepsilon_{nr}}{\sigma} \tag{3.11}$$

where, J_{nr} = non-recoverable creep compliance (kPa^{-1}); ε_{nr} = non-recovered strain at the end of a creep-recovery cycle, and σ = stress level (kPa). In this subtask, the MSCR test was employed to also characterise the storage stability of TPC modified asphalt binders based on J_{nr} values of the top and bottom section binder samples. The test temperature used was 60 °C. Recent advancements in the MSCR characterisation of modified binders have indicated that a steady-state is not achieved in the first ten MSCR cycles and can thus lead to higher variations in binder response (Golalipour, 2011; Golalipour et al., 2017). As a result, thirty MSCR cycles were employed, with J_{nr} data collected from the last five cycles, as previously reported by other researchers (García-Travé et al., 2016; Moreno-Navarro et al., 2019).

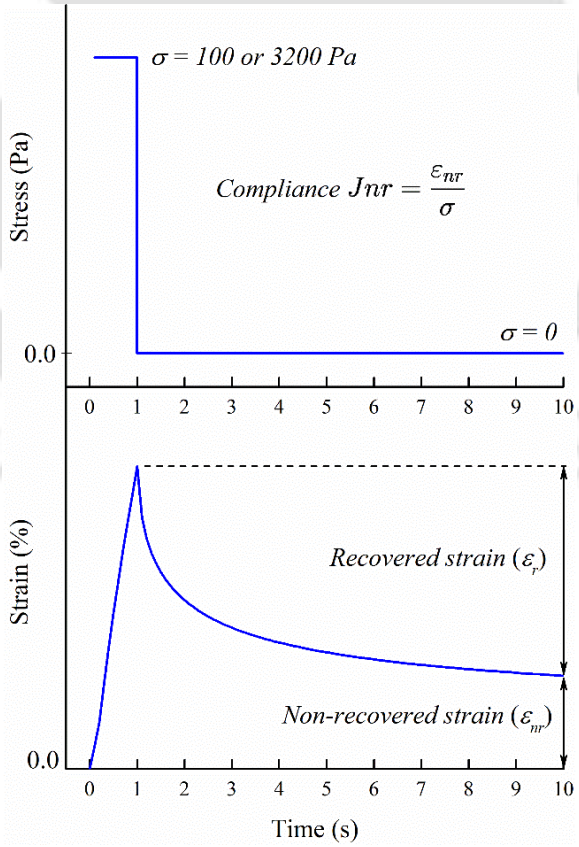

Figure 3.20 Stress and strain response in one MSCR creep-recovery cycle

***FTIR spectroscopy*:** To evaluate storage stability characteristics from a chemical perspective, FTIR spectroscopy was used to compare the proximity of infrared spectra of the top and bottom section binder samples. The procedure of performing FTIR analysis was the same as presented earlier under Task 1. It is briefly described again here, for reasons of completeness. A PerkinElmer UATR Two FTIR spectrometer operating in attenuated total reflection (ATR) mode was used to record FTIR spectra of the binders. Binder samples were dissolved in tetrahydrofuran [$(CH_2)_4O$] at 10% w/v (weight per volume). The solvent was allowed to evaporate for 5 min before acquiring the spectra. A 20 µl amount of the sample was dropped onto the sampling plate for obtaining the FTIR spectrum.

3.4.2.2 Subtask 2B: Storage stability evaluation of PPC modified binders

In Subtask 2B, rheological and spectroscopic evaluations were performed to determine the storage stability characteristics of PPC modified binders. Figure 3.21 shows the experimental plan for Subtask 2B. A PPC modified binder with 20% PPC dosage (with no sulfur) was used as the control. With understanding gained from the TPC storage stability evaluation results (Subtask 2A), elemental sulfur was only used and added to the control binder at three dosages (0.15, 0.30, and 0.45%). In addition to the conventionally used SPD parameter, characterisation of thermal storage stability was attempted using rheology-based separation indices (SIs) derived through temperature sweep, frequency sweep, and MSCR tests. These rheological SIs were based on complex modulus (G*), Superpave rutting parameter (G*/sin δ), Shenoy rutting parameter (SRP), zero shear viscosity (ZSV), and MSCR J_{nr}. Two formulations of each rheology-based separation index were studied: (1) ratio and (2) maximum-average difference formulations. The temperature and frequency dependencies of rheological SIs were also evaluated. FTIR spectroscopy was used to characterise storage stability by comparing the infrared spectra of the top and bottom section binder samples.

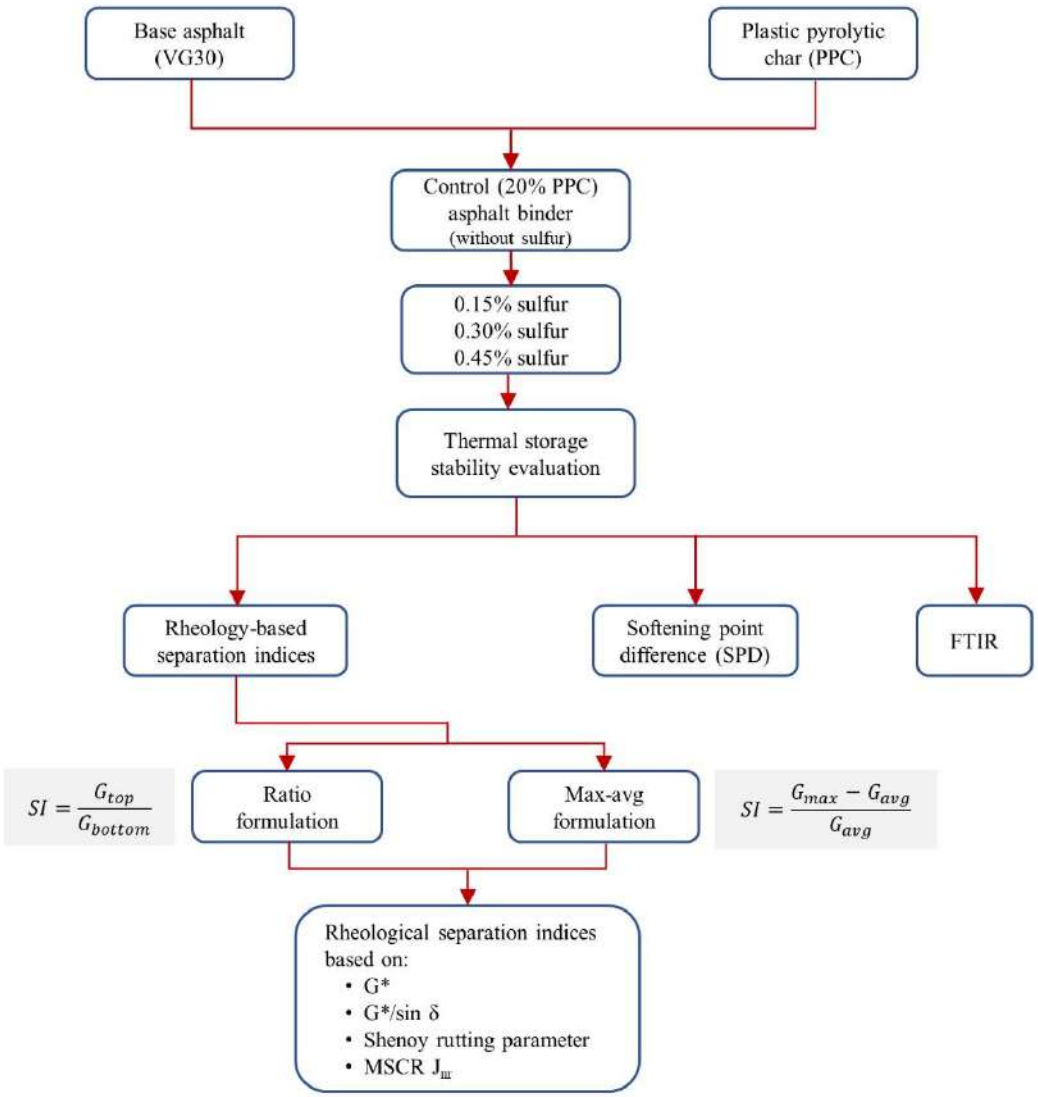

Figure 3.21 Experimental plan for Subtask 2B

The following paragraphs provide a brief outline of each experimental technique used along with the operating principles of the instruments.

Separation indices: Table 3.5 enlists the equations of the separation indices determined in this study on the asphalt binder formulations with and without PPC. In addition to SPD, storage stability was also evaluated through comparison of rheological parameters determined on the storage stability test's top and bottom segment binder samples after conditioning. In addition to conventional Superpave rutting parameter (G*/sin δ) used in performance grading to determine the binder permanent deformation resistance, Shenoy

rutting parameter (SRP), a refinement of the Superpave rutting parameter with the expression G*/(1–(1/(tan δ sin δ)), was also used. With the term (1–(1/(tan δ sin δ)) being more sensitive to δ than sin δ, SRP is reported to maximise the effects of elastic behaviour commonly observed in modified asphalt binders (Shenoy, 2001; Shenoy, 2004; Domingos and Faxina, 2016).

Separation index to characterise the storage stability is formulated in two ways: firstly, in a ratio form (ratio of a rheological property of the top to bottom segment of cigar tube test, the first column of Table 3.5) and secondly in a maximum-average difference form (abbreviated as 'max-avg', the second column of Table 3.5). Separation indices based on G*, G*/sin δ, SRP, and J_{nr} were used in both ratio and max-avg forms. Comparison based on the form of the index would be helpful to understand if the method of formulation of a separation index affects the ranking of binders concerning their storage stability. Further, since G* and δ are properties heavily dependent on temperature and frequency, it is of interest to evaluate the variation of a separation index for a range of temperatures and test frequencies. The separation indices based on G*, G*/sin δ, and SRP were determined as functions of temperature and frequency.

Table 3.5 Formulations and expressions for rheological separation indices of Subtask 2B

Ratio formulation	***Max-avg formulation***	***Remarks***
$\frac{[G^*]_{top}}{[G^*]_{bottom}}$	$\frac{[G^*]_{\max} - [G^*]_{avg}}{[G^*]_{avg}}$	SI based on complex modulus (G*)
$\frac{[G^*/\sin\delta]_{top}}{[G^*/\sin\delta]_{bottom}}$	$\frac{\left[G^*/\sin\delta\right]_{\max} - \left[G^*/\sin\delta\right]_{avg}}{\left[G^*/\sin\delta\right]_{avg}}$	SI based on Superpave rutting parameter (G*/sin δ)
$\frac{[SRP]_{top}}{[SRP]_{bottom}}$	$\frac{[SRP]_{\max} - [SRP]_{avg}}{[SRP]_{avg}}$	SI based on Shenoy rutting parameter G*/(1–(1/(tan δ sin δ))
$\frac{[J_{nr}]_{bottom}}{[J_{nr}]_{top}}$	$\frac{[J_{nr}]_{\max} - [J_{nr}]_{avg}}{[J_{nr}]_{avg}}$	SI based on MSCR unrecovered compliance (J_{nr}) at two stress levels (0.1 and 3.2 kPa)

Rheological tests for determination of separation indices: Three rheological tests were performed using DSR on the control and PPC modified asphalt binder samples extracted from the top and bottom segments in the cigar tube test: temperature sweep, frequency sweep, and MSCR. The 25 mm parallel plate geometry with 1 mm gap was used for all tests. In the temperature sweep test, the test temperature was varied from 40 to 80 °C at 10 rad/s (1.59 Hz) frequency. Test frequencies were varied from 0.1 to 100 rad/s in the frequency sweep test at a constant high pavement temperature of 60 °C. The strain amplitude was fixed at 0.1% for temperature and frequency sweep tests. In the MSCR test, a binder sample was subjected to two stress levels (0.1, and 3.2 kPa) for 30 creep-recovery cycles at each stress level. The average J_{nr} and recovery data of the last five MSCR cycles were used in the determination of separation indices. For an MSCR cycle, creep strain (ε_c: strain at the end of the 1 s creep), unrecovered strain (ε_{nr}: strain at the end of the 9 s recovery) and the recovered strain (ε_r) was measured to obtain the unrecovered creep compliance (J_{nr}) and percent recovery as per Equations 3.11 and 3.12:

$$\text{Recovery} = \frac{\varepsilon_r}{\varepsilon_c} \times 100 \tag{3.12}$$

where, ε_r = recovered strain; and ε_c = strain at the end of creep period.

3.4.3 Task 3: Characterisation of asphalt binders

Asphalt binders must be rheologically characterised since they are viscoelastic materials, and their rheological properties significantly impact the performance of asphalt pavements. Task 3 of this study covered the rheological characterisation of TPC and PPC modified binders and neat (control/unmodified) binders through frequency sweep, high-performance grade (PG), MSCR, G* and δ master curves, G*sin δ, linear amplitude sweep (LAS) tests, and an additional rutting characterisation. These tests encompassed characterisation at different temperatures, frequencies, strain levels, stress levels, and ageing states. The

evaluation of conventional and rheological parameters of the TPC and PPC modified binders was performed under the Subtask 3A. To further examine the binders' rutting performance, Subtask 3B included a multi-temperature (40, 50, 60, and 70 °C) and multi-parameter (Superpave rutting parameter; Shenoy rutting parameter; zero shear viscosity (ZSV); MSCR parameters) rutting characterisation. Chapter 6 of the thesis presents the results and discussion of works performed under Task 3. The experimental programme of two subtasks is discussed in the following subsections.

3.4.3.1 Subtask 3A: Conventional and rheological parameters

Subtask 3A of the study involved evaluating conventional and rheological parameters of the char-modified binders. Figure 3.22 shows the experimental plan for the subtask. The conventional parameters were evaluated on unaged binders and comprised penetration, softening point, and viscosity (at 135 °C) determinations. The rheological parameters for rutting characterisation were performed on both unaged and short-term aged binders (ageing state discussed later for each test).

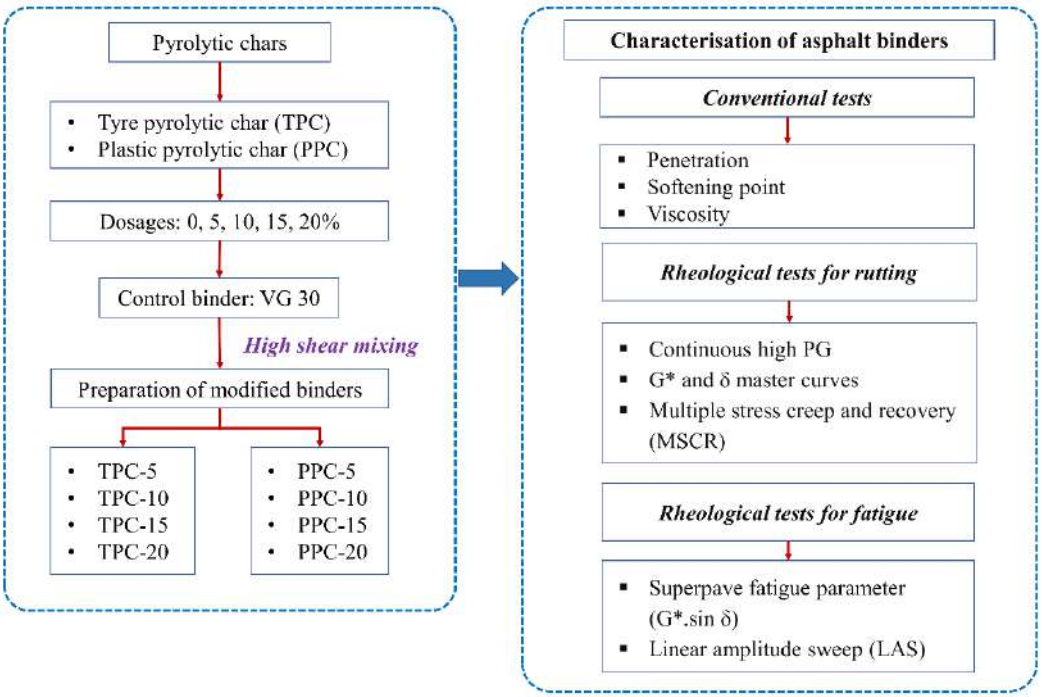

Figure 3.22 Experimental plan for Subtask 3A

The rheological parameters for fatigue characterisation were determined on long-term aged binders. The following paragraphs provide a brief outline of each experimental technique used along with the operating principles of the instruments.

Ageing of binders: During its service life, asphalt binder is subjected to a series of complex physio-chemical processes such as oxidisation, volatilisation, condensation, polymerisation, thixotropy (or steric hardening), causing the binder to become stiffer (harder) and brittle (Traxler, 1961; Petersen, 1984). This phenomenon is usually referred to as asphalt ageing. An asphalt binder ages in the following two main phases: (1) short-term ageing (manifests during production, placement, and compaction of the asphalt mixture), and (2) long-term ageing (manifests during the service life of the asphalt pavement when exposed to the proximate environment). Rolling thin film oven (RTFO) and pressure ageing vessel (PAV) are the two most commonly used devices for simulating short-term and long-term ageing of the binders in the laboratory, respectively (shown in Figure 3.23). In this study, short-term ageing of the binders was performed through a RTFO at 163 °C for 85 min under 4000 ml/min air flow rate per ASTM D2872 (2012). Short-term aged binders were further aged in PAV to obtain long-term aged binders. PAV ageing was performed at 100 °C at 2.1 MPa pressure for 20 h per ASTM D6521 (2018).

(a) (b)

Figure 3.23 (a) RTFO used for short-term ageing; (b) PAV used for long-term ageing

Conventional binder test parameters: The conventional parameters evaluated for the different binders included penetration (IS 1203, 1978), ring and ball softening point (IS 1205, 1978), and viscosity (at 135 °C) values. Original (unaged) binders were used for determination of the conventional parameters. The penetration test was carried out at 25 °C with a 100 g needle to penetrate the binder sample for 5 s, and the penetration was measured in tenths of mm. In softening point test, a ring held the binder sample immersed in water and was heated at a rate of 5 °C/min until a 3.5 g steel ball dropped by a fixed depth. The discussion on viscosity measurement is presented under Task 5.

Continuous high PG: Continuous high PG grades were determined based on DSR test results obtained on unaged and short-term aged binders. The testing was performed at 10 rad/s frequency and 12% strain (for unaged) and 10% strain (for short-term aged) binders per ASTM D6373 (2016). The Superpave rutting parameter G*/sin δ was determined at temperatures varying from 46 °C to 82 °C (at 6 °C intervals), and the temperatures corresponding to a G*/sin δ value of 1.0 and 2.2 kPa were noted for unaged and short-term aged binders, respectively, to obtain the continuous high temperature performance grade (PG). Continuous high PGs were used to calculate the discrete PG of the nine different asphalt binder blends formulated in the study.

Master curves for G* and δ: Master curves allow examination of the binder rheological responses in a broader frequency domain, beyond the frequencies experimentally measurable by a conventional rheometer. G* and δ master curves were constructed based on frequency sweep conducted at 10, 20, 30, 40, 50, 60, and 70 °C. Short-term aged binders were used in frequency sweeps. The reference temperature used was 20 °C, while the frequencies were varied from 0.1 to 100 rad/s at each temperature. The frequency sweeps were performed starting with the lowest temperature and testing at all frequencies (from highest to lowest). All frequency sweeps were performed using a 25 mm diameter DSR

spindle and 1 mm gap setting (except for frequency sweeps at temperatures below 40 °C for which an 8 mm diameter spindle and 2 mm gap was used). The sigmoidal model (Equation 3.13) was used to construct the G* and δ master curves.

$$\log|G^*| = v + \frac{\alpha}{1+e^{\beta+\psi \log f_r}} \tag{3.13}$$

Here, f_r is the reduced frequency, v is the lower asymptote, α is the difference between the values of the upper and lower asymptotes, β and ψ are the parameters defining the shape between the asymptotes and the location of the inflection point. A shift factor (a_T), which represents the temperature dependency of the material, determines the amount of shifting at each temperature T and is defined by Equation 3.14:

$$a_T = \frac{f_r}{f} \tag{3.14}$$

where, f is the loading frequency at temperature T, and f_r is the reduced frequency at the reference temperature. A third-order polynomial equation was used to model the shift factors at different temperatures (Equation 3.15).

$$a_T = a_0 + a_1 T + a_2 T^2 + a_3 T^3 \tag{3.15}$$

Figure 3.24 shows the individual measured data points from frequency sweep tests (as markers), and the G* master curve model function as a smooth line for the control binder.

MSCR test: The MSCR test was used to evaluate the rutting resistance of the different binder blends and was performed on short-term aged binders at a typical high pavement service temperature of 60 °C. According to ASTM D7405 (2020), the test was performed at two stress levels (0.1 and 3.2 kPa), with each cycle consisting of 1 s creep and 9 s recovery. Thirty cycles were used instead of ten MSCR cycles, as recommended in some recent studies (Golalipour et al., 2017). MSCR non-recoverable creep compliance (J_{nr}) and

recovery (*R*) were calculated from the last five creep-recovery cycles (Equations 3.11 and 3.12 presented earlier).

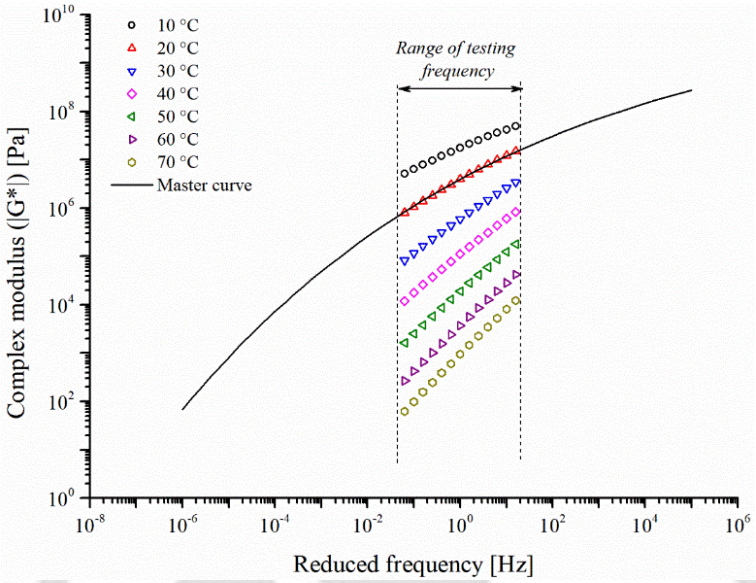

Figure 3.24 G* master curve for control binder showing data points from frequency sweep tests (as markers) and master curve model function as a smooth line

Rheological parameters for fatigue characterisation: The fatigue performance of the binder blends was determined through : (1) Superpave fatigue parameter (G*sin δ), and (2) linear amplitude sweep (LAS) test parameters. These tests were performed on long-term aged binders (aged on RTFO followed by PAV) using the 8 mm diameter DSR spindle and 2 mm gap setting. The reason for utilising a long-term aged binder is that it is thought that the essential period for fatigue cracking in a pavement is later in its service life.

Superpave fatigue parameter: The fatigue parameter (G*sin δ) is currently used in the Superpave PG system to quantify the binder's fatigue resistance. When a binder is subjected to cyclic sinusoidal loading, the dissipated energy per load cycle at a constant strain is expressed as per Equation 3.16:

$$W_c = \pi \cdot \varepsilon_0^2 \cdot (G^* \sin\delta) \tag{3.16}$$

where, W_c = dissipated energy per load cycle; and ε_0 = strain applied during the load cycle. An asphalt binder should be elastic but not too stiff in order to withstand fatigue cracking.

As a result, the G*sin δ parameter should be as low as possible. The parameter was measured on a range of temperatures (10 to 40 °C at a spacing of 3 °C) at 10 rad/s frequency and 1% strain using DSR (ASTM D6373, 2016). The value of G*sin δ is limited to a maximum of 5000 kPa in the Superpave PG specification. The temperature corresponding to a G*sin δ value of 5000 kPa was calculated and reported as the failure temperature with respect to fatigue cracking.

Linear amplitude sweep (LAS): The TPC and PPC modified binders' fatigue performance was also determined through the LAS test. The LAS test is used to evaluate the fatigue damage tolerance of asphalt binders in a shorter time due to an accelerated loading scheme using a sequence of progressively higher strain amplitudes. The test was performed and analysed according to AASHTO TP101 (2014) at an intermediate service temperature of 25 °C. The test included two steps, a frequency sweep and an amplitude sweep. In the first step of the LAS test, a frequency sweep (0.2 to 30 Hz) at a low strain level (0.1%) was performed, and the data acquired at 12 selected frequencies (0.2, 0.4, 0.6, 0.8, 1.0, 2.0, 4.0, 6.0, 8.0, 10, 20, and 30 Hz) were used to obtain material properties in an undamaged state. In the amplitude sweep, the binder specimen was subjected to accelerated fatigue damage with linear ramping of the strain (from 0.1% to 1%, and then increased to 30% at 1% interval) at 10 Hz frequency. Binder fatigue life (number of cycles to failure = N_f) was calculated from the LAS test using Equation 3.17. The parameters A and B of the fatigue equation are calculated from viscoelastic continuum damage (VECD) analysis per AASHTO TP101 (2014).

$$N_f = A.\varepsilon^{-B} \tag{3.17}$$

Here, N_f is the number of LAS cycles to failure; ε is the shear strain (%), and A, B are fatigue equation parameters.

3.4.3.2 Subtask 3B: Advanced rutting characterisation

Rutting is one of the most common types of asphalt pavement distresses. Under heavy traffic loads, rutting appears as a longitudinal depression along the wheel path. A critical rutting mitigation approach is to improve the rheological properties of asphalt binders. Although rutting is a high-service temperature phenomenon, it should be appreciated that the phenomenon does not occur at a single temperature and may mobilise over a range of 'high' temperatures that should reflect the high summer temperatures observed on a project location. Evaluation of rutting resistance of TPC and PPC modified binders under various temperatures and stress levels can be quite useful for comparison. In Subtask 3B, the rutting performance of modified binders was evaluated at multiple temperatures using five rutting related rheological parameters: (1) Superpave rutting parameter (G*/sin δ); (2) Shenoy rutting parameter; (3) zero shear viscosity (ZSV); (4) non-recoverable creep compliance (J_{nr}) from MSCR test; and (5) non-recoverable strain rate ($\Delta\varepsilon_{nr}$) from the MSCR test. Figure 3.25 shows the experimental plan of work elements under Subtask 3B. The following paragraphs provide a brief background and discussion of each of the five rutting factors and their methodology.

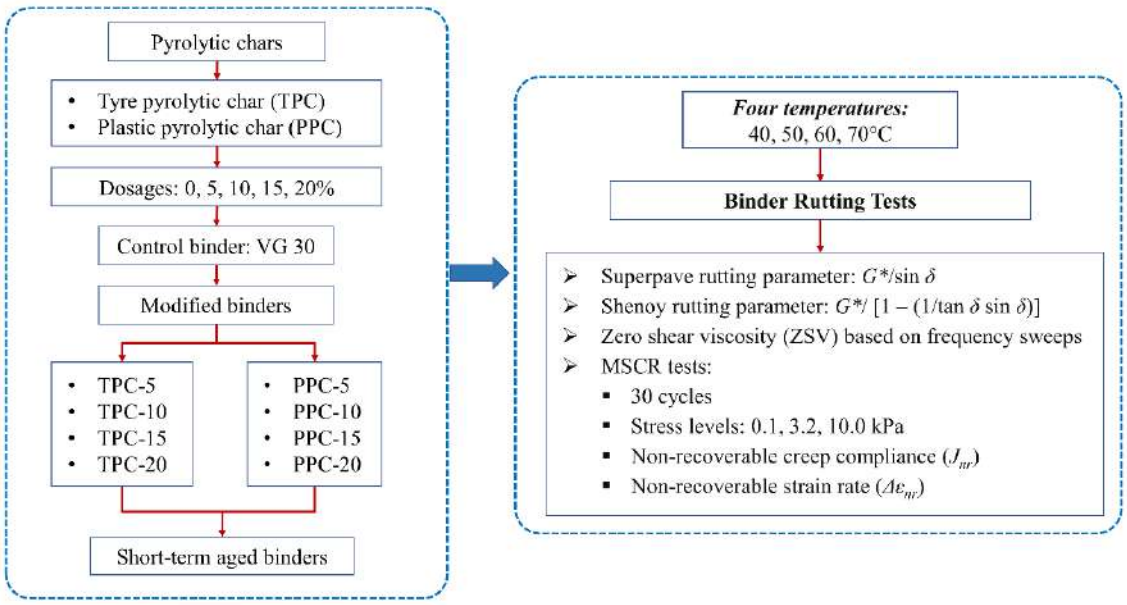

Figure 3.25 Experimental plan for Subtask 3B

***Background and methodology for advanced binder rutting characterisation*:** With the emergence of Superpave PG binder specifications in the 1990s, the degree of empiricism associated with conventional properties (such as penetration, softening point, Saybolt-Furol viscosity) was reduced to a great extent, and at the same time, a consensus was formed to use fundamental rheological methods for proper characterisation of asphalt binders considering the viscoelastic nature of the material. The Superpave rutting parameter (G*/sin δ) is based on the complex shear modulus (G*) and phase angle (δ) measured on DSR at a particular frequency and strain. The expression for G*/sin δ assumes rutting as a stress-controlled, cyclic loading phenomenon and is based on minimising the dissipated energy in each cycle of loading (W_c) subjected to constant stress given by Equation 3.18:

$$W_c = \pi \cdot \sigma_0^2 \cdot \frac{1}{G^*/\sin\delta} \tag{3.18}$$

where, σ_0 is the shear stress. Equation 3.18 indicates that to reduce the work dissipated per loading cycle, the parameter G*/sin δ should be increased, and therefore a higher value of this parameter indicates a better rutting resistance. Despite being included in the Superpave PG specifications for asphalt binders, many researchers have highlighted limitations of this parameter (Domingos and Faxina, 2016; Liu et al., 2021) and have put forth some refinements.

Shenoy (2001) proposed one such refinement termed the Shenoy rutting parameter presented in Equation 3.19.

$$\text{Shenoy rutting parameter} = \frac{G^*}{1 - \frac{1}{\tan\delta \sin\delta}} \tag{3.19}$$

The parameter is based on unrecovered strain and emphasises the effect of elasticity in terms of better sensitivity to δ. A lower unrecovered strain in the binder is associated with

an increased value of this parameter and is desirable for an improved rutting resistance. Despite the merit offered over the Superpave rutting parameter, this parameter has a limitation that the parameter's denominator vanishes when the phase angle is lower than 52°. In that scenario, Shenoy (2004) presented an alternative to use $(\sin \delta)^9$ in the denominator of the parameter. Superpave and Shenoy rutting parameters were measured following ASTM D6373 (2016) at 10 rad/s frequency and 10% strain.

Another rheological parameter quite often used for rutting characterisation is zero shear viscosity (ZSV). ZSV is an intrinsic characteristic of binder viscosity measured when the shear rate approaches zero, and the binder reaches a steady state of flow. Some of the frequently used models to estimate ZSV use complex viscosity (η^*) measurement from DSR with varying frequency. The Cross model, presented in Equation 3.20, was used to determine ZSV for asphalt binders measured through frequency sweep tests:

$$\eta^* = \frac{\eta_0 - \eta_\infty}{1 + (Kf)^m} + \eta_\infty \qquad (3.20)$$

where, η^* = complex viscosity at frequency f (rad/s), η_0 = zero shear viscosity, η_∞ = infinite shear viscosity at infinite frequency, K and m = model parameters. To measure ZSV, frequency sweep tests were conducted from 0.1 to 100 rad/s frequencies. A low strain of 0.1% was used to ensure the linearity of response of the binders at all frequencies and temperatures. A higher numerical value of ZSV is desirable for better resistance against rutting.

The widely preferred recent advancement in the rutting characterisation of binder is the MSCR test that acknowledges the significant role of non-recovered deformation of bitumen on the rutting performance. The concept of the MSCR test is that after shear stress is removed, the viscoelastic strain created in the creep portion may be recovered, allowing

the permanent (or unrecovered) strain to be separated from the overall strain, which is better connected with field rutting (Liu et al., 2021). The test methodology applies loading pulses with rest periods at multiple stress levels to simulate the actual traffic variables. The standard MSCR test comprises 10 cycles at two different stress levels (0.1 and 3.2 kPa), where one cycle includes a 1 s creep and a 9 s recovery time without any time lag between the cycles. Non-recoverable creep compliance (J_{nr}) is the MSCR parameter used for rutting characterisation and is the ratio of the unrecovered strain at the end of an MSCR cycle to the applied stress (Equation 3.11). J_{nr} offers a leap over other rutting parameters because of its suitability for characterising both neat and modified binders and is sensitive to temperature and stress levels. Percent recovery in an MSCR cycle is calculated from the peak (or creep) strain and the unrecovered strain as shown in Equation 3.12.

Recent advances in the MSCR methodology for characterisation of modified binders have indicated that a higher stress level than the currently used 0.1 and 3.2 kPa is needed to achieve a state of stress representative of that encountered by modified binders in pavements (Golalipour, 2011; Golalipour et al., 2017). A third stress level of 10 kPa was therefore used in this study. Further, thirty MSCR cycles were used, as recommended in some recent studies (García-Travé et al., 2016; Moreno-Navarro et al., 2019) and the J_{nr} and recovery data were obtained from the last five creep-recovery cycles.

Moreno-Navarro et al. (2019) pointed that the J_{nr} is calculated as the average value obtained for a specific number of creep-recovery cycles; however, it does not provide information on how the rutting behaviour evolves with the increasing number of MSCR cycles. They proposed a new parameter called the non-recoverable strain rate ($\Delta\varepsilon_{nr}$) given by Equation 3.21 and measured in the units of %/cycle:

$$\Delta\varepsilon_{nr} = \frac{\varepsilon_{nr,30} - \varepsilon_{nr,15}}{30 - 15} \tag{3.21}$$

where $\varepsilon_{nr,30}$ = cumulative non-recoverable strain after 30 cycles and $\varepsilon_{nr,30}$ = cumulative non-recoverable strain after 15 cycles. $\Delta\varepsilon_{nr}$ is the fifth advanced binder rutting characterisation parameter used in this study. The calculation of the parameter is schematically illustrated in Figure 3.26.

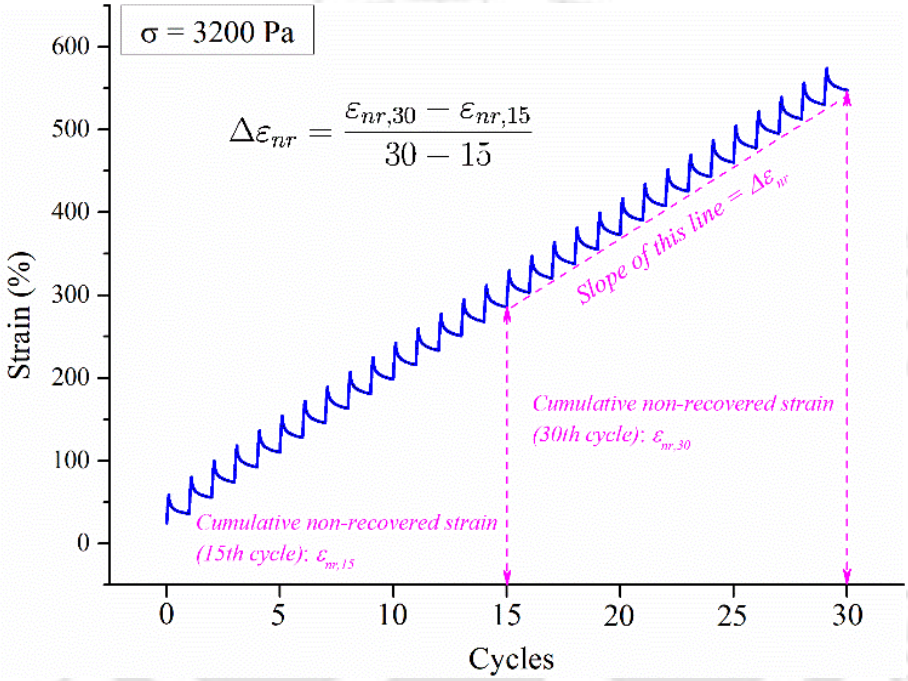

Figure 3.26 Illustration of MSCR non-recoverable strain rate ($\Delta\varepsilon_{nr}$) parameter

The parameter $\Delta\varepsilon_{nr}$ is analogous to the development of accumulated unrecovered strain as commonly found from the cyclic rutting tests performed on asphalt mixes (*e.g.*, dynamic creep test, cyclic triaxial test, wheel-tracking test). A higher $\Delta\varepsilon_{nr}$ would indicate a higher rate of the development of non-recoverable strain in the binder with the progression of MSCR cycles, and hence a lower rutting performance. In this manner, both J_{nr} and $\Delta\varepsilon_{nr}$ have the similar interpretation in terms of binder rutting resistance: lower values indicate better performance.

3.4.4 Task 4: Ageing characterisation of TPC and PPC modified binders

Asphalt is prone to chemical oxidation by reacting with ambient oxygen since it is a natural organic end product of crude petroleum derived from ancient organisms. Asphalt ageing is important in practice because it causes the asphalt to harden, resulting in a loss of favourable physical qualities. Oxidative age-hardening contributes significantly to pavement embrittlement in asphalt pavements, eventually leading to severe pavement cracking (Petersen, 2009; Sirin et al., 2018). The ageing of the asphalt binder occurs in two stages. The first stage is short-term ageing, which occurs during the asphalt mixture's production, placement, and compaction. Because of the high temperatures and huge surface area of the heated aggregates, asphalt binders are subjected to fast oxidation and volatilisation in this stage. The second stage is long-term ageing, which occurs much slowly and after the asphalt mixture has been placed and compacted and occurs during the pavement's service life. In this stage, volatilisation is minimal, and oxidation is thought to be the dominant ageing mechanism. It is therefore vital to understand and investigate the ageing properties of TPC and PPC modified binders.

Task 4 of this research study was carried out to evaluate the ageing resistance properties of TPC and PPC modified binders. Nine binder formulations evaluated were: control, TPC-10 and PPC-10 binders under three ageing states (unaged, short-term aged, and long-term aged). Under this task, to imitate short-term and long-term ageing conditions, the asphalt binders were first treated in a rolling thin film oven (RTFO) and then in a pressure ageing vessel (PAV). The characterisation of ageing characteristics behaviour was attempted using four rheological ageing indices based on complex modulus (G*), phase angle (δ), ZSV, and non-recoverable creep compliance (J_{nr}) from the MSCR test. These parameters were measured through a DSR. FTIR spectroscopy analysis was also then used to investigate changes in chemical composition due to ageing in the modified binders. Figure 3.27 shows

the experimental plan for Task 4. Chapter 6 of the thesis presents the results and discussion of works performed under Task 4. The following paragraphs provide a brief outline of the methodology used along with the operating principles of the instruments.

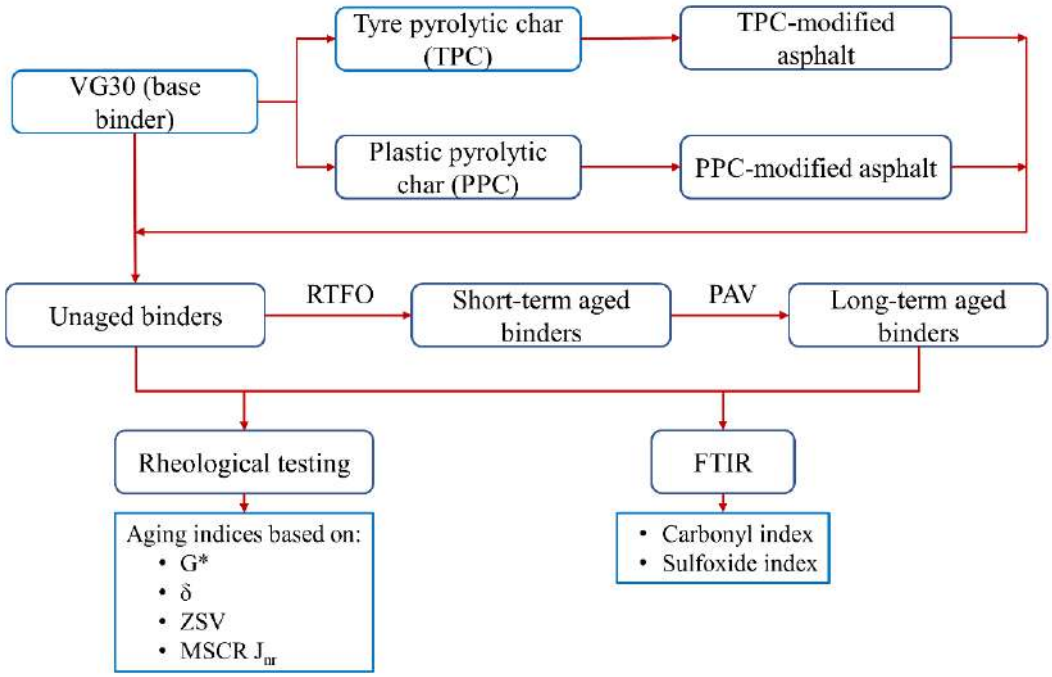

Figure 3.27 Experimental plan for Task 4

Short-term ageing: Short-term aged binders were obtained through a rolling thin film oven (RTFO) (Figure 3.23a) operating at 163 °C for 85 min and airflow of 4000 ml/min according to ASTM D2872 (2012). In this test, a 35 g well-heated asphalt binder sample is placed and spread in a glass bottle having a top aperture (Figure 3.28). The glass containers are positioned in a carriage with its horizontal axis and the bottle aperture facing a jet of air. The oven is set to 163 °C and the carriage is rotated at 15 rev/min for 85 min. This ageing technique exposes an asphalt binder film to heat and oxidation on a continual basis, simulating the conditions encountered in hot mix asphalt manufacturing (Shalaby, 2002).

Figure 3.28 RTFO glass bottle before (left) and after the test (right)

Long-term ageing: Long-term ageing is used to simulate several years of binder ageing in the field and makes use of the short-term aged binder. The pressure ageing vessel (PAV) shown in Figure 3.23b is the equipment used for this purpose. As compared to RTFO ageing that uses oven ageing, pressure is also used as a factor in the PAV treatment to cause accelerated ageing. The use of pressure stems from the fundamental understanding that asphalt oxidation is dependent on a physical diffusion process, and by increasing the pressure, oxygen can be forced much more quickly into the asphalt films (Bahia and Anderson, 1995b).

Figure 3.29 Binder samples in PAV pans after undergoing PAV ageing and before vacuum degassing

Binders were simulated for long-term ageing on the PAV according to ASTM D6521 (2018). The ageing temperature was 100 °C with air pressure maintained at 2.1 MPa for 20

h. All binder samples were then vacuum degassed at 170 °C under an absolute pressure of 15.0 kPa. Figure 3.29 shows PAV conditioned binder samples in standard pans before vacuum degassing.

Rheological ageing indices: To quantitatively characterise the ageing behaviour, four ageing indices (AI) were formulated, shown in Equations 3.22-3.25. These indices are based on binder complex modulus (G*), phase angle (δ), ZSV, and MSCR J_{nr} determined before and after being subjected to ageing. Rheological ageing indices, defined as the ratio of a parameter before and after ageing, have been used by other researchers in asphalt ageing studies (Iqbal et al., 2020; Wang et al., 2020b). The rheological indices are defined such that a lower value of each ageing index represents more minor changes due to ageing in the rheological property under consideration and, therefore, a lower ageing susceptibility. This definition allows convenience to interpret the rheological as well as FTIR-based indices.

$$AI(G^*) = \frac{G^* \text{ in aged state}}{G^* \text{ in unaged state}} \tag{3.22}$$

$$AI(\delta) = \frac{\delta \text{ in unaged state}}{\delta \text{ in aged state}} \tag{3.23}$$

$$AI(ZSV) = \frac{ZSV \text{ in aged state}}{ZSV \text{ in unaged state}} \tag{3.24}$$

$$AI(J_{nr}) = \frac{J_{nr} \text{ in unaged state}}{J_{nr} \text{ in aged state}} \tag{3.25}$$

Rheological tests: Rheological properties of the asphalt binders were measured on a DSR. Frequency sweeps were conducted in the range of 0.1-100 rad/s at 60 °C at low strain (to measure the binder properties in the linear viscoelastic domain) on binders of all three ageing states. G* and δ were determined at different frequencies. Based on complex

viscosity data derived from oscillatory frequency sweep tests, the ZSV of the binders was determined using the Cross-model (Equation 3.20). MSCR test was conducted at 60 °C to investigate the high-temperature rutting resistance of the binders under different ageing states. Two stress levels (0.1, 3.2 kPa) were used with 1 s creep and 9 s recovery intervals. A total of 20 cycles were used at 0.1 kPa (10 cycles for conditioning and subsequent 10 cycles for data acquisition), and 10 cycles were used at 3.2 kPa stress levels as per ASTM D7405 (2020). Non-recoverable creep compliance (J_{nr}) was calculated using Equation 3.11.

***FTIR spectroscopy*:** Chemical composition of asphalt binder changes with ageing. During oxidative ageing, the chemical groups in the asphalt binder react with oxygen, and therefore monitoring the changes in oxygen-based functional groups can be quite helpful to understand changes brought in the binder due to ageing. FTIR was used to observe the progress of chemical functionalities for control, TPC-modified and PPC-modified binders subjected to short- and long-term ageing. The FTIR methodology has been previously discussed under Tasks 2 and 3, and the same was followed in the case of this task. Quantitative analysis of the FTIR spectra was performed by calculating carbonyl (C=O) index (CI) and sulfoxide (S=O) index (SI) based on the peaks in distinct regions of the spectra. The increase in carbonyl and sulfoxide indices with ageing can be related to the simultaneous occurrence of oxidation, dehydrogenation, and crosslinking events throughout the ageing process (Singh et al., 2017). Figure 3.30 shows the distinct regions corresponding to CI and SI in shaded colours for an asphalt binder sample. The two indices are calculated using Equations 3.26-3.27:

$$CI = \frac{A_{1678-1725}}{\sum A} \tag{3.26}$$

$$SI = \frac{A_{1010-1043}}{\sum A} \tag{3.27}$$

where, $\sum A = A_{1010-1043} + A_{1350-1510} + A_{1535-1625} + A_{1678-1725}$

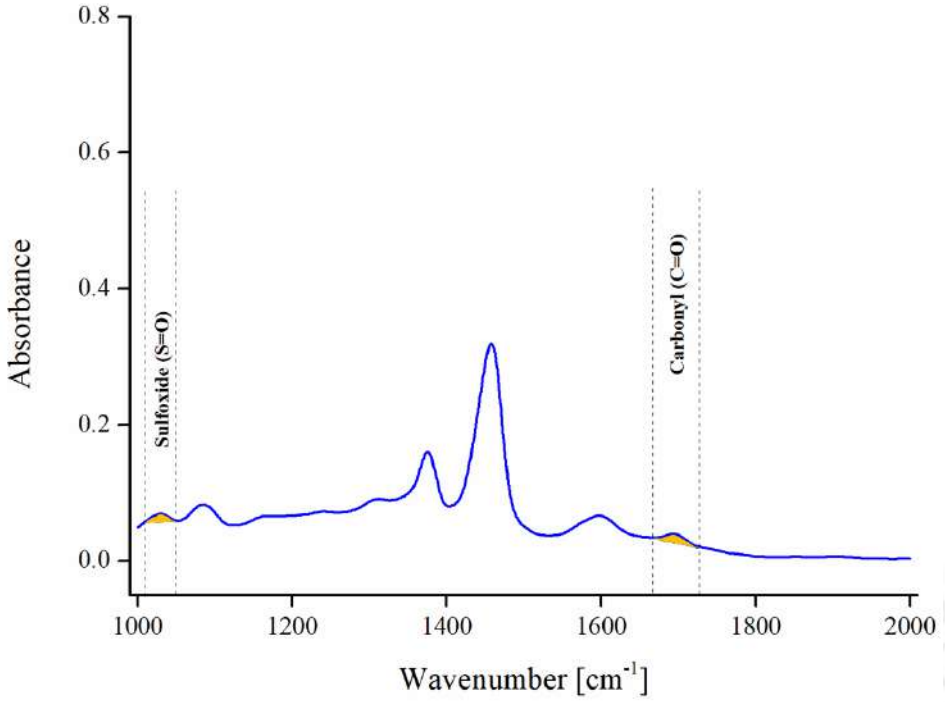

Figure 3.30 Illustration of areas under FTIR spectrum for carbonyl and sulfoxide indices

3.4.5 Task 5: Determination of production temperatures

Selecting the correct and reasonable production temperatures for modified asphalt binders is critical for the subsequent preparation of asphalt mixtures. The 'production' temperatures refer to the temperatures used to mix the aggregates and binder and the temperatures desired for compaction of the resulting asphalt mix to achieve the required in-situ density. Production temperatures are also known as 'mixing and compaction' temperatures.

Under this task, the production temperatures (mixing and compaction temperatures) were determined for the control, and TPC and PPC modified binders. Four different approaches, based on the rheological behaviour of modified asphalt binders, were used to determine the production temperatures. Figure 3.31 shows the experimental plan followed to evaluate the production temperatures of modified binders with different doses of TPC and PPC. The candidate methods included the conventional equiviscous (EV) method, high

shear viscosity (HSV) method, steady shear flow (SSF) method, and the phase angle (PA) method. The EV and HSV methods were implemented on a rotational viscometer, while the SSF and PA methods utilised the measurements through a DSR. The experimental techniques and operating principles are discussed as follows.

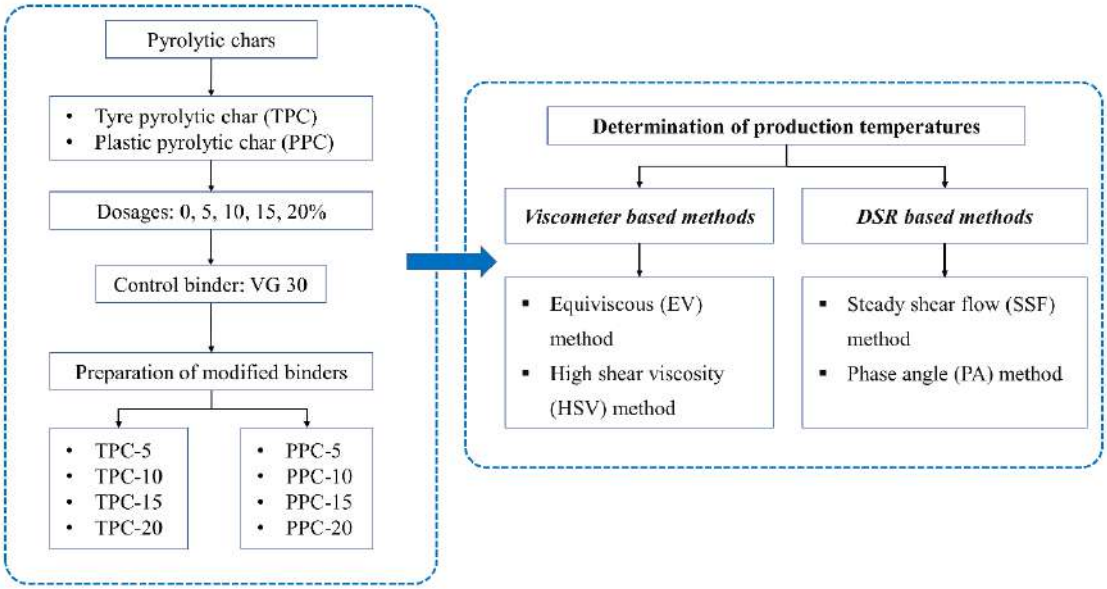

Figure 3.31 Experimental plan for Task 5

Rotational viscometer: The viscosity measurements on binders were made using a Brookfield DV-II+Pro rotational viscometer in accordance with ASTM D4402 (2015). The viscometer is shown in Figure 3.32a. The test setup consists of a temperature conditioning and controlling unit to maintain a constant temperature of asphalt sample during testing. Two spindles (#21 and #27) were used for viscosity measurement (Figure 3.32b). A 10.0 g binder sample was tested with a #27 cylindrical spindle, while 9.0 g sample was used with a #21 spindle. For viscosity measurement, the desired amount of asphalt binder was poured into the sample chamber and kept in the 'Thermosel' unit for a minimum of 10 min for temperature equilibration. The viscometer motor was then started at selected rotational speed to produce a resisting torque within 98% of the full-scale capacity of the instrument. The rotational speed was maintained for 5 min to allow the sample to equilibrate. After

that, the viscosity measurement was recorded in centipoise (cP) from the digital display of the viscometer.

(a) (b)

Figure 3.32 (a) Brookfield rotational viscometer, (b) spindles used in rotational viscometry

In a rotational viscometer, viscosity is calculated by computing the torque sufficient to keep a cylindrical spindle spinning at a constant speed while immersed in an asphalt binder sample at a constant temperature. The reported torque is directly proportional to the viscosity of the asphalt binder. The equations used for calculating viscosity from torque and speed (expressed in angular speed) are as follows (Al-Khateeb, 2020):

$$\eta = \frac{\sigma}{\gamma} \tag{3.28}$$

$$\sigma = \frac{\tau}{2\pi R_s^2 L} \tag{3.29}$$

$$\gamma = \frac{2\omega \cdot R_c^2 R_s^2}{x^2 \cdot \left(R_c^2 - R_s^2\right)} \tag{3.30}$$

Here, η = dynamic viscosity (Pa.s); σ = shear stress (Pa); γ = shear rate (s^{-1}); τ = torque; L = effective spindle length (m); R_s = spindle radius (m); R_c = container radius (m); ω =

rotational speed (rad/s); x = radial location to calculate shear rate (m). Built-in software of the viscometer typically facilitates these computations by recording torque (between 0 to 98% of the instrument's capacity) and then multiplying it by a set of constants specific to the equipment model and dividing the product by the current speed of the viscometer spindle in rotation per minute (RPM). The expression used by Brookfield DV-II+Pro rotational viscometer model is given below (Brookfield, 2021):

$$\text{Viscosity (cP)} = \frac{100}{RPM} \cdot TK \cdot SMC \cdot \text{Torque} \tag{3.31}$$

where, TK = torque constant; SMC = spindle multiplier constant; RPM = spindle speed in rpm; Torque = viscometer torque percentage.

The DSR was used for performing SSF and PA methods for the determination of production temperatures. The details on the basic measurement principle of DSR has been presented under Task 2. Chapter 7 of the thesis presents the results of work performed under Task 5. It was considered appropriate to include the detailed description of production temperature determination methodologies (EV, HSV, SSF, and PA methods) in Chapter 7 because it is presented alongside the results obtained for the different binders.

3.4.6 Task 6: Design and performance evaluation of mixtures

Task 6 of the study included designing and then evaluation of performance characteristics of asphalt mixes fabricated with control (unmodified) and TPC/PPC modified binders. Mix designs were performed for each of the nine binder formulations used in this study. Bituminous mixes are currently designed in India as per the Marshall method (MoRTH, 2013) and it was thus followed in the study for mix design. Under performance evaluation, asphalt mixes were evaluated for resistance against rutting (through static creep, dynamic creep, and Hamburg wheel tracking device (HWTD) tests), moisture damage (through tensile strength ratio (TSR) and retained Marshall stability (RMS) tests), cracking (through

semi-circular bend (SCB) test), and fatigue (through indirect tensile fatigue test (ITFT)). Leachate toxicity tests were also conducted on asphalt mixes to ensure that their use is safe for the environment. Pavement structural analysis was then further carried out using IITPAVE software based on the resilient modulus values of different mixes. Figure 3.33 presents the experimental plan for Task 6. The results and discussion for work performed under Task 6 are presented in Chapter 8 of the thesis.

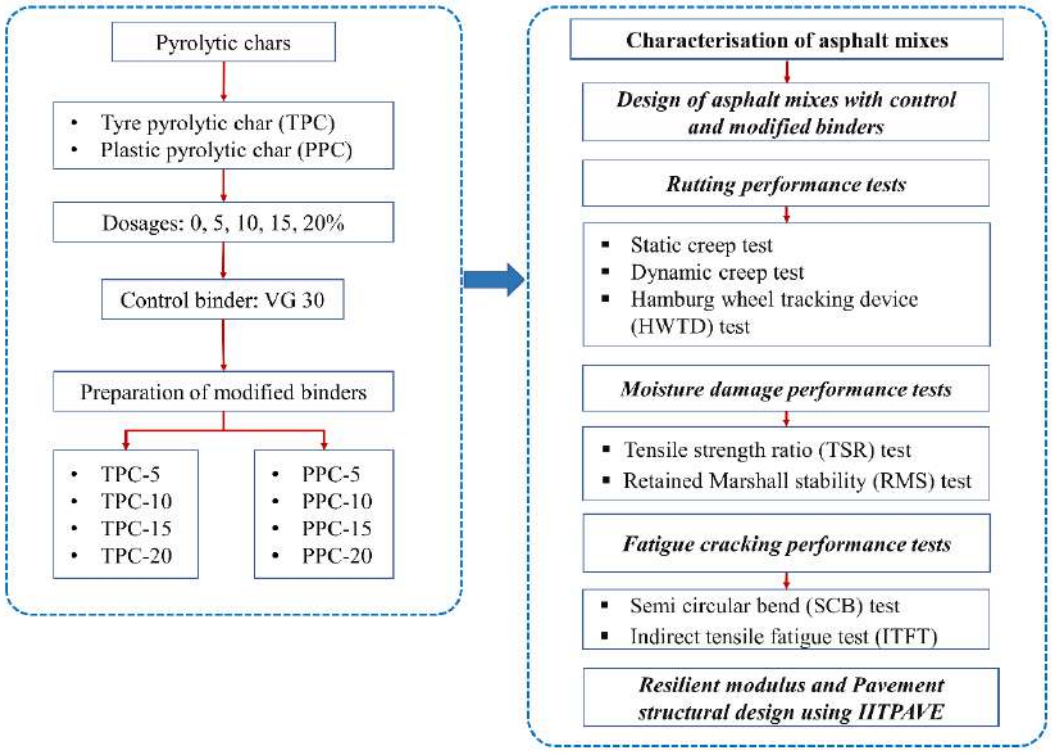

Figure 3.33 Experimental plan for Task 6

3.4.6.1 Design of asphalt mixes

Bituminous Concrete (BC) mix, a conventionally used as wearing course in India, with 13.2 mm nominal maximum aggregate size (NMAS) aggregate gradation (Figure 3.2), was used to fabricate the mixes per the specifications of the Ministry of Road Transport and Highways, India (MoRTH, 2013). Different mix designs were performed for each of the nine binders formulated in this study. Under mix design, three Marshall specimens of 100 mm diameter and about 63.5 mm height were prepared at five variable binder contents of

4.5, 5.0, 5.5, 6.0, and 6.5% (by weight of the mix). The compaction effort given to each specimen was 75 blows of the Marshall impact compactor on each face. The specimens were tested for volumetric parameters [air voids (VA), voids in mineral aggregates (VMA), and voids filled with bitumen (VFB)], and Marshall parameters (stability and flow). The optimum binder content (OBC) was selected as the one corresponding to 4% air voids content while satisfying the other mix design requirements for VMA, VFB, stability, and flow. Table 3.6 shows the mix design requirements for a BC-2 gradation mix as per MoRTH (2013) specifications.

Table 3.6 Requirements for a BC-2 mix (MoRTH, 2013)

Property	**Requirement**
Stability, kN at 60 °C	Min. 9 kN
Flow, mm	2-4
Air voids, %	3-5
Voids in mineral aggregates (VMA), %	Min. 14%
Voids filled with bitumen (VFB), %	65-75
Tensile strength ratio (TSR), %	Min. 80%

3.4.6.2 Preparation of asphalt mixes

The procedure stated in ASTM D6926 (2016) was followed to prepare asphalt mixes for mix design and performance evaluation. The aggregates obtained from the crusher plant were cleaned, dried, and sieved into the size fractions as needed for the selected BC-2 gradation. Aggregate batches were then prepared and placed in a hot air oven at 175 °C for at least 4 h. The asphalt binders were also heated to the corresponding mixing temperatures (the production temperatures are presented in Chapter 7). The required quantity of binder was then introduced to the heated aggregates and mixed for about 30-40 s at the respective mixing temperature. The prepared mix was transferred to a rectangular tray and allowed to condition for 2 h at the compaction temperature to undergo short-term ageing, as stipulated by AASHTO R30 (2006). The short-term ageing of the loose mix allows asphalt binder

absorption into the aggregates. The conditioned loose mix was then transferred to a heated Marshall mould and compacted with 75 blows on each face of a Marshall impact compactor. The hammer had a weight of 4.54 kg and a free fall of 457 mm. The procedure for mix preparation is illustrated stepwise in Figure 3.34. The compacted sample was extracted from the mould on the next day using an extruder device.

All loose mixtures for performance testing were short-term aged for 4 h at 135 °C following AASHTO R30 (2006) procedures. After the short-term ageing, the loose mixtures were heated in an oven to reach the desired compaction temperature before compaction. A gyratory compactor was then used to fabricate asphalt mixtures for performance characterisation. The discussion on the gyratory compactor is presented later in this section. The air void content for a particular performance test was precisely controlled by varying the number of gyrations during specimen compaction. This approach allowed analysis of the effect of pyrolytic char type and content without binder content or air void content as confounding variables.

3.4.6.3 Density-voids analysis and Marshall stability-flow tests

Density-voids analysis was performed to obtain the three principal mix volumetric parameters: air voids (VA), voids in mineral aggregates (VMA), and voids filled with bitumen (VFB). The essential parameters required for density-voids analysis are explained in the following paragraphs.

Bulk specific gravity of compacted mix (G_{mb}): G_{mb} of a compacted mix specimen is an important parameter used in calculating air voids and VMA and can also be used in the field to determine the relative degree of compaction. The G_{mb} was determined according to ASTM D2726 (2019). First, the mass of the dry specimen in the air was determined and designated as W_a. The specimen was then immersed in a water bath at 25±1 °C for 3 to 5 min, and the mass of the specimen in water was determined (W_w).

Figure 3.34 Steps in the preparation of asphalt mixes: (a) aggregate batches in oven, (b) placement of a heated batch in mixing bowl, (c) addition of binder, (d) isomantle used during mixing, (e) conditioning of loose mix, (f) compaction using automatic Marshall compactor, (g) prepared Marshall specimens

The immersed specimen was taken out from the water bath, surface dried by blotting with a damp towel, and the mass was determined as the saturated surface dry (SSD) mass (W_s). The G_{mb} was determined as follows:

$$G_{mb} = \frac{W_a}{W_s - W_w} \tag{3.32}$$

The difference (W_s – W_w) in Equation 3.32 measures the mass of a volume of water equal to the volume of the specimen.

Maximum specific gravity of loose mix (G_{mm}): G_{mm} of an asphalt mix is the specific gravity without considering the volume occupied by air voids. It is used to determine air voids and effective specific gravity of the aggregates (G_{se}) and helps set the target compaction level of paving mixes. The automatic vacuum sealing method stipulated by ASTM D6857 (2017) was followed for G_{mm} evaluation. The CoreLok® apparatus (InstroTek Inc., USA) was used to perform the method (Figure 3.35a).

(a)

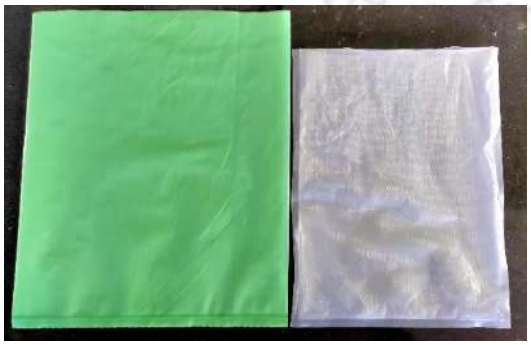

(b)

(c)

Figure 3.35 (a) CoreLok® device for G_{mm} determination, (b) external (left) and internal (right) bags, (c) asphalt mix specimen after vacuum conditioning

The required quantity of loose mix at room temperature, which was free of agglomerated particles larger than 6.3 mm, was placed in specially designed internal (white) and external (green) bags (Figure 3.35b). The bag containing the sample was placed in the vacuum chamber of the CoreLok® apparatus and subjected to 99% absolute vacuum pressure for 5 min. The vacuum chamber also seals the bag to maintain the vacuum when the bag is taken outside the chamber (Figure 3.35c). The bag was cut open inside water and weighed, allowing water to fill all accessible regions of the sample. G_{mm} is calculated using Equation 3.33:

$$G_{mm} = \frac{W_a}{W_{bag} + W_a - W_w - \frac{W_{bag}}{G_{bag}}} \tag{3.33}$$

Here, W_a = mass of dry mix sample in air; W_{bag} = combined mass of internal and external bags; W_w = mass of mix sample and bags underwater; G_{bag} = apparent specific gravity of the plastic bags (value supplied by the manufacturer).

Volumetric parameters: Figure 3.36 shows a schematic diagram of volumetric elements of a compacted asphalt mix. Air voids (VA) are the volume of air pockets present between asphalt binder coated aggregates in the compacted mix specimen. Voids in mineral aggregates (VMA) represent the volume of compacted mix not occupied by aggregates (considering the bulk aggregate volume). Voids filled with bitumen (VFB) represent the percentage of VMA occupied by asphalt binder, or the volume of effective asphalt expressed as a percentage of VMA. The three volumetric parameters are calculated using Equations 3.34-3.36:

$$VA = \left(1 - \frac{G_{mb}}{G_{mm}}\right) \times 100 \tag{3.34}$$

$$VMA = \left(1 - \frac{G_{mb} \cdot P_s}{G_{sb}}\right) \times 100 \tag{3.35}$$

$$VFB = \left(1 - \frac{VA}{VMA}\right) \times 100 \tag{3.36}$$

Here, VA = air voids (percentage of mix volume); G_{mb} = bulk specific gravity of compacted mix; G_{mm} = maximum specific gravity of mix; VMA = voids in mineral aggregates (percentage of mix volume); P_s = percent aggregate (by weight of mix); G_{sb} = bulk specific gravity of aggregates; VFB = voids filled with bitumen (percentage of VMA).

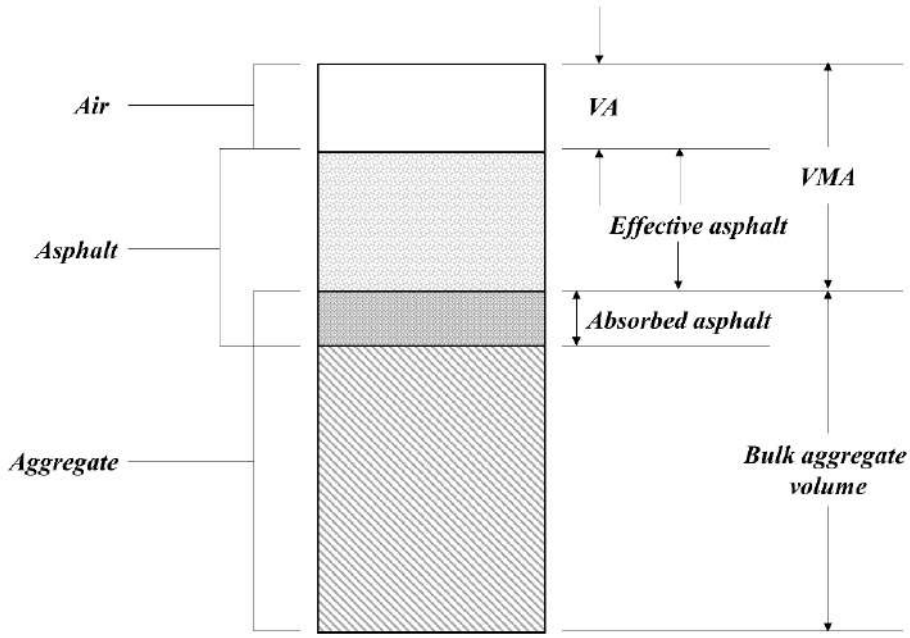

Figure 3.36 Schematic representation of volumetric elements of compacted asphalt mix

Marshall stability and flow tests: The maximum/peak load resisted by a compacted mix specimen subjected to a loading sequence with a constant deformation rate at 60 °C is known as Marshall stability. The deformation corresponding to the peak load is termed Marshall flow. Stability and flow, in addition to VA, VMA and VFB are used in the Marshall method of mix design. Stability and flow were evaluated in accordance with ASTM D6927 (2015) specifications. The digital Marshall apparatus used in this study is shown in Figure 3.37, along with a water bath, test jig with loading frame, and the personal computer connected with the loading frame to acquire the test data. The compacted mix specimen was conditioned in the water bath at 60 °C for 30 min before being tested. The

load was applied to the specimen at a rate of movement of 50 mm/min. Stability and flow were analysed by the software and displayed to the user.

Figure 3.37 Digital Marshall testing system: ① water bath, ② test jig with loading frame, ③ personal computer connected to loading frame

Preparation of asphalt mixes for performance evaluation using gyratory compactor: In a gyratory compactor, asphalt mix is compacted based on the 'shear compaction' principle, meaning that the compactor operates under a combination of vertical pressure and a shear displacement (Darku, 2003). These two compaction modes help to provide more realistic compaction of asphalt mixes compared to the Marshall impact compaction. ASTM D6925 (2015) specifications were followed for gyratory compaction to obtain mix specimens for further performance testing/evaluation. Figure 3.38a shows the gyratory compactor (electro-pneumatic type) along with a compacted 100 mm diameter specimen. During compaction, the loading ram applies a vertical pressure of 600 kPa while the mould containing the mix is positioned at a compaction angle of 1.25° and is rotated (gyrated) at a rate of 30 rpm (Figure 3.38b). The specimen height, density, shear stress, and ram pressure are recorded corresponding to each gyration. To obtain specimens with target air voids, the compactor was operated under height control mode, under which the compaction

would automatically terminate once the pre-set specimen height was attained. This allowed the specimen to reach the desired bulk density corresponding to the target air voids.

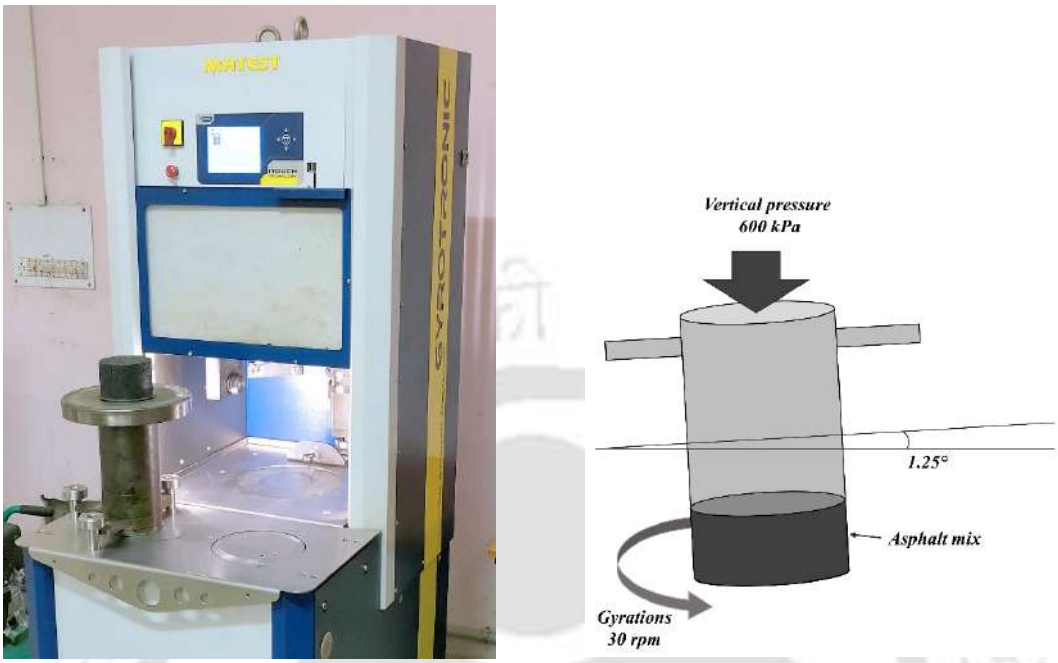

(a) (b)

Figure 3.38 (a) Superpave gyratory compactor, (b) principle of gyratory compaction

3.4.6.4 Toxicity characteristics

Toxicity characteristic leaching procedure (TCLP) test is generally recommended when industrial wastes/by-products are used as pavement materials (Oluwasola et al., 2016). The asphalt mixes prepared with TPC-20 and PPC-20 binders (the highest dosages) were evaluated for leaching potential as per the TCLP analysis prescribed by the Environmental Protection Agency (USA) Method 1311 (USEPA, 1992). The prepared mixes were passed through a 1.18 mm sieve to remove large particles, and the sieved material was oven-dried to remove any moisture and submitted to the USEPA procedure. The presence of metals was detected through atomic absorption spectroscopy (AAS).

3.4.6.5 Performance tests for characterisation of rutting behaviour

One of the critical distress types affecting asphalt pavement is permanent deformation, or rutting, which finally appears as surface depression along wheel paths. Rutting is the

accumulation of irreversible deformations caused by repeated wheel loading on the pavement (Mohammad et al., 2017). Three mechanical performance tests were employed to assess the rutting performance: static creep test, dynamic creep test, and Hamburg wheel tracking device (HWTD) test. All three tests were performed at 50 °C temperature with specimen air voids maintained at 7±0.5%.

Static creep test: A static creep test is performed to evaluate the behaviour of an asphalt mix under static loading conditions. In a static creep test, a constant load is applied for a set time and deformation is measured over time. The test was conducted in accordance with BS 598-111 (1995) using a universal testing machine (UTM). The test assembly is shown in Figure 3.39.

Figure 3.39 Test assembly for static and dynamic creep tests

The specimen was conditioned in an environmental chamber at the test temperature for 4 h before commencing the test. Initially, a static load of 10 kPa was applied for 600 s for conditioning. The specimen was then subjected to a static load of 100 kPa held constant for 1 h. After 1 h, the stress was released, allowing the specimen to recover the deformation for another 1 h. The axial deformation was measured using two LVDTs (linear variable displacement transducers). The axial strain at any time *t* was calculated by Equation 3.37:

$$\varepsilon(t) = \frac{\Delta h(t)}{h} \tag{3.37}$$

where, $\varepsilon(t)$ = axial strain at time t; $\Delta h(t)$ = axial deformation at time t; h = specimen height.

Dynamic creep test: The dynamic creep test measures accumulated or plastic strains, which contribute significantly to rutting in asphalt pavements. In this test, the specimen is subjected to a load cycle comprising a square load waveform (loading period followed by a rest period to allow the specimen deformation to recover). The test method used for the dynamic creep test (also called repeated load axial test) was BS DD 226 (1996). The test assembly for this test is the same as shown in Figure 3.39. A load of 10 kPa was applied for 600 s for proper seating of the specimen and the loading platens. The test then consisted of dynamically applying vertical stress of 100 kPa to a 100 mm diameter and 63.5 mm height specimen. The stress was applied for 1 s followed by a 1 s rest period (0.5 Hz frequency). A total of 10000 cycles (total test time = 20000 s) were applied. Prior to the commencement of the test, the test jig, specimen and all necessary accessories were conditioned at the test temperature for 4 h. LVDTs continuously measured the axial deformation undergone by the specimen. The deformation was then used to compute the axial strain of the specimen at the end of the rest period in each cycle. The accumulated (unrecovered) axial strain was used to measure the mix's permanent deformation performance.

HWTD test: The HWTD, which measures the combined effects of rutting and moisture damage, is gaining popularity due to its quick and dependable testing of various HMA mixes (Yildirim et al., 2007; Rahman and Hossain, 2014). AASHTO T324 (2016) specifications were used to perform the HWTD test on asphalt mixes fabricated with TPC and PPC modified binders. Figures 3.40a and 3.40b show the HWTD equipment and a test specimen undergoing the test. Figure 3.40c shows a specimen after the HWTD test.

(a)

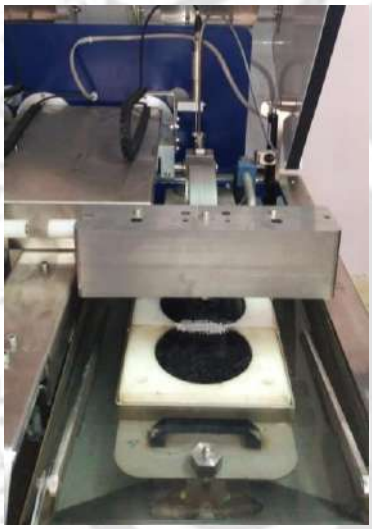

(b)

(c)

Figure 3.40 (a) HWTD equipment, (b) mix specimen being tested in HWTD, (c) specimen after undergoing HWTD test

Two 150 mm diameter SGC specimens (height: 60 mm) were fabricated. The two specimens were sawed off along a secant line and butted together in the HWTD mould. The specimen gap was filled by plaster of Paris slurry and allowed to set for 1 h. The specimens were then submerged in water at 50 °C and subjected to 20,000 passes of a 705 N loaded steel wheel. Prior to the commencement of the test, the specimens were allowed to equilibrate at the test temperature for 30 min. The primary rutting performance related parameter was the rut depth recorded as a function of passes of the loaded wheel.

3.4.6.6 Tests for characterisation of moisture damage resistance

Moisture-induced damage is one of the most common forms of flexible pavement distresses evident in the form of stripping and potholes. Loss of adhesion (between aggregate surface and binder) and loss of cohesion (within the binder or mastic) are two principle mechanisms that cause moisture-induced damage in the asphalt mix (Little et al., 2018). Two test methods were used for moisture damage performance assessment of mixes with TPC and PPC modified binders: (1) modified Lottman test or tensile strength ratio (TSR) test, and (2) retained Marshall stability (RMS) test. The specimens for the TSR test were prepared at 7±0.5% air voids, while those for the RMS test were fabricated at 6±0.5% air voids.

TSR test: The TSR test was performed in accordance with AASHTO T283 (2007) procedure. In the TSR test, six specimens were prepared for each mix/binder type at the target air voids. The specimens were divided into dry and wet subsets (with three specimens in each subset). Specimens of the dry subset were conditioned at 25 °C for 2 h in a water bath and subjected to indirect tensile strength (ITS) testing on a digital Marshall machine equipped with an ITS test jig (Figure 3.41). The load rate for the ITS testing was 50 mm/min. Specimens under the wet subset were vacuum saturated and then were wrapped and placed in plastic bags containing 10 ml water, followed by their placement in a freezer maintained at –18 °C for 16 h. Immediately after this freezing cycle, the specimens were placed in a water bath at 60 °C for 24 h for thawing. The ITS was then determined for the wet as well as dry subset after 2 h conditioning at 25 °C. The ITS is calculated from Equation 3.38, while Equation 3.39 shows the TSR calculations. Indian specifications (MoRTH, 2013) stipulate a minimum 80% TSR for an acceptable moisture damage performance.

$$ITS = \frac{2000P}{\pi hD} \tag{3.38}$$

$$TSR = \frac{ITS_{wet,avg}}{ITS_{dry,avg}} \times 100 \tag{3.39}$$

Here, *ITS* = indirect tensile strength, kPa; *P* = peak load, N; *h* = specimen height, mm; *D* = specimen diameter, mm; $ITS_{wet,\,avg}$ = average ITS of specimens in the wet subset; $ITS_{dry,\,avg}$ = average ITS of specimens in the dry subset.

Figure 3.41 ITS test jig and loading frame

RMS test: In the RMS test, the Marshall stability of unconditioned and conditioned specimens was determined. Figure 3.42 shows the test jig used in the determination of Marshall stability. Three specimens were fabricated under each subset (conditioned and unconditioned). The stability of unconditioned specimens was determined at 60 °C after 30 min soaking in a water bath. The moisture conditioned specimens were placed in a 60 °C water bath for 24 h, and then subjected to stability testing. RMS was calculated as the ratio of average stability of conditioned to unconditioned specimens (Equation 3.40). MoRTH (2013) recommends a minimum 75% RMS for acceptable mixes.

$$RMS = \frac{MS_{wet,avg}}{MS_{dry,avg}} \tag{3.40}$$

Here, $MS_{wet,\ avg}$ = average stability of specimens in the wet subset; $MS_{dry,\ avg}$ = average stability of specimens in the dry subset.

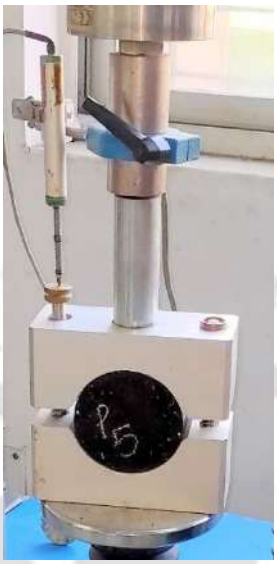

Figure 3.42 Marshall stability testing for RMS

3.4.6.7 Tests for characterisation of fatigue behaviour

Fatigue cracking is caused by the repeated action of wheel loads, which causes the nucleation of microcracks, which grow further to form larger macroscopic cracks (Little et al., 2018; Ahmed et al., 2019). Two test methods were used to evaluate mechanical performance at intermediate-service temperatures: (1) semi-circular bend (SCB) test and (2) indirect tensile fatigue test (ITFT). These test methods are quite different with respect to load application modes (monotonic in SCB and repeated in ITFT), specimen geometry (semi-circular notched specimen in SCB, and cylindrical specimen in ITFT), and analysis theories. Both tests were conducted at 25 °C, a temperature representing the intermediate-pavement service temperatures. For both tests, the specimen air voids were controlled at 4±0.5%.

SCB test: The SCB test is gaining popularity among researchers to characterise the fracture properties of asphalt mixes under monotonic loading conditions. In this test, a semi-circular

asphalt mix specimen with a central notch is mounted on a three-point load configuration (three roller supports) and loaded with a static loading from the top. Tensile stress develops due to the loading, and a crack forms at the notch's tip (Saha and Biligiri, 2016). The test was performed according to ASTM D8044 (2016) standard on 150 mm diameter and 57 mm thick specimens sawed and notched according to the standard requirements. Three specimens at each of the three notch depths (25, 32, and 38 mm) were prepared for each mixture type (Figure 3.43a). A pre-load of 45 N was applied for 30 s to ensure the specimen was correctly seated. A UTM with a 3-point bending configuration (shown in Figure 3.43b) was used to apply a monotonically increasing load with a 0.5 mm/min rate until the load decreased by 25% of the peak load. Corresponding to each notch depth, the strain energy to failure (U) was calculated using a numerical integration scheme recommended by ASTM D8044 (Equation 3.41).

$$U = \sum_{i=1}^{n} (u_{i+1} - u_i) \times P_i + \frac{1}{2} \times (u_{i+1} - u_i) \times (P_{i+1} - P_i) \tag{3.41}$$

Here, P_i and P_{i+1} are applied loads (kN) at i and $i+1$ load steps, and u_i and u_{i+1} are crosshead displacements (m) at i and $i+1$ load steps. From specimen width and the slope of the regression line between U and notch depth, the critical strain energy release rate (J_c) (also called the J-integral) was calculated (Equation 3.42).

$$J_c = \frac{-1}{h}\left(\frac{dU}{da}\right) \tag{3.42}$$

Here, J_c is critical strain energy release rate (kJ/m^2); h is sample thickness (m); a is notch depth (m); U is strain energy to failure (kJ), and dU/da is the rate of change of U with respect to a. The J_c is the main performance parameter derived from the SCB test with higher values desirable for better fracture resistance.

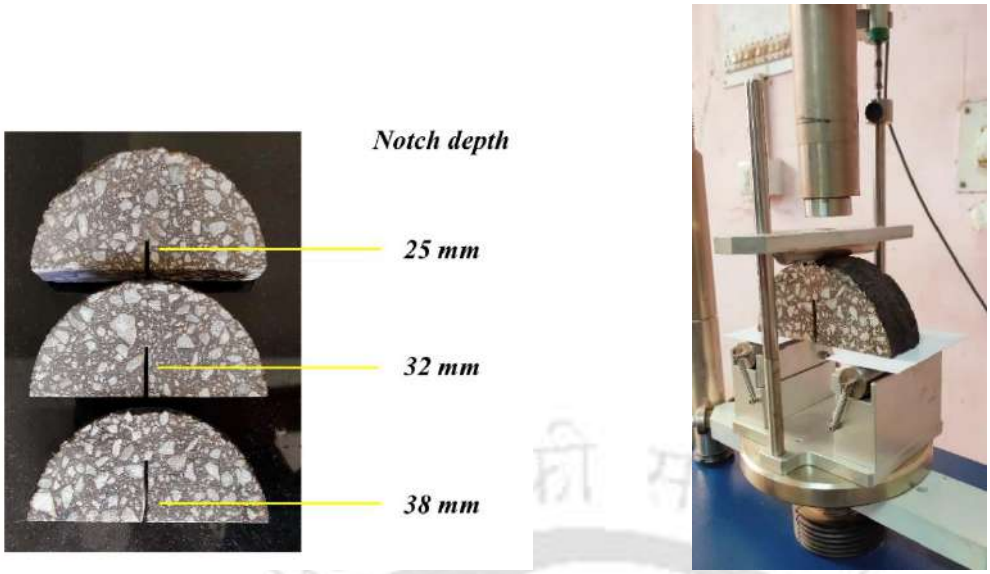

(a) (b)

Figure 3.43 (a) SCB specimens at different notch depths, (b) SCB testing in UTM

ITFT: The ITFT is considered as an economical and easily implementable test method to investigate the fatigue behaviour of asphalt mixes (Adedimila and Kennedy, 1976; Maggiore, 2014). This test requires no special specimen preparation steps (such as sawing, notching, or drilling), and it can be performed on cylindrical specimens prepared in the laboratory or cores extracted from pavements. The test evaluates the fatigue resistance of asphalt mixes subjected to repeated indirect tensile loads and was conducted according to BS EN 12697- 24 (2001) on a UTM. The asphalt mixture specimen diameter was 100 mm with a thickness of 63.5 mm. Before the test, the test jig, specimen, and all accessories were conditioned in an environmental chamber at 25 °C for 4 h. The ITFT was performed in stress-controlled mode with a stress of 500 kPa applied along the vertical direction to obtain a strain in the range of 100-400 $\mu\varepsilon$. The ITFT used a haversine stress wave with a 2 Hz frequency (0.1 s load followed by 0.4 s rest period). The test was continued till the test specimen failed by splitting along the vertical diameter. Fracture life was defined as the number of ITFT cycles to complete the fracture of the specimen and was used as the fatigue performance indicator. Figure 3.44 shows the test assembly for ITFT and a fractured specimen at the end of ITFT.

(a)

(b)

Figure 3.44 (a) Test assembly for ITFT, (b) fractured specimen in ITFT

3.4.6.8 Measurement of resilient modulus for structural analysis

The resilient modulus (M_R) is defined as the ratio of applied stress to recoverable strain (resilient strain). It is used as an input parameter in the design of flexible pavements in India to determine pavement layers' thickness (IRC 37, 2018). Resilient modulus of asphalt mixes with control and TPC/PPC modified binders was determined at 35 °C in accordance with AASHTO TP31 (1996). Three replicates were prepared for each mix type at 4% target air voids. Figure 3.45 shows a specimen placed in the resilient modulus test jig. A repetitive load level of 8.3% of the specimen ITS was used, obtained from interpolation between 15% and 5% recommended respectively for 25 °C and 40 °C temperatures (AASHTO TP31-1996). The specimen was subjected to a haversine shaped load waveform with 0.1 s load and 0.9 s rest period. The load pulse was applied 105 times, and the data from the last 5 pulses was used for M_R calculation. The specimen was axially rotated by 90°, and the procedure was repeated. The final M_R of the specimen was the average of the 10 measurements from both orientations. Equation 3.43 shows the calculation of M_R:

$$M_R = \frac{P(\mu + 0.27)}{\Delta H_r \cdot h} \tag{3.43}$$

where, M_R = resilient modulus (MPa); P = repeated vertical load (N); μ = Poisson's ratio (assumed 0.35); h = specimen height (mm); ΔH_r = recovered horizontal deformation (mm).

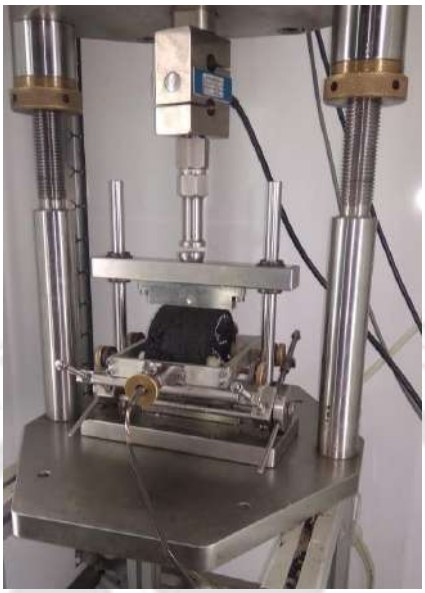

Figure 3.45 Test assembly for resilient modulus test

3.4.6.9 Pavement structural analysis

A flexible pavement consists of several courses/layers, including (from bottom to top): subgrade, granular layers (subbase and base), and bituminous layers (binder and wearing courses). A flexible pavement system composition recommended by IRC 37 (2018) for a 30 msa (million standard axles) design traffic level was considered. The analysis was performed using IITPAVE software, accompanying IRC 37 (2018) guidelines for flexible pavement design in India. The pavement composition was loaded with a single wheel load of 20 kN with a tyre pressure of 0.56 MPa. The strains at the following two critical locations in the pavement system were analysed using the software: (1) tensile strain at the bottom of the bituminous layer and (2) compressive strain at the top of the subgrade. The resilient modulus values of only the top wearing course were changed based on the experimental results obtained in this study. The critical strains and the subgrade rutting life, and bituminous layer fatigue life were compared for the different mixes. The results and discussion of Task 6 are presented in Chapter 8 of the thesis.

3.5 Summary

The details of materials selected in the study, including base asphalt binder, mineral aggregates, and pyrolytic chars, were discussed in this chapter. The experimental programme to achieve the objectives of the study was presented and discussed. Six tasks were formulated to achieve the objectives of the study. The details of work elements, experimental techniques, test methods, and operating principles of instruments adopted to investigate the properties of the materials, modified binders, and asphalt mixes were presented corresponding to each task.

Chapter 4

PHYSICO-CHEMICAL CHARACTERISATION OF MATERIALS

4.1 Introduction

The results of physico-chemical characterisation of pyrolytic chars and asphalt binders performed under Task 1 of the study are presented in this chapter. The physico-chemical properties of pyrolytic chars were investigated to understand the variations in the performance of the TPC/PPC modified binders and mixtures in a better manner. This chapter presents the results of the physical and chemical characterisation of the two pyrolytic chars (TPC and PPC) along with the microstructural and thermo-chemical characterisation of asphalt binders. The pyrolytic chars were analysed through: FESEM, EDX spectroscopy, BET surface area analysis, particle size distribution analysis, proximate analysis, FTIR spectroscopy, and TGA. The binders were analysed through TGA, FTIR spectroscopy, and optical microscopy.

4.2 Characterisation of Pyrolytic Chars

4.2.1 FESEM

The microscopic images of TPC and PPC were obtained through FESEM and are shown in Figure 4.1. Figure 4.1a shows that at low magnification (1000x), TPC appeared as agglomerates of smaller particles with a granular surface (Li et al., 2015; Sharma et al., 2021). At high magnification (150000x) shown in Figure 4.1b, the individual particles of carbon black present in TPC could be seen with sizes ranging between 40 and 50 nm. TPC exhibits hierarchical morphological features, which means that there are primary particles (sizes smaller than 100 nm) and aggregates and agglomerates of the particles (of larger

sizes) in irregular shapes. The primary particles tend to form aggregates due to covalent bonds and van der Waal forces (Cardona et al., 2018). The size of TPC is usually larger than the original carbon black used in tyre rubber. Char particles act as nuclei during pyrolysis, allowing carbon structures to develop by crosslinking or cyclisation (Cardona et al., 2018).

Smaller particles covered the surface of PPC (Figures 4.1c and 4.1d), with some particles even embedded inside the pores of the bigger particles. These smaller particles may also block the pores leading to a lower surface area (Xue et al., 2015). Some cubic-shaped features were observed in PPC microscopic images, which likely represent the catalyst (*e.g.*, zeolites) used in plastic pyrolysis.

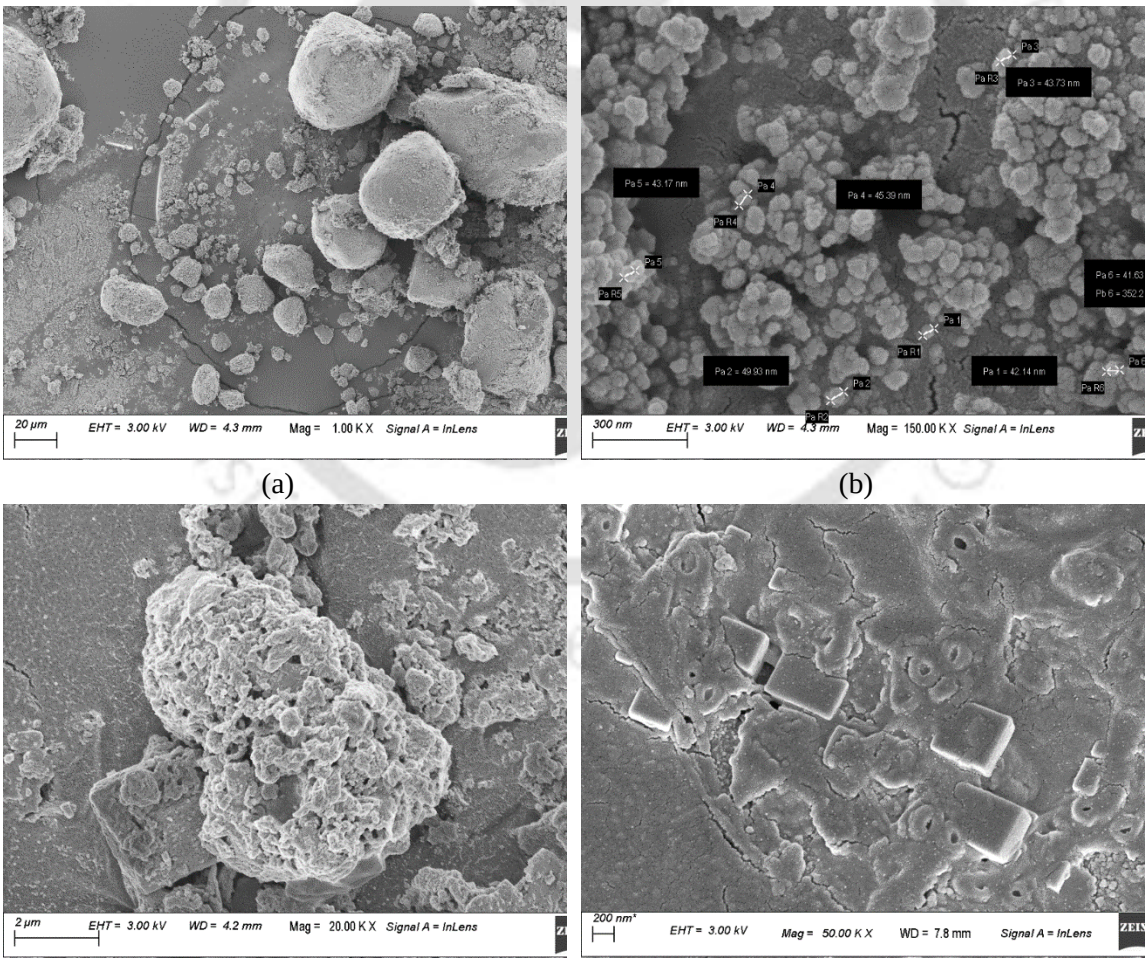

Figure 4.1 FESEM micrographs of (a) TPC at 1 KX, (b) TPC at 150 KX, (c) PPC at 20 KX, and (d) PPC at 50 KX

4.2.2 Surface area, size distribution, and proximate analysis

Table 4.1 presents and compares the properties of TPC and PPC. The surface area, measured through BET technique of TPC (47.4 m^2/g) was much higher than that of PPC (12.3 m^2/g). The TPC encompasses a blend of carbon blacks used in different parts of tyres (Martínez et al., 2019; Urrego-Yepes et al., 2021). Since each part of a tyre requires a specific carbon black, TPC particles generally contain a mixture of carbon blacks of varying sizes. Depending on the grade, tyre carbon blacks can have a specific surface area ranging from 10 m^2/g to about 150 m^2/g. This explains the higher BET surface area of TPC than PPC (carbon black is generally not present in PPC). Figure 4.2 shows the particle size distribution of the two pyrolytic chars. The finer particle size of TPC, as noted from Figure 4.2, also has a similar explanation as applicable for the surface area. The finer size of TPC also agrees with a higher specific surface area of TPC than PPC. The critical sizes (D_{30}, D_{50}, D_{60}, and D_{90}) of the chars are also presented in Table 4.1, showing that TPC particles are of finer size than PPC.

Table 4.1 Properties of the pyrolytic chars

Property	***TPC***	***PPC***
Specific gravity	1.707	1.740
BET surface area, m^2/g	47.4	12.3
Particle size analysis:		
D_{90}, µm	27.2	47.6
D_{60}, µm	12.0	27.2
D_{50}, µm	9.7	22.2
D_{30}, µm	5.4	7.1
Proximate analysis:		
Moisture, %	1.0	5.2
Fixed carbon, %	82.9	5.1
Ash content, %	12.1	62.0
Volatiles, %	4.0	27.7

D_{90}: Particle size at 90% passing; D_{60}: Particle size at 60% passing; D_{50}: Particle size at 50% passing; D_{30}: Particle size at 30% passing

In the proximate analysis, TPC contained mainly fixed carbon and ash, while ash and volatile matter were the main constituents in PPC. PPC showed a higher ash content than

TPC. Another observation is the comparatively higher volatile matter content in PPC than TPC. The volatile substance on the TPC surface indicates the presence of partially pyrolysed rubber and/or tarry compounds (Cardona-Uribe et al., 2021). The existence of certain non-devolatilised plastic and hydrocarbons (tarry compounds) leftover from parallel and/or secondary reactions during the pyrolysis process causes the volatile matter in PPC (Yousef et al., 2021). The proximate analysis results were similar to those reported in the literature (Cardona et al., 2018; Martín-Lara et al., 2021).

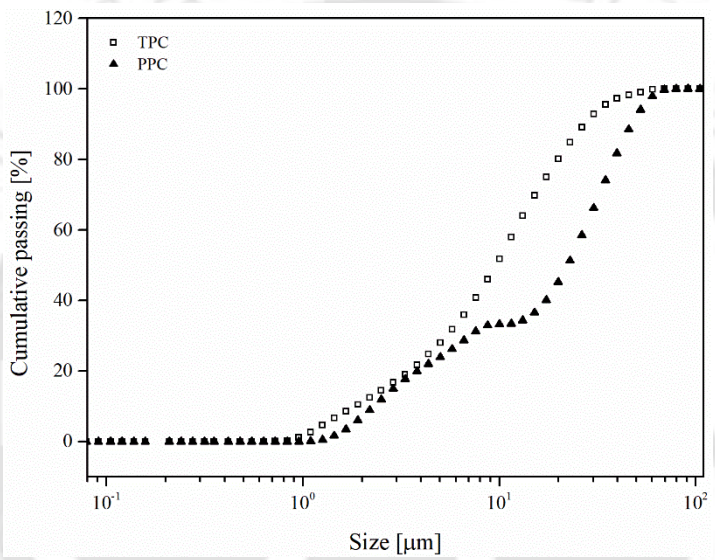

Figure 4.2 Particle size distribution of TPC and PPC

4.2.3 EDX analysis

EDX analysis generates information about the elemental composition of a sample. Figure 4.3 presents the results of EDX analysis of the two chars. The EDX analysis showed that carbon (C) and oxygen (O) were the major elements in TPC and PPC, although the carbon content was higher in TPC. In TPC, Zn is derived from zinc oxide which used as a catalyst in the tyre rubber vulcanisation process. The presence of sulfur (S) is from the vulcanised rubber used in tyre manufacturing, while Si derives from silicon dioxide added to provide flexibility to tyres. Other elements detected in TPC are Ca, and Cl which can be sourced to various additives (such as $CaCO_3$, chlorinated paraffins) used during tyre manufacturing.

In PPC, elements such as Ca, Fe, Mg, Al, Si, and O can be derived from catalysts used during plastic pyrolysis. Ca, Al, Si, and O can also be from clay (kaolin) and calcium carbonate, commonly used as fillers (reinforcing agents) during plastics manufacturing. Titanium (Ti) derives from titanium dioxide, one of the most common white pigmentation agents used in plastics. Mg can be due to magnesium hydroxide, one common inorganic flame-retardant additive used in plastics (Wang et al., 2018). Since a mixed plastic waste was used during plastic pyrolysis, a minor amount of Cl is also detected, which may be sourced from polyvinyl chloride.

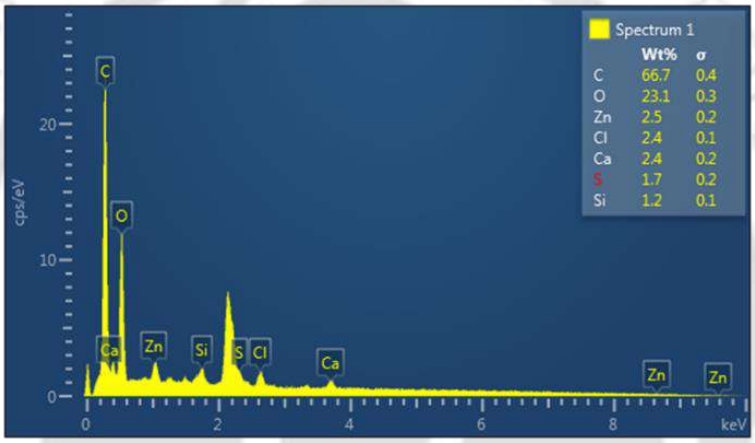

(a)

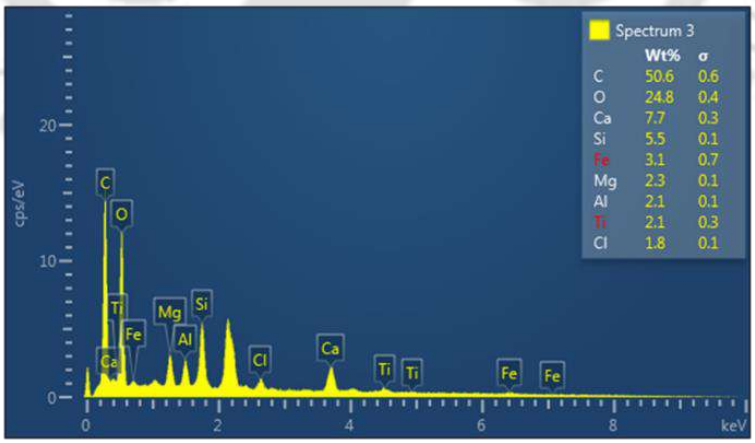

(b)

Figure 4.3 EDX analysis results of (a) TPC and (b) PPC

4.2.4 FTIR spectroscopy

An infrared absorption spectrum produced in FTIR spectroscopy is widely used to identify chemical bonds present in a material. Figure 4.4 presents the FTIR spectra of TPC and PPC for the wavenumber range 400-4000 cm^{-1}. The absorbance peak at 660 cm^{-1} in the FTIR spectrum of TPC (shown in Figure 4.4a) corresponds to the aliphatic halo compounds found in the catalysts used during the pyrolysis process of tyres. The peak at 910 cm^{-1} corresponds to C=C bending in-plane rocking vibration of alkene compound, and the bands at 1070 and 1185 cm^{-1} are due to coupled C-O stretching of ethers (O'reilly and Mosher, 1983). The spectrum peak observed at 1365 cm^{-1} belongs to the O-H bending of phenols (Sigmaaldrich, 2021). The peak at 1460 cm^{-1} represents the C-H bending of alkane compound and is explained by the creation of hydrocarbons such as methane and ethylene during the pyrolysis of tyres (Han et al., 2018). The peaks at 1640 and 1780 cm^{-1} correspond to C=C stretching of conjugated alkene and C=O stretching vibrations of lactone (Cardona et al., 2018; Li et al., 2018). The sharp and medium peaks at 2680, 2870, and 2980 cm^{-1} represent the C-H stretching vibrations of alkane compound class. The wide absorbance band near wavenumber 3540 cm^{-1} corresponds to OH stretching vibration of COOH and H_2O (Cardona et al., 2018; Li et al., 2018).

The strong peak observed in the FTIR spectrum of PPC (shown in Figure 4.4b) at 465 cm^{-1} corresponds to the bending vibration of O-Si-O (Dominic et al., 2013). The presence of Si was also confirmed in the EDX analysis of PPC. The absorption peaks observed around 670, 755, and 880 cm^{-1} belong to 1,2-disubstituted and 1,2,3-trisubstituted compound class of C-H bending, respectively, while the peak at 1020 cm^{-1} corresponds to the vibrations of the C-H bonds of aromatic ring (Martín-Lara et al., 2021). The peaks at 1370 and 1400 cm^{-1} wavenumbers correspond to the O-H bending of carboxylic groups. The strong peak around 1610 cm^{-1} represents the C=C stretching of α,β-unsaturated ketone

(Sogancioglu et al., 2017). The presence of long aliphatic chains is suggested by the peaks located at 2920 and 2850 cm^{-1} corresponding to the $–CH_3$ and $–CH_2$ groups. The strong and broad appearance of the peak around 3390 cm^{-1} belongs to the intermolecular bonded O-H stretching group (Sigmaaldrich, 2021). During plastic pyrolysis, a higher residence time and temperature provides an opportunity for secondary reactions that could include isomerisation, aromatisation, and hydrogenation/ dehydrogenation (Tiikma et al., 2007; Onwudili et al., 2009). These reactions reduce the oil yield by decomposition of liquids to aromatics and some gases, and the stripping of gases to form aromatics and, finally, char (Onwudili et al., 2009; Abbas-Abadi et al., 2013). Several FTIR spectrum peaks confirm the presence of aromatic groups in PPC.

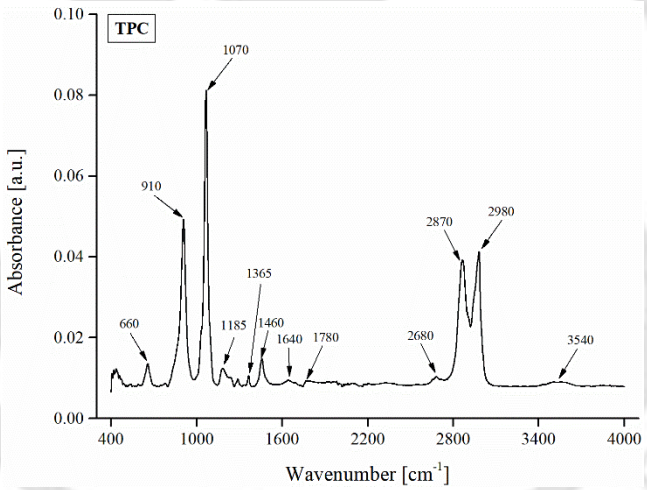

(a)

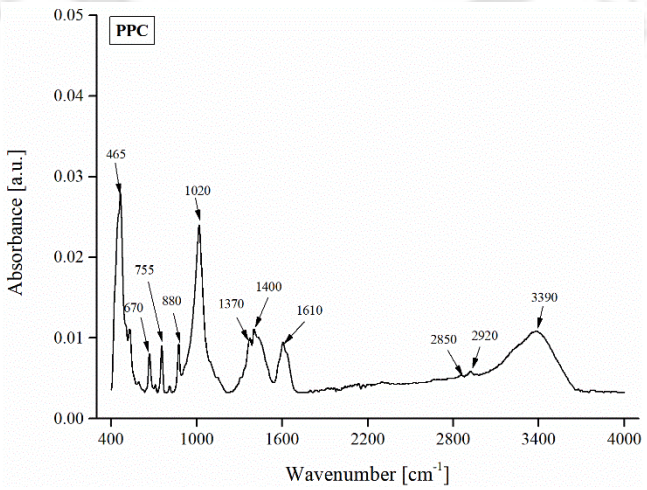

(b)

Figure 4.4 FTIR spectra of (a) TPC and (b) PPC

4.3 Thermogravimetric Analysis of Pyrolytic Chars and Binders

The thermogravimetric analysis (TGA) technique measures the mass change when a sample is heated at a constant rate, and evaluates a material's thermal stability. Figure 4.5 shows the mass loss (%) curves of TPC, PPC, and control binder alone, along with TPC-10, PPC-10, TPC-20, and PPC-20 modified binder blends. Three indicators were obtained from the TGA curves: (1) initial decomposition temperature (T_i, temperature at 5% mass loss), (2) temperature at maximum decomposition rate (T_{max}, identified from the differential of the thermogravimetric curve), and (3) residue (percent mass remaining after 1000 °C). Results of these temperatures are shown in Table 4.2. TGA curve for TPC showed a moderate but steady mass loss throughout the temperature range considered. For PPC, the TGA curve showed that by 1000 °C, it lost 53.4% weight. At the end of TGA, TPC residue was 75.4%, while the PPC residue was 46.6%, indicating that the TPC was decomposed to a much less extent than PPC. The initial mass loss in TPC below 500 °C is attributed mainly to the vaporisation of rubber residue coating the surface of the char. Beyond 500 °C, the mass loss can be ascribed to the pyrolysis of rubber residues trapped into the pores of the char (Cataldo, 2020). In TPC, the remnants at the end of TGA are a mixture of metals and compounds added during tyre manufacturing (Sharma et al., 2021).

Figure 4.5 further shows that control and modified binder blends underwent major decomposition at temperatures between 350 and 530 °C. The mass loss corresponds to the loss of lightweight constituents in asphalt binders (saturates and aromatics) (Padhan et al., 2020). As seen from T_{max} values in Table 4.2, the maximum mass loss rate occurred between 445-465 °C. The decomposition rate lowered beyond these temperatures until about 530 °C, where meagre decomposition rates could be seen since the asphalt binder was already carbonised. From the TGA curves in this region (530 °C and beyond), it was observed that the modified binders were more stable against mass loss than the control

binder. In fact, TPC-20 and PPC-20 binders suffered the least mass loss compared to the control. The nature of decomposition for control, TPC-10, PPC-10, and TPC-20 binders was similar with one reaction stage (350-530 °C). A minor deviation was observed only for PPC-20 binder with a small mass loss episode near 260 °C in addition to that at 350-530 °C temperatures.

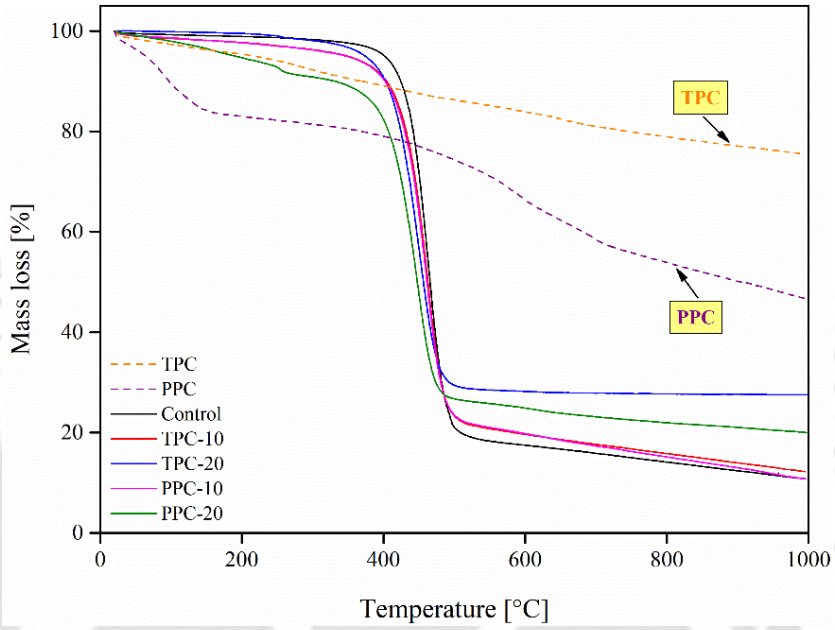

Figure 4.5 TGA results of pyrolytic chars and binders

Table 4.2 Results of TGA analysis of pyrolytic chars and asphalt binders

Pyrolytic char/Binder	*T_i, °C*	*T_{max}, °C*	*Residue, %*
TPC	216	283	75.4
PPC	64	97	46.6
Control binder	401	462	10.8
TPC-10 binder	349	465	12.2
TPC-20 binder	374	454	27.5
PPC-10 binder	347	462	10.7
PPC-20 binder	190	447	20.0

T_i: initial decomposition temperature
T_{max}: maximum decomposition temperature

Due to volatiles and lightweight substances in TPC and PPC, the T_i values for modified binders were lower than the control binder. However, except for PPC-20, all T_i values were higher than 345 °C, indicating that modified binders' thermal stability would not show a significant role under the usual production temperatures of bituminous mixes. Even for the PPC-20 binder, the T_i of 190 °C is still higher than the typical mixing and production temperatures of 150-180 °C. The trend of T_{max} is quite similar to that for T_i. Table 4.2 also shows the percent residue (mass of the material remaining at the end of TGA). The modified binders suffered lower final weight loss, although they had higher mass loss initially. This observation points to the fact that once the lightweight substances are decomposed before 530 °C, the chars contain heavy substances (such as a mixture of inorganics, metals, ash, *etc*.) that allow the modified binders to suffer less mass loss and thus have a higher residue.

An important observation can be made here for PPC and PPC-modified binders. Even though PPC particles showed a high mass loss in the 100-160 °C temperature range, the mass loss of PPC-10 and PPC-20 binders at these temperatures was much less. For example, at 160 °C (typical mixing temperature), mass loss of PPC particles, PPC-10 binder, and PPC-20 binder was found as 16.3%, 1.9%, and 3.9%, respectively. The blending of PPC-modified binders involved the pre-conditioning of PPC particles at 105 °C for 2 h, prior to blending. This helped to remove very lightweight constituents present in PPC. In the absence of such pre-conditioning, when PPC was added directly to the asphalt binder, one would notice generation of bubbles/foaming in the binder for 2 to 4 min after the addition of PPC, and this phenomenon subsided after 4-5 min. Such observations were also reported with graphene oxide modification in Wang et al. (2020a) study. In the present study, all PPC blends were prepared with the pre-conditioning step, and no foaming was therefore observed during the blend preparation.

4.4 Characterisation of Char-modified Binders

4.4.1 FTIR spectroscopy

Figure 4.6 shows the FTIR spectrum of the control binder, TPC-10, and PPC-10 modified binders. The band peaks observed at 625 and 660 cm^{-1} belong to aliphatic bromo compounds. However, the spectral peaks between 610 and 660 cm^{-1} can also be attributed to alkyne C-H bend (Coates, 2000). The band peaks appearing around 780, 840, and 910 cm^{-1} belong to C=C bending vibration of trisubstituted alkene, while peaks at 1030 and 1200 cm^{-1} are due to sulfoxide (S=O vibration) and C-O stretching, respectively (Nivitha et al., 2016). The characteristic bending vibration of methyl group appears at 1375 and 1460 cm^{-1} and indicates the symmetric and asymmetric bend of CH_3 (Sigmaaldrich, 2021). The spectral bands observed at 1590 cm^{-1} in the control binder and at 1640 cm^{-1} in TPC-10 and PPC-10 correspond to the C=C stretching of alkene while the band at 1750 cm^{-1} belongs to C=O stretching vibrations of lactone. The presence of aldehyde was attributed to C-H stretching vibration present at 2680 cm^{-1} wavenumber (Xu et al., 2020b), while peaks at 2850, 2920, and 2960 cm^{-1} are ascribed to aliphatic C-H stretching. The peak observed at 3060 cm^{-1} in spectra of base binder represents C-H stretching of alkene (Coates 2000). The peak observed at 3470 cm^{-1} in TPC-10 and PPC-10 and 3540 cm^{-1} in the base binder may belong to the O-H stretching group of carboxylic acid (Nivitha et al., 2016).

As evident from Figure 4.6, the absorbance peak observed at 625, 780, 1590, and 3060 cm^{-1} in the spectrum of the control binder disappeared in the FTIR spectra of TPC-10 and PPC-10 binders. Also, the intensity of spectral peaks at 840, 910, 1030, 2680, and 2960 cm^{-1} in TPC-10 and PPC-10 decreased notably compared to the base binder. The C=C stretching of alkene present in the base binder at 1590 cm^{-1} shifted to 1640 cm^{-1} in TPC-10 and PPC-10, while the aliphatic C-H stretching at 2920 cm^{-1} increased significantly in TPC-10 and PPC-10 binders in comparison to band intensity in the control binder.

Therefore, the disappearance of spectral peak or shift in peak position indicates that TPC and PPC have chemical interactions with the base binder during modification. Similar observations were also found in literature (Masson et al., 2003; Nivitha et al., 2016; Yan et al., 2021).

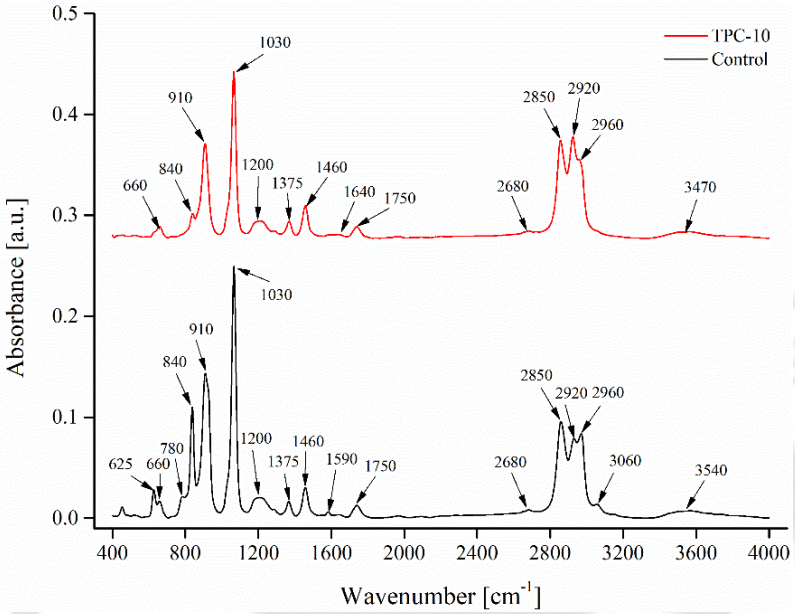

(a)

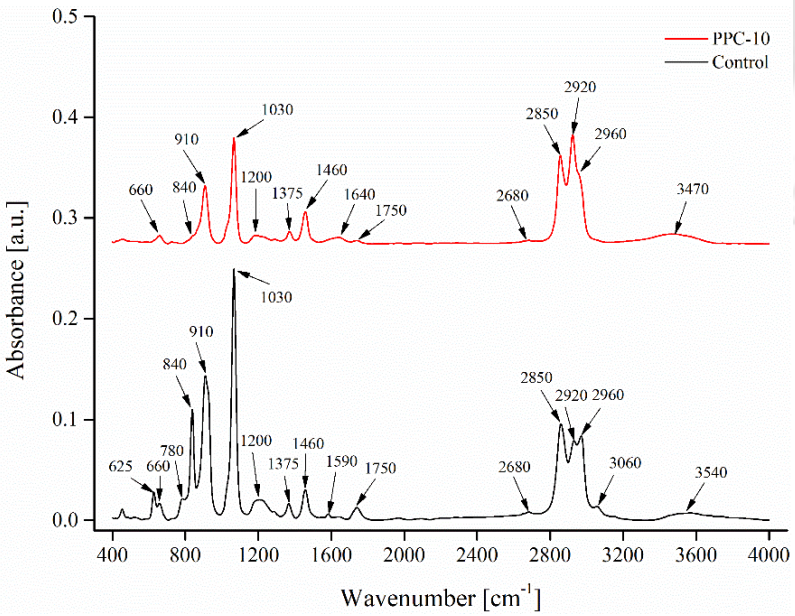

(b)

Figure 4.6 FTIR spectra comparison of control binder with (a) TPC-10 binder and (b) PPC-10 binder

4.4.2 Optical microscopy

The TPC and PPC-modified binders were visualised through an optical microscope for visual assessment at the microscopic level. Figure 4.7 shows the micrographs captured at 40x magnification. The orange/red colour represents the neat asphalt binder, and it forms the background for the images for the modified binders. The black areas indicate the TPC and PPC particles. The micrographs show that both modifiers are isolated and evenly dispersed in the binder with no significant agglomeration. Slight agglomeration is only observed at a high dosage of 20%, which is expected at such high modifier content. Further, the concentration of black areas (representing the modifiers) seems to increase with their content. A range of particles sizes can be observed from as large as 72 µm to as low as 0.3 µm (Figure 4.7i), which shows that the blending procedure used for the modification was able to avoid association/agglomeration of the particles and distribute the TPC and PPC particles uniformly.

4.5 Summary

This chapter presented the results of the physico-chemical characterisation of pyrolytic chars, control and the modified asphalt binder blends. Characterisation of the pyrolytic chars revealed that the TPC had finer size distribution, higher specific surface area, less volatile matter content, and higher fixed carbon content compared to the PPC. TGA results showed that the chars had an appreciable effect on the mass loss profile of the modified binders. FTIR spectroscopy showed that TPC and PPC interacted chemically with the base binder during modification. Optical microscopy showed a uniform distribution of TPC and PPC particles in the modified binders suggesting that the blending procedure used for fabrication of modified binder blends provided a good dispersion of the char particles.

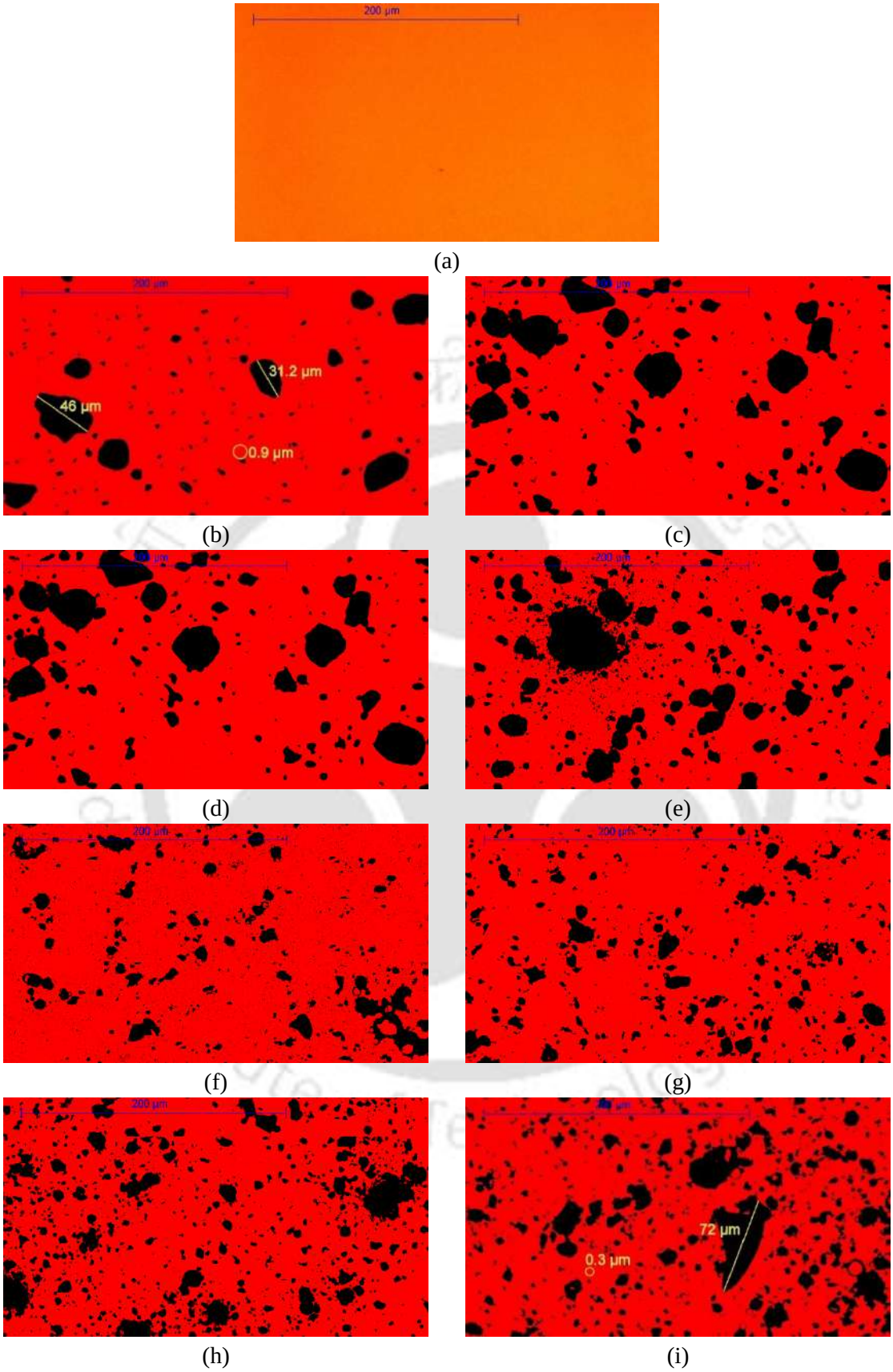

Figure 4.7 Optical microscopy images of binders (at 40x) (a) control, (b) TPC-5, (c) PPC-5, (d) TPC-10, (e) PPC-10, (f) TPC-15, (g) PPC-15, (h) TPC-20, (i) PPC-20

Chapter 5

STORAGE STABILITY OF CHAR MODIFIED ASPHALT BINDERS

5.1 Introduction

In this chapter, the results of thermal storage stability characterisation of TPC and PPC modified binders, under Task 2 of the study, are presented and discussed. Adequate storage stability is an important requirement with modified asphalt binders. Principal factors that cause concerns in regard to the storage stability of modified binders include the physical and chemical dissimilarities between the modifier and the asphalt binder such as density, solubility, viscosity, polarity, and molecular weight and structure (Al-Hadidy and Yi-qiu, 2009; tur Rasool et al., 2017; Liang et al., 2019). Cigar tube separation test is a widely used test to evaluate the storage stability characteristics of modified binders. The test measures the difference in properties between the top and bottom one-third portions of the binder sample in a tube after being subjected to extended periods (typically 48 h) of high temperature (typically 163 °C) storage. The procedure has been standardised as ASTM D7173 (2020). Poor storage stability leads to macroscopic separation of the two phases, causing a loss of uniformity and thus leading to an inconsistent binder quality and higher differences in the properties of the modified binder samples extracted from the top and bottom portions during the separation test.

The softening point, being an empirically defined value, may not be sufficient alone to understand the effect of storage stability phenomenon on binder's performance properties and may also be less sensitive to the differences in compatibility (Lu and Isacsson, 1997;

Liang et al., 2017; Zani et al., 2017). Based on softening point difference (SPD) alone, it is difficult to explain how the separation affects the rheological viscoelastic properties of the modified binder, which are more important from a performance perspective. Therefore, it is more beneficial to further evaluate the differences/changes through rheological determinations on the binder specimens conditioned for standard storage stability measurements.

The use of cross-linking agents is a well acknowledged method for achieving appropriate storage stability with modified asphalt binders. Polyphosphoric acid (PPA) is a commonly used mineral acid to enhance storage stability of modified binders and to modify paving grade asphalt binders, either by itself or in combination with different polymers (Fee et al., 2010). Sulfur is another commonly used cross-linking agent for improving the storage stability of polymer and rubber (natural and synthetic) modified asphalt binders. Sulfur forms bridges/networks by chemically cross-linking the polymer chains and grafting the polymer chains with asphalt components through sulfide and/or polysulfide bonds (Martínez-Estrada et al., 2010; Polacco et al., 2015).

The storage stability characteristics of TPC modified binders with different cross-linking agents are described in the next section of this chapter, as formulated in Subtask 2A. The results of the storage stability performance of PPC modified binders are then presented and discussed as part of Subtask 2B. The effect of use of cross-linking agents on the rheological characteristics of the binders is also studied through frequency sweep, temperature sweep, and MSCR tests. The evaluations are done for the highest (20%) dosages of both TPC and PPC in binder modification. The chapter then concludes with validation of the storage stability results for modified binders with other dosages.

5.2 Storage Stability Characterisation of TPC Modified Binders

5.2.1 Effect of PPA and sulfur on binder rheology

Frequency sweep: Frequency sweeps were conducted at a typical high pavement service temperature of 60 °C. A 60 °C temperature was selected since it is generally used to evaluate the binder performance at high pavement service temperatures. The results of storage modulus (G′) and loss modulus (G″) are shown in Figures 5.1a and 5.1b for binders with PPA and sulfur. The control binder in these results is the TPC-20 binder without any cross-linking agent.

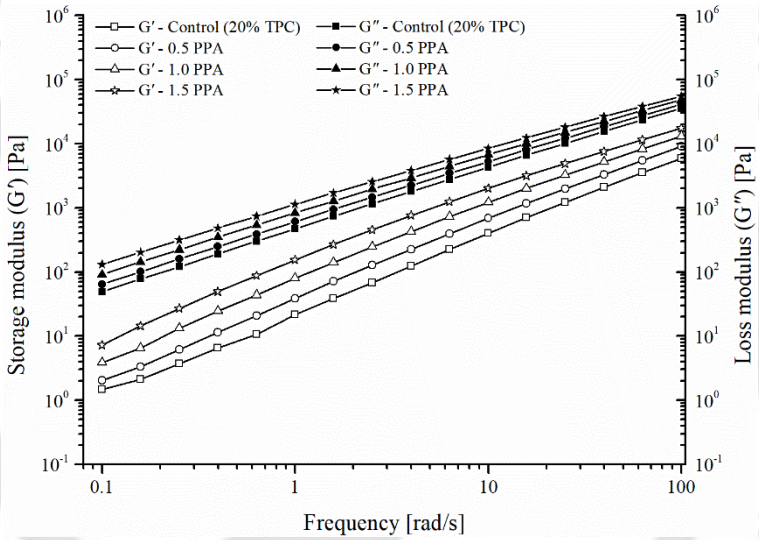

(a)

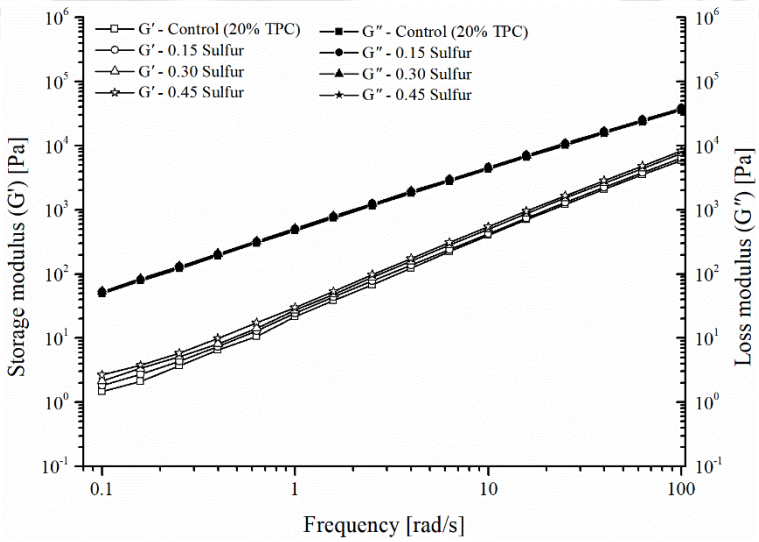

(b)

Figure 5.1 Frequency sweep results for TPC modified binders with: (a) PPA, and (b) sulfur

The loss modulus was higher than the storage modulus, which was expected at the high test temperature of 60 °C, where an asphalt binder's viscous (loss) component dominates over the elastic (storage) component. Over the range of frequencies (0.1 to 100 rad/s), an increase in PPA dosage showed greater changes in both storage and loss moduli. The higher increase observed in the storage modulus indicates that PPA significantly improves the elastic response of the TPC modified asphalt binder. With an increase in the load frequency, the differences among G′ (or G″) of the binders seemed to decrease. The addition of sulfur caused a small increase in the storage modulus and almost no change in the loss modulus.

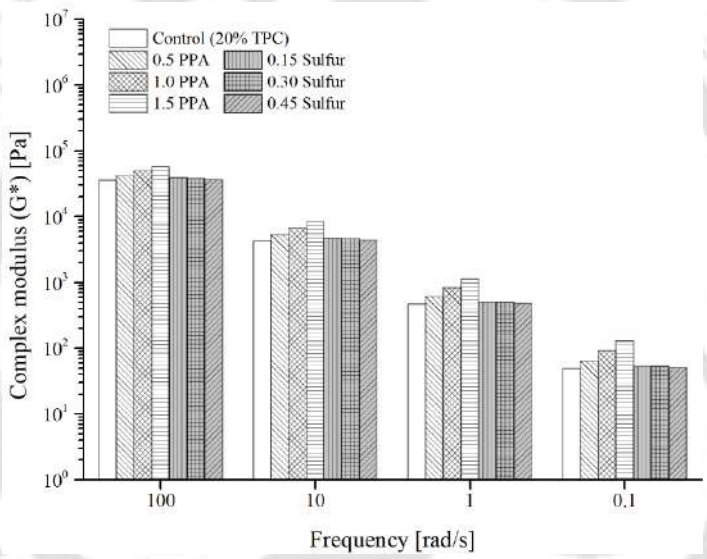

(a)

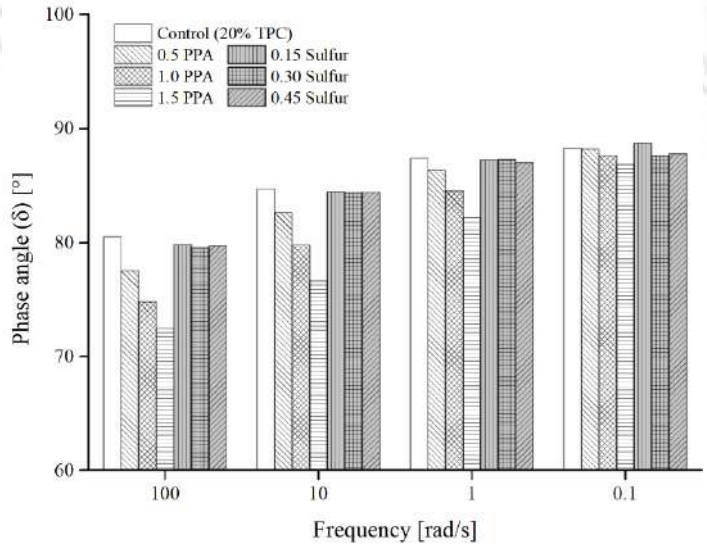

(b)

Figure 5.2 G* and δ at selected frequencies for TPC modified binders with PPA and sulfur: (a) G*, and (b) δ

Figure 5.2 presents the results of G* and δ at four selected frequencies (0.1, 1.0, 10, 100 rad/s) derived from the frequency sweep tests. Again, the values of G* increased, and δ decreased with increasing PPA contents, while the different doses of sulfur did not cause an appreciable change (increase or decrease) in the viscoelastic properties of the binders. The possible reasons for the observed trends are discussed in later part of this section.

The complex viscosity (η^*) data from frequency sweep tests were submitted to the Cross model (Equation 3.20) to derive the ZSV of the binders at 60 °C through nonlinear curve fitting. The model allows extrapolating the complex viscosity-frequency data to estimate the viscosity at zero frequency (the ZSV). Figure 5.3 shows the Cross model fit to the complex viscosity data for the control TPC modified binder and the TPC modified binders with different PPA and sulfur dosages. The model fitted the data quite well with a high coefficient of determination ($R^2 \approx 0.99$) in each case. The complex viscosity reduced with an increase in the load frequency. The addition of PPA caused a considerable increase in the complex viscosity values. The extrapolation of viscosity in the low-frequency region using the Cross model is also shown in Figure 5.3. Figure 5.4 depicts the ZSV values for the binders. It is again observed that the addition of PPA enhanced the ZSV values significantly while not much effect was seen with sulfur. Thus, PPA modification enhanced the binders' stiffness and high-temperature rutting resistance, whereas the effect of sulfur was minimal.

Temperature sweep: The temperature sweep test simulated the temperature variation of two viscoelastic parameters: G* and δ, over a range of temperatures (25 to 80 °C). Figures 5.5a and 5.5b present the results for binders with different dosages of PPA and sulfur, respectively. As expected, an increase in temperature caused a decline in G* and an increase in δ, signifying an increase in the viscous nature of the binders. As shown in Figure 5.5a, an increase in PPA dosage resulted in a higher G* and a lower δ and therefore, PPA

improved the stiffness of the binders in the range of temperatures considered. A higher increase in G* was observed at higher temperatures as seen from the vertical spread in the G* curves. The results indicated that PPA remarkably enhanced the high-temperature resistance to deformation of the TPC modified binder. Figure 5.5b indicates that the modification by sulfur did not show a noteworthy change in the G* and δ values throughout the test temperatures.

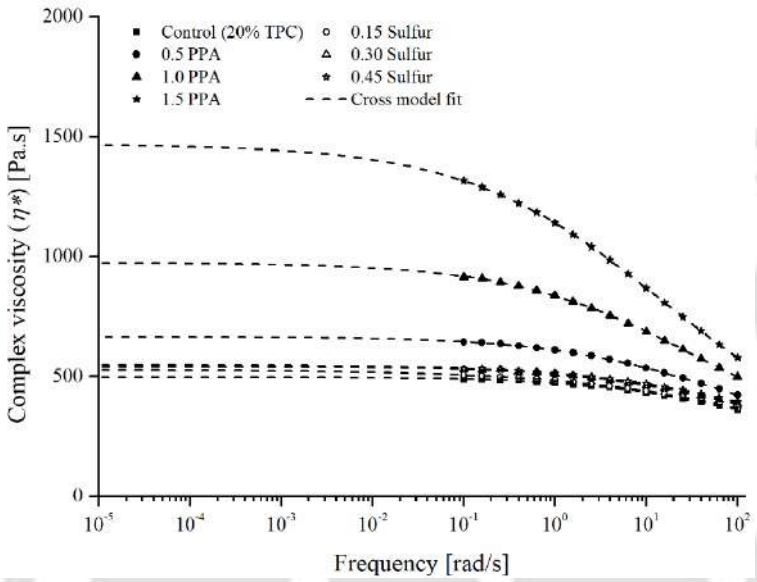

Figure 5.3 Complex viscosity-frequency results of TPC modified binders with PPA and sulfur: experimental data and fit by Cross model (extrapolated to low frequencies)

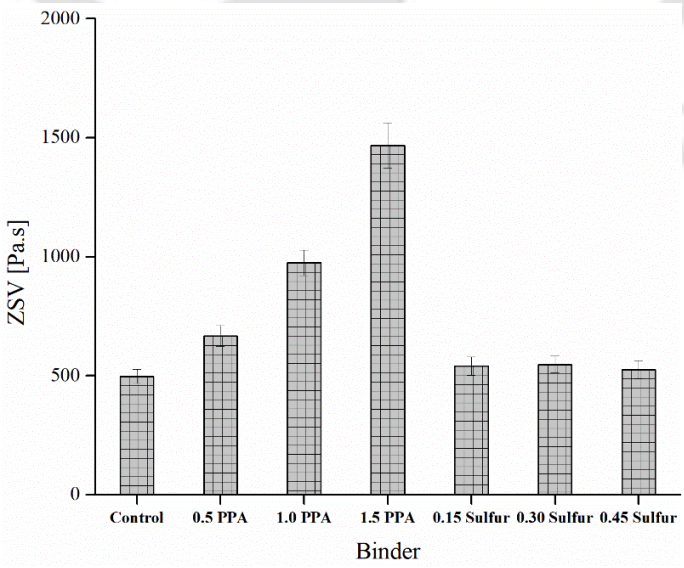

Figure 5.4 ZSV results for TPC modified binders with PPA and sulfur

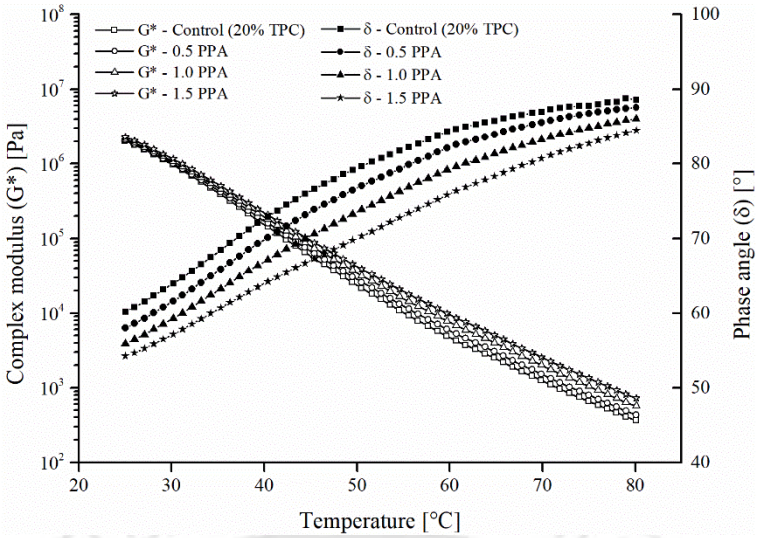

(a)

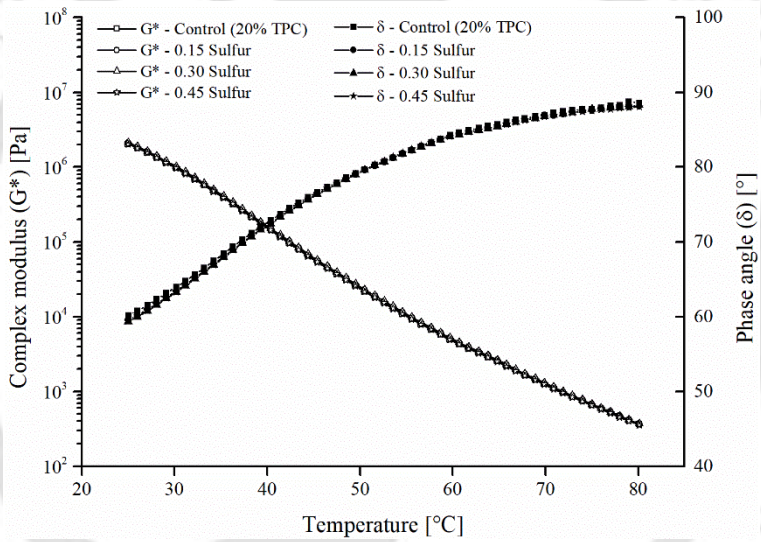

(b)

Figure 5.5 Temperature sweep results of TPC modified binders with (a) PPA, and (b) sulfur

MSCR: The J_{nr} results at the two stress levels (σ = 0.1 and 3.2 kPa) are shown in Figure 5.6 for the TPC modified binders with different doses of PPA and sulfur, respectively. The J_{nr} value significantly decreased with the use of PPA, implying that it prominently reduced the non-recovered strain at each stress level. For example, the J_{nr} at 3.2 kPa stress level reduced from 2.8 kPa^{-1} for the control modified binder to 2.2, 1.6, and 1.1 kPa^{-1} at PPA contents of 0.5%, 1.0%, and 1.5%, respectively. The results agree with observations made by other researchers on higher stiffness and high-temperature deformation resistance

achieved with PPA incorporation (Orange et al., 2004; Liang et al., 2017). In contrast, the J_{nr} values only showed minor changes at the different sulfur contents. These findings agree with frequency and temperature sweeps and further indicate that the addition of sulfur did not significantly affect the rheological characteristics of TPC modified binders.

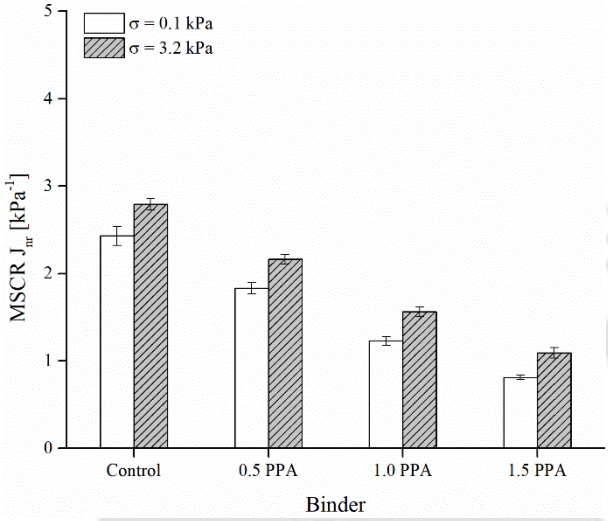

(a)

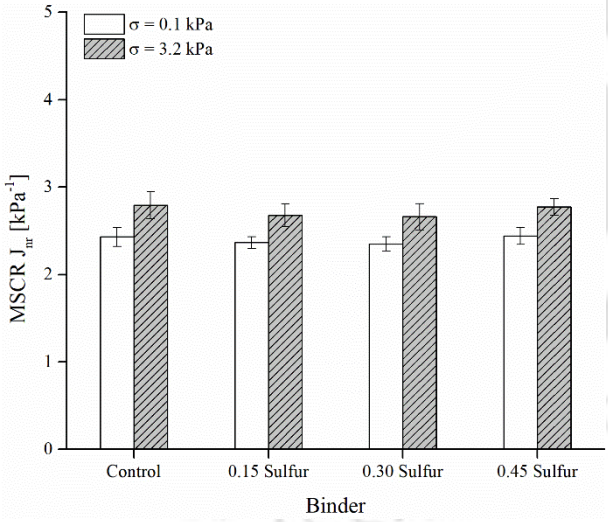

(b)

Figure 5.6 MSCR J_{nr} results for TPC modified binders with (a) PPA, and (b) sulfur

A discussion is now provided to explain the possible contributing mechanisms of the two cross-linking materials on the rheological parameters of TPC modified binders. To explain the high stiffening, better elasticity and higher rutting resistance with PPA, different possible mechanisms were explained by Baumgardner et al. (2005) using advanced

chemical analyses such as thin-layer chromatography (TLC), nuclear magnetic resonance (NMR), gel-permeation chromatography (GPC), and atomic force microscopy (AFM). The mechanisms explained/proposed were: (1) formation of PPA adducts through acidolysis of alkyl-aromatics; (2) alkylation of aromatic rings; (3) cross-linking of reactive asphalt segments forming a matrix of covalently bonded entities; (4) the formation of stiff ionic clusters by the aggregation of phosphate salts; and (5) PPA catalysed cyclisation of alkyl aromatics leading to a stiffer naphthene aromatics. However, the existence of a mechanism depended on the asphalt binder composition, and no single mechanism could thoroughly explain the effect of PPA. It is also well-accepted that the overall effect of PPA is to modify the solvation of asphaltenes, thus increasing the solid fraction and gel character of the asphalt resulting in a higher stiffening effect (Polacco et al., 2015; Liang et al., 2017).

The addition of sulfur did not show an appreciable effect on the rheology of TPC modified asphalt binders. In this study, it seems that the addition of sulfur in small dosages (0.15, 0.30, and 0.45%) did not impart a noticeable effect on the rheological characteristics. In a previous study by Wen et al. (2001), a similar conclusion was made that a low amount of sulfur (0.35% by weight of binder) brought no significant changes in the measured torque profile of a modified binder. It is to be noted that the interaction of sulfur with polymer/rubber is expected to be different than with carbonaceous additives such as TPC due to differences in the additive chemical structure. It was initially supposed that TPC particles interact with sulfur so that the effect of sulfur is masked. To assess this supposition, blends were prepared with the original base (unmodified) binder at the three sulfur dosages (0.15, 0.3, and 0.45%) and the results of G* at multiple test frequencies were compared with the TPC modified binders at the same sulfur dosages. Figure 5.7 shows that the addition of sulfur neither changed the rheology of the original base binder nor of the control binder (*i.e.*, TPC-20 binder without a cross-linking agent). The increase in G* in

TPC modified binders is only due to incorporating the TPC modifier. Thus, it is clear that sulfur, in the dosages considered in the study, did not affect the rheology of the modified binders. However, interestingly it was found (as shown in the next section) that sulfur did have a profound effect on the storage stability performance of the binders.

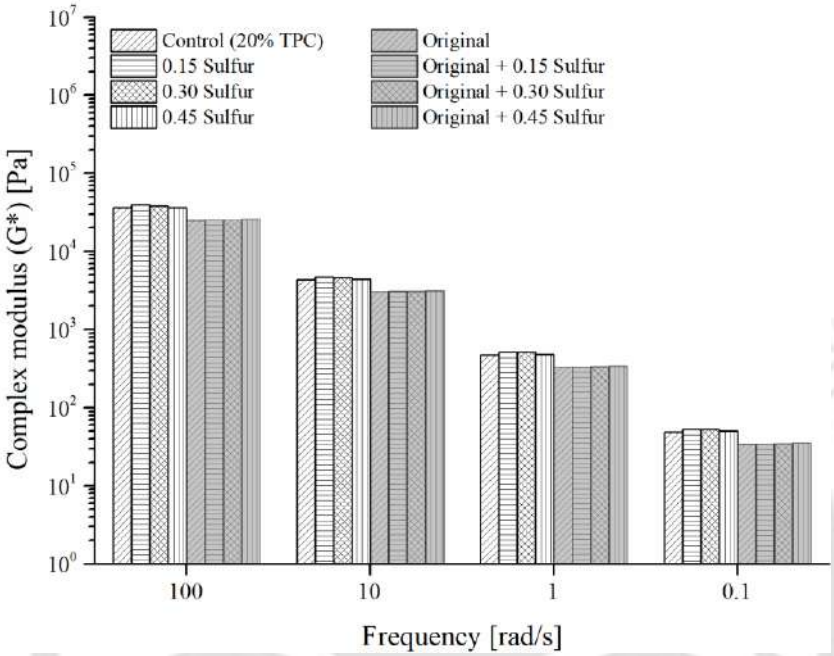

Figure 5.7 Effect of doses of sulfur on original and control (20% TPC) binders

5.2.2 Analysis of storage stability

Rheological separation indices and SPD: The TPC modified binder specimens after being subjected to the high temperature conditioning (at 163 °C for 48 h) as per the requirements of ASTM D7173 (2020), were collected from the bottom and top one-third sections of the cigar tube, and then examined for evaluation of SPD and other rheological based separation indices. Eight rheology-based separation indices (SIs) derived from temperature sweep and MSCR tests were employed in addition to the SPD. The details of the SIs were presented in Table 3.4. Figure 5.8 shows the results of different SIs used for the estimation of storage stability of the modified binders. The bars labelled 'conventional' represent the SI of samples without remixing protocol, and the bars labelled 'remixed' are for the results obtained on samples subjected to the remixing protocol. For remixing (explained in details

in Chapter 3), after being subjected to the 48 h static high-temperature storage at 163 °C, all modified binders were taken out of the oven, placed in a hot sand bath (163 °C), and gently stirred with a narrow glass rod. The sample tubes were then placed in a freezer prior to sawing. Remixed binder samples from to the top and bottom sections were extracted and subjected to the same testing regime as used for conventional (non-remixed) samples.

Rheological separation indices (SIs) (described in detail in Chapter 3) used to quantify storage separation are defined in two forms. In the first form, an SI is defined as the ratio of a rheological parameter measured for the sample extracted from top and the bottom sections. It follows that a binder with zero separation would have SI = 1 (values near 1 are desirable). In the second form, SI is defined as the difference between the maximum and the average values of a rheological parameter belonging to either the top or bottom section, expressed as a ratio of the average value (*i.e.*, $(X_{max} - X_{avg})/X_{avg}$, where X is a rheological parameter). In this case, an ideal binder with zero separation would have the same value for the maximum and the average, implying SI = 0 (values near 0 are desirable). In the present study, nine SIs (one SPD and eight rheology-based) were considered with the details of expressions presented in Table 3.4.

The SIs indicate that the control TPC modified binder suffered separation in the conventional testing approach. This was expected due to a high TPC concentration (20%) used and density difference of TPC particles (specific gravity: 1.71 g/cm^3) compared to the base asphalt binder (specific gravity: 1.03 g/cm^3), facilitating the migration of TPC particles to the bottom of the separation tube when subjected to prolonged static storage at high temperature (163 °C). Therefore, the rheological parameters and the softening point of the modified binders extracted from the bottom section showed a general increase (and a decrease in the case of J_{nr}) after the thermal storage because of a higher TPC concentration in the bottom section of the tube compared to the top one.

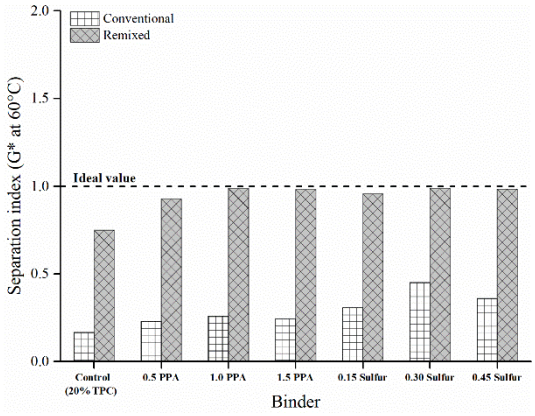

(a)

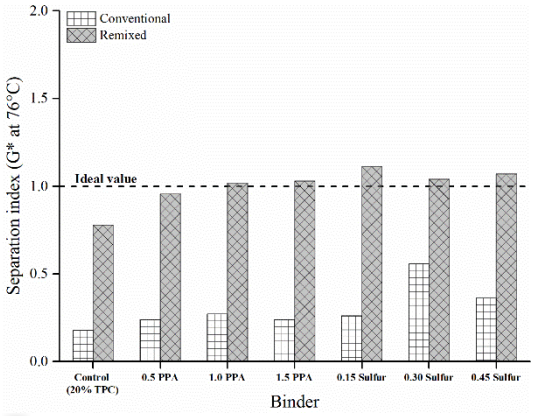

(b)

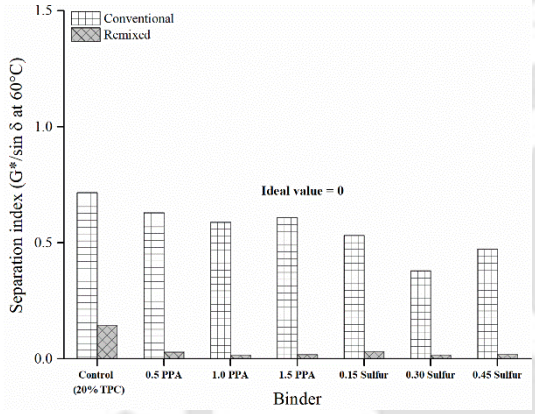

(c)

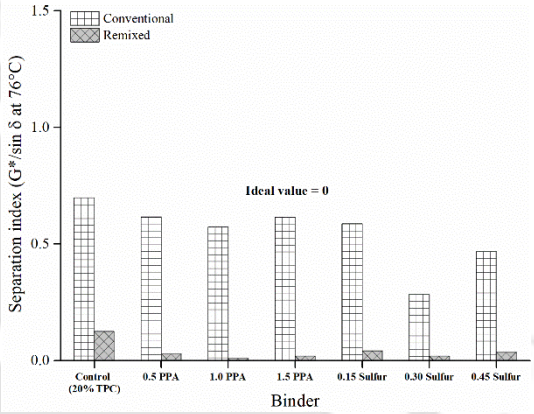

(d)

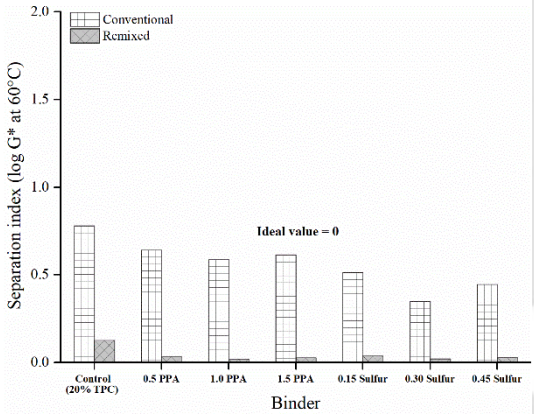

(e)

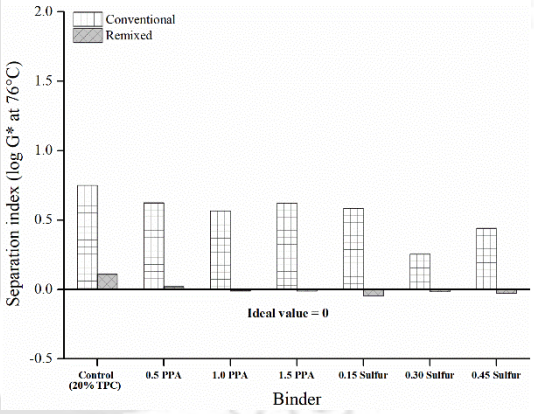

(f)

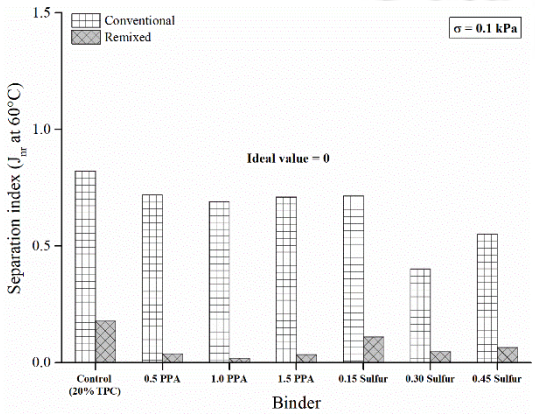

(g)

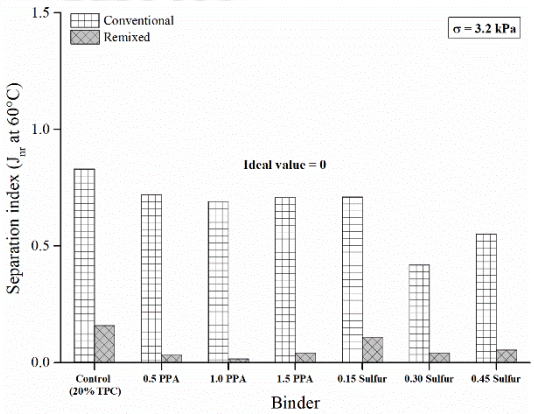

(h)

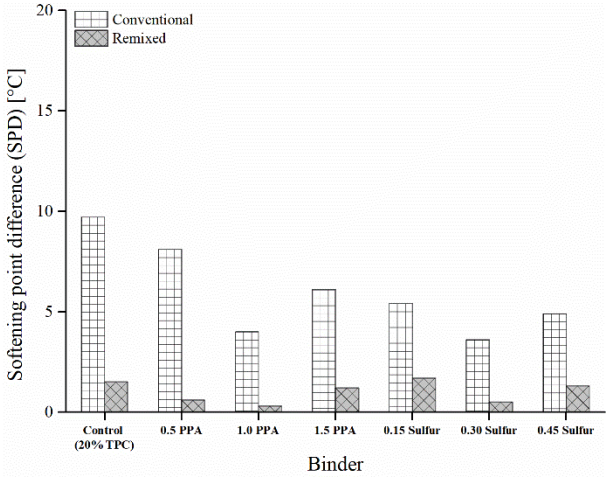

(i)

Figure 5.8 Results of different separation indices (a) SI based on G* at 60 °C, (b) SI based on G* at 76 °C, (c) SI based on G*/sin δ at 60 °C, (d) SI based on G*/sin δ at 76 °C, (e) SI based on log(G*) at 60 °C, (f) SI based on log(G*) at 76 °C, (g) SI based on J_{nr} at 0.1 kPa, (h) SI based on J_{nr} at 3.2 kPa, (i) SI based on SPD

The addition of PPA or sulfur improved storage stability as indicated by all the SIs. For TPC modified binders without incorporating the remixing protocol, the optimum result was observed at 1.0% dosage of PPA and 0.3% dosage of sulfur. After remixing, all SIs were found closer to their ideal values. Prior to remixing, the differences between the top and bottom sections were macroscopically apparent and could be discerned with a simple organoleptic observation. Remixing allowed the segregated TPC modified binder to regain an improved dispersion of TPC particles. The incorporation of PPA and sulfur into remixed samples resulted in almost negligible separation. Remixing improved storage stability performance of all binders and proved to be a valuable step considering the practical usage of TPC modified binders as it can radically reduce the separation tendencies of the modified binder even at a high TPC dosage of 20%.

The current in force Indian standards for polymer-modified bitumen (PMB) (IS 15462, 2019) and rubber modified bitumen (RMB) (IS 17079, 2019) stipulate maximum SPD limits of 3 °C and 4 °C for PMB and RMB, respectively. Although these requirements would not be strictly applicable to TPC modified binders given the inherent differences in

the modifier properties, the SPD results (Figure 5.8i) indicated that conventionally tested (without remixing) TPC modified binders with 1.0% PPA and 0.3% sulfur met the requirements for an RMB. Further, all TPC modified binders, including the control modified binder (without PPA and sulfur), met the requirements for both PMB and RMB if remixing was performed.

The likely contributing mechanisms of the two cross-linking materials on the thermal storage stability performance are now discussed. The addition of PPA and sulfur showed an improvement in storage stability before and after remixing. Deflocculation of asphaltenes is a widely accepted mechanism to explain the interaction of PPA with asphalt binder. It is believed that PPA breaks up agglomerates of asphaltenes either by neutralising polar groups, acid-base neutralisation, or esterification, thereby facilitating better dispersion of the asphaltene individual units in the maltene phase. Such dispersion allows the formation of a long-range network of asphaltenes that affects the rheology of the PPA modified binder (Marcant, 2004; Martin et al., 2004; Fee et al., 2010; Baldino et al., 2013).

Meanwhile, based on ultraviolet (UV) absorbance studies, Chaala et al. (1996) demonstrated that the TPC reduced the asphaltene concentration in the maltenes by 'trapping' some of the asphaltenes. The TPC particles were surrounded by a boundary layer (film) of about 2 nm thickness, principally composed of asphaltenes. The boundary layer concept between a polymer and asphalt has been observed to influence the compatibility and storage stability of polymer-asphalt blends significantly. A boundary layer is formed as the polymer absorbs light asphalt constituents such as saturates and aromatics. The higher thickness of the boundary layer enhances the binding between the polymer and the boundary layer, improving the stability of the modified binder (Zhang and Hu, 2013). In the present study, it is hypothesised that both effects co-occur: PPA helps to form the network of well-dispersed asphaltene units in the asphalt binder, and these asphaltene units

also occur on the boundary layer between the binder and the TPC particles, with the net effect that the TPC particles are dispersed relatively more uniformly. The network so formed within the binder can retain and reduce the TPC particles from settling down in the modified binder on prolonged thermal storage.

Considering the effect of sulfur, it is found to show a profound effect on improving the storage stability of TPC modified binders. Sulfur has been reported to function as an effective cross-linker with unsaturated polymers such as styrene-butadiene-styrene (SBS) as it creates covalent linkages through sulfide and/or polysulfide bonds between the chains of the polymer and also between the polymer and the asphalt molecules, and thus acts as a cross-linker by anchoring asphalt-rich and polymer-rich phases (Zhang et al., 2010; Polacco and Filippi, 2014). In SBS modified asphalts, the cross-linking mechanism of sulfur has been attributed to the presence of unsaturated C=C double bonds in the polybutadiene segment of SBS. Previous investigations (Cardona et al., 2018; Li et al., 2018) have identified C=C bonds in TPC, which were also recognised from the FTIR spectrum of the TPC (discussed in Chapter 4, Figure 4.4a). Therefore, it is very likely that physical or chemical interactions occur during the preparation of the TPC-sulfur modified asphalt, resulting in improved storage stability. However, the actual reactions and interactions could be more complex. The beneficial effect of sulfur is clearly present in the improvement of the storage stability, although the addition of sulfur did not have an appreciable effect on the rheological characteristics of the modified blends.

FTIR spectroscopy: FTIR spectrum was also studied to characterise PPA and sulfur's ability to enhance the storage stability of TPC modified binders. FTIR was performed on the control, 1.0% PPA, and 0.3% sulfur incorporated TPC modified binders and their corresponding top and bottom sections of the cigar tube. Figure 5.9 presents the FTIR spectra of the binders. It is seen that in all spectra, the major peaks occur at the same

locations. The two major absorbance peaks observed at 2921 and 2854 cm^{-1} correspond to aliphatic —C-H stretching and belong to —CH_2 and —CH_3 groups, respectively. The spectral peaks at 1458 and 1375 cm^{-1} are due to —CH_2 and —CH_3 groups, respectively, and assigned to —C-H bending vibrations. The FTIR spectra show the sulfoxide peak (S=O stretching) at 1070 cm^{-1}, aromatics and carbonyl around 1600 cm^{-1} and 1700 cm^{-1}, respectively. These peaks are identified and labelled based on asphalt FTIR literature (Mouillet et al., 2008; van den Bergh, 2011; Weigel and Stephan, 2017).

Figure 5.9a shows that the spectral curve for the control modified binder from the bottom part of the storage stability tube has higher absorbance peaks than the top part and the control TPC modified binder blend. This occurrence seems to be in direct relation to the TPC concentration in the binders (TPC concentration in bottom > blend > top). A similar observation was made by Lu et al. (1999), where a higher absorbance was observed for the top section of SBS-modified binders than the bottom section, and it was attributed to a higher SBS concentration in the top section binders than the bottom ones. FTIR spectra shown in Figure 5.9b correspond to TPC modified binders with 1.0% PPA. It is observed that the spectral curve of the bottom binder is now closer to the curve of the 1.0% PPA binder blend and the top section binder. On further examination of the relative positions of the FTIR spectra of binders with 0.3% sulfur (Figure 5.9c), it is seen that the differences are quite minor comparatively.

The interpretation that can be made here is that 1.0% PPA and 0.3% sulfur improve the storage stability of the TPC modified binders, imparting an increase in the homogeneity of the TPC modified binder identified by the proximity of the FTIR spectra. A similar interpretation was also made in a study by Zhang et al. (2018b), where they found a closer spectral trend for the original asphalt blend and the top and bottom sections of a bio-asphalt binder after thermal storage.

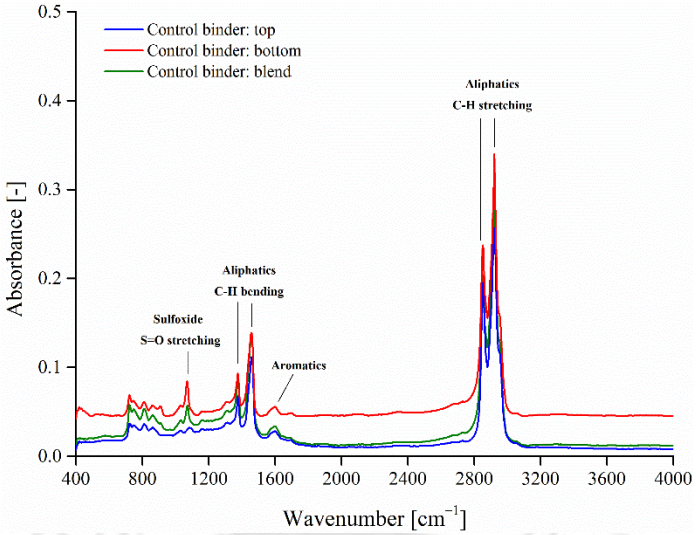

(a)

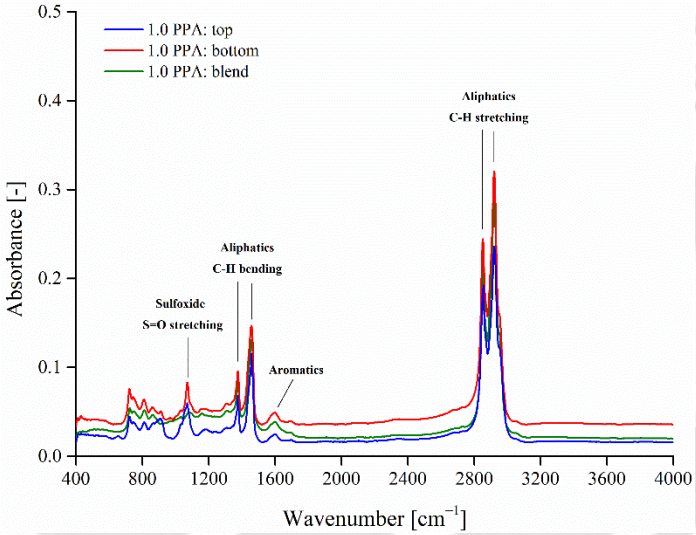

(b)

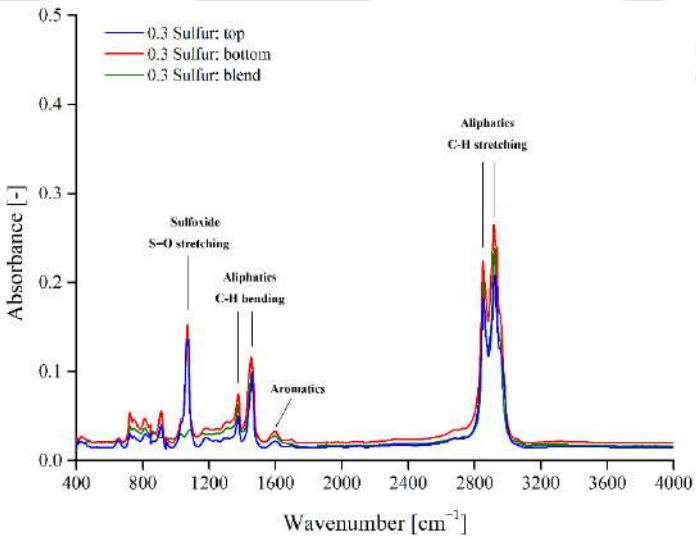

(c)

Figure 5.9 FTIR spectra of blend and top-bottom section binders for (a) control, (b) 1.0 PPA, and (c) 0.3 sulfur

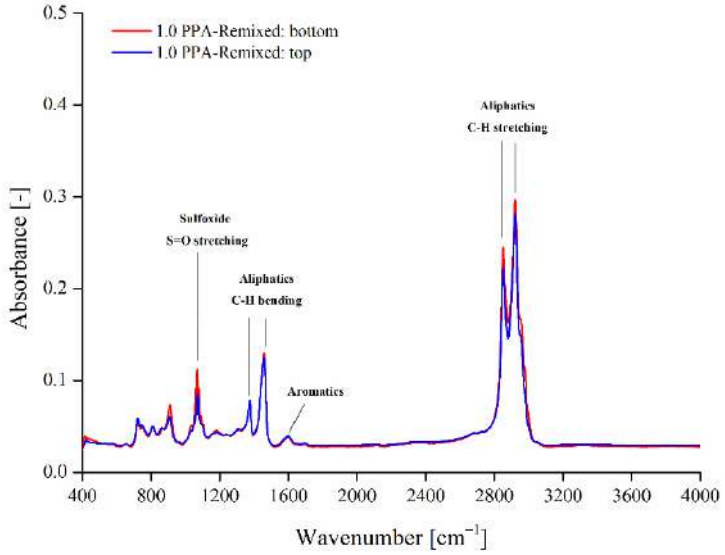

(a)

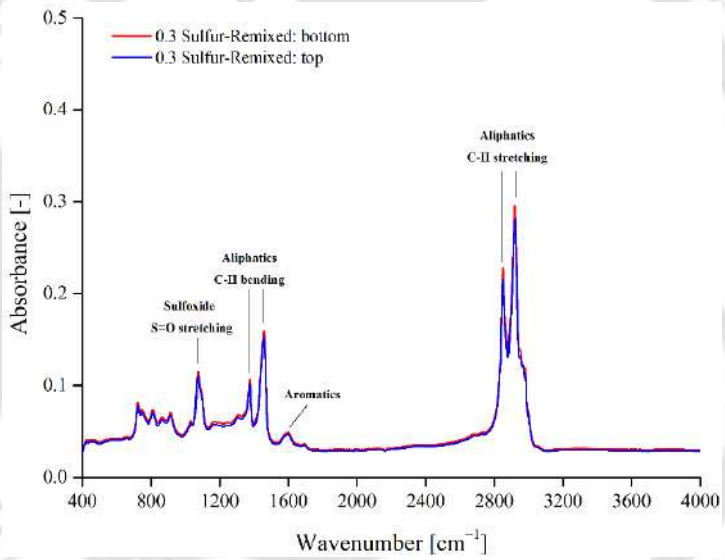

(b)

Figure 5.10 FTIR spectra of top-bottom sections of remixed binders for (a) 1.0 PPA, and (b) 0.3 sulfur

It is further observed from Figure 5.10 that the FTIR spectra are in close proximity to each other for the top and bottom sections after remixing of the binder for both 1.0% PPA and 0.3% sulfur. FTIR trends are also consistent with the rheological separation indices that showed that sulfur performed more profoundly than PPA in enhancing the storage stability of TPC modified binders.

5.2.3 Ranking of binders

The conventionally tested (tested without remixing) TPC modified binders were numerically assigned ranks from 1 to 7, with 1 being the best rank. Remixed binders were not considered for ranking as the differences between their SI values were very close to 0. The ranking results are shown in Table 5.1. All SIs assigned the first rank to the 0.3% sulfur binder. As expected, all SIs assigned the lowest rank to the control TPC modified binder. In general, the binders with sulfur produced better ranks than the binders with PPA. However, the 1.0% PPA binder had the best rank among the PPA modified binders, followed by 1.5% PPA and 0.5% PPA binder. The 0.3% sulfur binder had the best rank among the sulfur modified binders, followed by binders with 0.45% sulfur and 0.15% sulfur content. It is also observed that the ranks assigned by SPD were also close to those assigned by rheology-based SIs. The ranks indicate that TPC modified binders with sulfur have better storage stability performance than those with PPA.

Table 5.1 Binder rankings based on separation indices

Binder	SI-1	SI-2	SI-3	SI-4	SI-5	SI-6	SI-7	SI-8	SI-9
Control	7	7	7	7	7	7	7	7	7
0.5 PPA	6	6	6	6	6	6	6	6	6
1.0 PPA	4	3	3	3	4	3	4	3	2
1.5 PPA	5	5	4	4	5	5	5	5	5
0.15 Sulfur	3	4	5	5	3	4	3	4	4
0.30 Sulfur	1	1	1	1	1	1	1	1	1
0.45 Sulfur	2	2	2	2	2	2	2	2	3

SI-1: SI based on G*/sin δ at 60 °C
SI-2: SI based on G*/sin δ at 76 °C
SI-3: SI based on J_{nr} at 0.1 kPa
SI-4: SI based on J_{nr} at 3.2 kPa
SI-5: SI based on log(G*) at 60 °C
SI-6: SI based on log(G*) at 76 °C
SI-7: SI based on G* at 60 °C
SI-8: SI based on G* at 76 °C
SI-9: SI based on SPD

The preceding results revealed that sulfur, compared to PPA, had a superior effect in reducing the storage separation found through storage stability evaluations. As a result, only sulfur was used as a cross-linking material in the next phase of the storage stability

study with PPC modified binders. As detailed in the next section, PPC modified binders with varied sulfur doses were fabricated and tested for storage stability.

5.3 Storage Stability Characterisation of PPC Modified Binders

5.3.1 Effect of sulfur on binder rheology

Temperature sweep: The complex modulus (G*) and phase angle (δ) results measured over 40 to 80 °C temperature range during the temperature sweep test are shown in Figure 5.11. The control binder, in this case, is the PPC-20 binder without sulfur. With an increase in temperature, there was a decrease in G* and an increase in δ for all PPC modified asphalt binders as a higher temperature reduces the binder stiffness and elasticity. Further, the inset figures in Figure 5.11 show a small increase in G* and a small decrease in δ at all temperatures after adding sulfur. This indicates a slight improvement in the deformation resistance and elastic behaviour of PPC modified asphalt with sulfur addition. Averaged over the entire range of temperatures, sulfur increased G* by 4%, 7% and 8% respectively at 0.15%, 0.3% and 0.45% dosages compared to the control binder. It was also observed that the increase in G* and decrease in δ persisted over the entire temperature range.

Frequency sweep: The dependence of storage (G′) and loss moduli (G″) on the frequency at 60 °C test temperature is shown in Figure 5.12a. It is observed that the addition of sulfur content caused a small improvement in the storage and loss moduli of the binders. Similarly, Figure 5.12b shows a slight increase in G* and a slight decrease in δ values with increased sulfur content. To further investigate the interaction of sulfur with PPC modified binder, sulfur-asphalt blends without PPC were prepared at the same sulfur dosages with the unmodified (base) VG 30 binder. The G* of the unmodified and the PPC modified binders at selected frequencies with multiple sulfur dosages are presented in Figure 5.13.

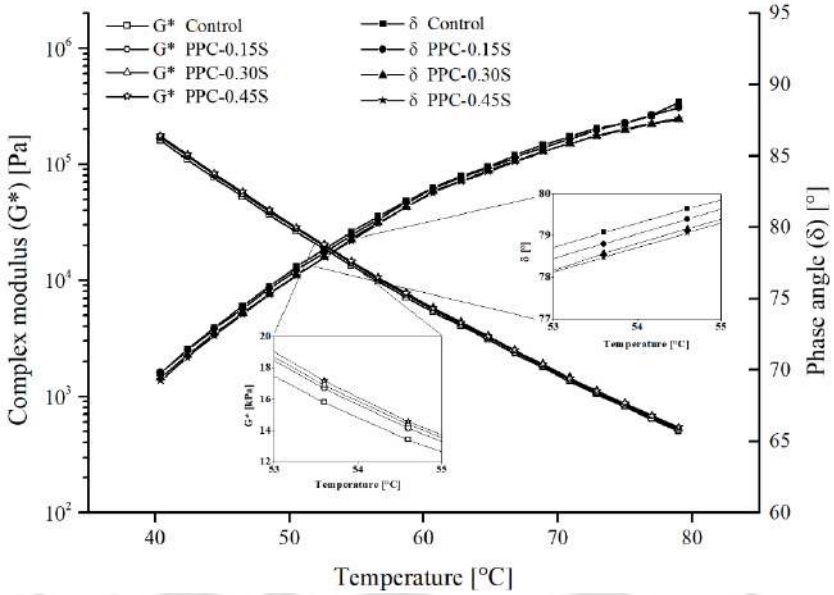

Figure 5.11 Temperature sweep results of PPC modified binders with different sulfur contents

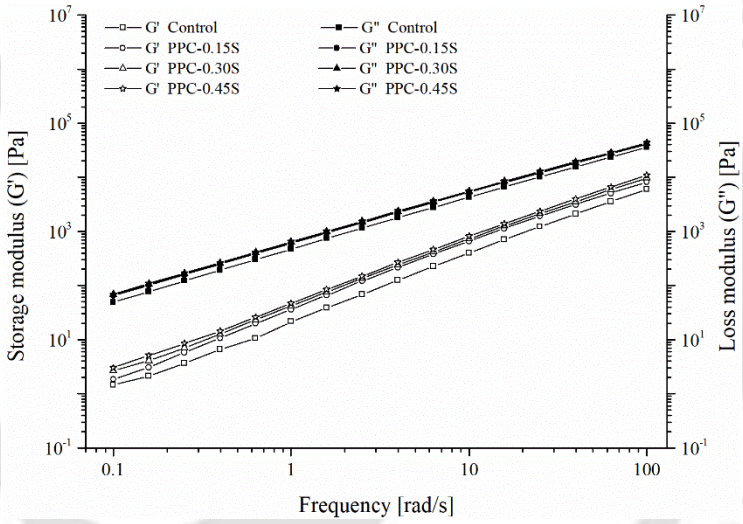

(a)

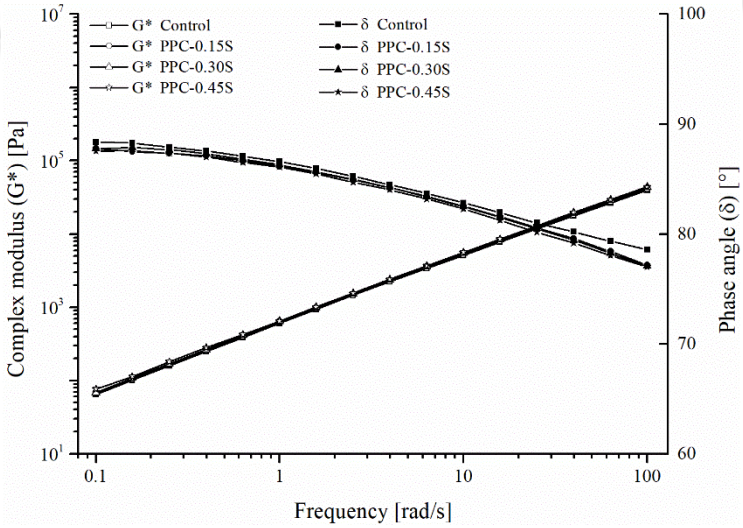

(b)

Figure 5.12 Frequency sweep results (a) storage and loss moduli (b) G* and δ

It is seen that the effect of sulfur was present in PPC modified binders, whereas almost constant G* values were obtained for the unmodified binder at multiple sulfur contents. It thus shows that sulfur interacted with PPC modified binders, and the interaction had a positive effect, no matter small, on the rheological performance.

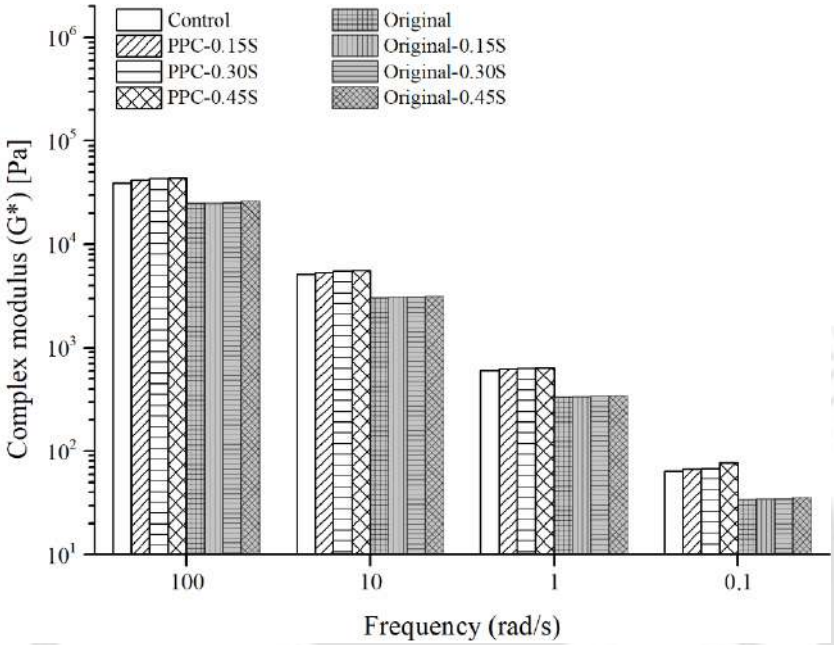

Figure 5.13 G* for unmodified and PPC modified binders with sulfur at multiple frequencies

The ZSV of the PPC modified binders was determined at 60 °C based on Cross model fit of complex viscosity (η*) versus frequency data from frequency sweep tests. The ZSV is determined as a steady-state viscosity at very low shear conditions, maintaining equilibrium without causing structural changes in the binder (Anderson et al., 2002; Liao and Chen, 2011). Figure 5.14a shows the Cross fit to the η*-frequency data for the PPC modified binders at different sulfur contents. A good fit can be seen in all cases with $R^2 \approx 0.99$. ZSV is used as a parameter reflecting the permanent deformation resistance of the binder. As shown in Figure 5.14b, the trend of ZSV was similar to that of other rheological variables with a slight increase at increasing sulfur dosages, indicating that the addition of sulfur slightly improved the permanent deformation behaviour of PPC modified binders.

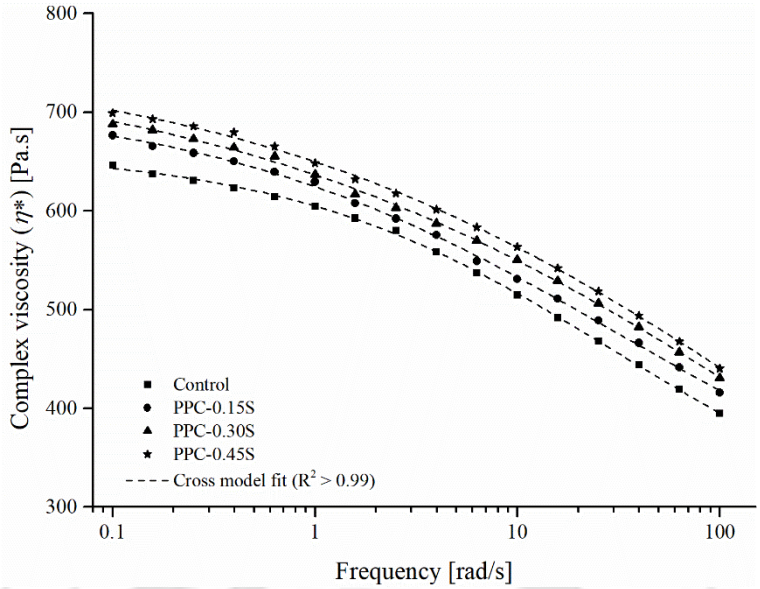

(a)

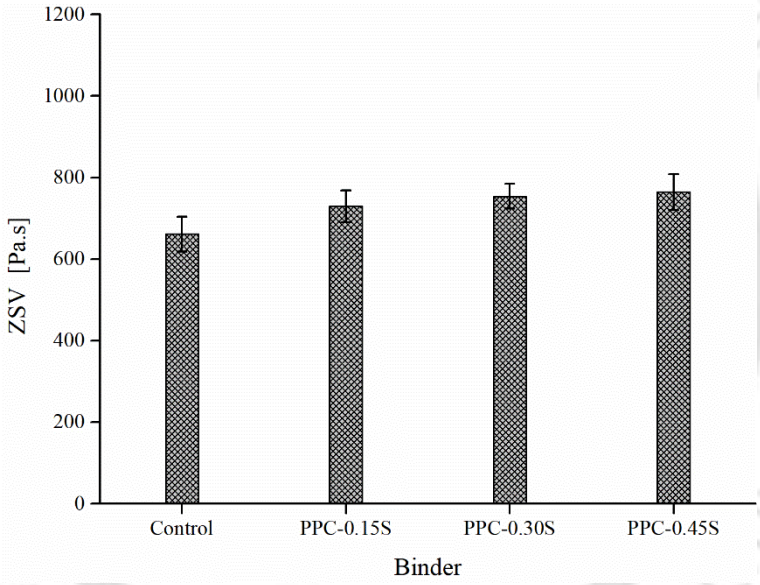

(b)

Figure 5.14 (a) Cross model fit to complex viscosity-frequency data for PPC modified binders, (b) ZSV results

MSCR: Figure 5.15a and 5.15b respectively present the results of MSCR J_{nr} and percent recovery of PPC modified binders at various sulfur contents and stress levels. The test was performed at 60 °C. The J_{nr} is a measure of the strain unrecovered at the end of the recovery period in MSCR creep-recovery cycles normalised to the stress applied, and therefore a lower value is desirable. Similarly, a higher recovery is desirable as it indicates a higher ability of the binder to restore the creep strains. The results from Figure 5.15a indicate that

the addition of sulfur had little to no effect on the MSCR J_{nr}. A similar observation can also be made for percent recovery at both stress levels (0.1 and 3.2 kPa) from Figure 5.15b.

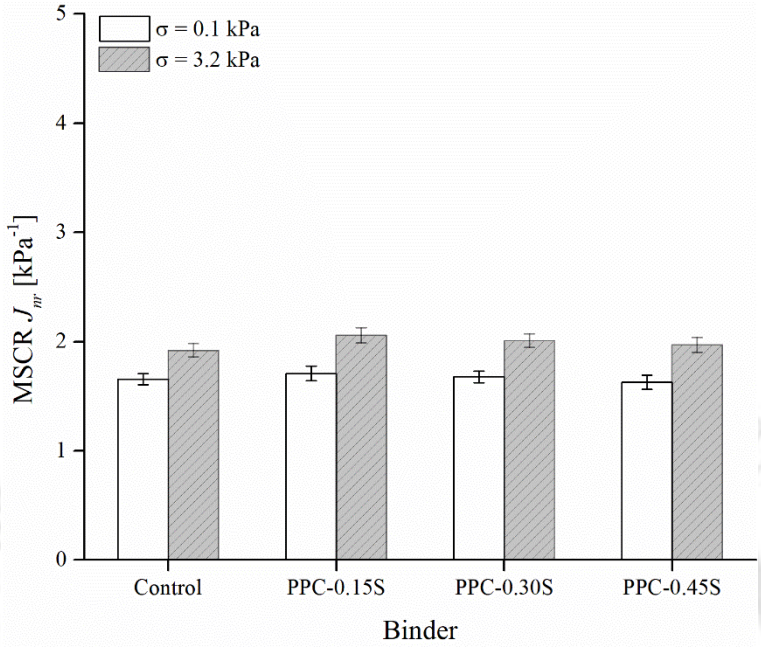

(a)

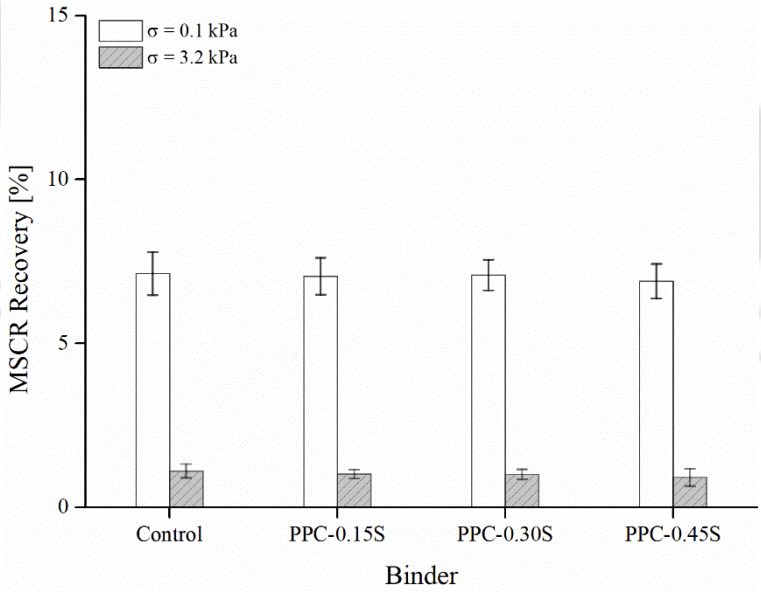

(b)

Figure 5.15 (a) MSCR J_{nr} results at different sulfur dosages, (b) MSCR recovery results at different sulfur dosages

Although previous studies reported a profound effect of sulfur in improving the rheological properties of binders modified with polymers/rubber (Polacco et al, 2015;

Liang et al., 2017; tur Rasool et al., 2017; Padhan et al., 2019); however, in this study, the findings with multiple sulfur dosages showed slight improvements to almost no change in the rheological parameters (G*, δ, G′, G″, ZSV, MSCR J_{nr}, and MSCR recovery). The chemical nature of polymers and rubber is much different from that of PPC, and hence the interactions of PPC with sulfur are expected to be different from the interactions with polymer/rubber. Nevertheless, sulfur's effect was still positive to slightly enhance the stiffness of the PPC modified binders as found from temperature and frequency sweep results.

5.3.2 Analysis of storage stability

Rheological SIs based on G*, G*/sin δ, and SRP: The details of the SIs used to evaluate the storage separation of PPC modified binders with different sulfur contents were presented in Table 3.5. SIs based on G*, G*/sin δ, and Shenoy rutting parameter (SRP) were used to characterise the storage stability of the binders as a function of temperature and frequency. These three SIs are presented as a function of temperatures from 40 to 80 °C (Figure 5.16) and frequencies from 0.1 to 100 rad/s (Figure 5.17) under both ratio and max-avg formulations. It is to be noted that values near 1 are desirable for SIs formulated in the ratio form, whereas a lower value (near 0) is desirable for SIs formulated in the max-avg form (the desirable values are also indicated in Figures 5.16 and 5.17).

The SI values became steady with fewer changes from temperatures of 55 to 80 °C. This observation is found valid for both ratio and max-avg forms of the indices. A crossover of SI based on SRP was observed for PPC-0.15S and PPC-0.45S binders near 46 °C, but beyond that, the trend of SI based on SRP with temperature was similar for other indices. The variation of SIs with frequency was relatively constant except for some variations observed at frequencies lower than 1 rad/s (Figure 5.17).

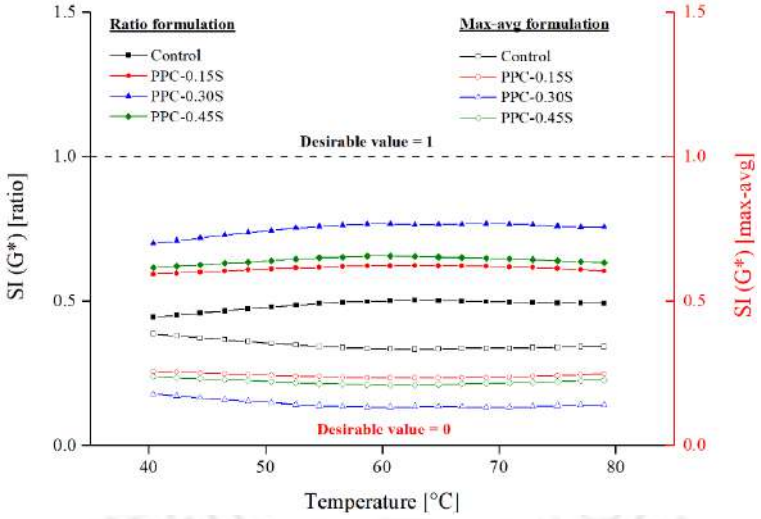

(a)

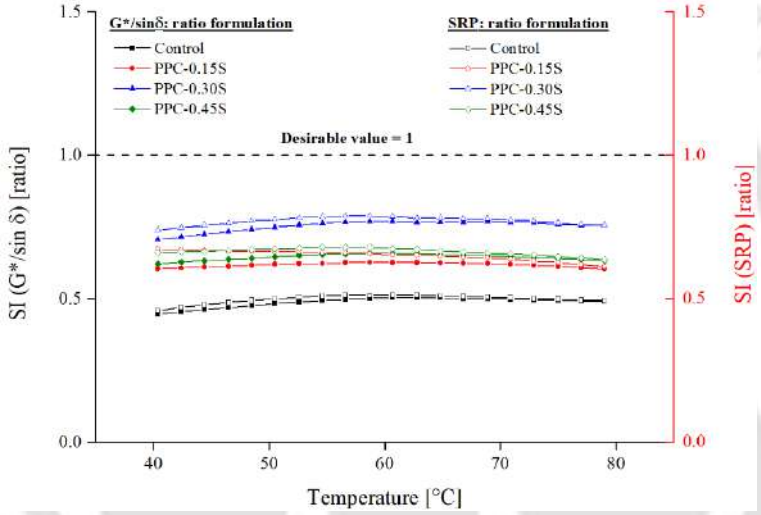

(b)

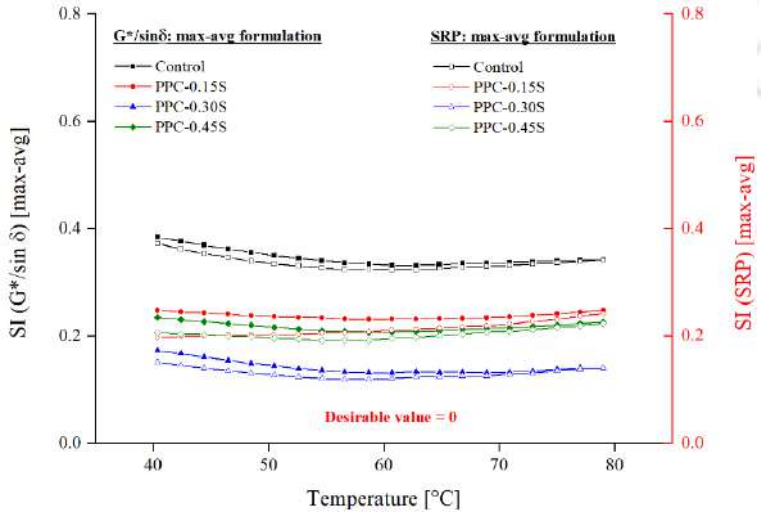

(c)

Figure 5.16 SIs as function of temperature: SI based on (a) ratio and max-avg formulations of G*, (b) ratio formulation of G*/sin δ and SRP, and (c) max-avg formulation of G*/sin δ and SRP

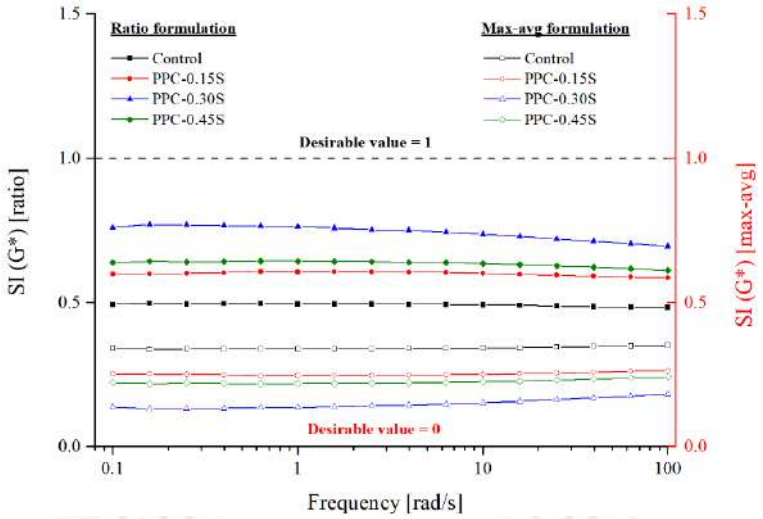

(a)

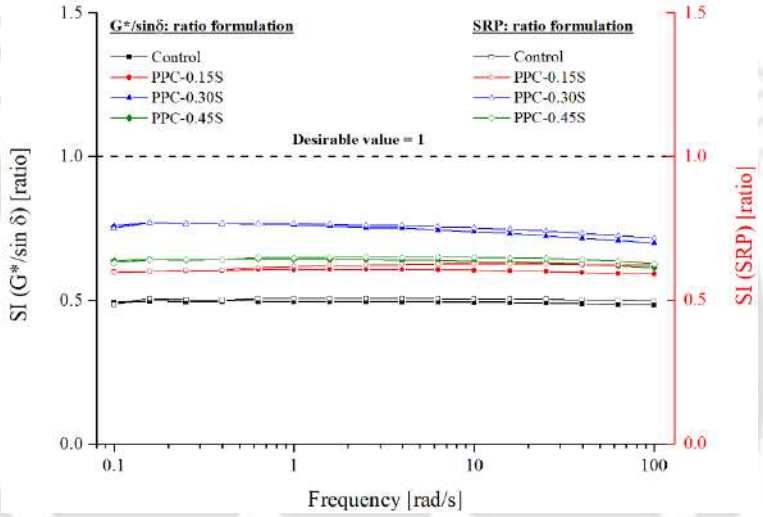

(b)

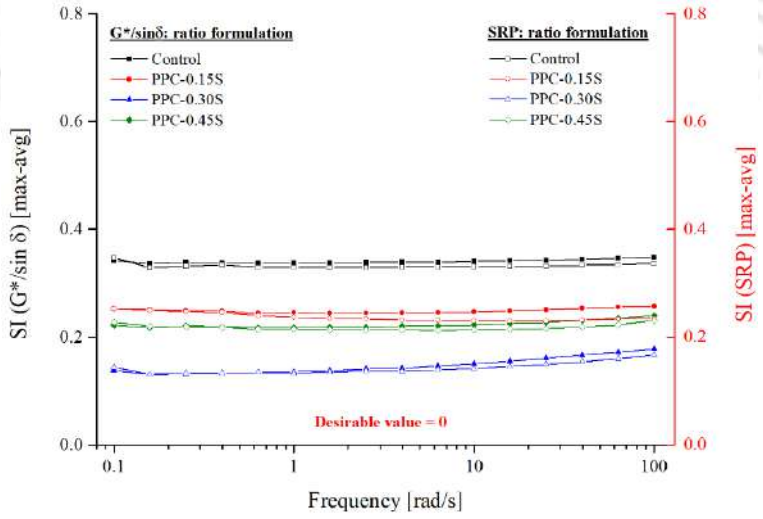

(c)

Figure 5.17 SIs as function of frequency: SI based on (a) ratio and max-avg formulations of G*, (b) ratio formulation of G*/sin δ and SRP, and (c) max-avg formulation of G*/sin δ and SRP

The results showed that the separation indices remained somewhat constant in the temperature range of 55 to 80 °C and frequency range of 1 to 100 rad/s, and therefore the use of any temperature or frequency within these ranges is expected to yield the same ranking of binder separation performance.

The control PPC modified binder showed poor storage stability due to the migration of PPC particles toward the bottom of the tube during hot storage. The migration is driven by gravitational forces and can be attributed to the density difference between PPC (specific gravity = 1.74) and the base asphalt binder (specific gravity = 1.03). The addition of sulfur improved the storage stability of the PPC modified binders, as seen from the increase in ratio-based indices and decrease in max-avg-based indices. The PPC-0.3S modified binder with 0.3% sulfur showed the best results considering all indices in both formulations. It is also seen that both ratio and max-avg formulations of the indices captured the differences in storage stability performance of the PPC modified binders at different sulfur dosages.

Statistical analysis: The SI results were submitted to one-way analysis of variance (ANOVA) conducted separately on temperature and frequency sweep test results obtained in ratio and max-avg forms at a 5% level of significance. Sulfur dosage was the independent variable, and the indices were response variables. Table 5.2 presents the multiple comparison results based on Tukey's honest significance difference approach. SI based on G*/sin δ and G*, whether in ratio or max-avg forms, were found to be statistically similar. Comparing the G*/sin δ and SRP based indices, in both ratio and max-avg forms, the SRP index yielded slightly higher performance in terms of separation index than the G*/sin δ index, especially at lower temperatures and higher frequencies (Figures 5.16b,c and 5.17b,c). This is attributed to the enhanced effect of the phase angle as the binder becomes increasingly elastic at lower temperatures and higher frequencies. Hence, the statistical analysis reported significant differences between SRP and other indices. The differences

between SRP and G*/sin δ based separation indices were reduced at higher temperatures and lower frequencies.

Table 5.2 Multiple comparison results from ANOVA

Comparison between SIs based on	***Formulation***	***TS data***		***FS data***	
		p-value	***S/NS***	***p-value***	***S/NS***
G* and G*/sin δ	Ratio	0.118	NS	0.675	NS
G* and SRP	Ratio	<0.001	S	<0.001	S
G*/sin δ and SRP	Ratio	<0.001	S	<0.001	S
G* and G*/sin δ	Max-avg	0.125	NS	0.612	NS
G* and SRP	Max-avg	<0.001	S	<0.001	S
G*/sin δ and SRP	Max-avg	<0.001	S	<0.001	S

Note: TS: temperature sweep; FS: frequency sweep; S: significant; NS: not significant

SPD and rheological SI based on MSCR: Figure 5.18 presents the SI derived from MSCR J_{nr} in ratio and max-avg forms. The PPC modified binder with 0.3% sulfur content again showed the least separation differences among all binders. The binders can be ranked as follows: PPC-0.3S > PPC-0.45S > PPC-0.15S > control (in high to low order of separation performance). The observations from J_{nr} based indices agree with those from G*, G*/sin δ and SRP based indices. According to the results shown in Figure 5.18, the separation indices determined by J_{nr} at 0.1 and 3.2 kPa stress levels were quite close to each other. The stress levels of 0.1 and 3.2 kPa provided similar separation indices in both ratio and max-avg formulations.

Figure 5.19 presents the SPD results of the binders. The current Indian specifications for polymer (IS 15642, 2019) and rubber modified (IS 17079, 2019) asphalt binders stipulate maximum SPD values of 3 and 4 °C, respectively, for judging the storage stability performance. Notably, these specifications are not directly applicable to PPC modified binders due to apparent differences in the nature of the modifiers. However, PPC modified

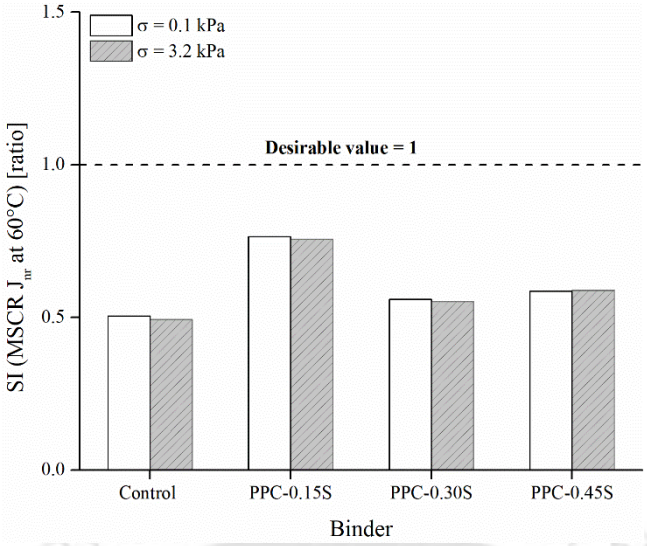

(a)

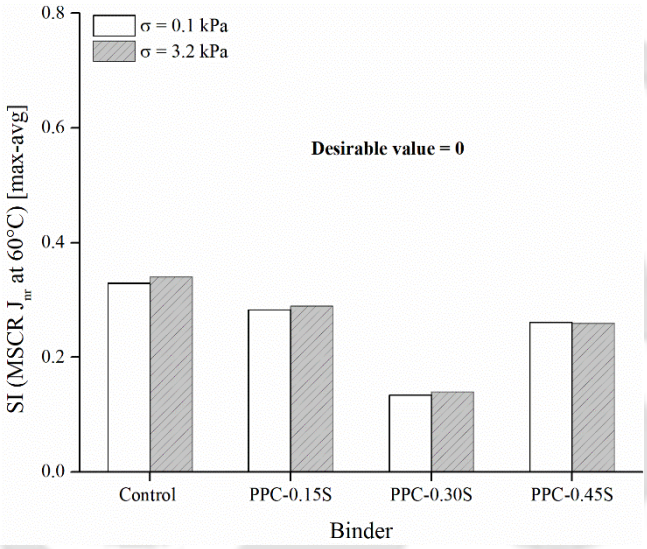

(b)

Figure 5.18 SI based on MSCR J_{nr}: (a) ratio form, (b) max-avg form

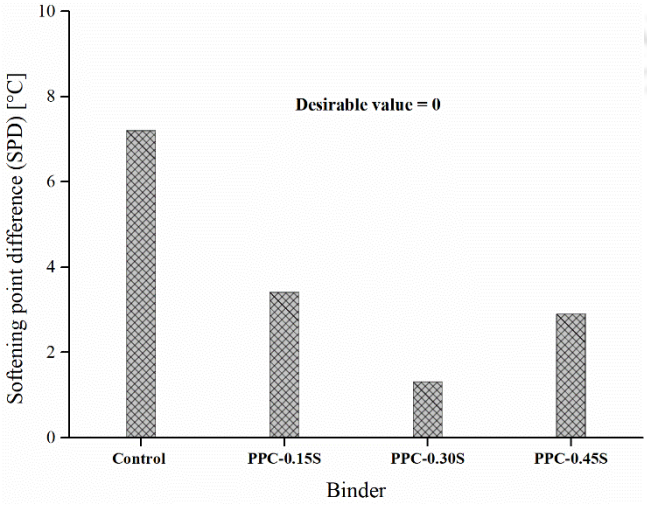

Figure 5.19 Softening point difference (SPD) results

binders with all sulfur dosages meet the criterion for rubber modified binders as SPDs are below 4 °C, whereas the binders with 0.3% and 0.45% sulfur also meet the criterion for polymer modified binders as SPD < 3 °C.

The ability of sulfur to improve storage stability in polymer/rubber modified asphalt binders has been primarily attributed to the reaction of sulfur with unsaturated C=C double bonds and the formation of interconnections cross-linking the polymer chains with themselves and with the asphalt (Polacco et al., 2015; Liang et al., 2017). The FTIR spectroscopy of PPC showed diverse chemical functional groups, including the C=C double bond (Figure 4.4b). Therefore, it is hypothesised that sulfur interacted with some PPC chemical functionalities that contributed to lower differences in the properties of top and bottom segments and thus produced a more storage stable PPC modified binder. This hypothesis is suggested on the basis of improved storage stability performance, and a further detailed investigation focused on the chemistry of sulfur in PPC modified asphalt binders will be helpful to identify the precise chemical mechanisms.

FTIR spectroscopy: FTIR analysis was conducted for the top and bottom sections of control, PPC-0.15S, PPC-0.30S, and PPC-0.45S binders. Figure 5.20 shows that major absorbance peaks occurred at the same locations for the studied binders. The corresponding functional groups at the observed absorbance peaks were identified based on the asphalt FTIR literature (Mouillet et al., 2008; Weigel and Stephan, 2017; Sigmaaldrich, 2021). The strong absorbance peaks between 2800 and 3000 cm^{-1} wavenumbers show the presence of aliphatic —C-H stretching of alkane compound class. The spectral peak at 1620 cm^{-1} corresponds to C=C stretching and belongs to unsaturated ketone. The absorptions peaks around 1465 cm^{-1} and 1380 cm^{-1} are assigned to —C-H bending and affiliated to aldehyde and alkane classes, respectively. The spectral peak at 1070 cm^{-1} is attributed to S=O stretching. Additionally, the absorbance peaks between 905-915 cm^{-1} and 790-840 cm^{-1}

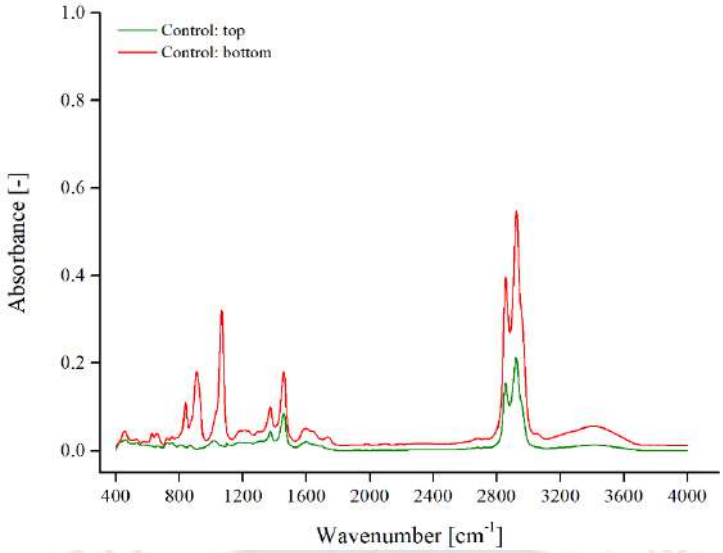

(a)

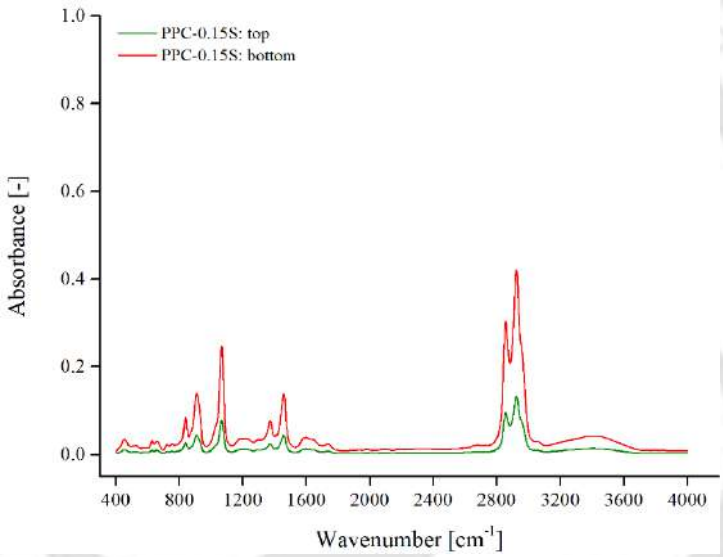

(b)

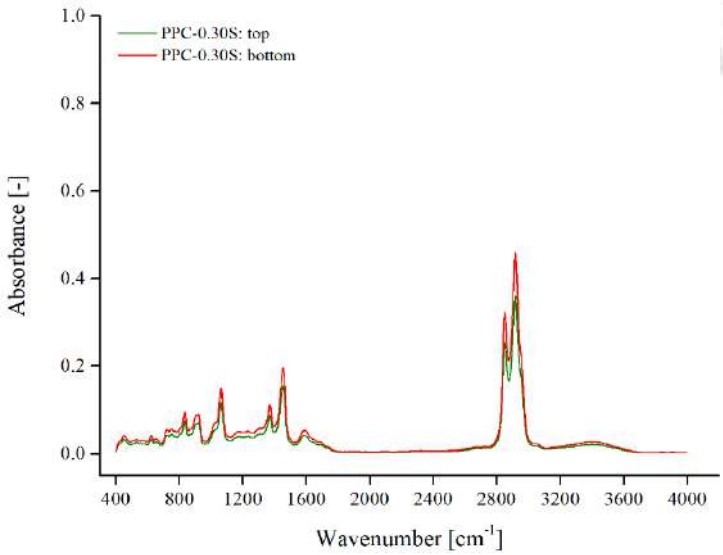

(c)

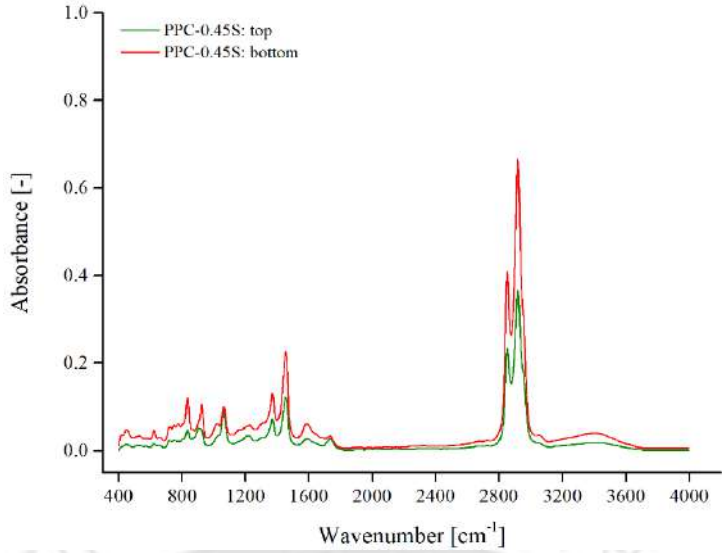

(d)

Figure 5.20 FTIR spectra of top and bottom segment binders (a) control, (b) PPC-0.15S, (c) PPC-0.3S, and (d) PPC-0.45S

suggest the presence of C=C bending and belong to monosubstituted and trisubstituted alkene, respectively.

A qualitative analysis was performed by inspecting the differences in the overall FTIR spectra between the top and bottom segment binders. It can be seen in Figure 5.20a that the spectral curve for the bottom segment of the control binder had a higher absorbance peak than the top segment suggesting that the bottom part had a higher concentration of PPC particles. A similar observation was reported by Lu et al. (1999) with higher absorbance peaks in the spectra of the top segment of an SBS-modified binder than the bottom segment, which was ascribed to the presence of higher SBS concentration in the top section. Figure 5.20c shows that the incorporation of sulfur enhanced the homogeneity as the spectral curve for top and bottom sections came closer at 0.3% sulfur and exhibited the least difference. A similar conclusion was also made by Zhang et al. (2018b), where the FTIR spectra of the top and bottom sections of a bio-asphalt binder were in close proximity after thermal storage. The observed trends for FTIR agree with the rheological SIs with the PPC-0.30S binder showing the best storage stability performance.

5.4 Validation of Storage Stability

The storage stability results of TPC and PPC modified binders presented in the previous sections revealed that a 0.3% sulfur dosage reduced separation well. TPC and PPC modified binders at all four contents (5, 10, 15, and 20%) were prepared with 0.3% sulfur dosage and then evaluated for storage stability test (ASTM D7173, 2020). The results of the high-temperature storage stability test evaluated through the SPD are shown in Figure 5.21.

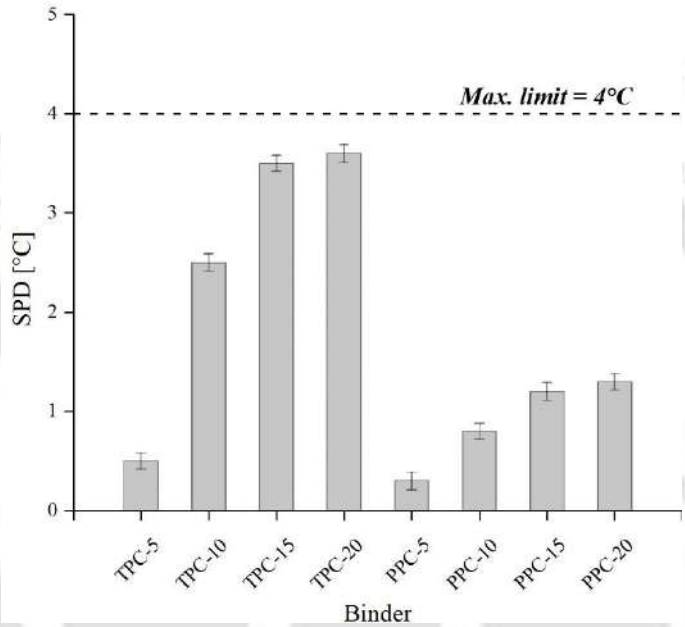

Figure 5.21 Validation of storage stability for all modified binders at 0.3% sulfur

Since the density of TPC and PPC was slightly higher than that of the base binder, the softening point of the binder from the lower section was higher than that of the top section of the tube. The difference between the softening points of the upper and lower parts increased with an increase in TPC and PPC dosage. In the absence of a current specification citing critical SPD limit for char modified binders, the limit for rubber-modified bitumen was used to compare the storage stability results. All modified binders had SPD less than 4 °C (critical limit set by IS 17079 (2019) for rubber-modified bitumen). The observed results showed that all modified binders were acceptably stable and therefore, a 0.3% sulfur dosage was used to prepare the TPC and PPC modified binders for further tests of the study.

5.5 Summary

This chapter described the thermal storage stability characteristics of TPC and PPC modified binders with different dosages of cross-linking agents PPA and sulfur. For TPC modified binders, three dosages of PPA and sulfur were used, while the storage stability performance of PPC modified binders was analysed with different sulfur contents. The effect of cross-linking agents on the rheological performance of the binders was also investigated through temperature sweep, frequency sweep, and MSCR tests. Several rheology based separation indices were used in addition to the conventionally used softening point difference (SPD). The rheological separation indices were based on frequency sweep, temperature sweep, and MSCR tests. The investigations were performed on binders fabricated with 20% dosages of TPC and PPC and later validated for binders with other TPC and PPC dosages.

Improved storage stability was found with the addition of sulfur to the TPC modified asphalt binder. The addition of PPA also enhanced the storage stability performance. PPA content of 1.0% and sulfur content of 0.3% produced the lowest separation indices as measured from SPD and rheological parameters. Remixing of the TPC modified binder had a significant positive effect on the thermal storage stability. The effect of PPA on the rheological characteristics of the TPC modified binders was significant, and it improved the performance compared to the negligible/marginal changes observed with sulfur. FTIR spectroscopic analysis indicated that the proximity of spectral trends improved with the addition of PPA and sulfur, with the best results obtained for remixed samples.

In the case of PPC modified binder, separation indices formulated in both forms (ratio form and maximum-average difference form) showed similar variation in storage stability performance. The variation of separation indices remained constant for temperatures of 55 to 80 °C and frequencies of 1 to 100 rad/s. The addition of sulfur had marked improvement

in storage stability of PPC modified binders. A sulfur dosage of 0.3% by weight of the binder showed the best separation performance among all dosages. Qualitative FTIR spectra analysis further showed that the closeness of spectral curves improved with the addition of sulfur. The 0.3% sulfur dosage was validated for TPC and PPC modified binders prepared at the other three char dosages (5, 10, and 15%).

Chapter 6

CHARACTERISATION OF CHAR MODIFIED ASPHALT BINDERS

6.1 Introduction

One of the key goals of the Strategic Highway Research Program (SHRP) was to figure out what physical properties of asphalt binders are connected to pavement performance and how to quantify them accurately (Anderson et al., 1994). The investigation found that many asphalt binder characterisation approaches were constrained by empiricism and oversimplification. The project's conclusions showed the importance of fundamental rheological characterisation while selecting asphalt binders (Bahia and Anderson, 1995a). The project marked a new beginning in the testing and grading of asphalt binders through the introduction of rheology based innovative test methods and parameters determined on a dynamic shear rheometer (DSR).

The rheological characteristics of asphalt binder play an important role in the performance of an asphalt pavement. The DSR enables measurement of rheological attributes of asphalt binders under different stress-strain-time-temperature combinations. The linear viscoelastic behaviour of binders is characterised by two main parameters: complex modulus (G*) and phase angle (δ). The parameters G*/sin δ and G*sin δ respectively measure the binder's contribution to rutting and fatigue resistance and are also included in the Superpave performance grading (PG) specifications (ASTM D6373, 2016). Recently, some new test procedures for asphalt binder rutting and fatigue characterisation have been investigated and suggested, which seek to overcome some shortcomings associated with the Superpave parameters based on G* and δ. Multiple stress creep and

recovery (MSCR) and linear amplitude sweep (LAS) tests are quite accepted new tests used to evaluate binders' rutting and fatigue performance, respectively. It is thus important to investigate the effect of incorporation of pyrolytic chars on the properties of asphalt binders through evaluation of rheological properties of the char-modified binders.

During the pavement service life, several complex physical and chemical processes occur in an asphalt binder, such as volatilisation, oxidation, and condensation, causing the asphalt binder to become harder and more brittle. This phenomenon is referred to as asphalt ageing and contributes significantly to embrittlement in asphalt pavements, eventually leading to pavement cracking (Petersen, 2009; Sirin et al., 2018; Wang et al., 2020b). Rolling thin film oven (RTFO) and pressure ageing vessel (PAV) test procedures are commonly used devices for laboratory simulation of short-term and long-term ageing of asphalt binders, respectively. To determine the level of changes caused by ageing, binder properties (such as rheological characteristics) need to be evaluated before and after ageing of asphalt binders. In addition, additional techniques/procedures for studying changes in asphalt chemical composition due to ageing are being used, with Fourier transform infrared (FTIR) spectroscopy being one of the most extensively employed.

This chapter describes the results of conventional and rheological properties of control and TPC/PPC modified asphalt binders with the experimental plan formulated under Task 3 of the study. The conventional tests performed on the binders were penetration, softening point, and viscosity. The different rheological tests performed on the binders were frequency sweep, temperature sweep, high performance grade (PG) measurement, MSCR test, G* and δ master curves, G*sin δ measurement, and LAS. To further examine the rutting performance of TPC and PPC modified binders, the chapter also presents the results of a multi-temperature and multi-parameter based rutting characterisation.

The chapter also investigates the ageing characteristics of the control and modified binders with the experimental plan formulated under Task 4. Four rheological ageing indices were used to assess the ageing properties of the binders and were based on G*, δ, ZSV, and MSCR non-recoverable creep compliance (J_{nr}). FTIR spectroscopy analysis was also then used to investigate changes in chemical composition due to ageing in the char modified binders through carbonyl and sulfoxide indices.

6.2 Conventional and Rheological Properties of Char Modified Binders

6.2.1 Conventional properties

The results of conventional tests, including penetration, softening point, and viscosity (at 135 °C), are presented in Figure 6.1. The addition of TPC and PPC decreased the penetration (Figure 6.1a) and increased the softening point (Figure 6.1b) values. The penetration values declined by 26, 34, 46, and 58% for each 5% increment in TPC dosage, while the reduction was 33, 44, 53, and 72% in PPC-modified binders with each 5% increment in PPC dosage. On the other hand, softening point values increased by about 14% for TPC-20 and PPC-20 compared to the control binder. The higher softening point and lower penetration can be attributed to the improved binder stiffness induced by the pyrolytic chars. The stiffening of the binder is due to the distinctive characteristics of pyrolytic char, which has a high surface area and oil absorption capacity, thus absorbing the binder's light fractions (Chaala et al., 1996; Wang et al., 2019).

Figure 6.1c shows the viscosities of asphalt binders at different TPC and PPC contents at 135 °C. The Superpave system specifies a maximum viscosity limit of 3 Pa.s (3000 cP) at 135 °C to ensure adequate workability and the ability to transport/pump the binder. Binders at all char dosages met this criterion with a maximum viscosity of 1.1 Pa.s (1100 cP) at 20% PPC dosage. The increase in pyrolytic char content increased the viscosity

values indicating the stiffening effect with the addition of the char. The viscosity of PPC modified binders was higher than that of TPC modified binders at each char dosage. For example, at 135 °C, PPC modified binders had 8, 14, 14, and 42% increase in viscosity at char contents of 5, 10, 15, and 20%, respectively, compared to the viscosity of TPC modified binders at these contents. The results indicate that the stiffening effect of PPC is higher than TPC, as also observed from penetration and softening point tests. Higher viscosity also indicates that the modification by TPC and PPC is expected to elevate the mixing and compaction temperatures (discussed in the Chapter 7).

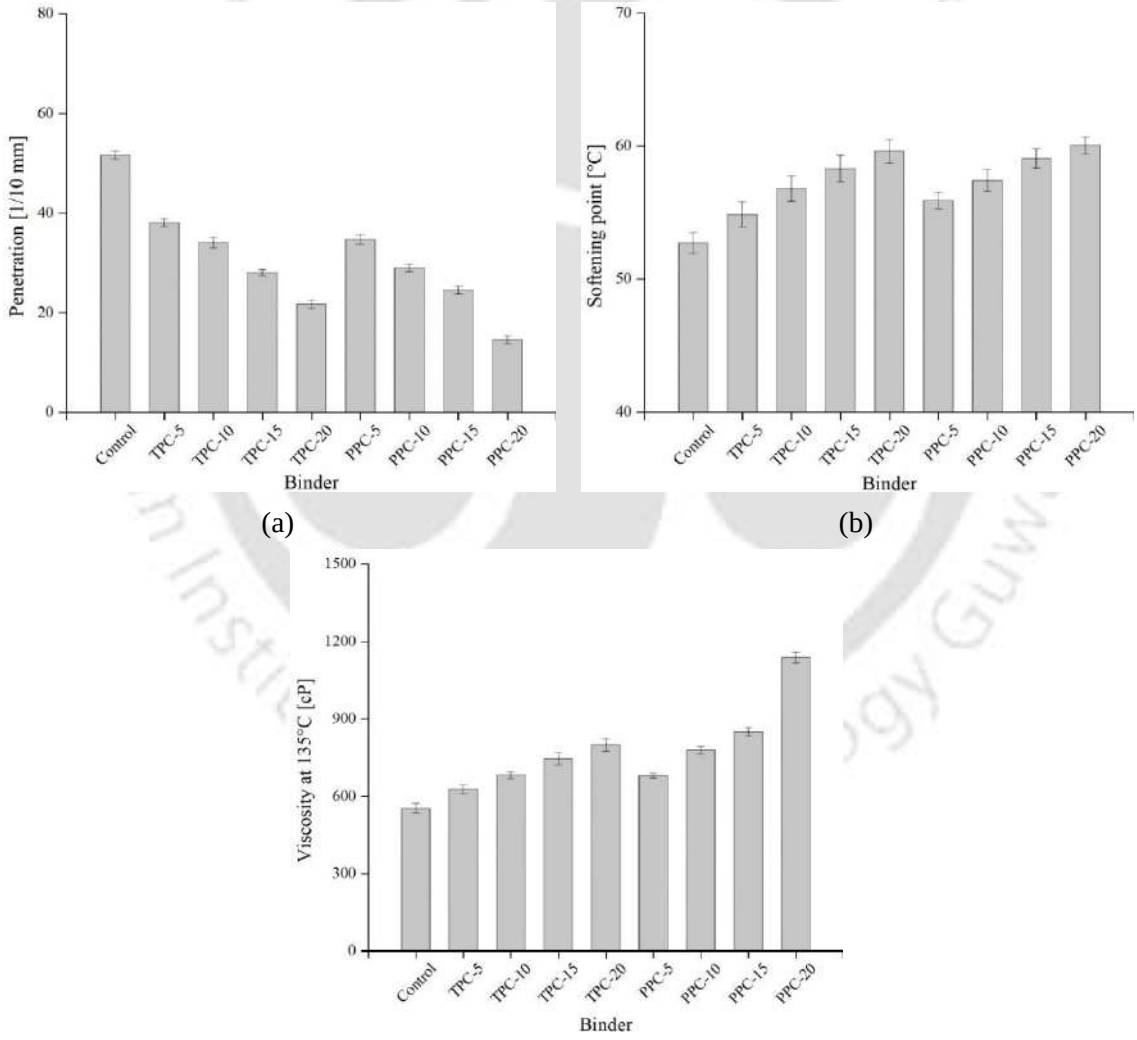

Figure 6.1 Conventional test results (a) penetration; (b) softening point; (c) viscosity at 135 °C

6.2.2 Continuous high PG

The failure temperatures are the temperatures where the Superpave rutting parameter G*/sin δ reaches the values of 1.0 kPa and 2.2 kPa, respectively, for unaged and short-term aged binders. The failure temperatures are also called continuous high PG. The Superpave high PG designation is decided based on the values of the failure temperature of the unaged and short-term aged binders and their comparison with the standard PG grades. As presented in Figure 6.2, the continuous PG temperatures increased with the addition of both pyrolytic chars. The control binder corresponded to a PG 64 as the failure temperature was 68 °C for unaged and 66.8 °C for short-term aged conditions. Even though the addition of TPC to the base binder increased the failure temperature, it did not shift the PG grade, and all TPC-modified binders were graded PG 64. On the other hand, PPC-modified binders had higher failure temperatures than the control and TPC-modified binders under both unaged and short-term aged conditions. PPC-5 and PPC-10 binders were graded PG 64 while PPC-15 and PPC-20 showed one-grade jump to PG 70.

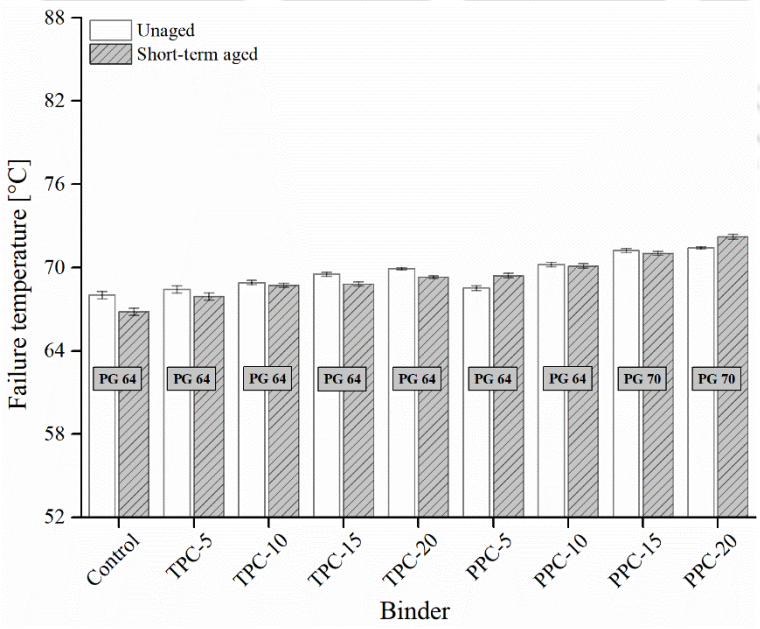

Figure 6.2 Failure temperatures under unaged and short-term aged conditions and high-PG grades

Further, the continuous grades of PPC-modified binders were relatively higher than those of TPC-modified binders. The results demonstrate that TPC and PPC incorporation improves binder resistance to permanent deformation, and the effect becomes more pronounced at higher TPC and PPC dosages.

6.2.3 Master curves for G and δ*

G* and δ master curves were constructed based on frequency sweeps conducted at 10, 20, 30, 40, 50, 60, and 70 °C. Short-term aged binders were used in frequency sweeps. The reference temperature used was 20 °C, while the frequencies were varied from 0.1 to 100 rad/s at each temperature. As shown in Figure 6.3, master curves of G* and δ were constructed at a reference temperature of 20 °C to observe the binder rheological response in a broader frequency domain. The behaviour of asphalt binder in the lower region of frequency in the master curve represents the high-temperature regime, while the higher frequency region corresponds to the low-temperature regime (Tarar et al., 2021). The sigmoidal model (Equation 3.13) was used to construct the G* and δ master curves. The smooth master curves of both G* and δ show that the time-temperature superposition principle worked effectively for TPC and PPC-modified binders. As evident from Figure 6.3b, the addition of PPC considerably increased the G* values at lower frequencies, implying improved deformation resistance at higher service temperatures, while in the higher frequencies (related to lower temperatures) also, a slight increment in G* was seen. Even though TPC-modified binders also had higher G* curves than the control binder in the whole frequency regime, the increase was relatively small compared to PPC.

The δ master curves for PPC-modified binders lay below that of the control binder in the whole frequency regime, and a significant decrease could be observed in the low-frequency regime (high-temperature region). The δ master curves decreased, but the reduction in TPC-modified binders was less noticeable. This indicates the elastic response

was higher in PPC-modified binders than TPC-modified ones. The observed trends show that both TPC and PPC stiffen the binder at lower frequencies, reducing rutting in high-temperature conditions while maintaining low-temperature characteristics nearly similar to the base binder. The effect with PPC modification was more noticeable than that with TPC modification.

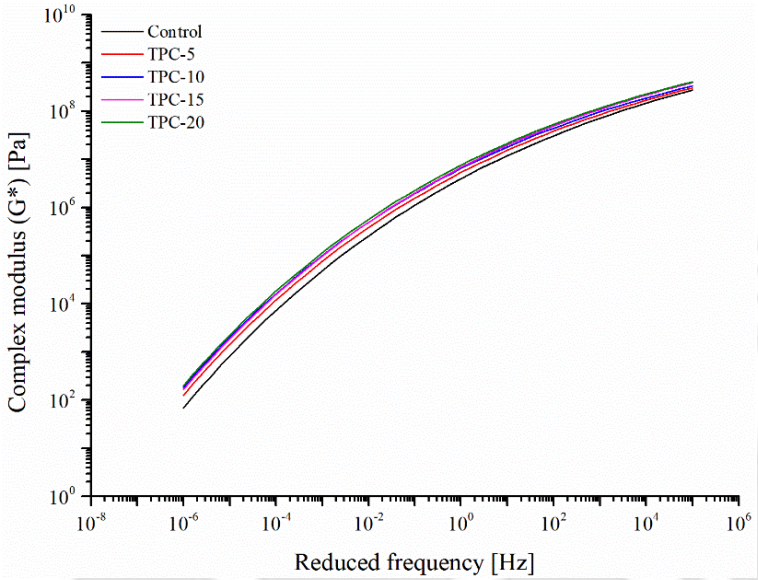

(a)

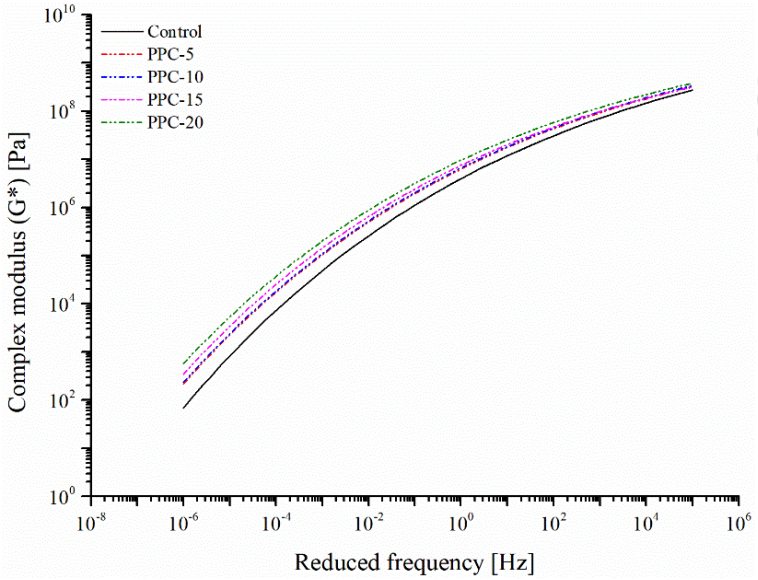

(b)

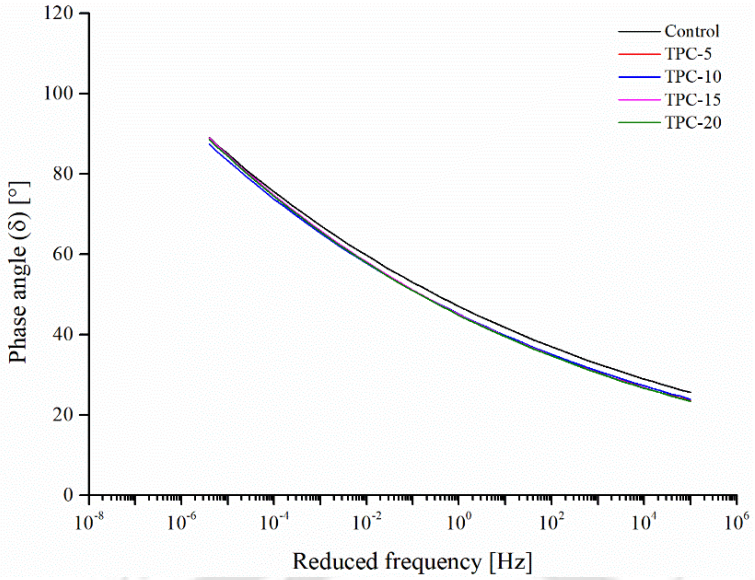

(c)

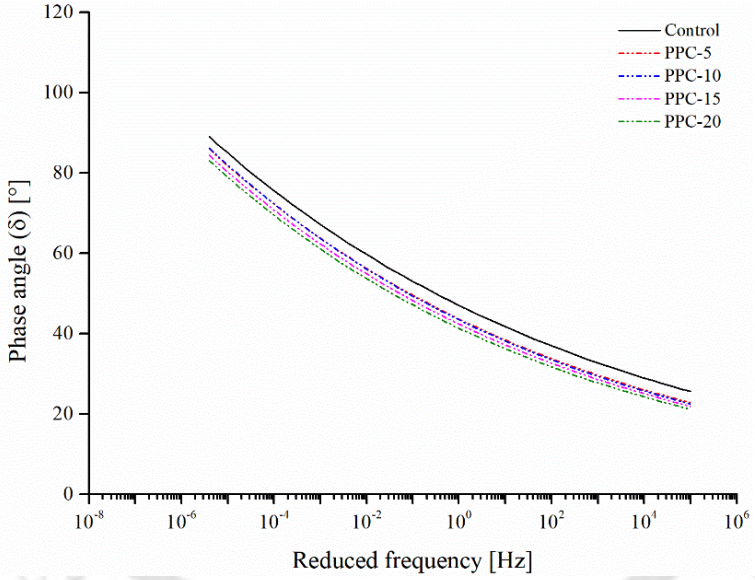

(d)

Figure 6.3 Master curves: (a) G* master curves for TPC-modified binders; (c) G* master curves for PPC-modified binders; (d) δ master curves for TPC-modified binders; (e) δ master curves for PPC-modified binders

6.2.4 Multiple stress creep and recovery (MSCR)

The MSCR test was carried out at two stress levels (0.1 and 3.2 kPa) and 60 °C temperature. To evaluate the performance of binders against rutting at high-temperature, the non-recoverable creep compliance (J_{nr}) at two stress levels of 0.1 and 3.2 kPa was acquired. J_{nr} variations for all binders are shown in Figure 6.4 at both stress levels. A lower J_{nr} at a given

stress level indicates a greater potential of the asphalt binder to resist permanent deformation at high temperatures. Figure 6.4 shows that J_{nr} values of the TPC and PPC-modified binders at both stress levels were lower than the control binder and J_{nr} values decreased with an increase in TPC and PPC dosage. Comparing the two pyrolytic chars, the PPC-modified binders had lower J_{nr} than TPC binders at both stress levels. At 3.2 kPa, the J_{nr} values for TPC-20 and PPC-20 binders were 43% and 67% lower than the control binder, respectively. This pattern indicates that the modified binders perform better at high temperatures when subjected to low and high stress levels. Furthermore, the J_{nr} difference (the percentage difference between J_{nr} values at 0.1 and 3.2 kPa stress levels) for all binders was within the standard limit of 75% maximum.

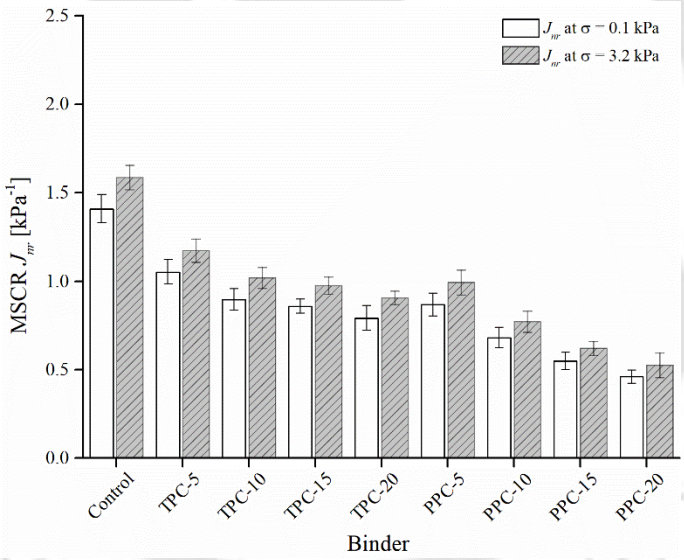

Figure 6.4 MSCR J_{nr} results at 0.1 kPa and 3.2 kPa stress levels

The MSCR recovery at both stress levels was measured to assess the binders' elastic response, and the results are shown in Figure 6.5. The MSCR recovery increased at both stress levels for both TPC and PPC-modified binders compared to the control binder. The PPC had a higher effect on recovery values than the TPC, as also observed from the phase angle master curves discussed previously. For example, TPC-20 showed 39% and 53% higher recovery than the control binder at 0.1 and 3.2 kPa stress levels, respectively, while

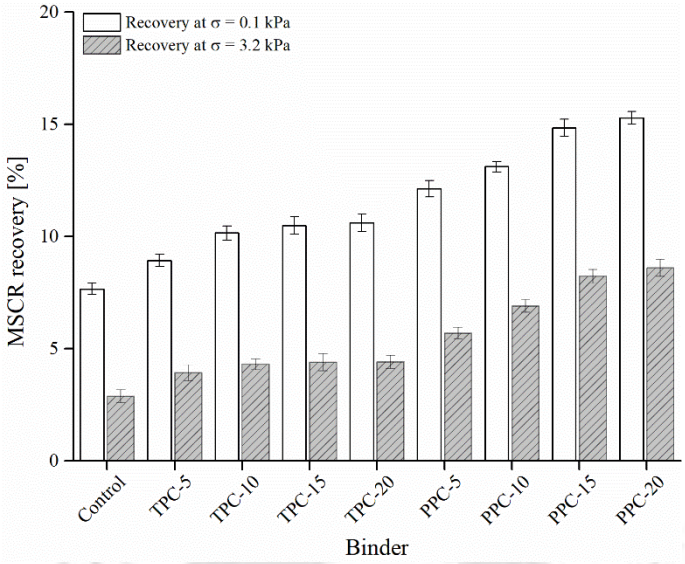

Figure 6.5 MSCR recovery results at 0.1 kPa and at 3.2 kPa stress levels

the subsequent increase for the PPC-20 binder was 100% and 199%.The observed MSCR results of TPC and PPC-modified binders indicate a better rutting performance at high temperatures. A similar significant reduction in J_{nr} and increase in recovery was also observed in a previous study for asphalt binders modified with carbon black from scrap tyre pyrolysis (Wang et al., 2019). It is noted that the results of MSCR are presented here at a single temperature (60 °C) only. The following section (Section 6.3) presents the results of advanced rutting characterisation performed with multi-temperature and multi-parameter based analysis. The possible contributory mechanisms for improved rutting resistance of the pyrolytic char modified binders are presented in Subsection 6.3.4.

*6.2.5 Superpave fatigue parameter (G*sin δ)*

G*sin δ of all binders was evaluated over a range of intermediate service temperatures varying from 10 to 40 °C (at 3 °C intervals). Figure 6.6 presents the results for TPC and PPC modified binders at various temperatures, while Figure 6.7 shows the failure temperatures (*i.e.*, the temperature corresponding to G*sin δ = 5000 kPa). The modified binders showed higher G*sin δ values than the control binder at all test temperatures, representing a lower fatigue resistance. An increase in TPC or PPC content increased the

G*sin δ values. Figure 6.7 shows that the failure temperatures of PPC modified binders are lower than TPC modified ones, indicating that the 5000 kPa limit for PPC modified binders is reached at much lower temperatures than TPC modified ones and therefore a better fatigue performance of PPC modified binder in terms of the G*sin δ parameter. This is attributed to lower phase angle values of PPC modified binders than TPC modified ones.

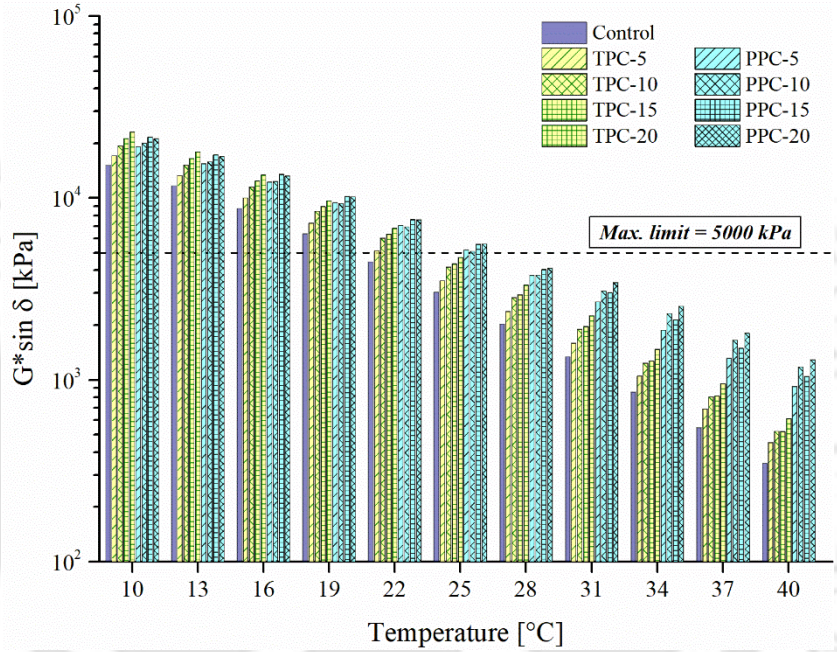

Figure 6.6 Superpave fatigue parameter results at intermediate temperatures

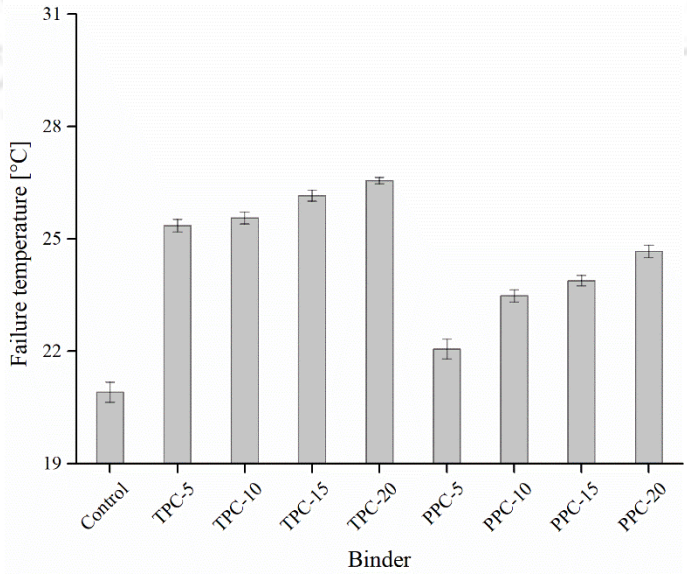

Figure 6.7 Failure temperatures under long-term aged conditions

It is to be noted that the Superpave fatigue parameter is based on the binder stiffness. Since the addition of pyrolytic chars increases the binder stiffness, the G*sin δ values also increase. Higher stiffness is desirable for rutting resistance but not for fatigue performance. However, the soundness of the Superpave fatigue parameter to evaluate fatigue performance has been called into question by many researchers. Key limitations associated with G*sin δ are: (i) because the parameter is based on linear viscoelasticity and is tested with a small amount of strain (usually 1%) and a few loading cycles, the amount of damage caused during testing is minimal (Stuart and Mogawer, 2002; Zhou et al., 2013; Hajj and Bhasin, 2018), (ii) G*sin δ relies on the loading mode because it is based on total energy dissipated per loading cycle under strain-controlled loading (Stuart and Mogawer, 2002; Delgadillo and Bahia, 2005), and (iv) energy expended during loading, as represented by G*sin δ, is mainly due to viscoelastic damping and does not include energy lost owing to fatigue damage (Delgadillo and Bahia, 2005). Therefore, to further assess the fatigue performance of pyrolytic char modified binders, LAS test was used and is discussed in the following subsection.

6.2.6 Linear amplitude sweep (LAS)

The load cycles to failure (N_f) derived from the LAS test at 2.5% and 5% strain levels are shown in Figure 6.8. A higher value of N_f is desirable for a binder to have enhanced performance against fatigue. With the incorporation of TPC and PPC, the N_f values increased compared to the control binder at both strain levels. However, there was a decrease in N_f after 10% dosage of both TPC and PPC. TPC-10 imparted an increase of 61% and 45% in fatigue life compared to the control binder at the strain levels of 2.5% and 5%, respectively, while the increase was 42% and 32% for the PPC-10 binder. The N_f results imply that the TPC and PPC can improve the fatigue resistance of binders under cyclic loading, and TPC has a higher effect on N_f values than PPC. It can be inferred from

the results that in conjunction with improved rutting characteristics, the addition of TPC and PPC to the binder also enhanced the fatigue performance up to 10% dosage.

Further, the trends of LAS were not found consistent with those the Superpave fatigue parameter G*sin δ considering the variation of char dosage. The most likely reason for this observation is that G*sin δ is evaluated at low strain and under linear viscoelastic conditions. On the other hand, the LAS test measures the fatigue-related properties in the nonlinear viscoelastic regime under high strain amplitudes. Further, the fatigue performance of asphalt mixtures fabricated with TPC and PPC modified binders was also evaluated under Task 6, and the results and possible contributing mechanisms are presented in Chapter 8.

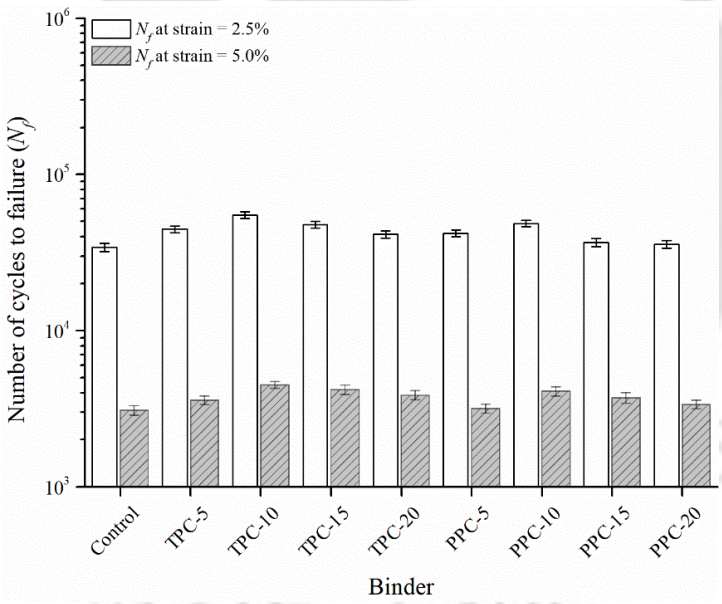

Figure 6.8 LAS N_f results at 2.5% and 5% strain levels

6.3 Advanced Rutting Characterisation

The advanced rutting characterisation of the TPC and PPC modified binders was performed according to the study's experimental plan formulated for Subtask 3B. Multiple temperatures (40, 50, 60, and 70 °C) and multiple binder rutting parameters were utilised (Superpave and Shenoy rutting parameters, ZSV, MSCR non-recoverable compliance and

MSCR non-recoverable strain rate) to further characterise the rutting performance of char modified binders at elevated temperatures. The following subsections present the results of the five binder rutting parameters at the different test temperatures. The section concludes with a discussion on contributing mechanisms to explain rutting performance.

6.3.1 Superpave and Shenoy rutting parameters

The Superpave rutting parameter (G*/sin δ) was one of the outcomes of the SHRP project and one of the first attempts to replace conventional and empirical binder properties with fundamental rheology based parameters (Domingos and Faxina, 2016). The Shenoy rutting parameter (Equation 3.19) is a refinement of the G*/sin δ parameter and is based on unrecovered strain and highlighted elasticity effects (δ). The parameter is based on unrecovered strain and emphasises the effect of elasticity in terms of better sensitivity to δ. A lower unrecovered strain in the binder is associated with an increased value of this parameter and is desirable for an improved rutting resistance. Superpave and Shenoy rutting parameters were measured following ASTM D6373 (2016) at 10 rad/s frequency and 10% strain. Figures 6.9 and 6.10 show the plots of Superpave and Shenoy rutting parameters at the four test temperatures for TPC and PPC modified binders.

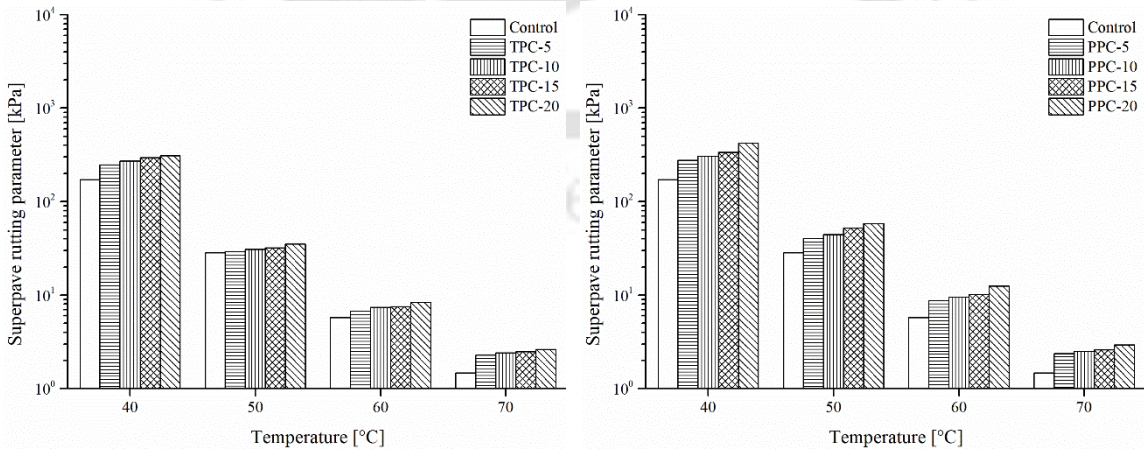

(a) (b)

Figure 6.9 Superpave rutting parameter results for (a) TPC modified binders, (b) PPC modified binders

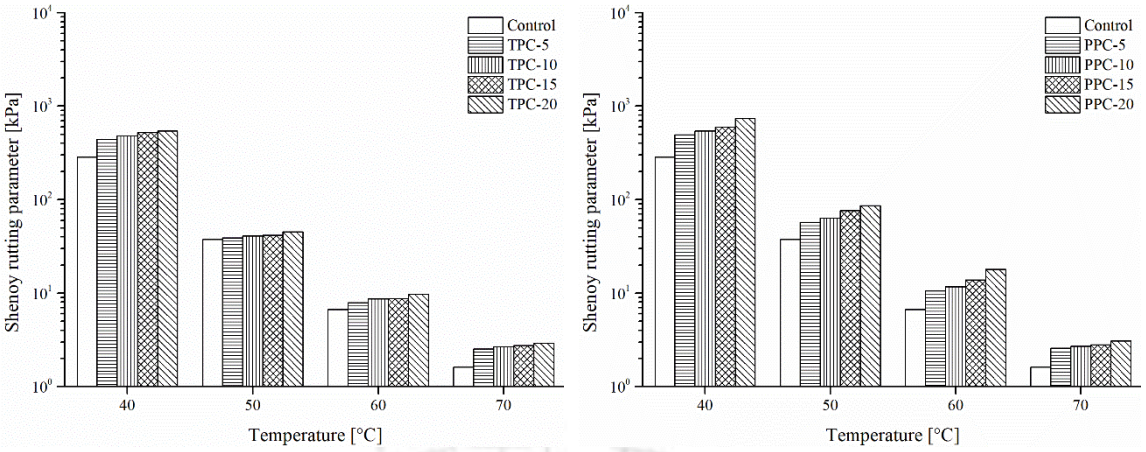

(a) (b)

Figure 6.10 Shenoy rutting parameter results for (a) TPC modified binders, (b) PPC modified binders

Both parameters showed a similar trend with respect to TPC and PPC dosage at all four test temperatures: the parameters increased with an increase in char content and decreased with the increase in temperature. The results indicate an improved rutting resistance of the binders with the addition of TPC and PPC. Wang et al. (2019) also reported similar results with pyrolytic tyre carbon black and reported the increased rutting resistance of binder with TPC due to the higher stiffness facilitated by the absorption of light fractions of the binder because of the high surface area of TPC. Similar improved rutting results with TPC were also found by Feng et al. (2016) and Li et al. (2018).

Averaged over all TPC and PPC dosages, the percent increase in Shenoy parameter over the Superpave parameter was 75, 37, 22, and 9% at 40, 50, 60, and 70 °C temperatures, respectively. The Shenoy parameter takes into consideration the emphasised influence of phase angle (or elasticity) on the potential of binder against permanent deformation, leading to a higher value of the Shenoy rutting parameter than the Superpave. Comparing the two pyrolytic chars, the PPC-modified binders had higher Superpave and Shenoy rutting parameters than TPC binders at all four temperatures. For example, at 70 °C, the TPC-5, TPC-10, TPC-15, and TPC-20 binders had Superpave parameters higher by 55, 64, 69, and

79%, respectively, compared to the control binder. Corresponding percent increase for PPC-5, PPC-10, PPC-15, and PPC-20 binders were 61, 70, 76, and 99%, respectively.

6.3.2 Zero shear viscosity (ZSV)

At typical high-service temperatures where rutting is most likely to mobilise, the modified asphalt binders often behave as non-Newtonian pseudoplastic fluids, implying that their viscosity decreases with an increase in shear rate or frequency. However, these binders behave as Newtonian fluids at low shear rates or frequencies. This viscosity, called the ZSV, is evaluated at shear rates/frequency approaching zero and thus independent of shear rate and can be used to evaluate the rutting resistance of the binders (Sybilski, 1996; Hajikarimi et al., 2015). The ZSV was estimated using the Cross model fit to the complex viscosity versus frequency data. The model parameters of the Cross model given in Equation 3.20 were estimated using nonlinear curve fitting analysis. The ZSVs of all TPC and PPC modified binders at the four temperatures were determined and are presented in Figure 6.11.

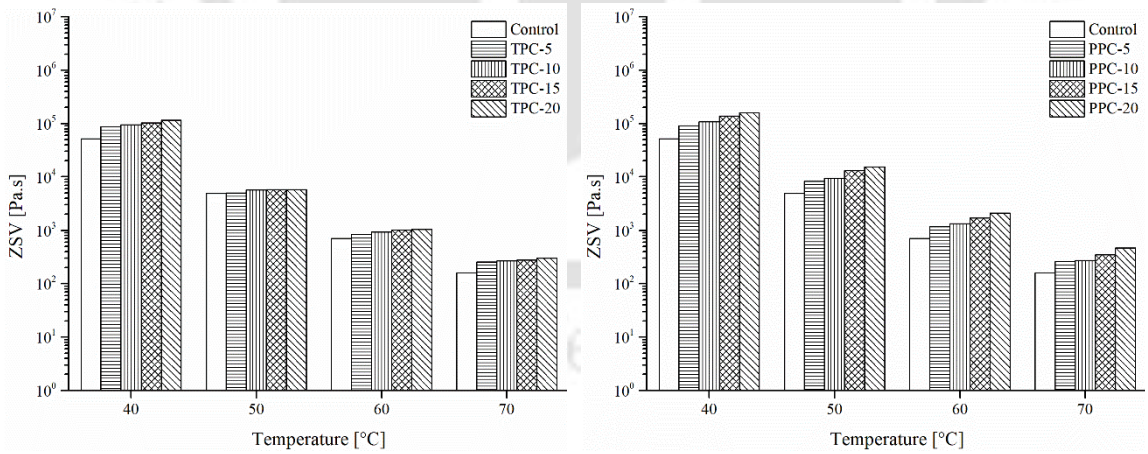

(a) (b)

Figure 6.11 ZSV results for (a) TPC modified binders, (b) PPC modified binders

As per the trends observed in Figure 6.11, the TPC and PPC modification increased the ZSV values at all four test temperatures, which is also consistent with the trends of Superpave and Shenoy rutting parameters. For instance, considering the 70 °C temperature,

a significant increase of 64, 71, 120 and 196% in ZSV values was found for subsequent PPC contents of 5, 10, 15 and 20%, respectively, compared to the control binder. Corresponding percent increase for TPC modified binders were 62, 70, 76, and 88%, respectively at 5, 10, 15 and 20% TPC contents. Comparing the two pyrolytic chars, the PPC-modified binders had higher ZSV values than TPC binders at all four temperatures.

6.3.3 Multiple stress creep and recovery (MSCR)

MSCR test is gaining wide popularity for rutting characterisation of asphalt binders with demonstrated correlations to field rutting performance (Liu et al., 2020). The test was originally developed as the US Federal Highway Administration (FHWA) research output to overcome deficiencies associated with the Superpave rutting parameter (D'Angelo et al., 2007). Recent advances in the MSCR methodology for characterisation of modified binders have indicated that a higher stress level than the currently used 0.1 and 3.2 kPa is needed to achieve a state of stress representative of that encountered by modified binders in pavements (Golalipour, 2011; Golalipour et al., 2017). A third stress level of 10 kPa was therefore used in this study. The standard MSCR test comprises 10 cycles at two different stress levels (0.1 and 3.2 kPa), where one cycle includes a 1 s creep and a 9 s recovery time without any time lag between the cycles. Further, thirty MSCR cycles were used, as recommended in some recent studies (García-Travé et al., 2016; Moreno-Navarro et al., 2019) and the J_{nr} and recovery data were obtained from the last five creep-recovery cycles.

The results of MSCR J_{nr} at the two stress levels (3.2 and 10 kPa) are shown in Figures 6.12 and 6.13 for the control and modified binders with different TPC and PPC dosages at the four test temperatures. The J_{nr} values decreased for the TPC and PPC modified binders, indicating that the modification by pyrolytic chars led to a lower plastic (unrecovered strain) at each stress level and test temperature hence a better permanent deformation resistance. Comparing the effect of the pyrolytic char type, the PPC-modified binders had

lower J_{nr} than TPC-modified binders at all stress levels and test temperatures. For example, considering 70 °C test temperature and 3.2 kPa stress level, a significant decrease of 35, 49, 59 and 65% in J_{nr} values were found for subsequent PPC contents of 5, 10, 15 and 20%, respectively, as compared to the control binder. Corresponding percent decrease for TPC modified binders were 26, 33, 39, and 42%, respectively at 5, 10, 15 and 20% TPC contents. The results indicate that the modified binders performed better at high temperatures when subjected to multiple stress levels.

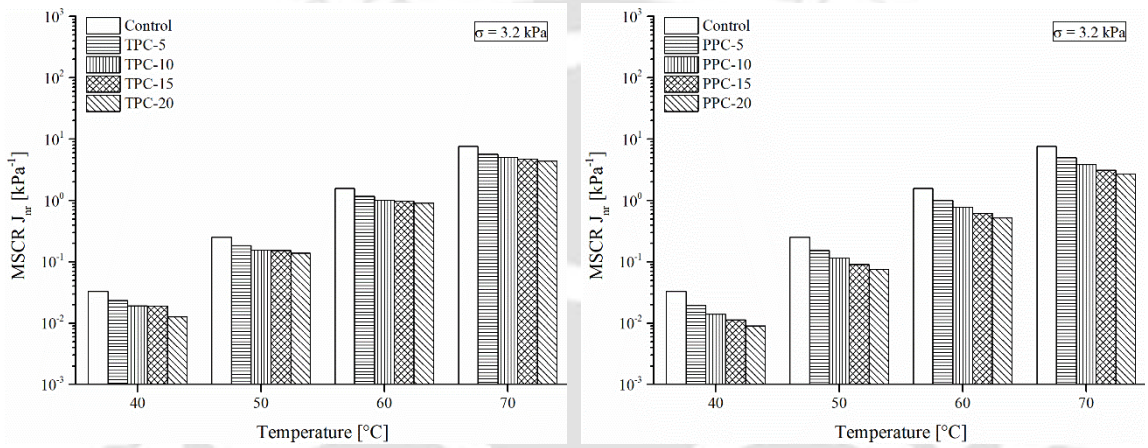

(a) (b)

Figure 6.12 MSCR J_{nr} at 3.2 kPa for (a) TPC modified binders, (b) PPC modified binders

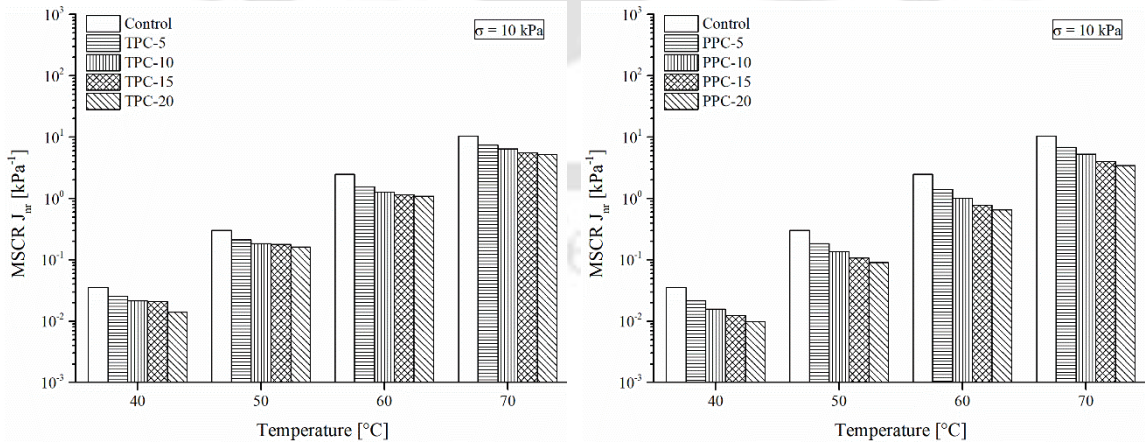

(a) (b)

Figure 6.13 MSCR J_{nr} at 10.0 kPa for (a) TPC modified binders, (b) PPC modified binders

Figures 6.14 and 6.15 show the results of MSCR percent recovery for all binders. The PPC had a higher effect on recovery values than the TPC. A slight improvement in recovery values was observed on the addition of TPC. As expected, the recovery decreased with an increase in test temperature and stress level. The recovery at 70 °C temperature is omitted because negative recoveries were observed. Possible reasons for negative recovery include instrument inertia and tertiary creep response of the binder under the combined influence of high stress levels and high temperatures (Liu et al., 2021). The current MSCR standard ASTM D7405 (2020) also recommends negative recovery to be treated as zero recovery.

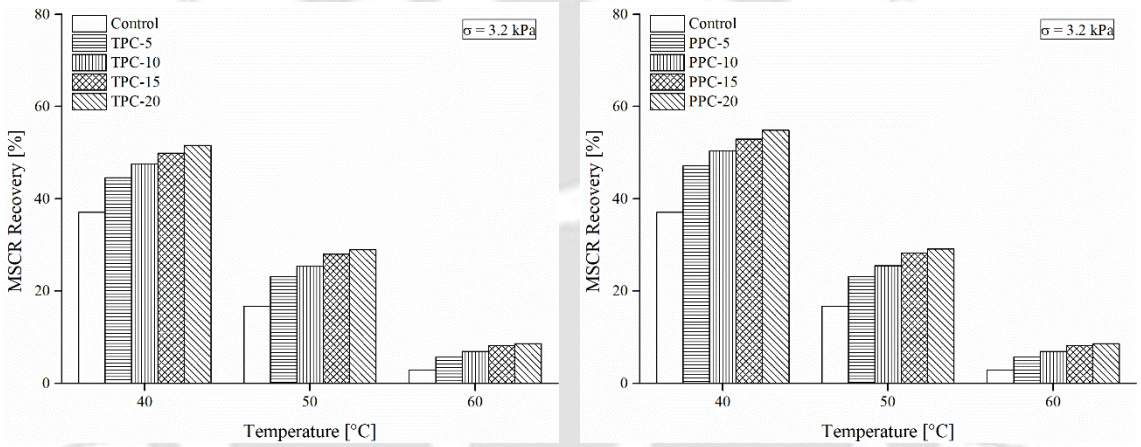

Figure 6.14 MSCR recovery at 3.2 kPa for (a) TPC modified binders, (b) PPC modified binders

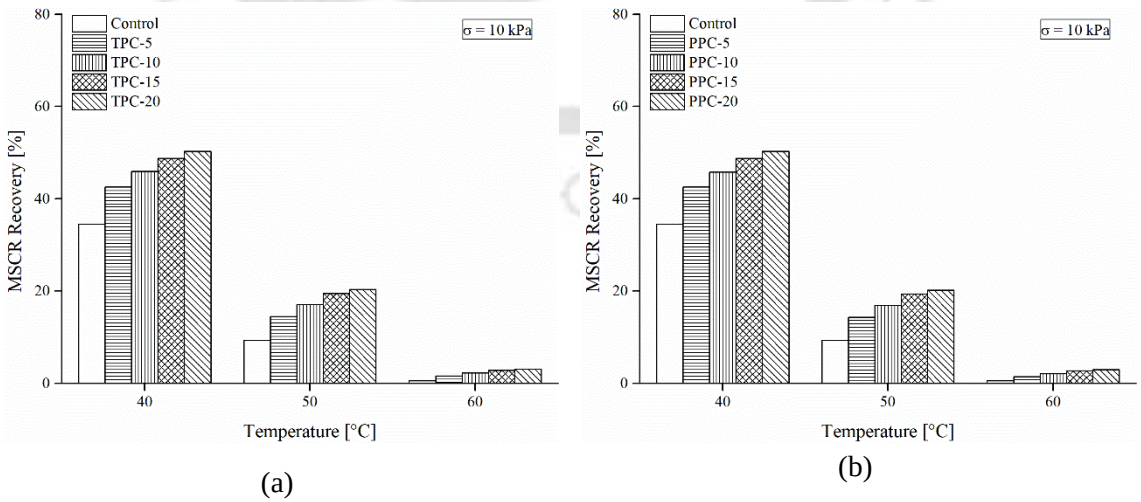

Figure 6.15 MSCR recovery at 10.0 kPa for (a) TPC modified binders, (b) PPC modified binders

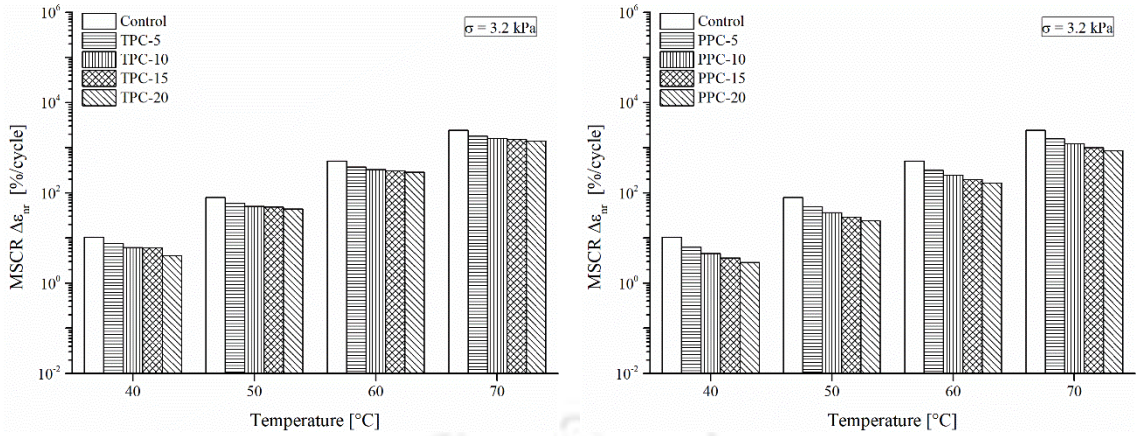

(a) (b)

Figure 6.16 MSCR $\Delta\varepsilon_{nr}$ at 3.2 kPa for (a) TPC modified binders, (b) PPC modified binders

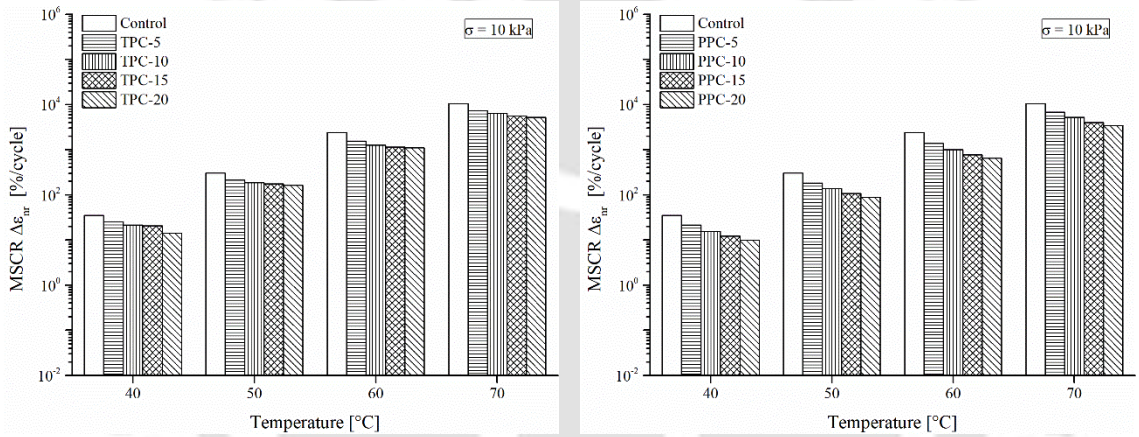

(a) (b)

Figure 6.17 MSCR $\Delta\varepsilon_{nr}$ at 10.0 kPa for (a) TPC modified binders, (b) PPC modified binders

Figures 6.16 and 6.17 present the results of the second MSCR rutting parameter: non-recoverable strain rate, $\Delta\varepsilon_{nr}$, given by Equation 3.21. The calculation of the parameter was also illustrated in Figure 3.26. The addition of TPC and PPC decreased the $\Delta\varepsilon_{nr}$ values, which is beneficial for rutting resistance as it indicates a lower rate of progression of the non-recovered strain with the evolution of the MSCR cycles. Similar to J_{nr}, the $\Delta\varepsilon_{nr}$ parameter also increased with an increase in temperature and stress level. Averaged over the four temperatures and three stress levels, the TPC dosages of 5, 10, 15, and 20% decreased the $\Delta\varepsilon_{nr}$ values by 27, 38, 41, and 49%, respectively. The PPC dosages of 5, 10,

15, and 20% decreased the $\Delta\varepsilon_{nr}$ values by 38, 53, 63, and 69%, respectively. Comparing the effect of the pyrolytic char type, the PPC-modified binders had lower $\Delta\varepsilon_{nr}$ than TPC binders at all stress levels and temperatures. The numerical values of $\Delta\varepsilon_{nr}$ are much higher than J_{nr} as the non-recovered strain values (constituting the numerator in Equation 3.21) increase rapidly with an increase in the stress level and temperature. The possible mechanisms for improved rutting resistance of the modified binders are presented now.

6.3.4 Discussion on rutting performance of char-modified binders

The results of rutting characterisation reveal that the trends of rutting resistance remain the same in all binder rutting parameters with respect to the TPC and PPC dosages. The improvement in stiffness of binders modified with both TPC and PPC is mainly attributed to the absorption of lightweight asphalt binder fractions (such as maltenes) by the chars and consequent stiffening. Similar results have also been reported in previous studies (Chaala et al., 1996; Wang et al., 2019). It was seen from the thermogravimetric analysis (TGA) curves (Figure 4.5) of TPC and PPC that PPC had a higher mass loss than TPC. This shows that there exist more lightweight compounds in PPC than TPC. This observation is also corroborated from proximate analysis results shown in Table 4.1, where PPC had a higher volatile matter content than TPC. It is hypothesised that these lightweight and volatile products interact with asphalt binder such that the interaction contributes to higher stiffness and elasticity in PPC-modified binders compared to TPC-modified ones. The higher elastic response was observed from master curves and MSCR recovery in PPC-modified binders. As also mentioned earlier, PPC may contain residual groups from the original polymer and therefore imparts a higher effect on the stiffness and elastic response of the binder than TPC. A piece of evidence for chemical interactions between chars and the base binder was identified through observing the changes in FTIR spectra of PPC and TPC-modified binders and comparing them with the control binder (Section 4.4.1).

6.4 Ageing Characterisation of Asphalt Binders

The ageing properties of asphalt binders were evaluated according to the experimental plan formulated for Task 4 of the study. The following subsections present the results of rheological tests (frequency sweep, ZSV, and MSCR) in three ageing states and the ageing indices based on these tests. The section concludes with the results of FTIR spectroscopy-based ageing indices (carbonyl and sulfoxide indices) and a discussion on contributing mechanisms for the ageing performance of char-modified binders.

6.4.1 Frequency sweep

The results of G* and δ measured at 60 °C for PPC and TPC modified asphalt (abbreviated as PPCMA and TPCMA) are presented in Figure 6.18 at 10 rad/s frequency. The G* describes the total resistance to deformation of a binder when subjected to a repeated sinusoidal shear load, whereas δ reflects the ratio of elastic and viscous behaviour of the binder. A higher G* and a lower δ are desirable attributes for an improved high-service temperature performance. It can be seen from Figure 6.18 that the addition of both TPC and PPC led to an increased G*, indicating that modification by both pyrolytic chars improved the stiffness of the binder. However, an appreciably lower δ was only observed for the PPC-modified binder. Comparing the G* and δ values of short-term and long-term aged binders with the unaged binder, it is seen that a higher degree of ageing caused a stiffer (higher G*) and more elastic (lower δ) response of the asphalt binder. Results indicate that both TPC and PPC had a positive effect on the deformation resistance of the binder.

The ageing indices derived from G* and δ are shown in Figures 6.19 and 6.20, respectively, at three frequencies (1, 10, and 100 rad/s). The rheological ageing indices were computed as the ratio of a rheological parameter before and after ageing and were presented in Equations 3.22-3.25. A lower value of the indices indicates lower changes in the material properties on ageing. Figures 6.20 and 6.21 show that the indices were the

lowest when TPC was used under both short- and long-term aged states and the three frequencies. It is noted that the differences in δ-based ageing index for unaged and short-term aged control and TPC-modified binders were relatively small; however, the differences became apparent when comparing the indices for the long-term aged binder, which showed that TPCMA had lower indices among all binders. It follows that the ageing susceptibility of the TPC-modified binder was the least. Lower frequencies led to higher ageing index values, suggesting that the effect of ageing was more severe at low frequencies (representing slower traffic speeds). A discussion on mechanisms contributing to the observed trends is provided later in this section.

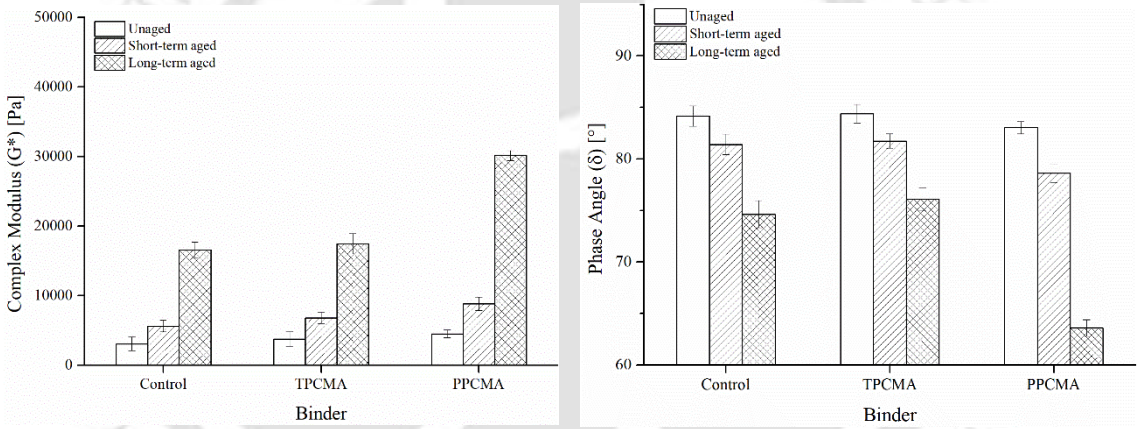

(a) (b)

Figure 6.18 Frequency sweep results at three ageing states for (a) G* (b) δ

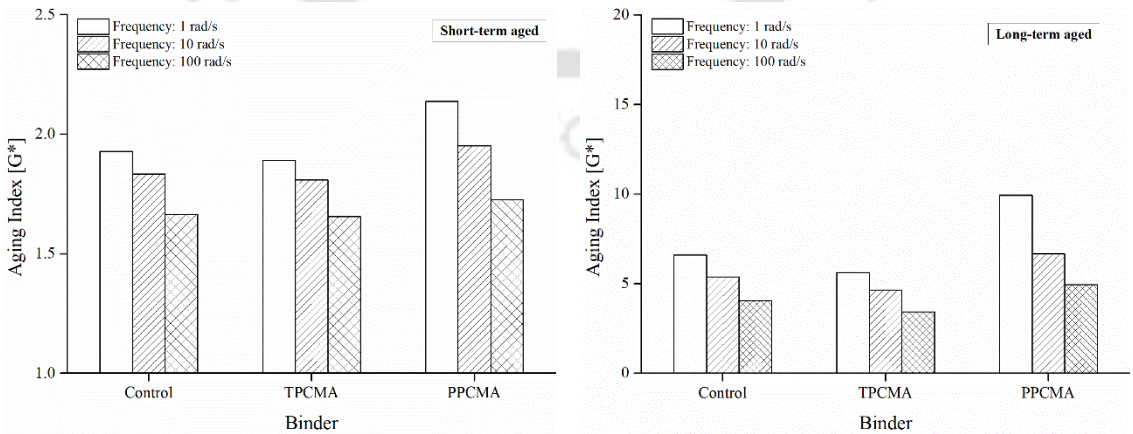

(a) (b)

Figure 6.19 Ageing index based on G* under (a) short-term ageing, (b) long-term ageing

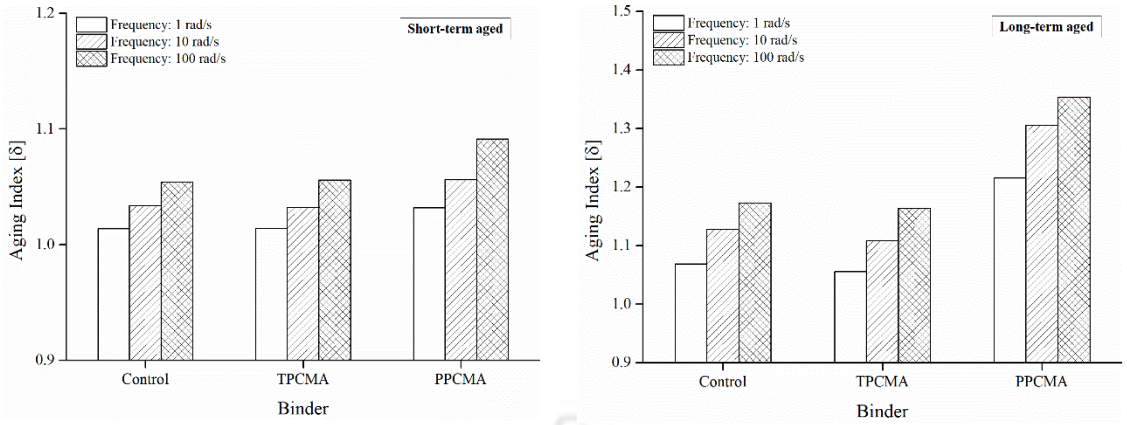

(a) (b)

Figure 6.20 Ageing index based on δ under (a) short-term ageing, (b) long-term ageing

6.4.2 Zero shear viscosity (ZSV)

ZSV indicates the viscosity of an asphalt binder under a very low shear rate (or frequency) and is often used as a parameter to evaluate the high-service temperature properties of asphalt binders. From Figure 6.21, it is seen that the ZSV of the asphalt binders increased with an increment in the ageing severity/period. A sharp increase in ZSV occurred from short-term to long-term aged conditions. The ZSV values of TPC and PPC-modified binders were higher than the control binder under the three ageing states, indicating that TPC and PPC improved the high-temperature performance of asphalt. This finding is consistent with the previous discussion based on G*.

The ageing index formulated based on ZSV is computed as the ratio of ZSV after and before ageing, and therefore a lower value indicates fewer changes in ZSV due to ageing. Figure 6.22 presents the result of the ZSV-based ageing index in short-term and long-term ageing conditions. The long-term ageing index is significantly higher than the short-term index. This is due to the higher severity of ageing undergone by the binder in the PAV process. Under both ageing conditions, the ageing index for TPC-modified binders is found to be the lowest. The G* and δ based ageing indices also ranked the binders in the same order.

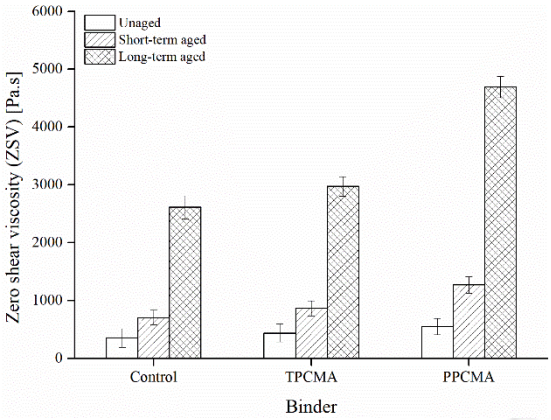

Figure 6.21 ZSV results at three ageing states

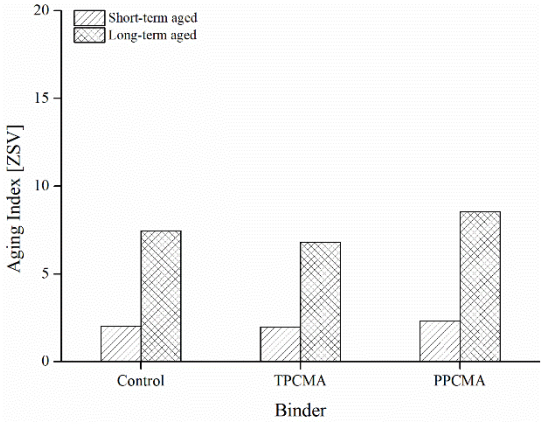

Figure 6.22 Ageing index based on ZSV

6.4.3 Multiple stress creep and recovery (MSCR)

The non-recoverable creep compliance (J_{nr}) from the MSCR test is commonly used to assess the high-temperature rutting performance of asphalt binders. Smaller the value of J_{nr}, the better the high-temperature resistance of the binder since it indicates lower unrecovered strain at the end of an MSCR creep-recovery cycle.

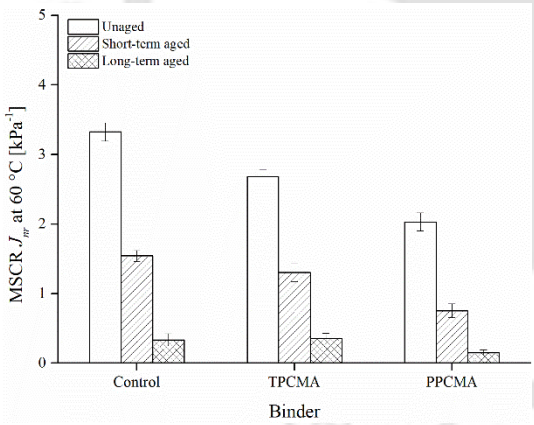

Figure 6.23 MSCR J_{nr} at three ageing states

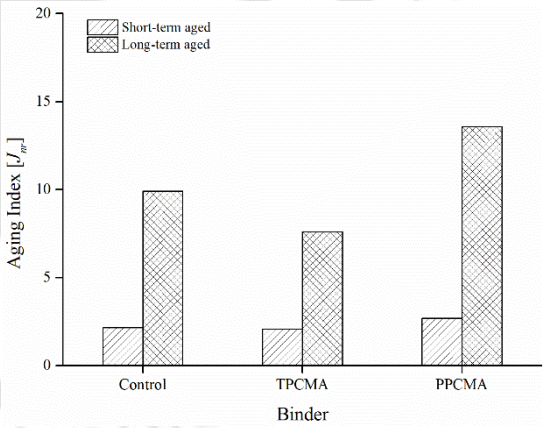

Figure 6.24 Ageing index based on J_{nr}

Figure 6.23 shows that ageing had a significant effect on the J_{nr} of binders. J_{nr} decreased with increasing ageing severity with a minimum value for the long-term aged binders. Both TPC and PPC reduced the J_{nr} values at the three ageing conditions compared to the base binder indicating the superior rutting resistance derived from the addition of the pyrolytic chars. The ageing index based on J_{nr} shown in Figure 6.24 ranks the binders in the same

order as for the indices based on G*, δ, and ZSV. The lowest index is observed for the TPC-modified binder, followed by the control and the PPC-modified binder. Now, a discussion is presented to explain the observed trends in the ageing performance of the binders.

6.4.4 Discussion on ageing performance of char-modified binders

Carbon black is added to tyre rubber during its manufacturing to improve its strength and aid in its resistance to abrasion. TPC, therefore, consists of the recovered carbon black, inorganic compounds used in tyre making, and condensed by-products formed during the pyrolysis (Helleur et al., 2001; Williams, 2013; Li et al., 2018). Carbon black has been reported to function as an effective antioxidant to the asphalt binders due to chemical species such as quinones, carboxyphenols, phenols, and lactones (Apeagyei, 2011). When subjected to ageing, these chemical species have a higher tendency to react with oxygen than the asphalt binder, leading to a better ageing resistance of the TPC modified binder. Wang et al. (2019) used an ageing index based on MSCR J_{nr} and reported improvements in binder ageing resistance with tyre pyrolytic carbon black and attributed them to the presence of functional groups that are more likely to react with oxygen than bitumen.

Another possible mechanism for better ageing resistance for TPC modified binder was reported by Wang et al. (2019) based on the results of electron spectroscopy for chemical analysis (ESCA), infrared, and ultraviolet spectroscopic studies on TPC modified bitumen by Chaala et al. (1996). When added to asphalt binder, the TPC particles absorb maltenes, and a thin boundary layer composed of asphaltenes exists on the TPC surface. Now, the ageing of bitumen is mainly related to the depletion of maltenes and the formation of more asphaltene-like compounds. When the binder is aged, such a system (TPC particle surrounded by asphaltenes) inhibits the depletion of maltenes and thus contributes to improving the binder ageing resistance.

Char obtained from waste plastic pyrolysis is reported to have higher amounts of volatile matter (Jamradloedluk and Lertsatitthanakorn, 2014; Saptoadi et al., 2016). Proximate analysis conducted on TPC and PPC revealed that volatile matter content in PPC was 27.7% compared to 4% in TPC (Table 4.1). The volatile matter becomes gaseous and will likely escape when the binder undergoes ageing at high temperatures (short-term ageing) or under a combination of high temperature and high pressure (long-term ageing). This, in turn, is expected to contribute to a higher ageing index of the PPC-modified asphalt binders.

6.4.5 FTIR spectroscopy for ageing performance

The chemical composition of an asphalt binder changes when the binder undergoes ageing. During oxidative ageing, the chemical groups in the asphalt binder react with oxygen, and therefore monitoring the changes in oxygen-based functional groups is helpful in understanding changes that occur in the binder due to ageing. FTIR spectroscopy was used to observe the progress of chemical functionalities for control, TPC-modified and PPC-modified binders subjected to short- and long-term ageing. FTIR spectra of the binders under different ageing states are shown in Figure 6.25. Peaks corresponding to two oxygenated functions, namely carbonyl (C=O, centred around 1700 cm^{-1}) and sulfoxide (S=O, centred around 1030 cm^{-1}), are widely used to evaluate changes caused due to ageing in asphalt binders (Lamontagne et al., 2001; Lu and Isacsson, 2002; Singh et al., 2017). Distinct regions corresponding to carbonyl and sulfoxide are also indicated in Figure 6.25. It can be seen that new carbonyl and sulfoxide functional groups are formed as the duration of ageing increases for all binders (indicated by a rise in the peaks). The carbonyl and sulfoxide groups are formed when other chemical bonds such as C–C and C=C dismantle and react with oxygen or when sulfur-based compounds of the asphalt react with oxygen (Lu and Isacsson, 2002; Qian et al., 2021).

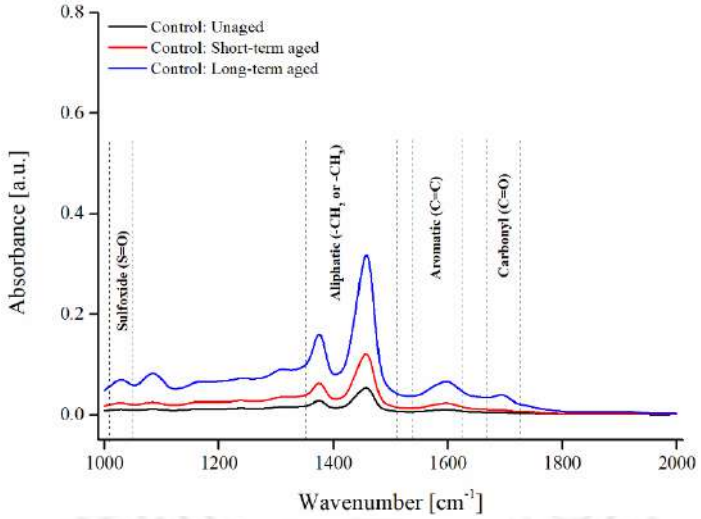

(a)

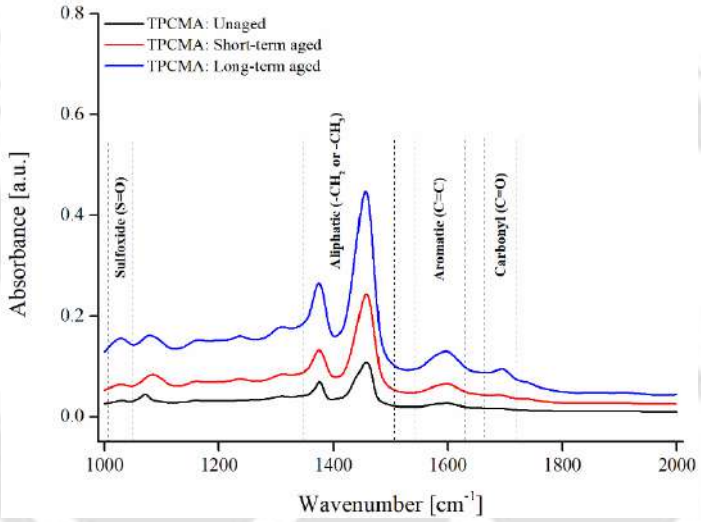

(b)

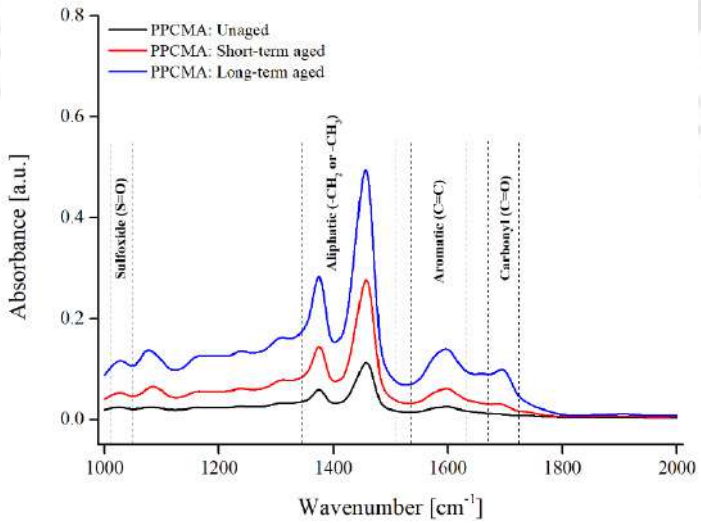

(c)

Figure 6.25 FTIR spectra under three ageing states for (a) control, (b) TPC modified binder, (c) PPC modified binder

Quantitative analysis of the FTIR spectra was performed by calculating carbonyl (C=O) index (CI) and sulfoxide (S=O) index (SI) based on the peaks in distinct regions of the spectra (Nivitha et al., 2016) as per Equations 3.26 and 3.27. Figure 6.26 shows the results of FTIR indices for all binders at different ageing conditions. In general, all indices consistently increased as the severity of ageing progressed in the order: unaged < short-term aged < long-term aged. The highest increase was found between the short-term and long-term aged conditions for all binders. The CI and SI were the lowest for the TPC-modified binder in the short- and long-term aged conditions. This indicates that the modification by TPC leads to the formation of fewer carbonyl and sulfoxide groups. Therefore, it is inferred that the addition of TPC can help inhibit the increase in chemical functionalities and improve the resistance to thermal-oxidative ageing. These findings also coincide with the observations from the rheological ageing indices.

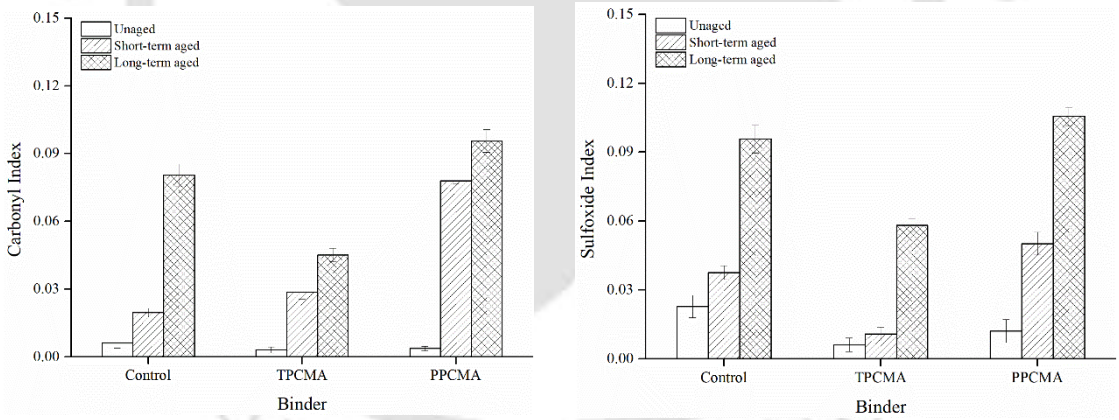

(a) (b)

Figure 6.26 (a) Carbonyl index, (b) Sulfoxide index

6.5 Summary

This chapter presented the results of conventional and rheological properties of control and TPC/PPC modified asphalt binders with the experimental plan formulated under Task 3 of the study. This was followed by presenting the ageing characteristics of the control and

char modified binders with the experimental plan formulated under Task 4.

Asphalt binder modification with TPC and PPC improved the rheological performance of binders as evidenced by continuous high PG, master curves, and MSCR tests on binders. For similar content of pyrolytic chars, each of five binder rutting parameters (Superpave and Shenoy rutting parameters, ZSV, MSCR J_{nr} and $\Delta\varepsilon_{nr}$) resulted in different percentage improvements compared to the control binder; nonetheless, the ranking of the binders remained consistent. The rutting performance improved with the increase in char dosages up to 20%. Based on the LAS fatigue test on binders, it was found that the optimum performance was achieved at 10% dosage of both TPC and PPC.

Rheological indices based on G*, δ, ZSV and J_{nr} ratio showed that TPC-modified asphalt binders showed the best ageing resistance compared to control and PPC-modified binders. FTIR spectroscopy results agreed with rheological ageing indices and indicated that the addition of TPC retarded the carbonyl and sulfoxide chemical groups formed due to ageing.

Chapter 7

MIXING AND COMPACTION TEMPERATURES

7.1 Introduction

Use of modified asphalt binders has been steadily increasing in asphalt pavement construction in response to increasing axle loads and tyre pressures, extreme temperature variations, and the need for an improved performance over the pavement service life. Selection of appropriate and reasonable production temperatures for different modified asphalt binders is quite essential and continuously researched. The 'production' temperatures collectively refer to the temperatures used for mixing the aggregates and the binder and the temperatures desired for compaction of the asphalt mixture to attain the requisite in-situ density, and are usually referred as 'mixing and compaction' temperatures.

The conventional approach used to determine mixing and compaction temperatures of neat/unmodified asphalt binders is the equiviscous method. This method and depends on the measurement of viscosity of the asphalt binder over a range of temperatures. The mixing temperature is determined as the temperature where the binder's viscosity is 0.17 ± 0.02 Pa.s, whereas the compaction temperature is the one for which the viscosity is in the range of 0.28 ± 0.03 Pa.s (Asphalt Institute, 1997). While being widely used for neat/unmodified binders, the equiviscous method often results in unduly high temperatures for modified binders. The high temperatures may cause unwarranted ageing of the binder, damage to the binder and/or modifier, increased fumes and emissions during mix preparation and compaction, and tender mixes during compaction (Yildirim et al., 2000; Azari et al., 2003; West et al., 2010). Higher production temperatures may also destroy the beneficial

properties expected from a modifier and may enhance the binder draindown in gap-graded and open-graded asphalt mixtures.

Many agencies recommend using production temperatures as endorsed by the manufacturer of the modified binder, which is often based on their prior experience with those binders. Several studies have been undertaken to investigate different approaches to arrive at reasonable/adequate production temperatures for different modified asphalt binders. Based on the shear-thinning phenomenon (pseudoplasticity) in modified binders, Yildirim et al. (2000) suggested a protocol for determining mixing and compaction temperatures that utilised the viscosity measured at varying shear rates on a rotational viscometer. The study estimated the actual shear rate experienced by asphalt binder films over aggregates during compaction in a gyratory compactor and reported it to be about 490 s^{-1}. This method is referred as the high shear viscosity (HSV) method. The method relies on estimating viscosity at a high shear rate of 500 s^{-1} and determining the mixing and compaction temperatures based on the same viscosity ranges as in the equiviscous method. The NCHRP Project 09-39 (West et al., 2010) explored two more methods for the estimation of mixing and compaction temperatures: the steady shear flow (SSF) method and the phase angle (PA) method. Both methods are based on measurements made on a DSR.

This chapter presents the results of mixing and compaction temperatures of control and char modified binders determined using four methodologies: equiviscous (EQ), HSV, SSF, and PA. A description of the four methods is first provided, followed by the mixing and compaction temperatures results obtained for the nine binders used in this study. The results of viscosity, high shear viscosity, steady shear viscosity, and phase angle master curves are also presented. The chapter concludes with the results of validation of the above-discussed methods and their results through fabrication of asphalt mixes.

7.2 Description of Methodologies

7.2.1 Equiviscous method

The equiviscous method determines temperatures that correspond to viscosity ranges specified for mixing (0.17 ± 0.02 Pa.s) and compaction (0.28 ± 0.03 Pa.s) temperatures. This method is recommended and widely used with unmodified/neat asphalt binders but often results in excessively high production temperatures when used for modified binders. Under this method, a viscosity-temperature line was first plotted based on viscosity measurements on a rotational viscometer at two temperatures (*e.g.* 135 and 165 °C). The viscosities were determined at a constant shear rate (20 rpm) on a Brookfield rotational viscometer as per ASTM D4402 (2015). For the viscosity-temperature relation, log-log viscosity is plotted versus log temperature (Rankine scale). Then, the temperatures are marked corresponding to the established mixing and compaction viscosity ranges. Figure 7.1 illustrates the evaluation for the control/base binder used in the study.

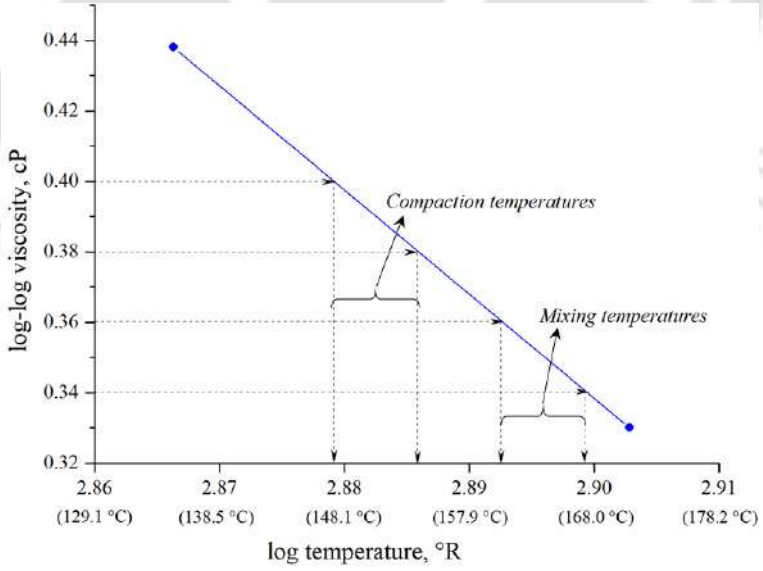

Figure 7.1 Illustration of equiviscous method for control binder

7.2.2 High shear rate viscosity method

The high shear rate viscosity (HSV) method considers the shear-thinning behaviour of the binders. The method was recommended by Yildirim et al. (2000) based on the finding that

actual shear rates experienced by asphalt binder films on aggregates are quite high than the shear rate used in rotational viscometer. The study estimated the shear rate when an asphalt mixture was compacted in a gyratory compactor as 490 s^{-1}. A rotational viscometer was used to measure viscosities at 135 and 165 °C at varying shear rates. To the viscosity-shear rate profile so obtained, the Cross-Williams model was fit, and the viscosity corresponding to a shear rate of 500 s^{-1} was estimated. Equation 7.1 presents the Cross-Williams model:

$$\eta = \eta_{\infty} + \frac{(\eta_o - \eta_{\infty})}{1 + (k\gamma)^n} \tag{7.1}$$

Here, η_{∞} *is* limiting viscosity, η_0 is the zero shear viscosity, γ is the shear rate, k and n are the model coefficients. Figure 7.2 illustrates a typical viscosity-shear rate profile obtained for the control binder and shows the Cross-Williams model fit. The HSVs so derived at 135 and 165 °C were plotted on a log-log viscosity versus log temperature chart, and a linear HSV-temperature line was derived. The mixing and compaction temperatures were derived for each binder using the mixing and compaction viscosities of 0.17 ± 0.02 Pa.s and 0.28 ± 0.03 Pa.s.

7.2.3 Steady shear flow (SSF) method

The SSF method was recommended for modified binders by NCHRP Project 09-39 (West et al., 2010). To perform this method, an Anton Paar MCR-102 dynamic shear rheometer (DSR) was employed. An unaged binder sample was placed between two parallel plates of 25 mm diameter and 500 µm gap setting for performing the rheological measurements. A lower gap is used in this method to avoid the flow of the sample between the plates when subjected to higher shear stresses. The sample was subjected to a range of shear stresses in flow mode (one-directional movement of the top plate of DSR) varying from 0.33 to 500 Pa at 76, 82 and 88 °C.

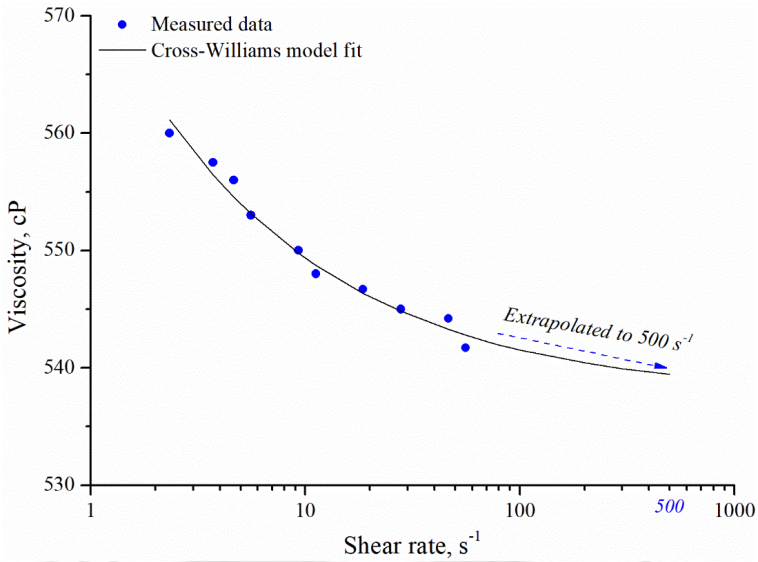

Figure 7.2 Illustration of HSV method for control binder at 135 °C

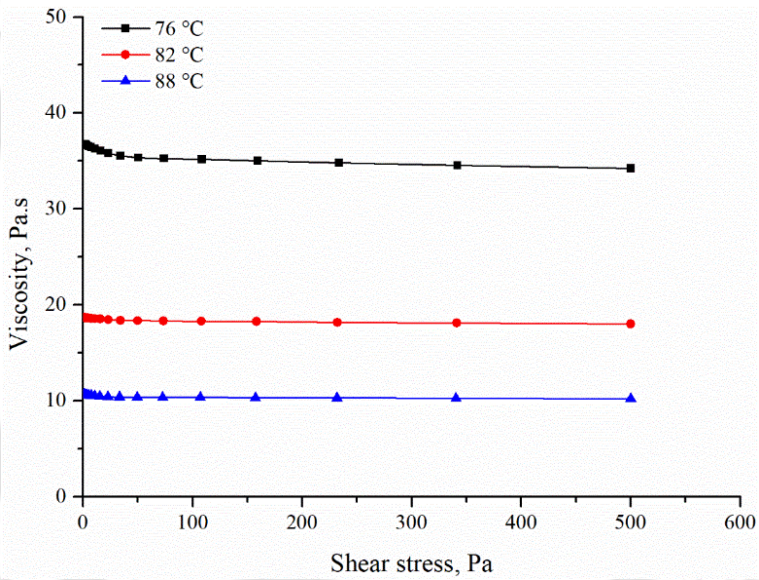

Figure 7.3 Illustration of SSF method for control binder

The viscosities measured at 500 Pa at each temperature were then used to construct the viscosity-temperature line. The line was then used to mark temperatures where the extrapolated viscosities of 0.17 ± 0.02 Pa.s (for mixing temperatures) and 0.35 ± 0.03 Pa.s (for compaction temperatures) were obtained. Figure 7.3 shows the viscosity-shear stress profile for the control binder at 76, 82 and 88 °C. There is a decrease in viscosity with an increase in shear stress, and the viscosity approaches a constant value (*i.e.* reaches a steady state) at 500 Pa stress level.

7.2.4 Phase angle method

The phase angle (PA) method was also developed during NCHRP Project 09-39 and was recommended for modified asphalt binders by West et al. (2010). Similar to viscosity, phase angle (δ) is a binder consistency parameter, and a measure of binder's consistency can be a good indicator of the binder's ability to coat the aggregates and densify the aggregates during mixing and compaction procedures (West et al., 2010). When an asphalt binder sample is subjected to sinusoidal shear loading in a DSR, the phase angle describes the time lag between the applied stress and the strain output. In this method, frequency sweeps were performed on unaged binder samples at four temperatures (50, 60, 70, and 80 °C) at 12% strain. Frequency was varied in three decades (0.1–1, 1–10, and 10–100 rad/s). Phase angle data were collected at each frequency and temperature, and phase angle master curves were developed for each binder at a reference temperature of 80 °C using a double-logistic model (Equation 7.2) (Asgharzadeh et al., 2013):

$$\delta = \delta_P - \delta_P \cdot H\left(f_r - f_P\right) \cdot \left(1 - \exp\left(-\left(S_R \cdot \log\left(\frac{f_r}{f_P}\right)\right)^2\right)\right) + \delta_L \cdot H\left(f_P - f_r\right) \cdot \left(1 - \exp\left(-\left(S_L \cdot \log\left(\frac{f_P}{f_r}\right)\right)^2\right)\right) \quad (7.2)$$

Here, f_r is the reduced frequency, f_P is the plateau frequency, δ_P is the plateau phase angle, H($f_r - f_P$) or H($f_P - f_r$) are Heaviside step functions, S_R represents the slope of the master curve to the right of plateau, δ_L denotes rise (or fall) on left side of plateau, S_L is the slope of the master curve to the left side of plateau. From the master curve, the frequency corresponding to phase angle of 86° is identified as ω_{86}. This phase angle represents the transition of the binder from purely viscous to viscoelastic (West et al., 2010). Findings of the NCHRP Project 09-39 determined a good correlation between ω_{86} and recommended mixing temperatures for different binder grades based on empirical equations shown as

Equations 7.3 and 7.4:

Mixing temperature: $$T_{mix}(°F) = 325(\omega_{86})^{-0.0135} \quad (7.3)$$

Compaction temperature: $$T_{comp}(°F) = 300(\omega_{86})^{-0.012} \quad (7.4)$$

Figure 7.4 illustrates the phase angle method and shows the master curve for the control binder. It is to be noted that, unlike the other three methods that give a 'range' of mixing and compaction temperatures, the phase angle method yields a single value for the mixing and the compaction temperature.

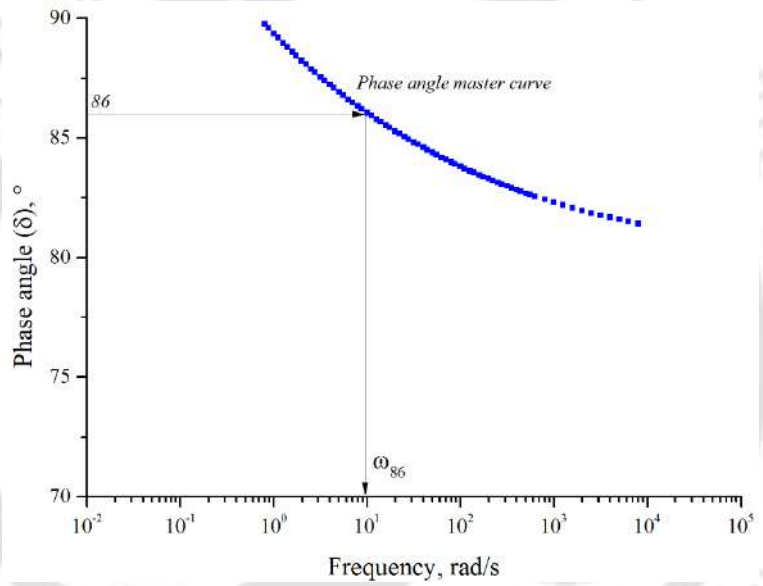

Figure 7.4 Illustration of phase angle method for control binder

7.3 Results of Production Temperatures

7.3.1 Viscosity profile

Figure 7.5 shows the viscosities of asphalt blends at different TPC and PPC contents when tested at 135 and 165 °C to analyse the production temperatures in the equiviscous method. As expected, the viscosity of all binders decreased as the temperature increased from 135 to 165 °C. At both temperatures, the increase in pyrolytic char content increased the viscosity values indicating the stiffening effect through the addition of the char. The

viscosity of PPC modified binders was higher than that for TPC modified binders at each char dosage. For example, at 135 °C, PPC modified binders showed 8%, 14%, 14%, and 42% higher viscosity values at char contents of 5%, 10%, 15%, and 20%, respectively, compared to the viscosity of TPC modified binders at these contents. The results indicate that the stiffening effect of PPC is higher than TPC, as also found from other rheological tests discussed in Chapter 6.

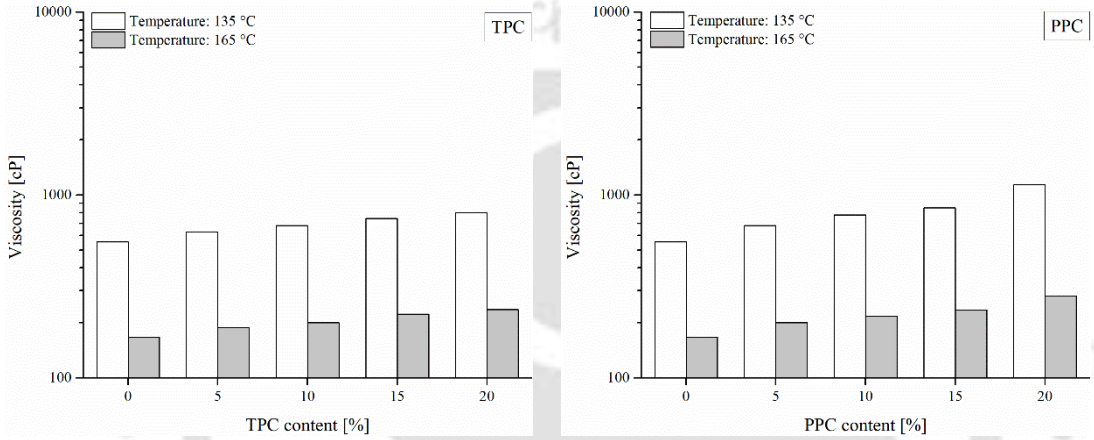

(a) (b)

Figure 7.5 Viscosity for binders modified with (a) TPC, and (b) PPC

The increase in viscosity with an increase in char content is attributed to the strong adsorption of bitumen compounds (especially maltene oils) on the surface of the char, which in turn reduce the binder's fluidity (Chaala et al., 1996; Darmstadt et al., 1996). Higher viscosity indicates that the modification by TPC and PPC is expected to elevate the mixing and compaction temperatures. Furthermore, the Superpave system specifies a maximum viscosity limit of 3 Pa.s (3000 cP) at 135 °C to ensure adequate workability and ability to transport/pump the binder. Binders at all char dosages met this criterion with a maximum viscosity of 1.1 Pa.s (1100 cP) at 20% PPC dosage.

7.3.2 High shear viscosity

Figure 7.6 shows the high shear viscosities of the binders at different TPC and PPC contents tested at 135 and 165 °C to analyse the production temperatures using the HSV method.

The high shear viscosity was obtained at 500 s^{-1} shear rate extrapolated from the Cross-Williams model. The trends for char dosages are the same as Figure 7.5, showing an increase in the viscosity with an increase in char dosage. Further, the viscosity values are higher for PPC modified binders than TPC modified ones. On average, the PPC modified binders have 27% and 15% higher viscosity than TPC modified ones at 135 °C and 165 °C, respectively.

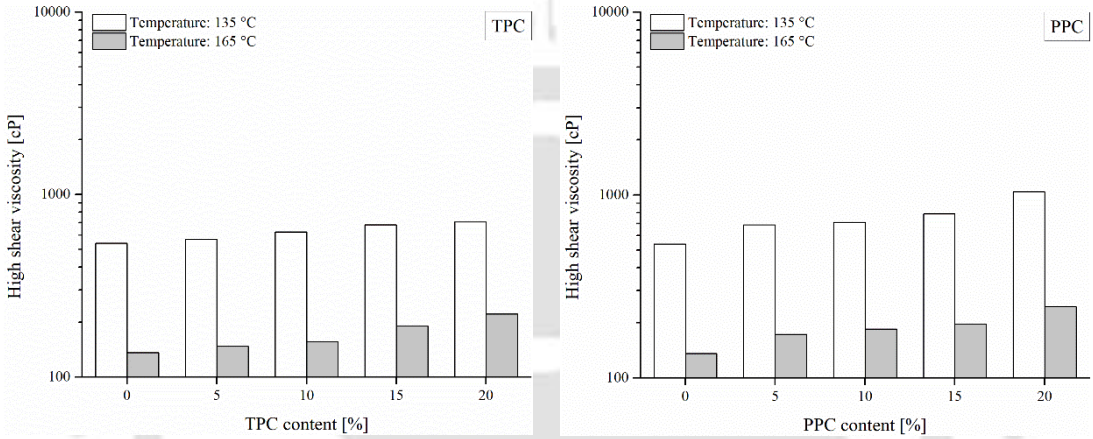

(a) (b)

Figure 7.6 High shear viscosity for binders modified with (a) TPC, and (b) PPC

The high shear viscosity values are comparatively lower than the viscosity obtained for the equiviscous method. Averaged for all binders, the high shear viscosities are 7.5% and 15% lower than the equiviscous viscosity at 135 °C and 165 °C, respectively. The lower HSV viscosities are due to the shear-thinning nature of the binders due to which they show a lower viscosity at higher shear rates. Since the limiting viscosities of the HSV and equiviscous methods are the same (0.17 ± 0.02 Pa.s and 0.28 ± 0.03 Pa.s for mixing and compaction temperatures, respectively), it is expected that the HSV production temperatures will be lower than the equiviscous temperatures. The production temperatures are presented in the Subsection 7.3.5.

7.3.3 Steady shear viscosity

The steady shear viscosity was measured at 500 Pa stress level, where the steady-state condition is attained for the binders (*i.e.*, almost constant viscosity with an increase in shear stress). The steady shear viscosities at the three test temperatures (76, 82, and 88 °C) for all binders are shown in Figure 7.7. Averaged for all binders, a 6 °C increase from 76 to 82 °C and from 82 to 88 °C caused 46% decrease in the viscosity. The viscosity values are higher for PPC modified binders than TPC modified ones by 71%, 63%, and 57% at 76 °C, 82 °C, and 88 °C temperatures. The higher viscosity of PPC modified binders is also consistent with equiviscous and HSV viscosities. To determine the mixing and compaction temperatures, the steady shear viscosity values are extrapolated to limiting viscosities of 0.17±0.02 Pa.s (for mixing temperatures) and 0.35±0.03 Pa.s (for compaction temperatures).

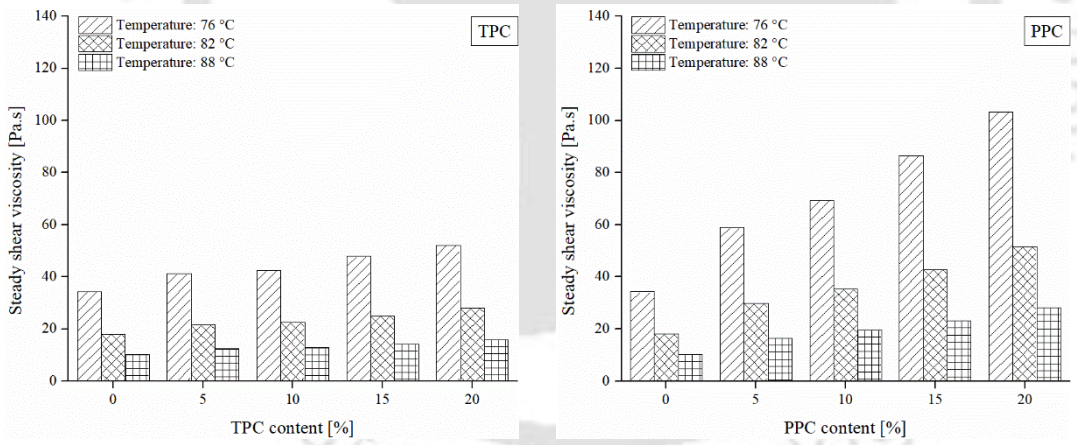

(a) (b)

Figure 7.7 Steady shear viscosity for binders modified with (a) TPC, and (b) PPC

7.3.4 Phase angle master curves

Phase angle master curves were developed using the time-temperature superposition principle (TTSP) at 80 °C reference temperature based on frequency sweeps performed at 50, 60, 70, and 80 °C. The master curves are shown in Figure 7.8. Throughout the frequency range, the phase angle master curves for PPC modified binders are lower than the control

binder. The master curves for the TPC modified binders were also lower than the control; however, the reduction was less pronounced. This observation implies that PPC modification has a higher elastic response than TPC modified binders. Similar results were also observed for viscosity results discussed earlier. The mixing and compaction temperatures calculated using the phase angle method use the frequency corresponding to a phase angle 86° and substituting in the empirical equations (Equations 7.3 and 7.4). Results of mixing and compaction temperatures obtained from all methods are discussed in the next section of the chapter.

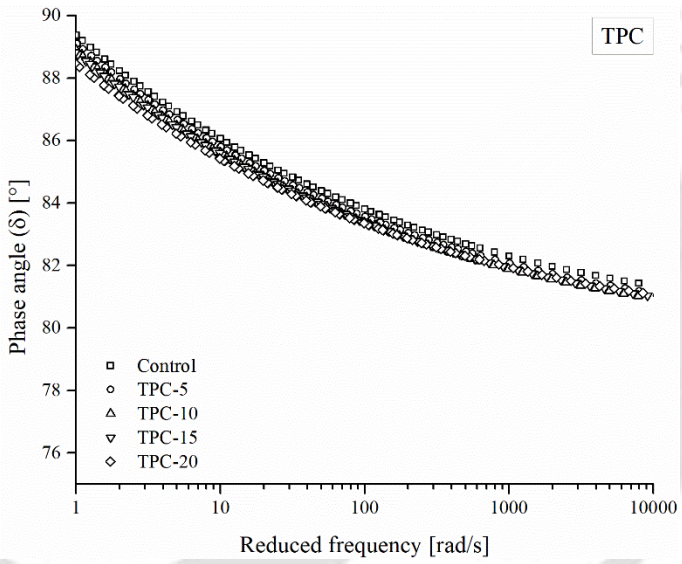

(a)

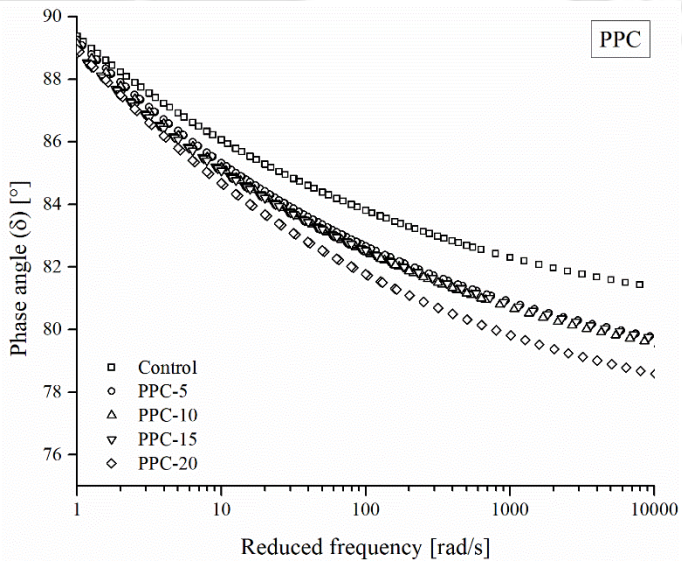

(b)

Figure 7.8 Phase angle master curves of: (a) TPC modified binders, (b) PPC modified binders

7.3.5 Mixing and compaction temperatures

Figure 7.9 presents the mixing and compaction temperatures (mid-values in case of ranges) found using the four different methods for all binders. In line with the existing literature, equiviscous method resulted in the highest mixing and compaction temperatures. Comparing the temperatures from HSV and equiviscous methods, it was seen that the HSV temperatures were slightly lower (about 5 °C and 4 °C lower for mixing and compaction temperatures, respectively) than the equiviscous temperatures. The production temperatures derived from SSF and PA methods were lower (about 14 °C and 11 °C lower for SSF and PA, respectively) than those obtained through the equiviscous method. The lower viscosities of HSV and SSF methods, than the equiviscous method, resulted in lower mixing and compaction temperatures. Both these methods capture the shear-thinning behaviour of the binders, and thus resulted in a lower viscosity at higher shear rates (HSV) or high shear stresses (SSF). The SSF mixing temperatures were 14 °C lower (on average) than the equiviscous mixing temperatures, while the reduction in compaction temperatures was 15 °C.

Not much variation in either mixing or compaction temperature is noted with an increase in the TPC dosage in the PA method. This is likely explained by the variation of phase angle master curves for TPC modified binders that showed quite proximity to one another. The values of ω_{86} derived from TPC phase angle master curves were close to each other, resulting in the production temperatures being quite near to each other. On the other hand, PPC dosages had a higher effect on mixing and compaction temperatures in all four methods. This observation is also consistent with the rheological findings of PPC modified binders (discussed in Chapter 6), where it was seen that PPC had more effect on binder stiffness parameters than TPC. The next section discusses the validation of the methods for use in the preparation of asphalt mixes.

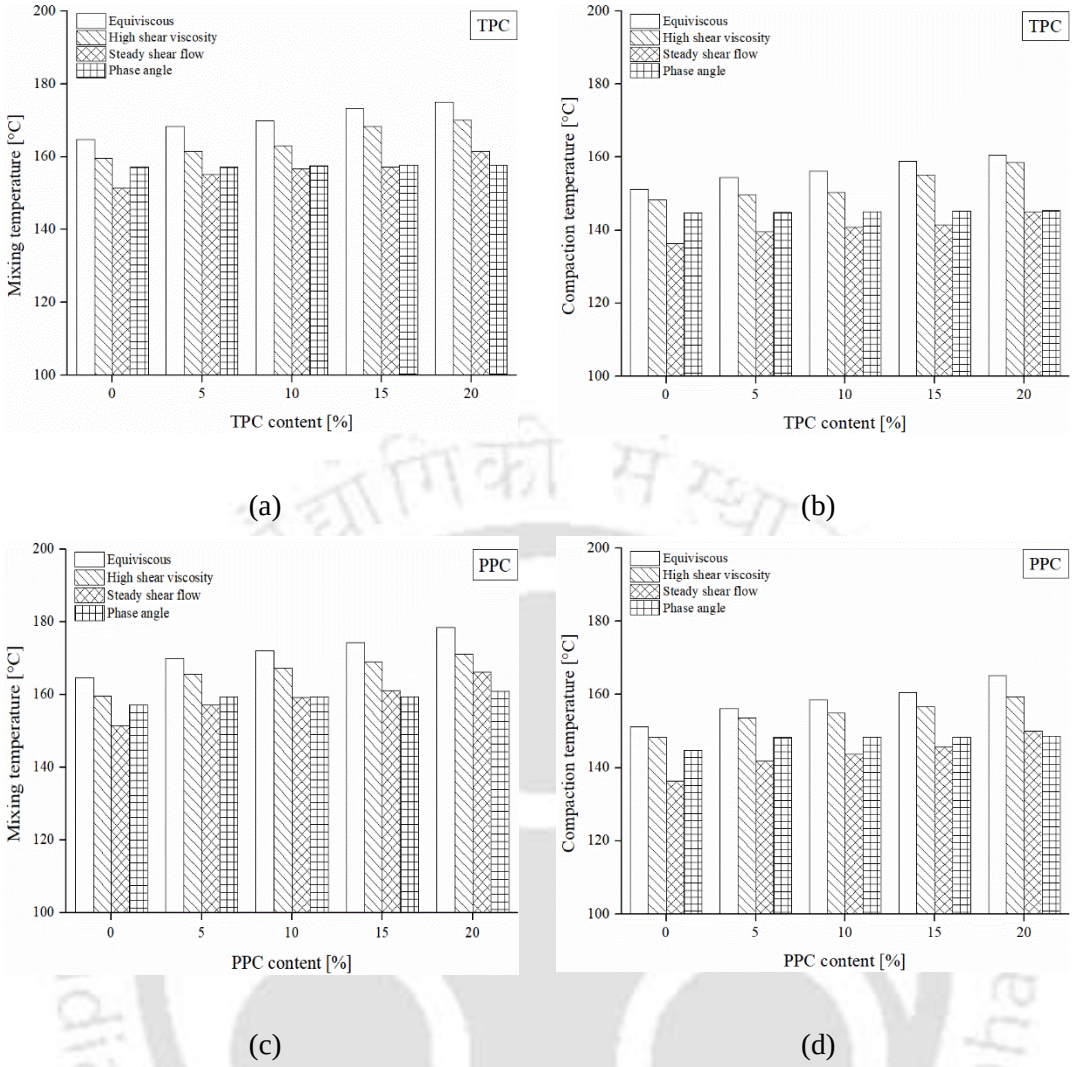

Figure 7.9 Production temperatures from all methods: (a) TPC mixing temperatures; (b) TPC compaction temperatures; (c) PPC mixing temperatures; (d) PPC compaction temperatures

7.3.6 Validation of production temperatures through asphalt mixtures

The production temperatures were determined based on measurements made on the binders alone. It was needed to select a method that could be used to prepare mixtures with the char modified binders in this study. Mixes were fabricated with the different binders following the mixing temperatures obtained from different methods to validate and finalise one method. The criterion adopted to select an acceptable mix was whether a complete aggregate coating could be obtained when an aggregate batch for preparing a single Marshall specimen was mixed with the binder for 60 s at the respective mixing temperature.

Figure 7.10 shows the photographs of loose mixes prepared at the different mixing temperatures with TPC-10 binder. Similar results were obtained for all other modified binders and are omitted to avoid excessive repetition. The mixes prepared at SSF and PA temperatures had some aggregate particles with inadequate binder coating, while a complete coating was observed for mixtures prepared at HSV and equiviscous temperatures. However, the equiviscous temperatures were observed quite high (such as 178 °C for the PPC-20 binder), which may require heating the modified binder to excessively high temperatures causing possible degradation and accelerated binder ageing. It was, therefore, decided to use the HSV temperatures for the fabrication of all mixes in this study. The HSV mixing temperatures can be approximated as 165±5 °C for mixing and 155±5 °C for compaction. It can also be noted that IRC 111 (2009) recommends mixed material temperatures (*i.e.*, mixing temperatures) of 150-165 °C and 160-170 °C for mixes made with VG 30 and VG 40 binders, respectively. The HSV mixing temperatures used for the mixes in this study also fall within the IRC specified ranges.

Figure 7.10 Photographs of TPC-10 mixes prepared using mixing temperatures derived from (left to right): EQ, HSV, SSF, and PA methods

7.4 Summary

In this chapter, the mixing and compaction temperatures (collectively called production temperatures) were determined for the control and modified binders at various dosages of

pyrolytic chars. Four methodologies were used: the traditional equiviscous (EQ) method, high shear viscosity (HSV) method, steady shear flow (SSF) method, and phase angle (PA) method. The equiviscous and HSV methods were based on measurements made with a rotational viscometer, while in the SSF and PA methods measurements were made on a DSR. An increase in the production temperatures with respect to TPC and PPC dosages was found across all the methods used. However, less variation was found for the TPC dosage, especially in the PA method. The production temperatures determined using the HSV, SSF, and PA methods were lower than those obtained through the equiviscous method. The production temperatures were further verified by fabricating mixtures and evaluating the binder coating, and the temperatures from the HSV method were found to be the most suitable. Therefore, for the next task (on evaluation of performance properties of the mixes), the HSV temperatures were used to fabricate the mixes.

Chapter 8

CHARACTERISATION OF ASPHALT MIXTURES

8.1 Introduction

Chapters 5, 6, and 7 of the thesis mainly focused on the characterisation and evaluation of char-modified asphalt binders, to understand their storage stability, rheology and production temperatures aspects. In the next phase of the work, asphalt mixtures were designed and fabricated with the TPC and PPC modified binders and then evaluated for different performance attributes related to resistance against rutting, moisture damage, cracking, and fatigue. The Marshall method of mix design, which is currently in force in India, was followed and conformity to the mix design specifications was checked for the mixtures designed with the nine different binders. Mix design parameters alone are not sufficient to ensure performance of the mixtures towards rutting, moisture damage, fatigue and cracking. It is therefore, critical to consider the laboratory scale attributes to evaluate the performance of asphalt mixtures fabricated with pyrolytic char modified binders.

This chapter presents and discusses the results of different design parameters and performance tests for evaluation of asphalt mixtures prepared with TPC and PPC modified binders. The mix design parameters/properties include the optimum binder content (OBC), volumetric properties (VMA and VFB), and Marshall properties (stability and flow). A leachate toxicity test was also conducted on asphalt mixtures to ensure that their use is safe for the environment. The asphalt mixtures were then evaluated for rutting (through static creep, dynamic creep, and HWTD tests), moisture damage (through TSR and RMS tests), cracking (through SCB test), and fatigue (through ITFT). Pavement structural analysis was

then carried out using IITPAVE software based on the resilient modulus of the mixtures. The chapter concludes with a discussion on the cost aspects of incorporation of pyrolytic chars in asphalt binder modification.

8.2 Mix Design of Bituminous Concrete

Bituminous concrete mixtures were prepared with the BC-2 aggregate gradation having 13.2 mm NMAS. Mix design was performed for each of the nine binders used in this study as per the Marshall mix design method. The mix design methodology was presented in Chapter 3. The OBC was the binder content corresponding to 4% air voids content, while satisfying the other mix design requirements for VMA, VFB, stability, and flow.

Figure 8.1a shows the OBC of all mixtures. The OBCs corresponding to control (unmodified binder), TPC-5, TPC-10, TPC-15, TPC-20, PPC-5, PPC-10, PPC-15, and PPC-20 modified binders were respectively determined as 5.5, 5.5, 5.5, 5.8, 5.85, 5.5, 5.75, 5.78, and 5.85%. A slight increase in the OBC with an increase in TPC and PPC dosage can be mainly attributed to a higher stiffness of modified binders, which demand higher binder to achieve the desired workability/air-void content. Figure 8.1b-e show the average volumetric (VMA and VFB) and Marshall properties (stability and flow) of all mixtures obtained at their respective OBC. The requirements stipulated by Indian specifications (MoRTH, 2013) are also shown in the sub-figures of Figure 8.1. It was observed that all mixtures fulfilled the VMA, VFB, stability, and flow requirements for a BC-2 mix. In particular, Figure 8.1d shows that control and the TPC and PPC mixtures met the Marshall stability criterion of 9 kN (minimum) for neat/virgin binder as well as the 12 kN (minimum) criterion stipulated for a modified binder (MoRTH, 2013). Flow values of all mixtures were within the prescribed range of 2 to 4 mm, indicating that the inclusion of pyrolytic chars did not result in excessive plasticity (indicated by too high flow) or brittleness (indicated by too low flow).

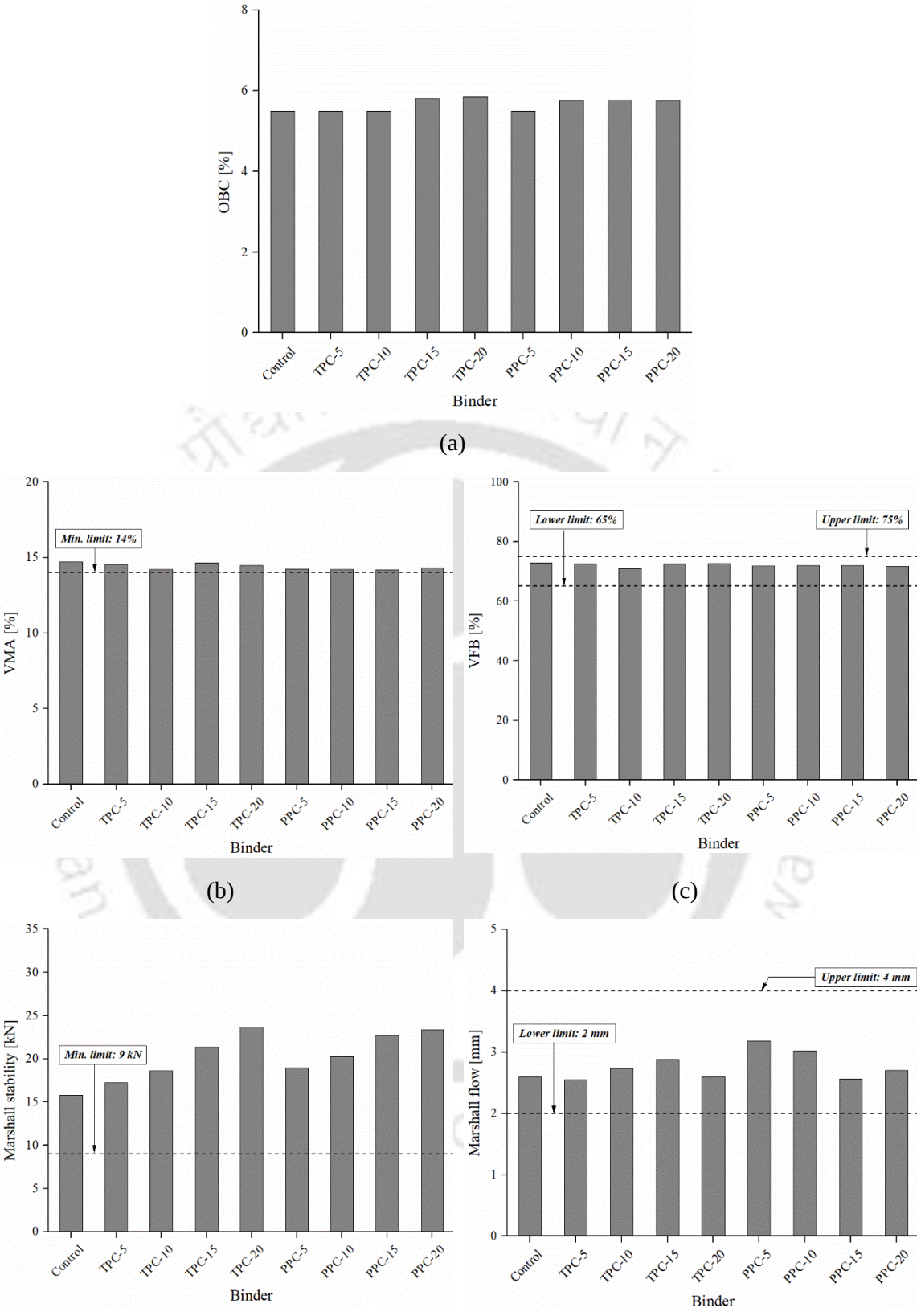

Figure 8.1 Mix design properties: (a) OBC, (b) VMA, (c) VFB, (d) stability, (e) flow

The OBC values of the mixtures with different pyrolytic char modified binders were quite close to 5.5 ± 0.3 % with a slight difference among each other. To make comparisons of performance properties among the nine mixtures, a single binder content of 5.5% was used to fabricate all mix specimens. A gyratory compactor was used to fabricate asphalt mixtures for performance characterisation. The required air void content for a particular performance test was then precisely controlled by varying the number of gyrations during the specimen compaction. This approach allowed analysis of the effect of pyrolytic char type and content without binder content or air void content as a confounding variable.

8.3 Toxicity Characteristics of Asphalt Mixtures

Toxicity characteristics leaching procedure (TCLP) tests were performed on the mixtures prepared with the modified binders at the highest (20%) TPC and PPC dosage. Table 8.1 presents the TCLP results of TPC-20 and PPC-20 mixtures, hazardous waste limits, and IS 10500 (2012) limits for drinking water. The criteria for hazardous waste limits for Cd, Cr, and Pb were based on USEPA (2020), while the limits for Fe, Mn, Zn, and Ni were based on 100 times the drinking water standards reported by Wartman et al. (2004).

Table 8.1 Results of TCLP analysis

Contaminant	Drinking water limit [a] (mg/L)	Hazardous waste limit (mg/L)	TCLP leachate concentration (mg/L)	
			TPC-20 mix	PPC-20 mix
Cadmium	0.003	1.0 [b]	0	0
Chromium	0.05	5.0 [b]	0	0
Lead	0.01	5.0 [b]	0	0
Manganese	0.1	10 [c]	0.081	0.474
Nickel	0.02	2 [c]	0	0
Total Iron	0.3	30 [c]	0	0
Zinc	5	500 [c]	0.533	0.781

[a] Specification limits from IS 10500 (2012)

[b] Specification limits from USEPA SW-846 (USEPA, 2020)

[c] Specification limit taken as 100 times the drinking water limit as reported by Wartman et al. (2004)

Based on these criteria, the detected concentrations of metals in TPC-20 and PPC-20 mixtures were well within the hazard limits. Only Mn and Zn were detected in the leachate from mixtures, while other metals were not present. Considering the environmental impact, it is evident that TPC and PPC can be safely used in asphalt modification for construction of asphalt pavements.

8.4 Rutting Performance of Asphalt Mixtures

Three mechanical performance tests were employed to assess the rutting/high-temperature performance of BC-2 mixtures: static creep, dynamic creep, and Hamburg wheel tracking device (HWTD) test. All tests were performed at 50 °C representing high pavement service temperature. The following subsections present and discuss the results of each test.

8.4.1 Static creep test

The static creep test was conducted with 100 kPa stress level for 1 h load and 1 h recovery duration. The strain-time response of all mixtures recorded in the test is shown in Figure 8.2a,b. At the beginning of the test, the strain increases at a faster rate and then the creep response becomes almost linear with time. After the creep stress is released, some elastic deformation is rapidly recovered, followed by a time-dependent recovery. The residual strain at the end of the test is the permanent strain and is used to compare the rutting performance of the mixtures. Figure 8.2a and 8.2b show that the strain-time plots of char-modified mixtures plotted below the control mix. An increase in TPC and PPC dosage caused the strain to decrease further, indicating that the char modified mixtures experienced lower strains than the control mix when subjected to the creep stress. The following two properties were derived from the strain-time plot: (1) permanent strain (unrecovered strain at the end of recovery duration, *i.e.*, at time = 7200 s), and (2) recovery (ratio of recovered strain to the total strain), where recovered strain is the difference between total and permanent strains, and total strain is the strain at the end of loading period (at 3600 s).

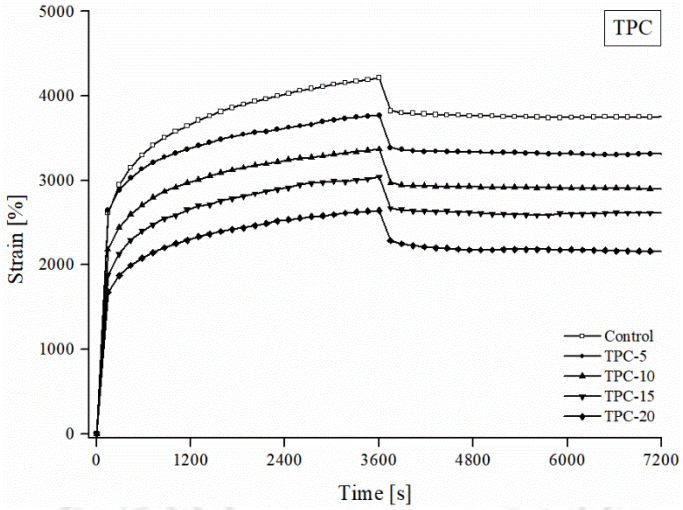

(a)

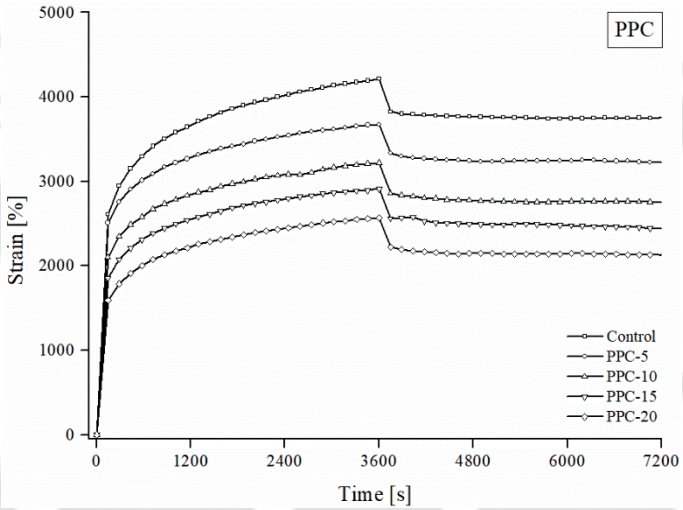

(b)

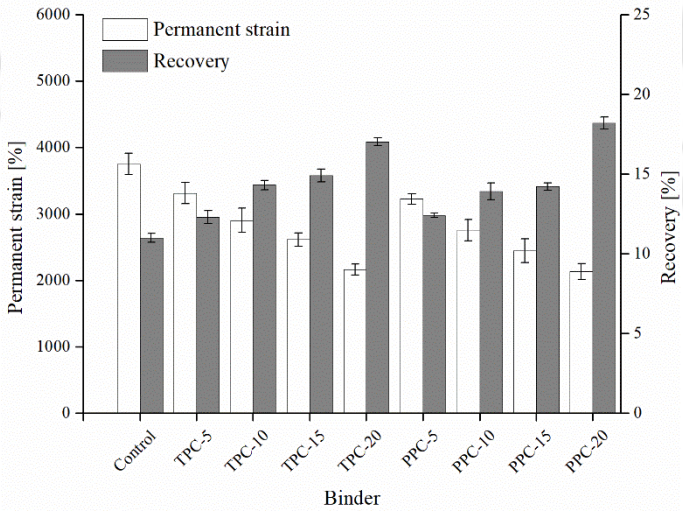

(c)

Figure 8.2 Results of static creep test: (a) strain-time plots for TPC mixtures, (b) strain-time plots for PPC mixtures, (c) permanent strain and recovery

Figure 8.2c presents the compiled results of permanent strain and percent recovery of all mixtures. In the case of both TPC and PPC mixtures, the incorporation of pyrolytic chars led to an appreciable decrease in the permanent strain. The TPC-5, TPC-10, TPC-15, and TPC-20 mixtures reduced the final strain by 12%, 23%, 30%, and 42%, respectively, compared to the control mix. Corresponding percent reductions for PPC-5, PPC-10, PPC-15, and PPC-20 mixtures were 14%, 27%, 35%, and 43%, respectively. Hence, the modified mixtures exhibited lower permanent deformation. Comparing the permanent strain results, one can also observe that PPC had a slightly higher effect on the permanent deformation performance of the mixtures than TPC. Further, the percent recovery increased with the char dosage in binder modification, indicating that a larger proportion of the total strain was recovered when modified binders were used.

8.4.2 Dynamic creep test

The dynamic creep test consisted of applying vertical stress of 100 kPa dynamically in a square load waveform (loading period followed by a rest period). The stress was applied for 1 s followed by a 1 s rest period (0.5 Hz frequency). The dynamic creep test results are presented in Figures 8.3a and 8.3b as accumulated (permanent) deformation versus load cycle curves for 10000 load cycles. The accumulated strain is the unrecovered strain left at the end of the rest period in a dynamic creep load cycle. A lower accumulated strain is desirable as it indicates higher resistance to rutting. Figure 8.3a and 8.3b show that the accumulated strain decreased with an increase in the TPC and PPC dosage. Initially, the accumulated strain increased faster in as the specimen underwent secondary compaction, which quickly reduced the air voids. Subsequently, in the creep phase, the rate of growth of the accumulated strain stabilised and increased somewhat linearly. It is noted that none of the mixtures reached the tertiary deformation phase up to 10000 cycles since no inflection point was observed in the strain-load cycles curves in Figures 8.3a and 8.3b.

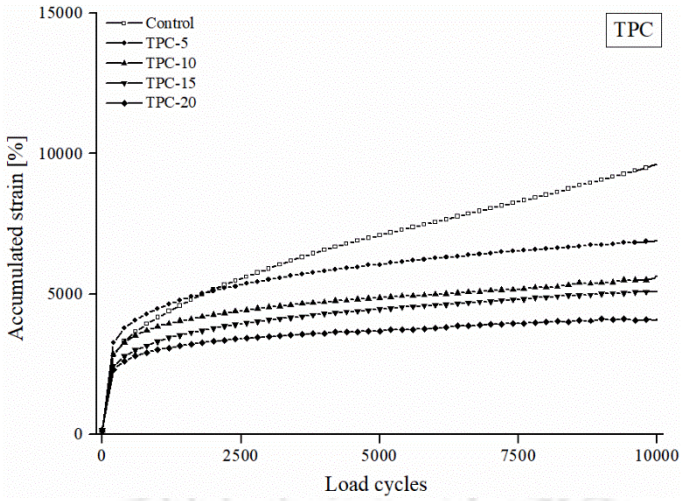

(a)

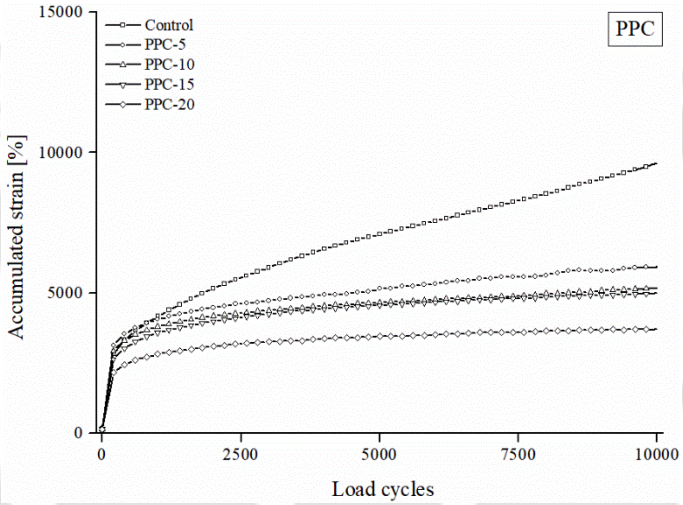

(b)

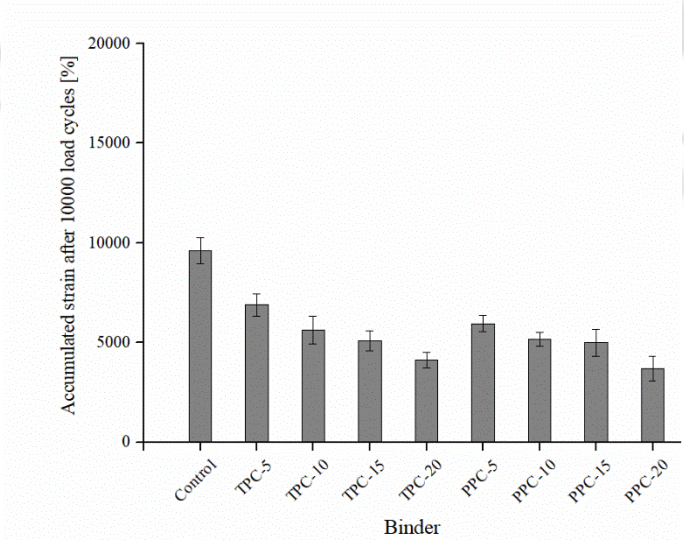

(c)

Figure 8.3 Results of dynamic creep test: (a) strain-load cycle plots for TPC mixtures, (b) strain-load cycle plots for PPC mixtures, (c) accumulated strain after 10000 load cycles

The effect of TPC and PPC dosages on the final accumulated strain value (strain at the end of the 10000th loading cycle) is presented in Figure 8.3c. In the case of both TPC and PPC mixtures, the incorporation of pyrolytic chars led to a decrease in the final accumulated strain. The TPC-5, TPC-10, TPC-15, and TPC-20 mixtures reduced the final strain by 28%, 41%, 47%, and 57%, respectively, compared to the control mix. Corresponding percent reductions for PPC-5, PPC-10, PPC-15, and PPC-20 mixtures were 38%, 46%, 48%, and 61%, respectively. BC mixtures with PPC modified binders performed better in permanent deformation as they reported lower accumulated strain values than TPC mixtures.

8.4.3 Hamburg wheel tracking device (HWTD) test

The HWTD test on asphalt mixtures was performed in accordance with AASHTO T324 (2016) specifications on specimens submerged in water at 50 °C, and subjected to 20000 passes of a 705 N loaded steel wheel. The HWTD test helps to evaluate the high-temperature performance of mixtures when submerged underwater. Figures 8.4a and 8.4b show the development of rut depth with HWTD passes for the different TPC and PPC modified BC-2 mixtures. The rut depth progression curves showed lower rut depths for mixtures with TPC and PPC modified binders. The rut depths further decreased with an increase in TPC and PPC content. All mixtures with pyrolytic char modified binders showed only the post-compaction (indicating secondary compaction and identified by a fast rut depth growth near the test's beginning) and the creep (indicated by linear growth of the rut depth) phases. However, the control mix with neat binder experienced all the three phases (post-compaction, creep, and stripping phases) within the 20000 HWTD passes. The stripping phase is indicated by the change in slope of the curve at the stripping inflection point of 11950 passes. None of the char-modified mixtures showed stripping up to 20000 passes (no stripping inflection point).

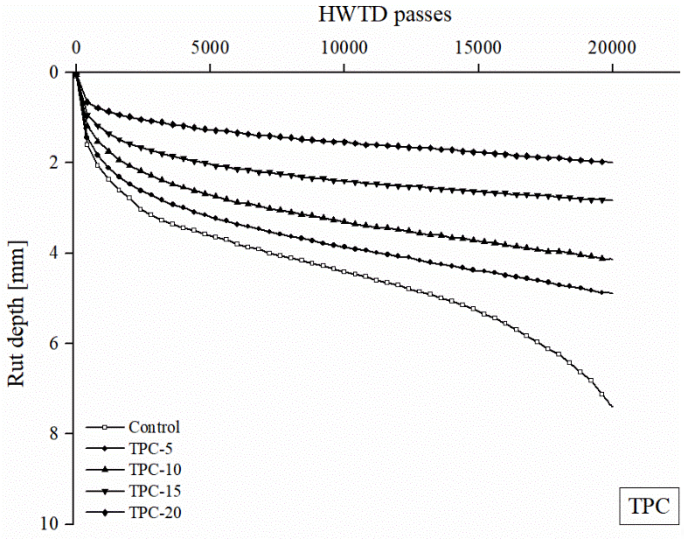

(a)

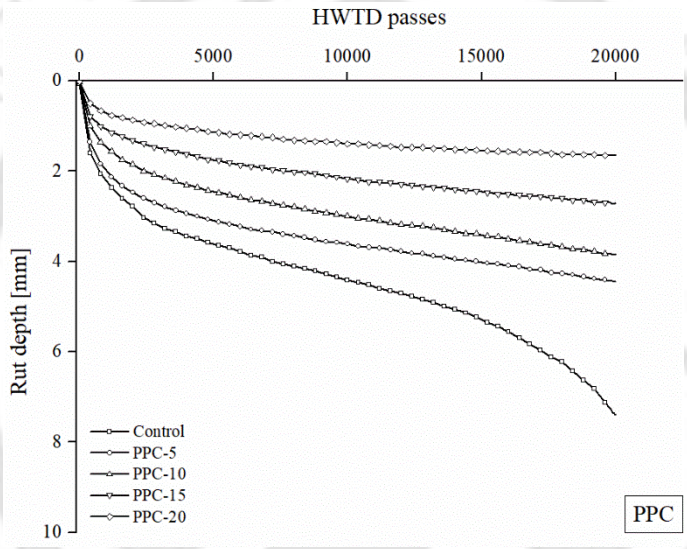

(b)

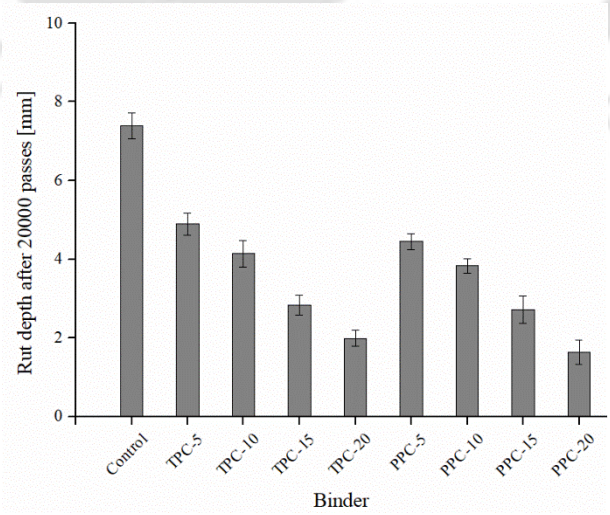

(c)

Figure 8.4 Results of HWTD tests: (a) rut depth-passes plots for TPC mixtures, (b) rut depth-passes plots for PPC mixtures, (c) rut depth after 20000 passes

The final rut depth after 20000 passes is further used to characterise the mix rutting performance (shown in Figure 8.4c). At the end of 20000 passes, the maximum rut depth was observed for the control mix as 7.4 mm. The mixtures with TPC-5, TPC-10, TPC-15, and TPC-20 binders showed a decrease in the rut depth by 34%, 44%, 62%, and 73%, respectively, compared to the control mix. Corresponding percent reductions for mixtures with PPC-5, PPC-10, PPC-15, and PPC-20 binders were 40%, 48%, 63%, and 78%, respectively. By comparison, the PPC mixtures showed a lower rut depth at a particular char content than the corresponding TPC mixtures. The results suggest that both TPC and PPC modified binders enhance the mix resistance to repeated wheel loads. The positive impact that TPC and PPC have on rutting performance also agrees with the rheological test results (MSCR, continuous high PG, master curves) of the char-modified binders presented in Chapter 6.

8.5 Moisture Damage Performance of Asphalt Mixtures

Two test methods were performed for moisture damage performance assessment of BC-2 mixtures with char-modified binders: modified Lottman test (TSR test) and retained Marshall stability (RMS). The following subsections present and discuss the results of each test.

8.5.1 Tensile strength ratio (TSR) test

Specimens of the dry (unconditioned) subset were conditioned at 25 °C for 2 h in a water bath and subjected to indirect tensile strength (ITS) evaluation. Under the conditioned ITS measurement, the BC-2 specimens were subjected to a freeze and thaw cycle of –18 °C for 16 h and 60 °C for 24 h, respectively. Figure 8.5a shows the dry and wet ITS values for all mixtures, while Figure 8.5b shows the TSR values. The dry ITS followed an increasing trend with an increase in TPC and PPC dosages from 0% (control mix) to TPC-20 and PPC-20 mixtures. However, the wet ITS increased from the control mix to the TPC-10 mix and

then decreased for TPC-15 and TPC-20 mixtures. A similar trend was observed in PPC mixtures (the wet ITS decreased for PPC-15 and PPC-20 mixtures after showing an increasing trend up to the PPC-10 mix). This shows that the wet ITS values of both TPC and PPC mixtures became susceptible to moisture conditioning at higher (15% and 20%) dosages. Modification up to 10% content of TPC and PPC helps to enhance the resistance to moisture damage as observed through the increase in the TSR values. At higher char dosage/content, a decrease was observed in the TSR values at 15% and 20% TPC and PPC contents. The TSR for the control mix was 96.1% which peaked at 98.9% for TPC-10 and 98.4% for PPC-10 mixtures and then reduced to 83.7% for TPC-20 and 85.9% for PPC-20 mixtures. The best performance in terms of TSR results were obtained for TPC-10 and PPC-10 mixtures. The TSR values of TPC-5, TPC-10, PPC-5, and PPC-10 mixtures were higher than the TSR for the control mix. There were only subtle differences between the results of TSR while comparing among the two chars. All the BC-2 mixtures with pyrolytic char modified binders satisfied the minimum 80% TSR criterion stipulated by the Indian specifications (MoRTH, 2013).

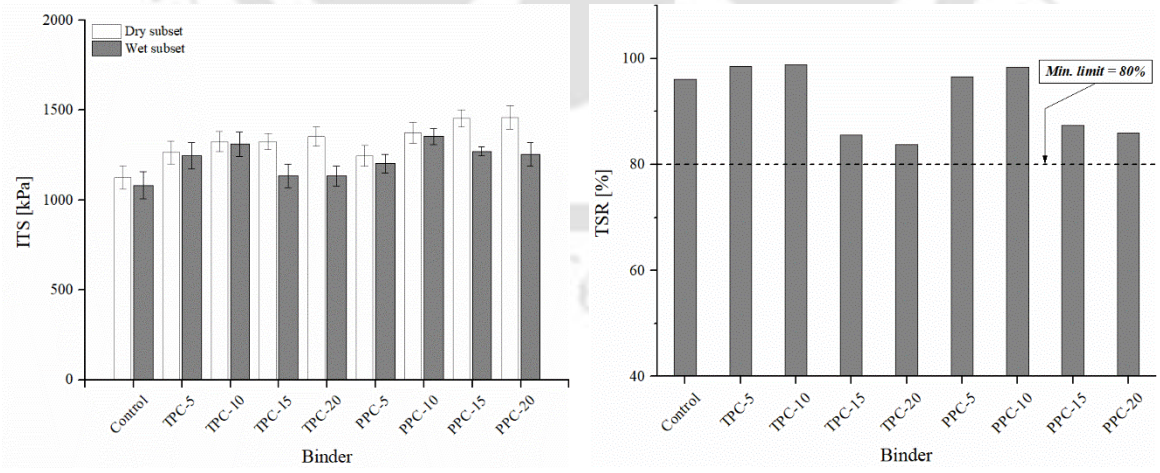

(a) (b)

Figure 8.5 (a) Results of dry and wet ITS, (b) TSR results

8.5.2 Retained Marshall stability (RMS) test

In the RMS test, the stability of unconditioned specimens was determined at 60 °C after 30 min soaking in a water bath. The moisture conditioned specimens were placed in a 60 °C water bath for 24 h, and then subjected to Marshall stability testing. The results of Marshall stability of unconditioned and moisture conditioned specimens and the RMS values are presented in Figure 8.6. RMS is the ratio of Marshall stability measured at 60 °C for moisture conditioned (or wet) to unconditioned (or dry) mix specimens. The unconditioned stability values consistently increased as the char dosage increased from 0% to 20% for both TPC and PPC mixtures.

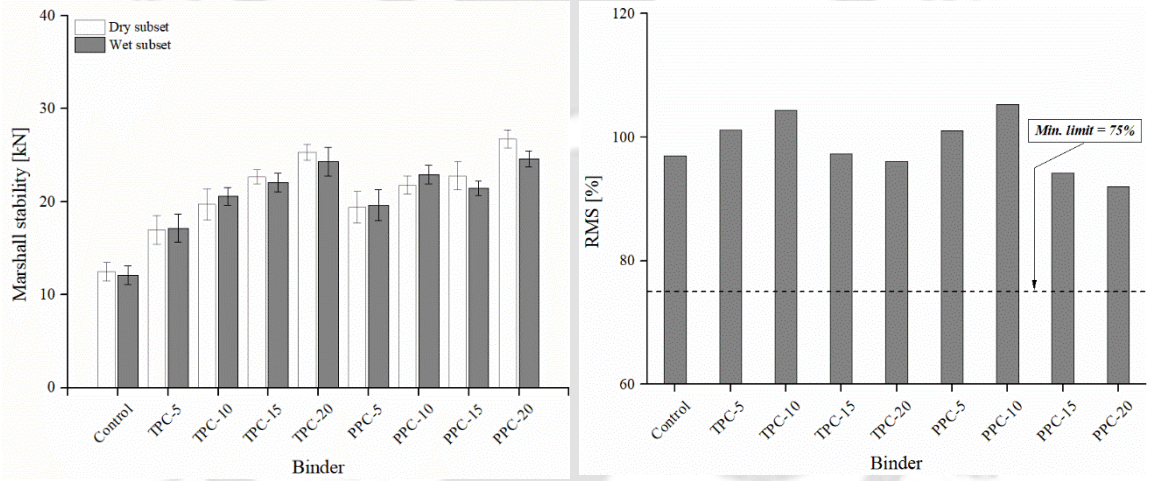

(a) (b)

Figure 8.6 (a) Results of dry and wet Marshall stability, (b) RMS results

The increase in unconditioned stability agrees with the binder stiffness and deformation resistance measured at 60 °C (such as the MSCR tests). The RMS values of mixtures increased up to 10% TPC and PPC contents, followed by a decrease at the higher TPC and PPC contents of 15% and 20%. The results of RMS and TSR test followed a similar trend and indicated that TPC-5, TPC-10, PPC-5, and PPC-10 mixtures have better moisture damage resistance than the control mix. BC-2 mixtures with TPC-5, TPC-10, PPC-5, and PPC-10 mixtures showed RMS values higher than 100%, indicating that the moisture conditioning did not have damaging effect on the mixture's stability (a surrogate measure

for compressive strength). Further, numerically the RMS values were higher than the TSR values for all mixtures. Compared to the TSR test, the moisture conditioning in the RMS test only included a thawing step and no freezing was applied. This may be the reason for higher RMS values than TSR for all mixtures. Finally, all TPC and PPC mixtures met the minimum 75% RMS requirement as per the Indian specifications (MoRTH, 2013).

8.6 Fatigue and Fracture Performance of Asphalt Mixtures

Two test methods were used to evaluate mechanical mix performance at intermediate service temperatures: SCB test for cracking and ITFT for fatigue. Both tests were conducted at 25 °C, a temperature representing the intermediate-service temperatures. The following subsections present and discuss the results of each test.

8.6.1 Semi-circular bend (SCB) test

The SCB test measured the crack resistance properties of asphalt mixtures subjected to static monotonic loading. J-integral (J_c) is the ratio of change in strain energy to a unit change in notch depth and has reported a good correlation with cracking observed in the field (Elseifi et al., 2012; Karimi et al., 2021). A higher value of J-integral shows higher resistance of the mix to crack initiation and propagation. The J-integral values of the TPC and PPC mixtures obtained from the SCB test are presented in Figure 8.7. Asphalt binder modification with TPC and PPC improved J-integral for 5% and 10% TPC and PPC modification levels, then a decrease in J-integral was observed at the higher (15% and 20%) modification levels. Except for the PPC-20 mix, all other TPC and PPC mixtures showed J-integral values quite higher than the control mix. The J-integral values for TPC-10 and PPC-10 mixtures were 150% and 67% higher than the control mix, respectively. The results show that TPC and PPC modification improved asphalt mixtures' cracking resistance, with TPC-10 and PPC-10 BC-2 mixtures having the best cracking performance. Comparing the effect of char type, no clear trend was observed between the TPC and PPC modified

mixtures, indicating that mixtures fabricated with both chars showed similar cracking performance.

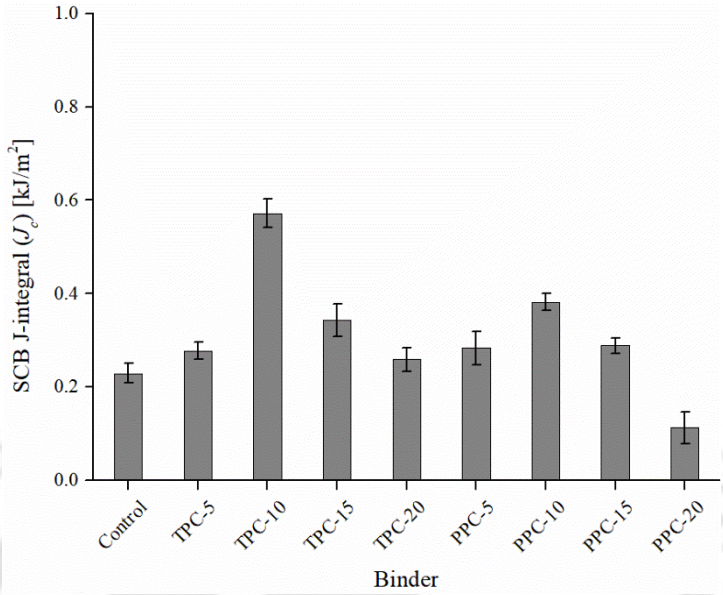

Figure 8.7 Results of J-integral from SCB tests

8.6.2 Indirect tensile fatigue test (ITFT)

Figure 8.8 presents the ITFT results where the asphalt mixtures' fracture life (the number of load cycles to failure) is presented. A higher fracture life indicates a better fatigue resistance. Figure 8.8 shows that mixtures fabricated with TPC and PPC modified binders exhibited higher fracture life than the control mix. The TPC-5, TPC-10, TPC-15, and TPC-20 mixtures showed fracture lives higher than the control mix by 89%, 225%, 120%, and 53%, respectively. Corresponding percent increase for PPC-5, PPC-10, PPC-15, and PPC-20 mixtures were 44%, 165%, 92%, and 25%, respectively. Similar to J-integral from the SCB test, the maximum fracture life was obtained for TPC-10 mix among all TPC mixtures and PPC-10 mix among all PPC mixtures. Comparing the effect of the pyrolytic chars, the TPC mixtures showed a 23% higher fracture life (on average) than PPC mixtures.

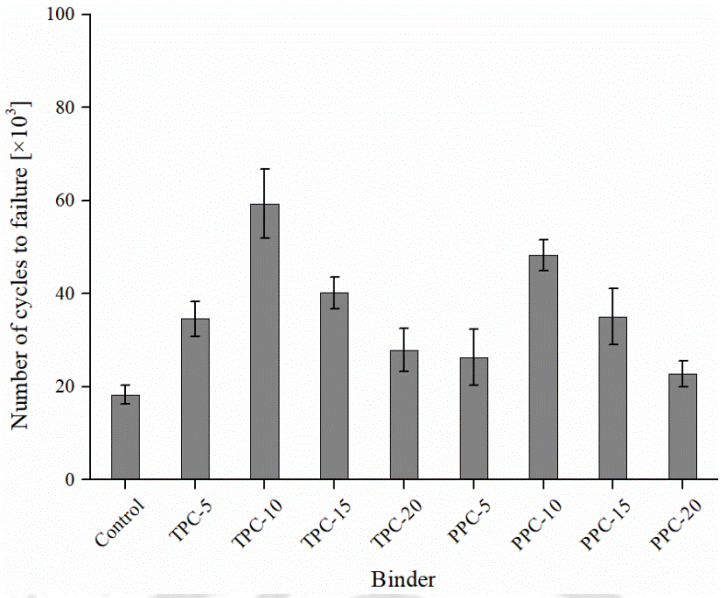

Figure 8.8 Results of fracture life from ITFT

The adhesion of the asphalt binder to the aggregate is critical to the mixture's resistance to moisture and fatigue cracking (Zhou et al., 2020). The results of moisture damage and intermediate temperature performance (cracking and fatigue) suggest that better adhesion between the aggregates and modified binders prevails up to 10% pyrolytic char content and then declines at higher dosages of 15% and 20%. It is possible that at higher TPC and PPC dosages (15% and 20%), there is relatively high stiffness/brittleness in the binders that causes relatively more rapid propagation of microcracks leading to shorter fracture life, decrease in J-integral, and lower TSR/RMS. Further, the trends of SCB and ITFT are also consistent with those from LAS test on asphalt binders (showing that a 10% dosage provides the optimum results), but not with the Superpave fatigue parameter G*sin δ. The most likely reason for this observation is that G*sin δ is evaluated at low strain and under linear viscoelastic conditions. On the other hand, LAS measures the fatigue-related properties in the nonlinear viscoelastic regime under high strain amplitudes. Similarly, the ITFT fracture life is the number of load cycles to specimen failure, while SCB J-integral is based on specimen strain energy to failure.

8.7 Pavement Structural Analysis

8.7.1 Resilient modulus

The resilient modulus (M_R) of asphalt mixtures with TPC and PPC modified binders was evaluated at 35 °C (annual average pavement temperature recommended by IRC 37, 2018). M_R at 35 °C is a vital material parameter used as an input in the mechanistic-empirical pavement design procedure followed in India based on linear elastic layer theory. Figure 8.9 shows the results of M_R for all mixtures. The results indicate that the resilient modulus of asphalt mixtures increased with the increment of char content for both TPC and PPC mixtures. TPC-20 and PPC-20 mixtures showed the highest resilient modulus values among all mixtures. An increase in TPC dosage from 5% to 20% increased the M_R values by 24% to 82%, respectively, compared to the control mix with unmodified binder. Increase in PPC dosage from 5% to 20% increased the M_R values by 35% to 90%, respectively, compared to the control mix. The trends of resilient modulus agree with the results of other high-temperature/rutting performance tests of the BC-2 mixtures (dynamic creep, static creep, and HWTD tests). As discussed in the next section, the resilient modulus values were used in the pavement structural analysis performed using IITPAVE software.

8.7.2 Structural analysis using IITPAVE software

A flexible pavement system composition recommended by IRC 37 (2018) for 30 msa (million standard axles) traffic level was considered and is shown in Figure 8.10. The pavement consists of a bituminous layer with two courses (wearing and binder courses), a granular layer with two courses (base and subbase), and the soil subgrade. The thickness (t), elastic modulus (E), and Poisson's ratio (μ) for each layer are also indicated in Figure 8.10. Resilient modulus values of different BC-2 mixtures were considered for elastic modulus of wearing course in the pavement composition shown in Figure 8.10.

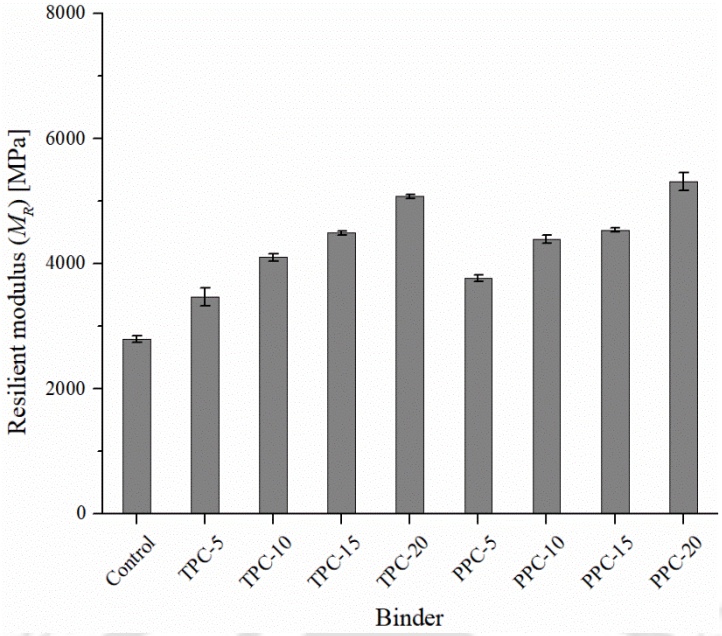

Figure 8.9 Results of resilient modulus of mixtures at 35 °C

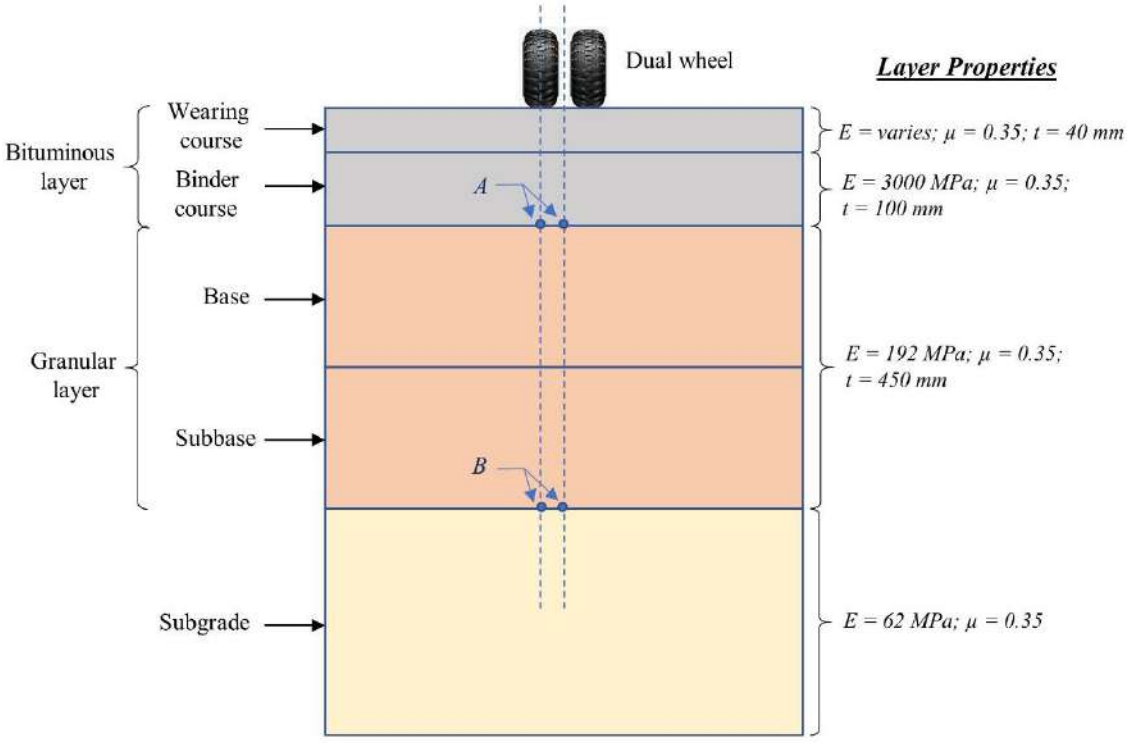

Figure 8.10 Flexible pavement composition considered for 30 msa traffic level
(Note: E = resilient modulus; μ = Poisson's ratio; t = thickness)

Critical mechanistic parameters are the strains at two locations in the pavement system: (1) tensile strain (ε_t) at the bottom of the bituminous layer (point A in Figure 8.10), and (2) compressive strain (ε_c) at the top of the subgrade (point B in Figure 8.10). The resilient

modulus values of only the top wearing course were changed based on the results obtained in the previous section for char-modified BC-2 mixtures, and the critical strain values at the two critical points were analysed using the IITPAVE software (a linear elastic layered pavement software used for mechanistic-empirical pavement design in India). The IITPAVE software considers a flexible pavement as a multi-layered linear elastic structure and computes stresses and strains at important locations in the pavement structure. For the design traffic of 30 msa, the allowable compressive strain (ε_c) was obtained from rutting equation (Equation 8.1) as 416 με.

$$T_R = 1.410 \times 10^{-8} \cdot \left(\varepsilon_c\right)^{-4.5337} \tag{8.1}$$

$$T_F = 0.5161 \times 10^{-4} \cdot C \cdot \left(\varepsilon_t\right)^{-3.89} \cdot \left(M_{R,b}\right)^{-0.854} \tag{8.2}$$

In Equation 8.1, T_R = subgrade rutting life (msa); ε_c = vertical compressive strain at the top of the subgrade. Similarly, for the 30 msa design traffic, the allowable tensile strain (ε_t) was obtained from fatigue equation (Equation 8.2) as 203 με. In Equation 8.2, T_F = fatigue life of bituminous layer (msa); ε_t = horizontal tensile strain at the bottom of the binder course; $M_{R,b}$ = resilient modulus of the bituminous mix used in the binder course. The factor *'C'* in Equation 8.2 takes into consideration the effect of volumetrics (air voids and effective binder content by volume) of the binder course layer and was assumed as 2.35 (IRC 37, 2018).

By changing the resilient modulus values of the topmost pavement layer, the strains at the critical locations (ε_t and ε_c) were determined using IITPAVE software. The results of computed strains and the corresponding rutting and fatigue life are shown in Figure 8.11. With incorporation of PPC and TPC modified binders, all BC-2 mixtures showed critical compressive and tensile strains lower than the allowable values. The increase in TPC and PPC dosage further reduced both critical strains, indicating that the pavement system

consisting of wearing course with TPC and PPC modified binders can withstand higher traffic repetitions than the pavement system with control mix used in the wearing course.

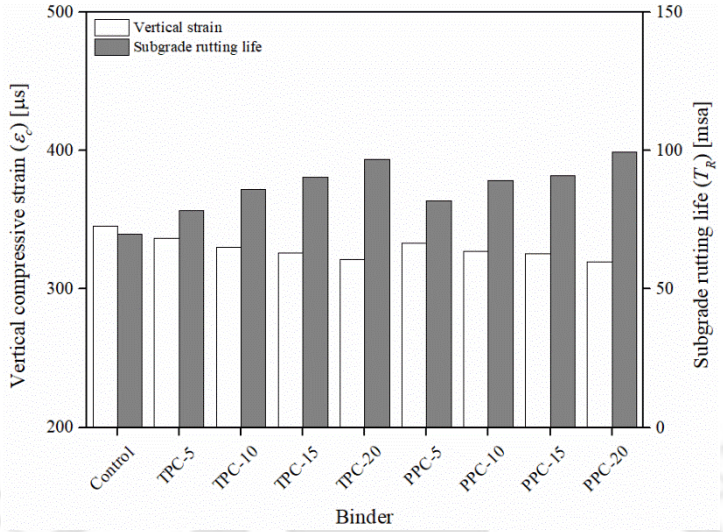

(a)

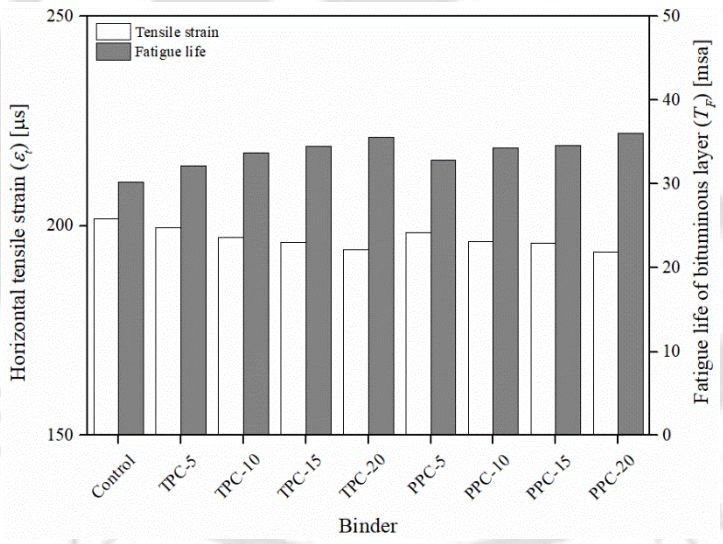

(b)

Figure 8.11 Results of pavement structural analysis: (a) ε_c and T_R, (b) ε_t and T_F

The design traffic level corresponding to the critical compressive and tensile strains was determined based on fatigue and rutting equations (Equations 8.1 and 8.2) and are also presented in Figure 8.11. The TPC-5, TPC-10, TPC-15, and TPC-20 mixtures are capable for bearing a traffic (based on compressive strain) higher than the control mix by 12%, 23%, 29%, and 39%, respectively. Corresponding percent increase in the amount of

allowable traffic for PPC-5, PPC-10, PPC-15, and PPC-20 mixtures were 17%, 27%, 30%, and 42%, respectively. The TPC-5, TPC-10, TPC-15, and TPC-20 mixtures showed design traffic (based on tensile strain) higher than the control mix by 6%, 11%, 14%, and 18%, respectively. Corresponding percent increase for PPC-5, PPC-10, PPC-15, and PPC-20 mixtures were 9%, 13%, 14%, and 19%, respectively. Therefore, the use of TPC and PPC contributes to an increased traffic/load carrying capacity of the pavement structure.

8.8 Cost Considerations

Information was gathered from different pyrolysis plant owners and bitumen suppliers regarding the current price of pyrolytic chars and bituminous binders. The char prices range from INR 2.50 to 4.00 per kg, with the price of TPC generally being slightly higher than PPC because TPC contains carbon black, which can be later recovered. Information provided by pyrolysis plant owners revealed that the chars are also sold as low-grade fuel in brick kilns at quite low prices (about INR 4 per kg ~ USD 0.05 per kg), else discarded in nearby landfills/open areas. The price of a VG 30 bitumen was obtained as INR 45-50 per kg. Compared to other common polymer modifiers, the price of the pyrolytic chars is much lower (the price of styrene-butadiene-styrene (SBS) co-polymer is about INR 200 per kg). Therefore, the price of TPC and PPC modified asphalt binders is expected to be quite lower than the polymer modified binders. The blending process of the chars with the unmodified binder will also entail some additional costs for the preparation of the modified binder, quite similar to that in the case of polymer modification. The cost of a product generally lowers through technological advancements, up-gradation of equipment and large-scale production. Therefore, continued research in the application of waste tyres and plastic pyrolytic chars will positively impact the economics of the pyrolysis process and development of the product (*i.e.*, pyrolytic char modified asphalt).

8.9 Summary

This chapter presented and discussed the results of mix design properties, performance tests for rutting, moisture damage, cracking, and fatigue of asphalt mixtures prepared with TPC and PPC modified asphalt binders. Bituminous concrete mixtures prepared with all TPC and PPC dosages met all volumetric (VMA, VFB) and Marshall (stability and flow) requirements, as specified by the Ministry of Road Transport and Highways. Asphalt binder modification with TPC and PPC improved the rutting resistance of mixtures, as evidenced by static creep, dynamic creep, and HWTD tests. The rutting performance improved with an increase in TPC and PPC dosages up to 20%. Comparing the fatigue, cracking, and moisture damage results, the optimum performance was achieved at 10% dosage of both TPC and PPC. Pavement structural analysis conducted with IITPAVE software showed that the use of TPC and PPC in the top wearing course layer contributed to increased traffic carrying capacity of the pavement, owing to the higher resilient modulus. The chapter concluded with remarks pertaining to cost considerations with the use of pyrolytic chars and showed that the char modification will be quite economical and provides a significant enhancement in the performance and traffic/load carrying capacity of corresponding asphalt mixtures.

Chapter 9

SUMMARY AND CONCLUSIONS

9.1 Summary of the Research

There has been a significant drive toward establishing sustainable solutions for managing post-consumer tyre and plastic waste streams in recent years. In this direction, pyrolysis technology has garnered broad scientific interest to reduce waste volume while allowing for energy valorisation and overcoming the challenges/concerns associated with the disposal of waste tyres and plastics. The two main pyrolysis products are the liquid oils and gases, which have good potential as fuels, monomers, and precursors to valuable petrochemicals. The third product, the solid carbonaceous pyrolytic char, is often regarded as a by-product with limited high-value application opportunities. The use of pyrolytic chars in asphalt binder modification is an emerging area of research. Positive results reported with other carbon-based asphalt modifiers, and the possibility of using a carbonaceous by-product of the waste pyrolysis process, motivated the present study on tyre pyrolytic char (TPC) and plastic pyrolytic char (PPC) modified asphalt binders and mixtures.

This study evaluated the effect of incorporation of TPC and PPC on the characteristics of asphalt binders, mix design parameters and the performance of bituminous concrete mixes containing TPC and PPC modified asphalt binders. The study focused on a multi-faceted investigation considering (a) characterisation of the two pyrolytic chars (TPC and PPC), (2) characterisation of the TPC and PPC-modified asphalt binders focusing on conventional, thermal storage stability, rheological, ageing, microscopic, and thermo-

chemical evaluations, and (3) characterisation of asphalt mixtures fabricated with TPC and PPC-modified asphalt binders focusing on their design, and performance against rutting, moisture damage, cracking, and fatigue. Leachate toxicity tests were also conducted on asphalt mixtures fabricated with TPC and PPC modified binders to ensure that their use is safe for the environment. Pavement structural analysis was then carried out using IITPAVE software based on the resilient modulus of the mixes. A total of nine modified binders were studied with a control binder and four binders, each with TPC and PPC-modification levels of 5, 10, 15, and 20%.

The objectives of this study were grouped into six independent tasks. Each task was carried out separately to fulfil the objectives framed for this study. Task 1 of the study involved the physical and chemical characterisation of TPC and PPC and the microstructural and thermo-chemical characterisation of asphalt binders. Task 2 of the study involved evaluating the storage stability of the TPC and PPC modified binders. The thermal storage stability was evaluated at multiple dosages of two cross-linking agents: polyphosphoric acid (PPA) and sulfur. Task 3 of this study covered the rheological characterisation of TPC and PPC modified binders through frequency sweep, high-performance grade (PG) measurement, MSCR evaluation, master curves for G* and δ, G*sin δ evaluation, linear amplitude sweep (LAS) tests, and an additional high temperature/rutting assessment. Task 4 of this research study aimed to evaluate the ageing resistance characteristics/properties of TPC and PPC modified binders using rheology-based and FTIR spectroscopy-based ageing indices. Under Task 5, the production temperatures (mixing and compaction temperatures) were determined for the control, and TPC and PPC modified binders using four approaches: equiviscous method, high shear viscosity method, steady shear flow method, and phase angle method. Task 6 of the study included mix design and evaluation of performance of asphalt (bituminous concrete)

mixtures fabricated with control and TPC/PPC modified binders. For performance evaluation, asphalt mixtures were evaluated for resistance against rutting (through static creep, dynamic creep, and Hamburg wheel tracking device (HWTD) tests), moisture damage (through tensile strength ratio (TSR) and retained Marshall stability (RMS) tests), cracking (through semi-circular bend (SCB) test), and fatigue (through indirect tensile fatigue test (ITFT)).

9.2 Conclusions

Based on the experimentations and analyses performed in the present study, the conclusive remarks corresponding to each task and recommendations are presented below:

- **Task 1:** Characterisation of the two pyrolytic chars showed that TPC and PPC had different microscopic morphology, particle size distribution, chemical composition, proximate composition, FTIR, and TGA behaviour. TPC had a finer particle size distribution with a lower volatile matter content and more stable TGA characteristics than PPC. FTIR spectroscopy showed that TPC and PPC interacted chemically with the base binder during modification. Optical microscopy showed that the blending parameters employed for char modification avoided agglomeration and distributed the TPC and PPC particles uniformly.

- **Task 2:** Improved storage stability was found with the addition of sulfur to TPC modified asphalt binder. The addition of PPA also enhanced the storage stability performance. PPA content of 1.0% and sulfur content of 0.3% were found to produce the lowest separation as measured from different rheological and FTIR based storage stability measurements/analyses. The TPC modified binders with sulfur produced better ranks of their storage stability performance than binders with PPA. Storage stability analysis of PPC modified binders was performed at multiple

sulfur dosages, and 0.3% dosage showed the best performance. Qualitative FTIR spectra analysis further showed that the closeness of spectral curves improved at the optimum dosage of sulfur. The 0.3% sulfur dosage was validated for TPC and PPC modified binders prepared at the three char (5, 10, and 15%) dosages/contents.

- **Task 3:** Asphalt binder modification with TPC and PPC improved the rheological performance of control/neat binders as evidenced through continuous high PG, master curves, and MSCR tests on the binders. For similar content of pyrolytic chars, each of five binder rutting parameters (Superpave and Shenoy rutting parameters, ZSV, MSCR J_{nr} and $\Delta\varepsilon_{nr}$) resulted in different percentage improvements compared to the control binder with a consistent ranking of the binders. The rutting performance improved with the increase in char dosages up to 20%. Based on the LAS fatigue test on binders, it was found that the optimum fatigue performance was achieved at 10% dosage of both TPC and PPC.
- **Task 4:** Under evaluation of ageing resistance, rheological indices based on the G*, δ, ZSV and J_{nr} ratio, showed that TPC-modified asphalt binder suffered less ageing compared to the control and PPC-modified binders. FTIR results also indicated that the addition of TPC retarded the carbonyl and sulfoxide chemical groups formed due to ageing and thus improved the binder ageing resistance.
- **Task 5:** An increase in the production temperatures was observed concerning the content of pyrolytic char across all four methods employed in the study (EQ, HSV, SSF, and PA). The production temperatures derived from SSF and PA were lower than those obtained through the HSV and equiviscous methods. The production temperatures were further verified by preparing mixes and evaluating the binder coating, and the temperatures from the HSV method were found the most suitable for fabrication of bituminous concrete mixes with pyrolytic char modified binders.

- **Task 6:** Leaching tests showed that TPC and PPC could be safely used in asphalt mixtures for pavement construction. Stiffness and rutting performance of the mixtures showed a consistent increase with an increase in TPC and PPC dosage up to 20%, as also observed in binder testing. Comparing the fatigue, cracking, and moisture damage results, it was found that the optimum performance was achieved at 10% dosage of both TPC and PPC. On average, mixtures with TPC-10 and PPC-10 binders showed 46% lower rut depth, 108% higher SCB J-integral value, and 195% higher fracture life than the control mixes. Pavement structural analysis conducted with IITPAVE software showed that the use of TPC and PPC in the top wearing course layer contributed to increased traffic carrying capacity of the pavement, owing to the higher resilient modulus.
- **Main Contribution and Recommendations**: This study evaluated the properties of asphalt binders and mixes modified at different dosages of pyrolytic chars derived as by-products from the pyrolysis of waste tyres and plastics. The study involved a multi-faceted investigation with a physico-chemical characterisation of the two pyrolytic chars (TPC and PPC); characterisation of the TPC and PPC-modified asphalt binders focusing on conventional, rheological, ageing, microscopic, and thermo-chemical tests; and characterisation of asphalt mixtures in terms of design, rutting, moisture damage, cracking, and fatigue performance. The study showed that the use of TPC and PPC in asphalt binder modification is promising for pavement construction from the environment and leaching considerations. The overall findings of this study show that 10% dosage of these chars is a quite favourable dosage considering rheological characteristics and the improvements in rutting, cracking, and fatigue performance of asphalt mixtures. From overall considerations of asphalt binder rheology and bituminous concrete

mix characteristics, it is recommended to use a 10% dosage of the TPC and PPC in asphalt binder modification. The 10% pyrolytic char dosage showed appreciable improvements in the mix rutting, cracking, moisture damage, and fatigue performance.

9.3 Recommendations for Future Research

The present study was a laboratory-based investigation of the properties of asphalt binders and mixtures with tyre and plastic pyrolytic chars (TPC and PPC). Trial pavement sections are recommended to be constructed with pyrolytic char modified binders with regular monitoring of the sections to gain further confidence. Studies can also be conducted with pre-treatment of chars such as surface activation and palletisation before modification with asphalt binders. Low-temperature binder rheological performance can be carried out to understand the role of pyrolytic chars on low-temperature binder properties. Advanced tools such as molecular dynamics simulation can be further attempted to study the microscopic properties of pyrolytic char modified binders prepared with multiple char sources. ■

REFERENCES

AASHTO R30. (2006). *Standard practice for mixture conditioning of hot mix asphalt (HMA).* American Association of State Highway and Transportation Officials, Washington, DC.

AASHTO T283. (2007). *Standard method of test for resistance of compacted asphalt mixtures to moisture-induced damage*. American Association of State and Highway Transportation Officials, Washington, DC.

AASHTO T324. (2016). *Standard method of test for Hamburg wheel-track testing of compacted asphalt mixtures.* American Association of State Highway and Transportation Officials, Washington, DC.

AASHTO TP101. (2014). *Standard method of test for estimating fatigue resistance of asphalt binders using the linear amplitude sweep*. American Association of State Highway and Transportation Officials, Washington, DC.

AASHTO TP31. (1996). *Standard test method for determining the resilient modulus of bituminous mixtures by indirect tension*. American Association of State Highway and Transportation Officials, Washington DC.

Abbas-Abadi, M. S., Haghighi, M. N., and Yeganeh, H. (2013). Evaluation of pyrolysis product of virgin high density polyethylene degradation using different process parameters in a stirred reactor. *Fuel Processing Technology, 109*, 90-95.

Abtahi, S. M., Sheikhzadeh, M., and Hejazi, S. M. (2010). Fiber-reinforced asphalt-concrete–a review. *Construction and Building Materials*, *24*(6), 871-877.

Adedimila, A. S., and Kennedy, T. W. (1976). Repeated-load indirect tensile fatigue characteristics of asphalt mixtures. *Transportation Research Record*, *595*, 25-33.

AG:PT/T108. (2006). *Segregation of polymer modified binders*. Austroads, Sydney, Australia.

Ahmed, T. M., Al-Khalid, H., and Ahmed, T. Y. (2019). Review of techniques, approaches and criteria of hot-mix asphalt fatigue. *Journal of Materials in Civil Engineering*, *31*(12), 03119004.

Ahmedzade, P., and Geckil, T. (2007). Influence of carbon black on the mechanical and electrical properties of asphalt mixtures. *Indian Journal of Engineering & Materials Sciences*, 14, 358-364.

Al-Abdul Wahhab, H. I., Dalhat, M. A., and Habib, M. A. (2017). Storage stability and high-temperature performance of asphalt binder modified with recycled plastic. *Road Materials and Pavement Design*, *18*(5), 1117-1134.

Al-Hadidy, A. I., and Yi-qiu, T. (2009). Effect of polyethylene on life of flexible pavements. *Construction and Building Materials*, *23*(3), 1456-1464.

Al-Khateeb, G. G. (2020). *Traffic and Pavement Engineering*. CRC Press.

Alliotti, A. G. (1962). Carbon black-its nature and possible effects on the characteristics of bituminous road binders. In *Australian Road Research Board (ARRB) Conference, 1st*, 1962, Canberra, Australia.

Anderson, D. A., Bahia, H. U., Christensen, D. W., Dongre, R., Sharma, M. G., Antle, C. E., and Button, J. (1994). *Binder characterization and evaluation, Volume 3: Physical characterization*. SHRP-A-369, National Research Council, Washington DC.

Anderson, D. A., Le Hir, Y. M., Planche, J. P., Martin, D., and Shenoy, A. (2002). Zero shear viscosity of asphalt binders. *Transportation Research Record*, *1810*(1), 54-62.

Anton Paar. (2021). BET theory. Accessed on November 16, 2021 from: https://wiki.anton-paar.com/in-en/bet-theory/

Apeagyei, A. K. (2011). Laboratory evaluation of antioxidants for asphalt binders. *Construction and Building Materials*, *25*(1), 47-53.

Asgharzadeh, S. M., Tabatabaee, N., Naderi, K., and Partl, M. (2013). An empirical model for modified bituminous binder master curves. *Materials and Structures*, *46*(9), 1459-1471.

Asphalt Institute. (1997). *Mix design methods for asphalt concrete and other hot-mix types:* Manual Series No. 2 (MS-2) (6th Ed.). Lexington, KY, Asphalt Institute.

ASTM D2726. (2019). *Standard test method for bulk specific gravity and density of non-absorptive compacted asphalt mixtures*. ASTM International, West Conshohocken, PA.

ASTM D2872. (2012). *Standard test method for effect of heat and air on a moving film of asphalt (rolling thin-film oven test).* ASTM International, West Conshohocken, PA.

ASTM D3172. (2013). *Standard practice for proximate analysis of coal and coke*. ASTM International, West Conshohocken, PA.

ASTM D3173. (2017). *Standard test method for moisture in the analysis sample of coal and coke*. ASTM International, West Conshohocken, PA.

ASTM D3174. (2012). *Standard test method for ash in the analysis sample of coal and coke from coal*. ASTM International, West Conshohocken, PA.

ASTM D3175. (2020). *Standard test method for volatile matter in the analysis sample of coal and coke*. ASTM International, West Conshohocken, PA.

ASTM D4402. (2015). *Standard test method for viscosity determination of asphalt at elevated temperatures using a rotational viscometer*. ASTM International, West

Conshohocken, PA.

ASTM D6373. (2016). *Standard specification for performance graded asphalt binder*. ASTM International, West Conshohocken, PA.

ASTM D6521. (2018). *Standard practice for accelerated aging of asphalt binder using a pressurized aging vessel (PAV).* ASTM International, West Conshohocken, PA.

ASTM D6857. (2017). *Standard test method for maximum specific gravity and density of asphalt mixtures using automatic vacuum sealing method*. ASTM International, West Conshohocken, PA.

ASTM D6925. (2015). *Standard test method for preparation and determination of the relative density of asphalt mix specimens by means of the Superpave gyratory compactor.* ASTM International, West Conshohocken, PA.

ASTM D6926. (2016). *Standard practice for preparation of asphalt mixture specimens using Marshall apparatus.* ASTM International, West Conshohocken, PA.

ASTM D6927. (2015). *Standard test method for Marshall stability and flow of asphalt mixtures.* ASTM International, West Conshohocken, PA.

ASTM D7173. (2020). *Standard practice for determining the separation tendency of polymer from polymer modified asphalt*. ASTM International, West Conshohocken, PA, 2020.

ASTM D7175. (2015). *Standard test method for determining the rheological properties of asphalt binder using a dynamic shear rheometer.* ASTM International, West Conshohocken, PA.

ASTM D7405. (2020). *Standard test method for multiple stress creep and recovery (MSCR) of asphalt binder using a dynamic shear rheometer*. ASTM International, West Conshohocken.

ASTM D8044. (2016). *Standard test method for evaluation of asphalt mixture cracking resistance using the semi-circular bend test (SCB) at intermediate temperatures*. ASTM International, West Conshohocken, PA.

Azari, H., McCuen, R. H., and Stuart, K. D. (2003). Optimum compaction temperature for modified binders. *Journal of Transportation Engineering*, *129*(5), 531-537.

Bahia, H. U., and Anderson, D. A. (1995a). The new proposed rheological properties of asphalt binders: Why are they required and how do they compare to conventional properties. In *Physical properties of asphalt cement binders*. STP 1241, ASTM International.

Bahia, H. U., and Anderson, D. A. (1995b). The pressure aging vessel (PAV): A test to simulate rheological changes due to field aging. In *Physical properties of asphalt cement binders*. STP 1241, ASTM International.

Baldino, N., Gabriele, D., Lupi, F. R., Rossi, C. O., Caputo, P., and Falvo, T. (2013). Rheological effects on bitumen of polyphosphoric acid (PPA) addition. *Construction and Building Materials*, *40*, 397-404.

Bao, D. X., Yu, Y. Y., and Zhao, Q. M. (2020). Evaluation of the chemical composition and rheological properties of bio-asphalt from different biomass sources. *Road Materials and Pavement Design*, *21*(7), 1829-1843.

Baumgardner, G. L., Masson, J. F., Hardee, J. R., Menapace, A. M. and Williams, A. G. (2005). Polyphosphoric acid modified asphalt: proposed mechanisms. *Journal of the Association of Asphalt Paving Technologists*, 74, 283–306.

Bernardo, M., Lapa, N., Gonçalves, M., Mendes, B., Pinto, F., Fonseca, I., and Lopes, H. (2012). Physico-chemical properties of chars obtained in the co-pyrolysis of waste mixtures. *Journal of Hazardous Materials*, *219-220*, 196-202.

Brookfield. (2021). Brookfield DV-II+Pro Viscometer Operating Instructions Manual No. M03-165-F0612. Brookfield Engineering Laboratories, Inc. Accessed on November 16, 2021 from: https://www.brookfieldengineering.com/-/media/ametekbrookfield/manuals/obsolete%20manuals/dviipro%20m03165f0612.pdf?la=en&fbclid=IwAR2sRzHX9LS4LzT6khm0enZi6cKau4k06x3lJVi6zP3NapN1u6Iap29dv9M

BS 598-111. (1995). *Method for determining resistance to permanent deformation of bituminous mixtures subject to unconfined uniaxial loading*. Brussels: European Committee for Standardization (CEN).

BS DD 226. (1996). *Method for determining resistance to permanent deformation of bituminous mixtures subject to unconfined dynamic loading*. Brussels: European Committee for Standardization (CEN).

BS EN 12697-24. (2001). *Bituminous mixtures—Test methods for hot mix asphalt—Part 24: Resistance to fatigue*. BSI Standards Publication: London, UK.

Buekens, A. G., and Huang, H. (1998). Catalytic plastics cracking for recovery of gasoline-range hydrocarbons from municipal plastic wastes. *Resources, Conservation and Recycling*, *23*(3), 163-181.

Button, J. W., Little, D. N., Kim, Y., and Ahmed, J. (1987). Mechanistic evaluation of selected asphalt additives (With discussion). In *Association of Asphalt Paving Technologists Proceedings*, *56*, 62-90.

Cardona, N., Campuzano, F., Betancur, M., Jaramillo, L., and Martínez, J. D. (2018). Possibilities of carbon black recovery from waste tyre pyrolysis to be used as additive in rubber goods-A review. In *IOP Conference Series: Materials Science and Engineering*, *437*, 012012.

Cardona-Uribe, N., Betancur, M., and Martínez, J. D. (2021). Towards the chemical upgrading of the recovered carbon black derived from pyrolysis of end-of-life

tires. *Sustainable Materials and Technologies*, *28*, e00287.

Cataldo, F. (2020). Further insight into some properties of pyrolytic carbon black obtained from scrap truck tires. *Fullerenes, Nanotubes and Carbon Nanostructures*, *28*(12), 995-1001.

Cataldo, F. (2021). Pyrolytic carbon black from truck tires: some new analytical approaches. *Fullerenes, Nanotubes and Carbon Nanostructures*, *29*(4), 304-314.

Celoglu, M. E., Yilmaz, M., Kok, B. V., and Yalcin, E. (2016). Effects of various biochars on the high temperature performance of bituminous binder. In *6th Euraphalt & Eurobitume Congress,* 1-3 June 2016, Prague, Czech Republic.

Chaala, A., Roy, C., and Ait-Kadi, A. (1996). Rheological properties of bitumen modified with pyrolytic carbon black. *Fuel*, *75*(13), 1575-1583.

Chebil, S., Chaala, A., and Roy, C. (1996). Modification of bitumen with scrap tyre pyrolytic carbon black. Comparison with commercial carbon black Part I: mechanical and rheological properties. *Polymer Recycling*, *2*(4), 257.

Chebil, S., Chaala, A., and Roy, C. (2000). Use of softwood bark charcoal as a modifier for road bitumen. *Fuel*, *79*(6), 671-683.

Chen, D., Yin, L., Wang, H., and He, P. (2014). Pyrolysis technologies for municipal solid waste: a review. *Waste Management*, *34*(12), 2466-2486.

Coates, J. (2000). Interpretation of infrared spectra, A practical approach. In *Encyclopedia of Analytical Chemistry.* John Wiley & Sons.

Cong, P., Xu, P., and Chen, S. (2014). Effects of carbon black on the anti aging, rheological and conductive properties of SBS/asphalt/carbon black composites. *Construction and Building Materials*, *52*, 306-313.

Czajczyńska, D., Anguilano, L., Ghazal, H., Krzyżyńska, R., Reynolds, A. J., Spencer, N., and Jouhara, H. (2017). Potential of pyrolysis processes in the waste management sector. *Thermal Science and Engineering Progress*, *3*, 171-197.

Dahiya, A. (Ed.) (2014). *Bioenergy: Biomass to Biofuels*, 1st Ed., Academic Press.

D'Angelo, J. A. (2009). The relationship of the MSCR test to rutting. *Road Materials and Pavement Design*, *10*(sup1), 61-80.

D'Angelo, J., Kluttz, R., Dongre, R. N., Stephens, K., and Zanzotto, L. (2007). Revision of the Superpave high temperature binder specification: the multiple stress creep recovery test (With discussion). *Journal of the Association of Asphalt Paving Technologists*, 76, 123-162.

Darku, D. D. (2003). *Evaluation of the Superpave gyratory compactor to assess the rutting resistance of asphalt mixtures*. Ph.D. Dissertation, University of Florida.

Darmstadt, H., Chaala, A., Roy, C., and Kaliaguine, S. (1996). SIMS and ESCA characterization of bitumen reinforced with pyrolytic carbon black. *Fuel*, *75*(2), 125-

132.

Delgadillo, R., and Bahia, H. (2005). Rational fatigue limits for asphalt binders derived from pavement analysis. *Journal of the Association of Asphalt Paving Technologists*, 74, 97-138.

Domingos, M. D. I., and Faxina, A. L. (2016). Susceptibility of asphalt binders to rutting: Literature review. *Journal of Materials in Civil Engineering*, *28*(2), 04015134.

Dominic, M., Begum, P. M. S., Joseph, R., Joseph, D., Kumar, P., and Ayswarya, E. P. (2013). Synthesis, characterization and application of rice husk nanosilica in natural rubber. *International Journal of Science, Environment and Technology*, *2*(5), 1027-1035.

Dong, W., Ma, F., Li, C., Fu, Z., Huang, Y., and Liu, J. (2020). Evaluation of anti-aging performance of biochar modified asphalt binder. *Coatings*, *10*(11), 1037.

Elseifi, M. A., Mohammad, L. N., Ying, H., and Cooper III, S. (2012). Modeling and evaluation of the cracking resistance of asphalt mixtures using the semi-circular bending test at intermediate temperatures. *Road Materials and Pavement Design*, *13*(sup1), 124-139.

Eze, W. U., Umunakwe, R., Obasi, H. C., Ugbaja, M. I., Uche, C. C., and Madufor, I. C. (2021). Plastics waste management: A review of pyrolysis technology. *Clean Technologies and Recycling*, *1*(1), 50-69.

Fader, J. H., Faulkner, B. P., and Unterweger, R. J. (1997). Using pyrolyzed carbon black (CBp) from waste tires in asphalt pavements, Rubber Division Meeting, American Chemical Society, 21-24 October, 1997, Cleveland, Ohio.

Fee, D., Maldonado, R., Reinke, G., and Romagosa, H. (2010). Polyphosphoric acid modification of asphalt. *Transportation Research Record*, *2179*(1), 49-57.

Feng, Z. G., Rao, W. Y., Chen, C., Tian, B., Li, X. J., Li, P. L., and Guo, Q. L. (2016). Performance evaluation of bitumen modified with pyrolysis carbon black made from waste tyres. *Construction and Building Materials*, *111*, 495-501.

Feng, Z., Zhao, P., Li, X., and Zhu, L. (2021). Preparation and properties of bitumen modified with waste rubber pyrolytic carbon black. *Construction and Building Materials*, *282*, 122697.

Gan, X., and Zhang, W. (2021). Application of biochar from crop straw in asphalt modification. *PloS ONE*, *16*(2), e0247390.

Gao, F. (2010). *Pyrolysis of waste plastics into fuels*. Ph.D. Dissertation, Department of Chemical and Process Engineering, University of Canterbury.

Gao, Y., Wu, X., Islam, S., and Hossain, M. (2019). Evaluation of carbon char in hot-mix asphalt mixture. In *Airfield and Highway Pavements 2019: Testing and Characterization of Pavement Materials*. Reston, VA: American Society of Civil

Engineers, 154-163.

García-Travé, G., Tauste, R., Moreno-Navarro, F., Sol-Sánchez, M., and Rubio-Gámez, M. C. (2016). Use of reclaimed geomembranes for modification of mechanical performance of bituminous binders. *Journal of Materials in Civil Engineering*, *28*(7), 04016021.

Geckil, T., Ahmedzade, P., and Alatas, T. (2018). Effect of carbon black on the high and low temperature properties of bitumen. *International Journal of Civil Engineering*, *16*(2), 207-218.

Geyer, R., Jambeck, J. R., and Law, K. L. (2017). Production, use, and fate of all plastics ever made. *Science Advances*, *3*(7), e1700782.

Girimath, S., and Singh, D. (2019). Effects of bio-oil on performance characteristics of base and recycled asphalt pavement binders. *Construction and Building Materials, 227*, 116684.

Gogoi, R., Biligiri, K. P., and Das, N. C. (2016). Performance prediction analyses of styrene-butadiene rubber and crumb rubber materials in asphalt road applications. *Materials and Structures*, *49*(9), 3479-3493.

Golalipour, A. (2011). *Modification of multiple stress creep and recovery test procedure and usage in specification.* Masters Dissertation, University of Wisconsin-Madison.

Golalipour, A., Bahia, H. U., and Tabatabaee, H. A. (2017). Critical considerations toward better implementation of the multiple stress creep and recovery test. *Journal of Materials in Civil Engineering*, *29*(5), 04016295.

Goli, A., Ziari, H., and Amini, A. (2017). Influence of carbon nanotubes on performance properties and storage stability of SBS modified asphalt binders. *Journal of Materials in Civil Engineering*, *29*(8), 04017070.

Hajikarimi, P., Rahi, M., and Nejad, F. M. (2015). Comparing different rutting specification parameters using high temperature characteristics of rubber-modified asphalt binders. *Road Materials and Pavement Design, 16*(4), 751-766.

Hajj, R., and Bhasin, A. (2018). The search for a measure of fatigue cracking in asphalt binders–A review of different approaches. *International Journal of Pavement Engineering*, 19(3), 205-219.

Han, J., Li, W., Liu, D., Qin, L., Chen, W., and Xing, F. (2018). Pyrolysis characteristic and mechanism of waste tyre: A thermogravimetry-mass spectrometry analysis. *Journal of Analytical and Applied Pyrolysis*, *129*, 1-5.

Helleur, R., Popovic, N., Ikura, M., Stanciulescu, M., and Liu, D. (2001). Characterization and potential applications of pyrolytic char from ablative pyrolysis of used tires. *Journal of Analytical and Applied Pyrolysis*, *58-59*, 813-824.

Hou, X., Lv, S., Chen, Z., and Xiao, F. (2018). Applications of Fourier transform infrared spectroscopy technologies on asphalt materials. *Measurement, 121*, 304-316.

Hu, Y., Attia, M., Tsabet, E., Mohaddespour, A., Munir, M. T., and Farag, S. (2021). Valorization of waste tire by pyrolysis and hydrothermal liquefaction: a mini-review. *Journal of Material Cycles and Waste Management*, *23*, 1737-1750.

Iqbal, M., Hussain, A., Khattak, A., and Ahmad, K. (2020). Improving the aging resistance of asphalt by addition of polyethylene and sulphur. *Civil Engineering Journal*, *6*(5), 1017-1030.

IRC 111. (2009). *Specification for dense graded bituminous mix*. Indian Road Congress, New Delhi.

IRC 37. (2018). *Guidelines for the design of flexible pavements*, Indian Road Congress, New Delhi.

IS 10500. (2012). *Drinking water specification*. Bureau of Indian Standards, New Delhi.

IS 1203. (1978). *Determination of penetration.* Bureau of Indian Standards, New Delhi.

IS 1205. (1978). *Determination of softening point.* Bureau of Indian Standards, New Delhi.

IS 1206. (Part II) (1978). *Determination of viscosity: Part II Absolute viscosity.* Bureau of Indian Standards, New Delhi.

IS 1206. (Part III) (1978). *Determination of viscosity: Part III Kinematic viscosity.* Bureau of Indian Standards, New Delhi.

IS 1208. (1978). *Determination of ductility.* Bureau of Indian Standards, New Delhi.

IS 1209. (1978). *Determination of flash point and fire point*. Bureau of Indian Standards, New Delhi.

IS 1216. (1978). *Determination of solubility in carbon disulphide or trichloroethylene*. Bureau of Indian Standards, New Delhi.

IS 15462. (2019). *Polymer modified bitumen (PMB) – Specification*. Bureau of Indian Standards, New Delhi.

IS 17079. (2019). *Rubber modified bitumen (RMB) – Specification*. Bureau of Indian Standards, New Delhi.

IS 2386. (Part I) (1963). *Methods of test for aggregates for concrete - Part I Particle size and shape*. Bureau of Indian Standards, New Delhi.

IS 2386. (Part III) (1963). *Methods of test for aggregates for concrete - Part III Specific gravity, density, voids, absorption and bulking*. Bureau of Indian Standards, New Delhi.

IS 2386. (Part IV) (1963). *Methods of test for aggregates for concrete - Part IV Mechanical properties*. Bureau of Indian Standards, New Delhi.

IS 2720. (Part III) (1980). *Methods of test for soils: Part III Determination of specific gravity, Section 1 Fine grained soils*. Bureau of Indian Standards, New Delhi.

IS 6241. (1971). *Method of test for determination of stripping value of road aggregates*.

Bureau of Indian Standards, New Delhi.

IS 73. (2013). *Paving bitumen – Specification*. Bureau of Indian Standards, New Delhi.

Jamradloedluk, J., and Lertsatitthanakorn, C. (2014). Characterization and utilization of char derived from fast pyrolysis of plastic wastes. *Procedia Engineering*, *69*, 1437-1442.

Jerin, T., Mahzabin, S., Siddique, S., Elma, T. A., Hossain, M. I., and Islam, M. R. (2020). Modified asphalt with carbon black from scrap tire pyrolysis. In *International Conference on Transportation and Development 2020*, Reston, VA: American Society of Civil Engineers, 72-82.

Julaganti, A., Choudhary, R., and Kumar, A. (2019). Permanent deformation characteristics of warm asphalt binders under reduced aging conditions. *KSCE Journal of Civil Engineering*, *23*(1), 160-172.

Kalantar, Z. N., Karim, M. R., and Mahrez, A. (2012). A review of using waste and virgin polymer in pavement. *Construction and Building Materials*, 33, 55-62.

Karimi, M. M., Dehaghi, E. A., and Behnood, A. (2021). A fracture-based approach to characterize long-term performance of asphalt mixes under moisture and freeze-thaw conditions. *Engineering Fracture Mechanics*, *241*, 107418.

Karthikeyan, S., Sathiskumar, C., and Moorthy, R. S. (2012). Effect of process parameters on tire pyrolysis: A review, *Journal of Scientific & Industrial Research*, *71*, 309-315.

Khedaywi, T. S. (2014). Study on utilising waste toner in asphalt cement. *Road Materials and Pavement Design*, 15(2), 446-454.

Khosla, N. P. (1991). Effect of the use of modifiers on performance of asphaltic pavements. *Transportation Research Record*, *1317*, 10-22.

Krishnan, J. M. and Rajagopal, K. R. (2003). Review of the uses and modeling of bitumen from ancient to modern times. *Applied Mechanics Reviews*, *56*(2), 149-214.

Kumar, A., Choudhary, R., Narzari, R., Kataki, R., and Shukla, S. K. (2018). Evaluation of bio-asphalt binders modified with biochar: a pyrolysis by-product of *Mesua ferrea* seed cover waste. *Cogent Engineering*, *5*(1), 1548534.

Kumar, P., and Gupta, A. (2010). Provision of rigid, semi rigid and flexible pavements as rural roads. *New Building Materials & Construction World*, *16*(3), 160-167.

Lamontagne, J., Dumas, P., Mouillet, V., and Kister, J. (2001). Comparison by Fourier transform infrared (FTIR) spectroscopy of different ageing techniques: application to road bitumens. *Fuel*, *80*(4), 483-488.

Lei, Y., Wang, H., Chen, X., Yang, X., You, Z., Dong, S., and Gao, J. (2018). Shear property, high-temperature rheological performance and low-temperature flexibility of asphalt mastics modified with bio-oil. *Construction and Building Materials*, *174*, 30-37.

Leng, Z., Tan, Z., Yu, H., and Guo, J. (2019). Improvement of storage stability of SBS-modified asphalt with nanoclay using a new mixing method. *Road Materials and Pavement Design*, *20*(7), 1601-1614.

Lesueur, D., Dekker, D. L., and Planche, J. P. (1995). Comparison of carbon black from pyrolized tires to other fillers as asphalt rheology modifiers. *Transportation Research Record*, *1515*, 47-55.

Levendis, Y. A., Atal, A., Carlson, J., Dunayevskiy, Y., and Vouros, P. (1996). Comparative study on the combustion and emissions of waste tire crumb and pulverized coal. *Environmental Science & Technology*, *30*(9), 2742-2754.

Li, G., Shen, B., and Lu, F. (2015). The mechanism of sulfur component in pyrolyzed char from waste tire on the elemental mercury removal. *Chemical Engineering Journal*, *273*, 446-454.

Li, C., Fan, Z., Wu, S., Li, Y., Gan, Y., and Zhang, A. (2018). Effect of carbon black nanoparticles from the pyrolysis of discarded tires on the performance of asphalt and its mixtures. *Applied Sciences*, *8*(4), 624.

Liang, M., Xin, X., Fan, W., Wang, H., Jiang, H., Zhang, J., and Yao, Z. (2019). Phase behavior and hot storage characteristics of asphalt modified with various polyethylene: Experimental and numerical characterizations. *Construction and Building Materials*, *203*, 608-620.

Liang, P., Liang, M., Fan, W., Zhang, Y., Qian, C., and Ren, S. (2017). Improving thermo-rheological behavior and compatibility of SBR modified asphalt by addition of polyphosphoric acid (PPA). *Construction and Building Materials*, *139*, 183-192.

Liao, M. C., and Chen, J. S. (2011). Zero shear viscosity of bitumen-filler mastics. *Journal of Materials in Civil Engineering*, *23*(12), 1672-1680.

Little, D. N., Allen, D. H., and Bhasin, A. (2018). *Modeling and design of flexible pavements and materials*. Springer International Publishing.

Liu, H., Zeiada, W., Al-Khateeb, G. G., Shanableh, A., and Samarai, M. (2021). Use of the multiple stress creep recovery (MSCR) test to characterize the rutting potential of asphalt binders: A literature review. *Construction and Building Materials*, *269*, 121320.

Lopez, A., De Marco, I., Caballero, B. M., Laresgoiti, M. F., and Adrados, A. (2011). Influence of time and temperature on pyrolysis of plastic wastes in a semi-batch reactor. *Chemical Engineering Journal*, *173*(1), 62-71.

Lu, X., and Isacsson, U. (1997). Compatibility and storage stability of styrene-butadiene-styrene copolymer modified bitumens. *Materials and Structures*, *30*(10), 618-626.

Lu, X., and Isacsson, U. (2002). Effect of ageing on bitumen chemistry and rheology. *Construction and Building materials*, *16*(1), 15-22.

Lu, X., Isacsson, U., and Ekblad, J. (1999). Phase separation of SBS polymer modified bitumens. *Journal of Materials in Civil Engineering*, *11*(1), 51-57.

Ma, F., Dai, J., Fu, Z., Li, C., Wen, Y., Jia, M., Jia, M., Wang, Y. and Shi, K. (2022). Biochar for asphalt modification: A case of high-temperature properties improvement. *Science of The Total Environment*, *804*, 150194.

Maggiore, C. (2014). *A comparison of different test and analysis methods for asphalt fatigue*, Ph.D. Dissertation, University of Nottingham.

Malvern Panalytical. (2021). Laser diffraction: Particle size distribution from nanometers to millimetres, Accessed on November 16, 2021 from: https://www.malvernpanalytical.com/en/products/technology/light-scattering/laser-diffraction

Maqsood, T., Dai, J., Zhang, Y., Guang, M., and Li, B. (2021). Pyrolysis of plastic species: a review of resources and products. *Journal of Analytical and Applied Pyrolysis*, *159*, 105295.

Marcant, B. (2004). *Polyphosphoric acid modification of asphalt*. Presented at Asphalt Institute Spring Meeting, Washington, D.C., 28 April, 2004.

Marsac, P., Piérard, N., Porot, L., Van den Bergh, W., Grenfell, J., Mouillet, V., Pouget, S., Besamusca, J., Farcas, F., Gabet, T., and Hugener, M. (2014). Potential and limits of FTIR methods for reclaimed asphalt characterisation. *Materials and Structures*, *47*, 1273-1286.

Martin, J. V., Orange, G., and Marcant, B. (2004). *Effect of polyphosphoric acid on aging behaviour of bituminous binder*. Presented at Petersen Asphalt Research Conference, Cheyenne, Wyoming, 21-23 June, 2004.

Martin, K.G. (1962). Preliminary microviscometer studies of carbon black/rubber/bitumen dispersions. In *Proceedings of the Australian Road Research Board (ARRB) Conference*, Canberra, Australia, *1*, 895–911.

Martínez, J. D. (2021). An overview of the end-of-life tires status in some Latin American countries: Proposing pyrolysis for a circular economy. *Renewable and Sustainable Energy Reviews*, *144*, 111032.

Martínez, J. D., Cardona-Uribe, N., Murillo, R., García, T., and López, J. M. (2019). Carbon black recovery from waste tire pyrolysis by demineralization: Production and application in rubber compounding. *Waste Management*, *85*, 574-584.

Martínez, J. D., Puy, N., Murillo, R., García, T., Navarro, M. V., and Mastral, A. M. (2013). Waste tyre pyrolysis–A review. *Renewable and Sustainable Energy Reviews*, *23*, 179-213.

Martínez-Estrada, A., Chávez-Castellanos, A. E., Herrera-Alonso, M., and Herrera-Nájera, R. (2010). Comparative study of the effect of sulfur on the morphology and rheological properties of SB-and SBS-modified asphalt. *Journal of Applied Polymer*

Science, *115*(6), 3409-3422.

Martín-Lara, M. A., Piñar, A., Ligero, A., Blázquez, G., and Calero, M. (2021). Characterization and use of char produced from pyrolysis of post-consumer mixed plastic waste. *Water*, *13*(9), 1188.

Masson, J. F., Collins, P., Robertson, G., Woods, J. R., and Margeson, J. (2003). Thermodynamics, phase diagrams, and stability of bitumen− polymer blends. *Energy Fuels*, *17*(3), 714-724.

Mastral, A. M., Murillo, R., Callén, M. S., and Garcıa, T. (1999). Application of coal conversion technology to tire processing. *Fuel Processing Technology*, *60*(3), 231-242.

Miandad, R., Barakat, M. A., Aburiazaiza, A. S., Rehan, M., and Nizami, A. S. (2016). Catalytic pyrolysis of plastic waste: A review. *Process Safety and Environmental Protection*, *102*, 822-838.

Mohammad, L. N., Elseifi, M., Cao, W., Raghavendra, A., and Ye, M. (2017). Evaluation of various Hamburg wheel-tracking devices and AASHTO T324 specification for rutting testing of asphalt mixtures. *Road Materials and Pavement Design*, *18*(sup4), 128-143.

Moldoveanu, S. (2005). *Analytical pyrolysis of synthetic organic polymers*. Elsevier Science B.V., Amsterdam, The Netherlands.

Moraes, M. S. A., Georges, F., Almeida, S. R., Damasceno, F. C., da Silva Maciel, G. P., Zini, C. A., Jacques, R. A., and Caramão, E. B. (2012). Analysis of products from pyrolysis of Brazilian sugar cane straw. *Fuel Processing Technology*, *101*, 35-43.

Moreno-Navarro, F., Tauste, R., Sol-Sánchez, M., and Rubio-Gámez, M. C. (2019). New approach for characterising the performance of asphalt binders through the multiple stress creep and recovery test. *Road Materials and Pavement Design*, *20*(sup1), S500-S520.

MoRTH. (2013). *Specifications for road and bridge works*: *Fifth revision*. Ministry of Road Transport and Highways, Govt. of India.

MoRTH. (2021). *Annual Report 2021-2021*, Ministry of Road Transport and Highways, Govt. of India, New Delhi.

Mouillet, V., Farcas, F., and Besson, S. (2008). Ageing by UV radiation of an elastomer modified bitumen. *Fuel*, *87*(12), 2408-2419.

Nivitha, M. R., Prasad, E., and Krishnan, J. M. (2016). Ageing in modified bitumen using FTIR spectroscopy. *International Journal of Pavement Engineering*, *17*(7), 565-577.

Oluwasola, E. A., Hainin, M. R., and Aziz, M. M. A. (2016). Comparative evaluation of dense-graded and gap-graded asphalt mix incorporating electric arc furnace steel slag and copper mine tailings. *Journal of Cleaner Production*, *122*, 315-325.

Onwudili, J. A., Insura, N., and Williams, P. T. (2009). Composition of products from the pyrolysis of polyethylene and polystyrene in a closed batch reactor: Effects of temperature and residence time. *Journal of Analytical and Applied Pyrolysis*, *86*(2), 293-303.

Orange, G., Martin, J. V., Menapace, A., Hemsley, M., and Baumgardner, G. L. (2004). Rutting and moisture resistance of asphalt mixtures containing polymer and polyphosphoric acid modified bitumen. *Road Materials and Pavement Design*, *5*(3), 323-354.

O'reilly, J. M., and Mosher, R. A. (1983). Functional groups in carbon black by FTIR spectroscopy. *Carbon*, *21*(1), 47-51.

Padhan, R. K., Gupta, A. A., and Sreeram, A. (2019). Effect of cross-linking agent on ethylene vinyl acetate/polyoctenamer modified bitumen. *Road Materials and Pavement Design*, *20*(7), 1615-1623.

Padhan, R. K., Sreeram, A., and Gupta, A. (2020). Evaluation of trans-polyoctenamer and cross-linking agents on the performance of waste polystyrene modified asphalt. *Road Materials and Pavement Design*, *21*(4), 1170-1182.

Park, T., Lee, K., Salgado, R., Lovell, C. W., and Coree, B. J. (1997). Use of pyrolyzed carbon black as additive in hot mix asphalt. *Journal of Transportation Engineering*, *123*(6), 489-494.

Petersen, J. C. (1984). Chemical composition of asphalt as related to asphalt durability: State of the Art. *Transportation Research Record*, *999*, 13-30.

Petersen, J. C. (2009). *A review of the fundamentals of asphalt oxidation: chemical, physicochemical, physical property, and durability relationships*. Transportation Research Circular, E-C140, Transportation Research Board.

Polacco, G., and Filippi, S. (2014). Vulcanization accelerators as alternative to elemental sulfur to produce storage stable SBS modified asphalts. *Construction and Building Materials*, *58*, 94-100.

Polacco, G., Filippi, S., Merusi, F., and Stastna, G. (2015). A review of the fundamentals of polymer-modified asphalts: Asphalt/polymer interactions and principles of compatibility. *Advances in Colloid and Interface Science*, *224*, 72-112.

Qian, G., Yu, H., Jin, D., Bai, X., and Gong, X. (2021). Different water environment coupled with ultraviolet radiation on ageing of asphalt binder. *Road Materials and Pavement Design*, *22*(10), 2410-2423.

Quek, A., and Balasubramanian, R. (2013). Liquefaction of waste tires by pyrolysis for oil and chemicals—A review. *Journal of Analytical and Applied Pyrolysis*, *101*, 1-16.

Radboud University. (2021). Information on the FESEM (Field-emission Scanning Electron Microscope), Accessed on November 16, 2021 from: https://www.vcbio.science.ru.nl/public/pdf/fesem_info_eng.pdf

Rahman, F., and Hossain, M. (2014). *Review and analysis of Hamburg wheel tracking device test data*, Report No. KS-14-1. Kansas. Dept. of Transportation.

Rahman, M. T., Mohajerani, A., and Giustozzi, F. (2020). Recycling of waste materials for asphalt concrete and bitumen: A review. *Materials*, *13*(7), 1495.

Raja, P. M. V., and Barron, A. R. (2021). BET surface area analysis of nanoparticles. Rice University. Accessed on November 16, 2021 from: https://chem.libretexts.org/Bookshelves/Analytical_Chemistry/Physical_Methods_in_Chemistry_and_Nano_Science_(Barron)/02%3A_Physical_and_Thermal_Analysis/2.03%3A_BET_Surface_Area_Analysis_of_Nanoparticles

Rostler, F. S., White, R. M., and Dannenberg, E. M. (1977). Carbon black as a reinforcing agent for asphalt. In *Association of Asphalt Paving Technologists Proceedings*, *46*, 376-410.

Saboo, N., and Kumar, P. (2016). Analysis of different test methods for quantifying rutting susceptibility of asphalt binders. *Journal of Materials in Civil Engineering*, *28*(7), 04016024.

Saha, G., and Biligiri, K. P. (2016). Fracture properties of asphalt mixtures using semi-circular bending test: A state-of-the-art review and future research. *Construction and Building Materials*, *105*, 103-112.

Sanchez, X., Somers, T., Dhasmana, H., and Owolabi, O. (2020). Effect of biochar on the basic characteristics of asphalt mixtures. In *Advances in Materials and Pavement Performance Prediction II*, CRC Press, 343-346.

Saptoadi, H., Rohmat, T. A., and Sutoyo. (2016). Combustion of char from plastic wastes pyrolysis. In *AIP Conference Proceedings*, *1737*(1), 030006.

Sasaki, I., Yamaguchi, K., and Meiarashi, S. (2003). Aging and rheological properties of carbon black modified asphalt binders. *Proceedings of the 21st ARRB and 11th REAAA Conference*, Cairns, Australia, 18-23 May, 2003.

Sathiskumar, C., and Karthikeyan, S. (2019). Recycling of waste tires and its energy storage application of by-products–a review. *Sustainable Materials and Technologies*, *22*, e00125.

Scheirs, J., and Kaminsky, W. (Eds.). (2006). *Feedstock recycling and pyrolysis of waste plastics: converting waste plastics into diesel and other fuels*. John Wiley & Sons Incorporated.

Shalaby, A. (2002). Modelling short-term aging of asphalt binders using the rolling thin film oven test. *Canadian Journal of Civil Engineering*, *29*(1), 135-144.

Sharma, A., Sharma, A., Joshi, J. B., Jain, R. K., and Kasilingam, R. (2021). Application

of high-grade carbon produced from tyre waste using advanced thermo-chemical technology. *Materials Today: Proceedings*, *43*(5), 3117-3120.

Sharuddin, S. D. A., Abnisa, F., Daud, W. M. A. W., and Aroua, M. K. (2016). A review on pyrolysis of plastic wastes. *Energy Conversion and Management*, *115*, 308-326.

Shenoy, A. (2001). Refinement of the Superpave specification parameter for performance grading of asphalt. *Journal of Transportation Engineering*, *127*(5), 357-362.

Shenoy, A. (2004). A comprehensive treatise of the high temperature specification parameter| G*|/(1-(1/tanδ sinδ)) for performance grading of asphalts. *Applied Rheology*, *14*(6), 303-314.

Sigmaaldrich. (2021). IR Spectrum Table and Chart. Merck. Accessed on November 16, 2021 from: https://www.sigmaaldrich.com/IN/en/technical-documents/technical-article/analytical-chemistry/photometry-and-reflectometry/ir-spectrum-table

Singh, B., Saboo, N., and Kumar, P. (2017). Use of Fourier transform infrared spectroscopy to study ageing characteristics of asphalt binders. *Petroleum Science and Technology*, *35*(16), 1648-1654.

Sirin, O., Paul, D. K., and Kassem, E. (2018). State of the art study on aging of asphalt mixtures and use of antioxidant additives. *Advances in Civil Engineering*, *2018*, 3428961.

Smith, B. C. (2011). *Fundamentals of Fourier transform infrared spectroscopy*. 2nd Ed. CRC press.

Sogancioglu, M., Yel, E., and Ahmetli, G. (2017). Pyrolysis of waste high density polyethylene (HDPE) and low density polyethylene (LDPE) plastics and production of epoxy composites with their pyrolysis chars. *Journal of Cleaner Production*, *165*, 369-381.

Solaimanian, M., Kennedy, T., and Tripathi, R. (1998). Performance characteristics of asphalt binders and mixtures modified by waste toner. *Transportation Research Record*, *1638*, 120-128.

Speight, J. G. (2015). *Handbook of coal analysis*. John Wiley & Sons.

Stuart, K. D., and Mogawer, W. S. (2002). Validation of the Superpave asphalt binder fatigue cracking parameter using the FHWA's accelerated loading facility. *Journal of the Association of Asphalt Paving Technologists*, *71*, 116-146.

Sybilski, D. (1996). Zero-shear viscosity of bituminous binder and its relation to bituminous mixture's rutting resistance. *Transportation Research Record*, *1535*(1), 15-21.

Taha, R., Ali, G., and Delwar, M. (1998). Evaluation of coke dust-modified asphalt using Superpave. *Journal of Materials in Civil Engineering*, *10*(3), 174-179.

Tarar, M. A., Khan, A. H., Rehman, Z. U., and Inam, A. (2021). Changes in the rheological characteristics of asphalt binders modified with soybean-derived materials. *International Journal of Pavement Engineering*, *22*(2), 233-248.

Thermo Nicolet. (2001). Introduction to Fourier transform infrared spectrometry, Accessed on November 16, 2021 from: https://www.chem.uci.edu/~dmitryf/manuals/Fundamentals/FTIR%20principles.pdf

Tiikma, L., Tamvelius, H., and Luik, L. (2007). Coprocessing of heavy shale oil with polyethylene waste. *Journal of Analytical and Applied Pyrolysis*, *79*(1-2), 191-195.

Traxler, R. N. (1961). Relation between asphalt composition and hardening by volatilization and oxidation. In *Association of Asphalt Paving Technologists Proceedings 30*, 359-377.

tur Rasool, R., Wang, S., Zhang, Y., Li, Y., and Zhang, G. (2017). Improving the aging resistance of SBS modified asphalt with the addition of highly reclaimed rubber. *Construction and Building Materials*, *145*, 126-134.

University of Georgia. (2017). More than 8.3 billion tons of plastics made: Most has now been discarded. Science Daily. Accessed on November 16, 2021 from: https://www.sciencedaily.com/releases/2017/07/170719140939.htm

University of Washington. (2020). Energy dispersive X-ray spectroscopy. Clean Energy Institute, University of Washington. Accessed on November 16, 2021 from: http://www.cei.washington.edu/education/science-of-solar/energy-dispersive-x-ray-spectroscopy/

Urrego-Yepes, W., Cardona-Uribe, N., Vargas-Isaza, C. A., and Martínez, J. D. (2021). Incorporating the recovered carbon black produced in an industrial-scale waste tire pyrolysis plant into a natural rubber formulation. *Journal of Environmental Management*, *287*, 112292.

USEPA. (1992). *SW-846 Test Method 1311: Toxicity characteristic leaching procedure*. U.S. Environmental Protection Agency (US EPA), Washington, DC.

USEPA. (2020). *SW-846 Chapter 7: Introductory and regulatory definitions pertaining to hazardous waste characteristics*. U.S. Environmental Protection Agency (US EPA), Washington, DC.

Vallerga, B. A., and Gridley, P. F. (1980). Carbon black reinforcement of asphalts in paving mixtures. In *Asphalt Pavement Construction: New Materials and Techniques*. STP 724, ASTM International, American Society of Testing and Materials, 110-128.

van den Bergh, W. (2011). *The effect of ageing on the fatigue and healing properties of bituminous mortars*. Doctoral Dissertation, Technische Universiteit Delft.

Wang, C., Wang, Y., and Han, Z. (2018). Enhanced flame retardancy of polyethylene/magnesium hydroxide with polycarbosilane. *Scientific Reports*, *8*,

14494.

Wang, H., Lu, G., Feng, S., Wen, X., and Yang, J. (2019). Characterization of bitumen modified with pyrolytic carbon black from scrap tires. *Sustainability*, *11*(6), 1631.

Wang, R., Xiong, Y., Yue, M., Hao, M., and Yue, J. (2020a). Investigating the effectiveness of carbon nanomaterials on asphalt binders from hot storage stability, thermodynamics, and mechanism perspectives. *Journal of Cleaner Production*, *276*, 124180.

Wang, F., Xiao, Y., Cui, P., Lin, J., Li, M., and Chen, Z. (2020b). Correlation of asphalt performance indicators and aging Degrees: A review. *Construction and Building Materials*, *250*, 118824.

Wartman, J., Grubb, D. G., and Nasim, A. S. M. (2004). Select engineering characteristics of crushed glass. *Journal of Materials in Civil Engineering*, *16*(6), 526-539.

Weigel, S., and Stephan, D. (2017). The prediction of bitumen properties based on FTIR and multivariate analysis methods. *Fuel*, *208*, 655-661.

Wen, G., Zhang, Y., Zhang, Y., Sun, K., and Chen, Z. (2001). Vulcanization characteristics of asphalt/SBS blends in the presence of sulfur. *Journal of Applied Polymer Science*, *82*(4), 989-996.

West, R. C., Watson, D. E., Turner, P. A., and Casola, J. R. (2010). *Mixing and compaction temperatures of asphalt binders in hot-mix asphalt*. NCHRP Report 648, Transportation Research Board, Washington, DC.

Wijesekara, D. A., Sargent, P., Ennis, C. J., and Hughes, D. (2021). Prospects of using chars derived from mixed post waste plastic pyrolysis in civil engineering applications. *Journal of Cleaner Production*, 317, 128212.

Williams, P. T. (2013). Pyrolysis of waste tyres: A review. *Waste Management*, *33*(8), 1714-1728.

Wyrzykowska-Ceradini, B., Gullett, B. K., Tabor, D., and Touati, A. (2011). Waste combustion as a source of ambient air polybrominated diphenylethers (PBDEs). *Atmospheric Environment*, *45*(24), 4008-4014.

Xu, O., Rangaraju, P. R., Wang, S., and Xiao, F. (2017). Comparison of rheological properties and hot storage characteristics of asphalt binders modified with devulcanized ground tire rubber and other modifiers. *Construction and Building Materials*, *154*, 841-848.

Xu, J., Yu, J., Xu, J., Sun, C., He, W., Huang, J., and Li, G. (2020a). High-value utilization of waste tires: A review with focus on modified carbon black from pyrolysis. *Science of The Total Environment*, *742*, 140235.

Xu, Z. X., Cheng, J. H., Song, H., Wang, Q., He, Z. X., Li, B., Duan, P. G., and Hu, X. (2020b). Production of bio-fuel from plant oil asphalt via pyrolysis. *Journal of the*

Energy Institute, *93*(5), 1763-1772.

Xue, Y., Zhou, S., Brown, R. C., Kelkar, A., and Bai, X. (2015). Fast pyrolysis of biomass and waste plastic in a fluidized bed reactor. *Fuel*, *156*, 40-46.

Yamaguchi, K., Sasaki, I., Nishizaki, I., Meiarashi, S., and Moriyoshi, A. (2005). Reinforcing effects of carbon black on asphalt binder for pavement. *Journal of the Japan Petroleum Institute*, *48*(6), 373-379.

Yan, K., Liu, W., You, L., Ou, J., and Zhang, M. (2021). Evaluation of waste cooling oil and European Rock Asphalt modified asphalt with laboratory tests and economic cost comparison. *Journal of Cleaner Production*, *310*, 127364.

Yang, X., and You, Z. (2015). High temperature performance evaluation of bio-oil modified asphalt binders using the DSR and MSCR tests. *Construction and Building Materials*, *76*, 380-387.

Yang, X., You, Z., and Dai, Q. (2013). Performance evaluation of asphalt binder modified by bio-oil generated from waste wood resources. *International Journal of Pavement Research & Technology*, *6*(4), 431-439.

Yang, X., You, Z., Dai, Q., and Mills-Beale, J. (2014). Mechanical performance of asphalt mixtures modified by bio-oils derived from waste wood resources. *Construction and Building Materials*, *51*, 424-431.

Yao, Z., and Monismith, C. L. (1986). Behavior of asphalt mixtures with carbon black reinforcement. In *Association of Asphalt Paving Technologists Proceedings*, *55*, 564-585.

Yildirim, Y. (2007). Polymer modified asphalt binders. *Construction and Building Materials*, *21*(1), 66-72.

Yildirim, Y., Hazlett, D., and Davio, R. (2004). Toner-modified asphalt demonstration projects. *Resources, Conservation and Recycling*, *42*(3), 295-308.

Yildirim, Y., Jayawickrama, P. W., Hossain, M. S., Alhabshi, A., Yildirim, C., Smit, A. F., and Little, D. (2007). *Hamburg wheel tracking database analysis*, Report No. FHWA/TX-05/0-1707-7, Texas Department of Transportation, Austin, Texas.

Yildirim, Y., Solaimanian, M., and Kennedy, T. W. (2000). *Mixing and compaction temperatures for hot mix asphalt concrete*, Report No. 1250-5. Center for Transportation Research, University of Texas at Austin.

Yousef, S., Eimontas, J., Striūgas, N., and Abdelnaby, M. A. (2021). Gasification kinetics of char derived from metallised food packaging plastics waste pyrolysis. *Energy*, 122070.

Yousefi, A. A., Ait-Kadi, A., and Roy, C. (2000). Effect of used-tire-derived pyrolytic oil residue on the properties of polymer-modified asphalts. *Fuel*, *79*(8), 975-986.

Youtcheff, J., Wijayatilleke, N., and Shenoy, A. (2005). *Evaluation of the laboratory*

asphalt stability test, Report No. FHWA-HRT-04-111, Federal Highway Administration, Virginia.

Zani, L., Giustozzi, F., and Harvey, J. (2017). Effect of storage stability on chemical and rheological properties of polymer-modified asphalt binders for road pavement construction. *Construction and Building Materials*, *145*, 326-335.

Zhang, F., and Hu, C. (2013). The research for SBS and SBR compound modified asphalts with polyphosphoric acid and sulfur. *Construction and Building Materials*, *43*, 461-468.

Zhang, F., Yu, J., and Wu, S. (2010). Effect of ageing on rheological properties of storage-stable SBS/sulfur-modified asphalts. *Journal of Hazardous Materials*, *182*(1-3), 507-517.

Zhang, R., Dai, Q., You, Z., Wang, H., and Peng, C. (2018a). Rheological performance of bio-char modified asphalt with different particle sizes. *Applied Sciences*, *8*(9), 1665.

Zhang, R., Wang, H., Jiang, X., You, Z., Yang, X., and Ye, M. (2018b). Thermal storage stability of bio-oil modified asphalt. *Journal of Materials in Civil Engineering*, *30*(4), 04018054.

Zhang, R., You, Z., Wang, H., Ye, M., Yap, Y. K., and Si, C. (2019). The impact of bio-oil as rejuvenator for aged asphalt binder. *Construction and building materials*, *196*, 134-143.

Zhao, S., Huang, B., Shu, X., and Ye, P. (2014a). Laboratory investigation of biochar-modified asphalt mixture. *Transportation Research Record*, *2445*(1), 56-63.

Zhao, S., Huang, B., Ye, X. P., Shu, X., and Jia, X. (2014b). Utilizing bio-char as a bio-modifier for asphalt cement: A sustainable application of bio-fuel by-product. *Fuel*, *133*, 52-62.

Zhou, F., Mogawer, W., Li, H., Andriescu, A., and Copeland, A. (2013). Evaluation of fatigue tests for characterizing asphalt binders. *Journal of Materials in Civil Engineering*, *25*(5), 610-617.

Zhou, L., Huang, W., Zhang, Y., Lv, Q., Yan, C., and Jiao, Y. (2020). Evaluation of the adhesion and healing properties of modified asphalt binders. *Construction and Building Materials*, *251*, 119026.

PUBLICATIONS

Journals

1. **Abhinay Kumar**, Rajan Choudhary, and Ankush Kumar (2021). Rheological, mechanical, and chemical characterization of asphalt binders and mixtures with waste tire and plastic pyrolytic chars, Journal of Materials in Civil Engineering, ASCE, 34(6), 04022093:1-19. DOI: 10.1061/(ASCE)MT.1943-5533.0004234

2. **Abhinay Kumar**, Rajan Choudhary, and Ankush Kumar (2021). Storage stability of waste tire pyrolytic char modified asphalt binders: Rheological and chemical characterization, Journal of Materials in Civil Engineering, ASCE, 34(3), 04021489:1-17. DOI: 10.1061/(ASCE)MT.1943-5533.0004129

3. **Abhinay Kumar**, Rajan Choudhary, and Ankush Kumar (2021). Characterization of thermal storage stability of waste plastic pyrolytic char modified asphalt binders with sulfur, PLoS ONE, Public Library of Science, USA, 16(3): e0248465. DOI: 10.1371/journal.pone.0248465

4. **Abhinay Kumar**, Rajan Choudhary, and Ankush Kumar (2021). Aging characteristics of asphalt binders modified with waste tire and plastic pyrolytic chars, PLoS ONE, Public Library of Science, USA, 16(8): e0256030. DOI: 10.1371/journal.pone.0256030

5. **Abhinay Kumar**, Rajan Choudhary, and Ankush Kumar (2021). A study on production temperatures of asphalt binders modified with waste tyre pyrolytic char, International Journal of Pavement Engineering & Asphalt Technology, 22, 56-68. DOI: 10.1515/ijpeat-2016-0044

6. **Abhinay Kumar**, and Rajan Choudhary (2020). Use of waste tyre pyrolytic products for asphalt binder modification, International Journal of Pavement Engineering & Asphalt Technology, 21, 35-51. DOI: 10.1515/ijpeat-2016-0031

Book Chapters

1. **Abhinay Kumar**, Rajan Choudhary, and Ankush Kumar (2021). Evaluation of rutting properties of asphalt binders and mixtures with tire pyrolytic char, 12th International Conference on Road and Airfield Pavement Technology (ICPT-2021), Colombo, Sri Lanka, 14-16 July, 2021. [*Published as a Book Chapter in Lecture Notes in Civil Engineering, Springer. DOI: 10.1007/978-3-030-87379-0_60*]

2. **Abhinay Kumar**, Rajan Choudhary, and Ankush Kumar (2020). Arrhenius based high-temperature performance evaluation of asphalt binders modified with waste

plastic pyrolytic char, 2nd International Conference on Recent Developments in Sustainable Infrastructure (ICRDSI-2020), Kalinga Institute of Industrial Technology, Bhubaneswar, Odisha, 19-21 December, 2020. [*Accepted for Publication as a Book Chapter in Lecture Notes in Civil Engineering, Springer*] *[Received Overall Best Paper Award of the Conference]*

3. **Abhinay Kumar**, Rajan Choudhary, and Ankush Kumar (2020). Use of char derived from waste plastic pyrolysis for asphalt binder modification, 3rd International Conference on Innovative Technologies for Clean and Sustainable Development: ITCSD 2020, Chandigarh, India, 19-21 February, 2020. [*Published as a Book Chapter in RILEM Book Series-ITCSD 2020, Springer. DOI: 10.1007/978-3-030-51485-3*]

Conferences

1. **Abhinay Kumar**, Rajan Choudhary, and Ankush Kumar (2020). Evaluation of aging behavior of asphalt binders modified with chars from pyrolysis of tyre and plastic wastes, International Conference on Civil Engineering Trends and Challenges for Sustainability (CTCS), 22-23 December, 2020, NMAM Institute of Technology, Nitte, Karnataka.

2. **Abhinay Kumar**, Rajan Choudhary, and Ankush Kumar (2020). High temperature characterization of waste plastic pyrolytic char modified asphalt binders, International Conference on Engineering Sciences and Technologies for Environmental Care (ESTEC-2020), 20-22 February, 2020, CSIR-NEIST, Jorhat.

3. **Abhinay Kumar**, Rajan Choudhary, and Ankush Kumar (2020). Use of products from pyrolysis of wastes in asphalt binder modification: A review, RECYCLE-2020: 3rd International Conference on Waste Management, 13-14 February, 2020, IIT Guwahati, Assam.

Manuscript Under Preparation

1. **Abhinay Kumar** and Rajan Choudhary (2021). Performance evaluation of asphalt binders and mixtures prepared with waste tire and plastic pyrolytic chars, *Under Preparation.*